THE UNIVERSITY
of EDINBURGH

The University Of Edinburgh

College of Medicine and Veterinary Medicine

Novel Imaging and Blood Biomarkers in Acute Aortic Syndrome

By

Maaz Bin Junaid Syed

Doctoral thesis
PhD Cardiovascular Sciences
Primary Supervisor: Professor David E Newby
British Heart Foundation Department for Cardiovascular Sciences

December 2021

In the name of God, the Most Merciful, the most Beneficent

I dedicate this thesis to my son, *Eesa Bin Maaz Syed*, and beautiful wife, *Yusra Makhdoomi*. I also dedicate this work to my loving parents, *Junaid-ul-Islam Syed* and *Zeenat Alvi Syed*, to whom I am forever indebted. Finally, I dedicate this thesis to my brother and his wife, *Talha Bin Junaid Syed* and *Syeda Humera Zia*, who are my closest and dearest family.

Acknowledgements

I would like to acknowledge the support of Professor David Newby and his team of senior researchers, including Professor Marc Dweck, Dr Tim Clark, Dr Adriana Tavarez, Dr Christophe Lucatelli and Professor Edwin van Beek.

I would also like to acknowledge the fantastic team at the Edinburgh Imaging Facility and the Clinical Research Facility, both of which are affiliated with the Queens Medical Research Institute, University of Edinburgh and NHS Lothian. I would like to thank Professor James Dear, Dr Anna-Maria Choy and their respective teams.

Contents

Declarations

Study design, funding and regulatory approvals

I performed a literature review and designed the study for this thesis with the support of Professor David Newby. We obtained a Clinical Research Fellowship grant from the British Heart Foundation. Again, I drafted the study proposal for this under the supervision of Professor D Newby. I also applied for regulatory approval to ensure the study was delivered safely. Finally, I registered the study in an open-access database prior to patient recruitment.

Patient recruitment, clinical assessment and blood collection

I consented and recruited study participants. I also performed a structured clinical assessment and collected blood samples from all participants. I would like to thank the Clinical Research Facility for processing the majority of blood samples collected from patients. I processed the blood samples from a small cohort of patients during the COVID pandemic during which time activity at the Clinical Research Facility was redirected.

Computed tomography, positron emission tomography scans and image analysis

I worked in a team consisting of a senior radiographer, medical physicists and radiophysicist to develop a safe computed tomography and positron emission tomography imaging protocol for study participants. I would like to thank the radiochemistry group for developing the ^{18}F-sodium fluoride radiotracer. I supervised the PET/CT scans for study participants. I would like to thank the staff at the Queens Medical Research Institute Imaging Department for acquiring, anonymising and storing imaging acquired in this study. I performed the image analysis of all participants in the study. This included image

analysis related to both computed tomography and positron emission tomography.

Biomarker Analysis

Biomarker analysis was performed by independent teams blinded to the clinical characteristics of study participants. I transported blood samples to Dr Anna-Maria Choy's Cardiovascular research team at the University of Dundee who quantified plasma Desmosine concentrations. I also provided blood samples to Professor James Dear's research team at the Queens Medical Research Institute at the University of Edinburgh who measured miRNA expression. I am grateful to both teams for their expertise.

Compilation of results, data analysis and manuscript authoring

I compiled the data into secure data structures and performed all aspects of the statistical analysis. I authored this manuscript, again under the supervision of Professor David Newby and my PhD co-supervisor, Professor Marc Dweck.

General Support

I would like to thank *Dr Alexander J Fletcher* and *Mr Samuel Debono* for their support during this research period, including the development of novel analytical techniques, discussions related to strategic direction and general delivery of the research project.

Abstract

Background

Acute aortic syndrome is an unpredictable and catastrophic condition. It is characterised by medial degeneration which is beyond the resolution of conventional anatomical imaging. Here, we investigate ^{18}F-sodium fluoride positron emission tomography and computed tomography (PET/CT) and circulating biomarkers in patients with acute aortic syndrome.

Methods

We performed ^{18}F-sodium fluoride PET/CT in 56 patients with aortic dissection, intramural haematoma or penetrating aortic ulcers and 20 healthy controls. First, we characterised radiotracer uptake in relation to demographic and clinical factors (**Chapter 3**). Next, we investigated the role of ^{18}F-sodium fluoride PET/CT and disease progression in patients with aortic dissection or intramural haematomas (**Chapter 4**). In a sub-study, we measured plasma desmosine concentration in patients with acute aortic syndrome and investigated these in relation to aortic expansion (**Chapter 5**). Finally, we identified candidate miRNAs and measured their circulating expression in patients with acute aortic syndrome. Again, we related these to disease characteristics and progression (**Chapter 6**).

Results

Patients with acute aortic syndrome had increased ^{18}F-sodium fluoride PET/CT signal compared to healthy controls (tissue-to-background ratio 2.08±0.45 vs 1.36 ±0.39, p<0.001). ^{18}F-Sodium fluoride uptake concentrated at the site of intimal disruption (+32.5%, p<0.001). Radiotracer uptake in the false lumen was associated with aortic expansion independent of aortic diameter (+7.1 mm/yr, p=0.011). Peak ^{18}F-sodium fluoride uptake was independently associated with aortic rupture, repair or aorta-related death (hazard ratio 8.6 [95% CI, 1.1-68.1], p=0.041). Plasma desmosine concentrations were also elevated in patients (0.58±0.26 vs 0.27±0.07 ng/mL, p<0.001) and peaked at presentation (0.82±0.17 ng/mL, p<0.001). Plasma desmosine concentration was associated with aortic expansion, again, independent of aortic diameter (β=+2mm/yr, p<0.001). We identified 16 candidate circulating miRNA, several of which were associated with aortic diameter, expansion and ^{18}F-sodium fluoride uptake. miRNA expression was independently associated with major adverse aortic events (hazard ratio 3.32 (1.71-6.46), p<0.001).

Conclusion

This is the largest PET study in patients with acute aortic syndrome and the first to use ^{18}F-sodium fluoride PET/CT. In this proof-of-concept study, we demonstrate the potential for ^{18}F-sodium fluoride PET/CT to detect acute aortic syndrome and improve risk stratification. Desmosine is a promising circulating biomarker in this condition and may play a role in diagnosis. Finally, we identified a miRNA signature associated with major adverse aortic events following acute aortic syndrome.

Lay Summary

The aorta is the main blood vessel of the body that carries blood out of the heart. In acute aortic syndrome, the blood vessel is damaged by a tear or bleed. This weakens the aorta. The damaged aorta may balloon up or burst. This can cause death. It is difficult to know which aortas will cause problems.

^{18}F-Sodium fluoride positron emission tomography and computed tomography (PET/CT) is a new type of scan that finds damaged parts of the aorta. It has never been used in patients with acute aortic syndrome. We found that ^{18}F-Sodium fluoride (PET/CT) could find damaged areas of the blood vessels in patients with acute aortic syndrome. Patients with more damage were likely to run in to problems such as ballooning of the aorta, the aorta bursting or needing an operation.

We also did some new blood tests in patients with acute aortic syndrome. One of these blood tests is called Desmosine. This is raised in the blood when the aorta is damaged. Again, desmosine has never been tested in patients with acute aortic syndrome. We found that patients with acute aortic syndrome had high desmosine, even when they saw doctors for the first time with this disease. This means that desmosine could one day be used to find patients with acute aortic syndrome. Patients with high desmosine in their blood also had more damaged aortas that grew quickly.

We performed new genetic tests on patients with acute aortic syndrome. We measured micro-ribose nucleic acids (miRNA). miRNA control the way genes work. We found 16 miRNA that are important in patients with acute aortic syndrome and tested them in the blood. We found that miRNA may tell us how damaged the aorta is. miRNA may also tell

us who has severe disease or need an operation. miRNA may one day help us find acute aortic syndrome patients who may develop problems with their aorta.

This is the first time ^{18}F-sodium fluoride PET/CT, desmosine or miRNA have been used to find damaged aortas in patients with acute aortic syndrome. These tests may help us find patients with the most severe disease and one day help us treat patients better.

Chapter 1

Introduction

1.1 The Aorta

The aorta is the main blood vessel of the body that carries blood from of the heart during systole. It is composed of three layers, each with distinct biological functions. The aorta is an elastic artery that propagates blood flow by recoiling during cardiac relaxation. The aorta experiences enormous haemodynamic stresses during the cardiac cycle. Genetic abnormalities may alter the cellular composition of the aorta. The aorta is also subject to metabolic insults from external irritants such as cigarette smoke and hypertension. In combination, these pathological processes weaken the aortic wall and make it prone to dilatation. The damaged aorta may ultimately rupture. This catastrophic event is often fatal.

1.1.1 Anatomy

The aorta is anatomically divided into the ascending aorta, aortic arch, descending thoracic aorta and abdominal aorta. These division are defined by distinct anatomical landmarks and this classification system is useful for the detection and management of aortic diseases.

The aorta arises from the aortic annulus at the outflow of the left ventricle and the aortic

valve. The aortic valve prevents retrograde flow of blood from the aorta into the heart during cardiac relaxation. Immediately distal to the aortic valve are the two coronary arteries which perfuse the myocardium. Mean aortic root diameter varies between 2.1 and 4.3cm and is associated with patient age, sex and body surface area (Devereux et al. 2012).

The ascending aorta is located within the anterior mediastinum and is the first segment to carry blood from the heart. This aortic segment faces extreme pressure changes during cardiac systole and thus has strong elastic properties. The ascending aorta also has the widest diameter which typically measures less than 3.5 cm (Paruchuri et al. 2015). The ascending aorta transitions into the aortic arch at the transthoracic plane. This imaginary boundary separates the superior and inferior mediastinum. The transthoracic plane runs through the sternal angle and the T4/T5 vertebra. Here, the aortic arch gives rise to the major arterial supply to the head, neck, limbs and spinal cord through the brachiocephalic trunk, left common carotid artery and left subclavian artery. The aortic arch hooks posteriorly and inferiorly to descend into the posterior mediastinum where it transitions into the descending thoracic aorta, again at the transthoracic plane. The descending thoracic aorta contains numerous small branches that perfuse the chest wall and contribute to spinal cord perfusion. This relatively straight section of aorta facilitates arterial flow to the lower half of the body.

Emergence of the aorta from the diaphragm at the T12 level marks its transition into the abdominal aorta. The abdominal aorta is further divided into the suprarenal, juxtarenal and infrarenal aorta as dictated by the position of the blood supply to the kidneys. The suprarenal aorta is a short arterial segment which gives rise to critical arteries that supply the fore- and midgut, including the hepatobiliary system. These are the coeliac trunk and the superior mesenteric arteries. Next, the juxtarenal aorta contains the origin of the renal arteries and serves as an important clinical landmark. Finally, the infrarenal aorta perfuses the hindgut and pelvis through the inferior mesenteric artery before terminating at the bifurcation around the T10 vertebral level. Here, the aorta divides in to the left and right common iliac arteries to supply the pelvis and lower limbs. The normal infrarenal aortic diameter ranges from 17 to 20mm which again, is influenced by age, sex and body surface area (Sonesson et al. 1994).

1.1.2 Cellular composition of the aorta

The aorta is composed of three distinct layers. First, the innermost tunica intima contains the endothelium and subendothelial structures which transmit biomechanical, chemical and immunological signals from luminal blood flow to the aortic wall. Second, the thicker medial layer is chiefly composed of vascular smooth muscle cells suspended within an extracellular matrix rich in elastin and collagen. These contractile units provide the aorta with its characteristic elastic properties. Finally, the external adventitial layer forms a loose but strong mesh of para-aortic structures that modulate aortic wall biology in response to external neurohormonal stimuli.

The vascular endothelium is a thin smooth non-fenestrated sheet of inner lining composed of polygonal-shaped endothelial cells with an antithrombotic coating of glycocalyx. Endothelial cells overlap with adjacent cellular structures and are connected by well-developed tight junctions which regulate substrate transfer. The adjacent basal lamina forms a collagen-rich barrier between the endothelium and deeper intimal layer to control cellular migration, vascular regeneration and blood clotting. The endothelium also produces proteoglycans. These are macromolecules that influence vascular wall biology lipid metabolism and thrombosis. The internal elastic lamina is rich in elastin which acts as a controlled barrier for the migration of macromolecules and cellular structures into the aortic media.

The tunica media consists primarily of highly organised smooth muscle cells suspended in elastin and collagen. This layer is the chief determinant of arterial properties and dictates arterial distensibility. Arterial smooth muscle cells are normally found in their contractile state. Smooth muscle cells are surrounded by a basement membrane which contains collagen and proteoglycans. These prevent cellular migration and lock vascular smooth muscle cells in place. The media contains well defined contractile complexes that function in tandem to facilitate propagation of blood along the arterial system.

The tunica adventitia is an ill-defined loose layer that is in continuity with peri-vascular connective tissue. The aorta is relatively scarce in adventitial tissue compared to smaller vessels. Aortic adventitia contains fibroblasts, myofibroblasts and pluripotent cells with

the potential to differentiate in to specialised subtypes in response to physiological stimuli. The neurological supply to the aorta is contained within the adventitia, which controls arterial vasomotor tone. The adventitia also contains vasa vasorum. These single-cell thick capillary networks provide oxygenated blood to the vessel wall. Importantly, large arteries such as the aorta, have an extensive network of vasa vasorum that also extend towards the outer most layer of the media.

1.1.3 Mechanical properties of the aorta

The aorta experiences strong haemodynamic forces during the cardiac cycle in the form of strain and shear stress. Circumferential strain is exerted perpendicular to the aortic wall. Strain is the product of blood pressure and vessel radius, whilst being inversely associated with wall thickness. In contrast, shear stress is the force experienced parallel to the aortic wall and is related to blood viscosity, flow rate and, again, vessel radius. Both, circumferential strain and shear stress act in a synergistic pattern such that the total pressure within the arterial segments remains constant.

Acute changes in shear stress results in the release of vasoactive components that modulate vascular tone. Sustained shear stress, however, results in vascular remodelling in the form of morphological alterations and change in cell wall composition. This adaptive response induces three changes within smooth muscle cells driven by endothelial nitric oxide production. First, they undergo a change in phenotype from contractile to excretory states to increase production of the extracellular matrix. Second, smooth muscle cells undergo hypertrophy to accommodate the increased force. Finally, vascular smooth muscle cells change their orientation resulting in dysregulation of an otherwise highly organised architecture. Sustained expression of nitric oxide, however, also activates matrix metalloproteinases that ultimately lead to a degradation of the extracellular matrix and cellular apoptosis. The result is reduced vascular stretch leading to increased arterial blood pressure. This also increases strain on the arterial wall leading to pressure-related crush, thus driving a positive feedback loop of endothelial dysfunction and adverse aortic remodelling.

1.2 Disease processes affecting the aorta

1.2.1 Atherosclerosis

Atherosclerosis is a multifocal immuno-inflammatory condition of medium and large-sized arteries (Teague et al. 2017). Exposure to risk factors such as hypertension, hypercholesterolaemia and smoking creates a systemic environment that encourages endothelial dysfunction (Davignon and Ganz 2004), oxidation of lipoproteins (Pirillo et al. 2018), production of free oxygen radicals (Mullick et al. 2008) and leukocyte migration (Newby 2016). Accumulation of oxidised lipoproteins within the vessel wall forms fatty streaks. Macrophages migrate across the endothelium to phagocytose these lipid-rich proteins. The high intracellular cholesterol content of macrophages induces pathways of cell death. The resultant debris, along with necrotic endothelial and smooth muscle cells, forms the principal constituent of the lipid-rich core (Figure 1.1) (Stary et al. 1995).

Atherosclerotic plaques consist of necrotic debris contained by outward remodelling and a fibrous cap within the intimal surface. Vulnerable plaques are prone to rupture and have patho-anatomical features, such as large lipid-rich necrotic cores contained by a thin (<65 μm) macrophage-rich fibrous cap (Virmani et al. 2003). In metabolically active plaques, macrophages accumulate in the fibrous cap and degrade the extracellular matrix that is produced by vascular smooth muscle cells (Newby 2016). The necrotic core creates a microenvironment of hypoxia that stimulates angiogenesis (Sluimer et al. 2008).

Calcium deposition in vessel wall inflammation occurs as a macrophage-mediated reparative response to oxidised lipid deposition and endothelial dysfunction. However, rather than being a passive by-product of degradation, the process of vascular calcification is active and controlled. Calcification in atherosclerosis primarily affects the intima. This is in contrast to medial calcification typically observed in patients with diabetes or chronic kidney disease, which adopts a concentric transmural morphology (Fuery et al. 2017). The initiation of vascular calcification occurs on a microscopic level and involves the deposition of calcium and phosphate-rich hydroxyapatite crystals (Hirsch et al. 1993). This early stage of “microcalcification” signifies intense biological activity and is associated with increased plaque vulnerability. In contrast, the larger established deposits of macroscopic

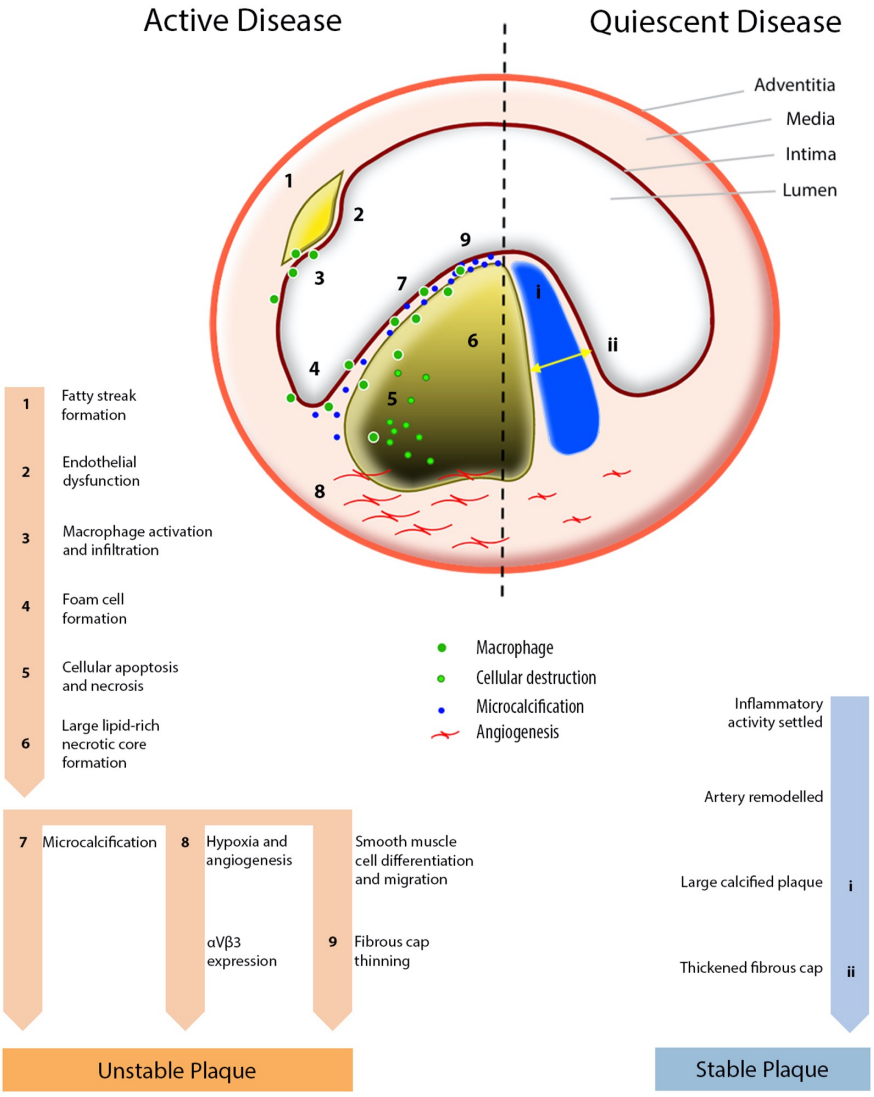

Figure 1.1: **Pathophysiology of atherosclerosis.** Arterial cross-section showing that active atherosclerotic disease is characterised by intense biological activity resulting from macrophage infiltration in response to the subendothelial accumulation of oxidised lipoproteins. A cascade of events leads to cell death and the formation of a lipid-rich necrotic core. Localised hypoxia from the lipid-rich core promotes $\alpha_v\beta_3$ expression and angiogenesis. Thinning of the fibrous cap results from macrophage infiltration and loss of vascular smooth muscle cells. Cell death around the necrotic core leads to microcalcification. This biologically active plaque is at high risk of rupture. In contrast, quiescent atherosclerotic disease represents chronic healed inflammation with positive remodelling. Calcification of the fibrous cap adds stability. This quiescent plaque is at low risk of rupture.

calcification that ultimately develop are associated with plaque stability and a more quiescent phase of disease.

Vulnerable plaques have a thin fibrous cap that is devoid of vascular smooth muscle cells and exhibits intense macrophage recruitment (Virmani et al. 2003). Rupture of the thin fibrous cap exposes the lipid-rich necrotic core to luminal flowing blood, initiating rapid and aggressive thrombosis that can cause vascular occlusion. However, plaque rupture is frequently silent and subclinical. Over time, vascular remodelling incorporates the exposed thrombus and the degree of stenosis may worsen.

Angiogenesis and collateralisation can partially compensate for reduced blood flow caused by increasingly stenotic vessels. However, if arterial disruption is rapid, this compensatory angiogenesis has had insufficient time to occur, and the resultant ischaemia is more severe. Thus, vulnerable plaque rupture may cause sudden arterial occlusion, loss of tissue perfusion and catastrophic end-organ infarction. Prompt therapeutic reperfusion is required to minimise irreversible tissue loss in a highly time-dependent process (Emberson et al. 2014).

1.2.2 Medial Degeneration

Degenerative aortopathies include inflammatory mediated processes that are distinct from atherosclerosis because they are characterised by medial atrophy rather than intimal proliferation (Figure 1.2)(Shen and LeMaire 2017). Consequent thinning, weakening and stiffening of the aortic wall leaves it vulnerable to dilatation and rupture. Inflammation in degenerative aortopathies primarily affect the media and adventitia.

The chief immune mediator in aortic aneurysm formation appears to be CD4+ T-lymphocytes through the production of interferon-γ (Xiong et al. 2004). Whereas Th1 cells contribute to atherosclerosis, Th2 cells are strongly implicated in aneurysmal disease. These produce interleukin-4, interleukin-5 and interleukin-13, which stimulate natural killer cells to produce matrix metalloproteinases (MMP) and cause medial smooth muscle atrophy (Shen and LeMaire 2017). Th17 are common to both, atherosclerotic and aneurysmal disease. They promote macrophage activation by releasing tumour necrosis

factor-α, interleukin-6 and interleukin-1. These cytokines have downstream effects that promote MMP-9 expression and smooth muscle loss (Bersi et al. 2017).

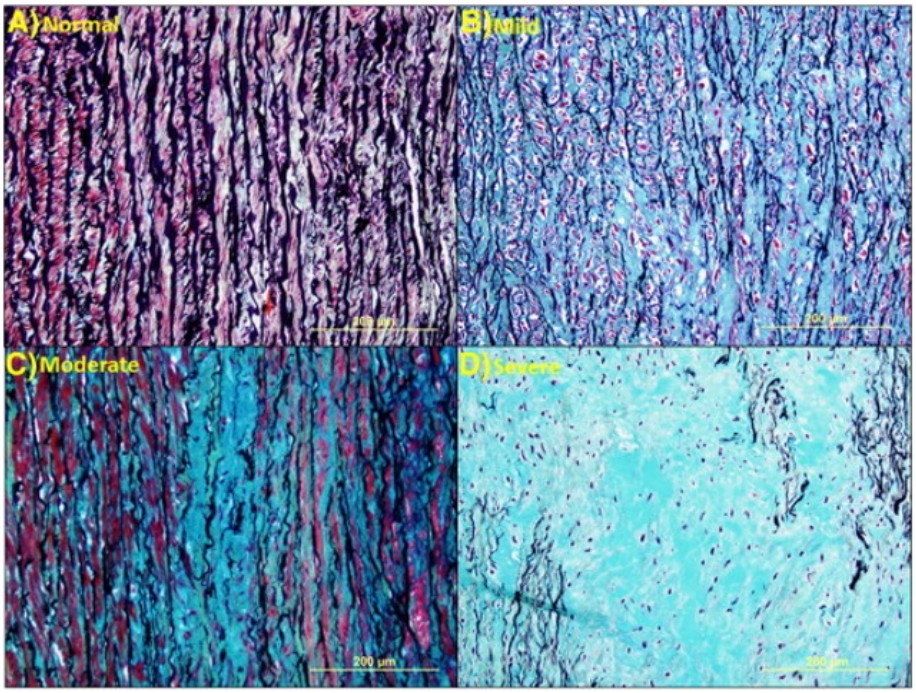

Figure 1.2: **Medial Degeneration.** Histologic images showing grades of medial degeneration. (**A**) Normal aorta. (**B**) Mild medial degeneration characterized by pooling of proteoglycan between elastic lamellae. (**C**) Moderate medial degeneration with focal loss of elastic lamellae and proteoglycan deposition. (**D**) Severe medial degeneration with marked loss of elastic lamellae, SMCs, and extensive proteoglycan deposition. All Movat pentachrome stain (Ladich et al 2016).

Degenerative aortopathy is driven by complex interplay of genetic and environmental pathological processes. These result in thinning of the medial layer, loss of cellular architecture, reduction in cellular density and abnormal extracellular matrix function. External stimuli, such as cigarette smoking and hypertension, cause chronic endothelial agitation that drive vascular smooth muscle cells to undergo morphological and functional changes. Chronic endothelial dysfunction causes pathological aortic remodelling by activating matrix metalloproteinases that cause disproportionate loss of cellular elastin and disruption of the basal lamellae that lock vascular smooth muscle cells in place. Loss of cellular architecture results in smooth muscle cell migration away from the media (Michel, Jondeau, and Milewicz 2018). A combination of reduced cellular density

and loss of extracellular matrix results in large vacuous spaces within the aortic wall which are occupied by pooling of proteoglycans - a phenomenon previously termed cystic medial necrosis (J. H. Lee et al. 2020).

In patients with connective tissue dysfunction, genetic abnormalities alter contractile units that are essential to arterial function. The fibrillin-1 (FBN1) gene, for instance, is responsible for the formation of a fibrillin mesh essential to the development of healthy arterial tissue. Fibrillin fibres act as a scaffold for tropoelastin deposition which is the precursor step for mature elastin synthesis (Dietz and Pyeritz 1995). Abnormalities in the fibrillin-1 gene result in abnormal fibrillin function and consequent elastinopathy that characterises connective tissue disorders such as Marfan Syndrome. The transforming growth factor-β (TGF-β) pathway modulates the closely related small mothers against decapentaplegic (SMAD) gene and is implicated in the development of Loeys-Dietz Syndrome. TGF-β signalling follows 2 distinct and well-investigated pathways: SMAD (canonical), or p38/extracellular signal-regulated kinase/c-Jun N-terminal kinase (noncanonical) (Holm et al. 2011). A multitude of genetic abnormalities may lead to thoracic aortopathy by inducing medial degeneration which in turn drives inflammation. Examples of these genes include FBN1, TGFBR1, TGBR2, BGN, SMAD3, SKI, BGN, COL3A1, COL1A1, COL1A2 and SLC2A10 (Fletcher et al. 2020). More genetic defects are constantly being discovered. Patients with arterial connective tissue disorders thus contain vulnerable aortas that are prone to developing aortic aneurysms or acute aortic syndrome.

1.2.3 Calcification

Vascular calcification is a healing response to inflammation and tissue degradation. Detection of the early stages of microcalcification therefore acts as a surrogate of early vascular injury within aortas. By comparison, detection of the latter stage of macrocalcification is associated with inflammation that is healing or burnt out.

Vascular calcification starts at a microscopic level and at a scale that is beyond the resolution of anatomical imaging modalities. Pathology such as elastin breaks or atherosclerotic plaque rupture causes increased metabolic activity in the vessel wall, which is reflected in the deposition of tiny calcium-containing crystals (Hirsch et al. 1993). This early-stage

microcalcification signifies intense biological activity and exerts its own effects on vascular tissue.

Necrosis and inflammation are the key pathological processes that ultimately lead to vascular calcification. Detecting microcalcification allows early identification of cell death associated with increased inflammatory activity that is likely to cause morphological changes over time. Microcalcification co-localises with cell death and can be considered a marker of necrosis-derived inflammatory activity (Proudfoot et al. 2000; Aghagolzadeh et al. 2016). Necrosis causes the spillage of intra-cellular calcium and phosphate. This triggers the formation of inflammatory mediators that drive microcalcification.

Vascular smooth muscle cells within the arterial wall produce components of the extracellular matrix. Cellular necrosis and inflammatory infiltrates cause the release of calcium. Macrophages, for instance, produce calcifying matrix vesicles that contribute to microcalcification (New et al. 2013). Extracellular calcium triggers a functional change in vascular smooth muscle cells which undergo vesicle-mediated calcification themselves (Reynolds et al. 2004). A reduction in vascular smooth muscle cell numbers further destabilises the aortic wall through a reduction in extracellular matrix formation. Here, microcalcification propagates further calcification thus creating a positive feedback loop. Deposits of microcalcification within the media is also associated with elastin breaks. This mechanism of microcalcification has been observed within the aortic wall of patients with connective tissue disorders (Wanga et al. 2017).

Eventually, calcium coalesces in to larger mature fragments. Inflammatory activity within the arterial tree is cyclical – it undergoes periods of elevated and reduced metabolic activity. Hence, established calcified plaque, in itself, is not a marker of active arterial disease. It may equally have formed many years ago and instead reflect a dormant disease process.

Calcium deposition is dynamic and present throughout the arterial tree. The mechanism of vessel wall calcification differs based on predisposing risk factors. It can take many forms and can affect the vessel intima or media. Rather than being a passive by-product of degradation, calcium deposition is active and controlled (Tabas and Bornfeldt 2016).

Atherosclerotic injury predominantly affects the intima and is associated with intimal calcification (Fuery et al. 2017). Conversely, calcification in medial degeneration adopts a crescentic transmural morphology involving the tunica media. Whilst the triggers for intimal and medial calcification may be different, many of the subsequent pathways appear to be shared (Fuery et al. 2017).

1.3 Acute Aortic Syndrome

Acute aortic syndrome is a clinical emergency resulting from intimal disruption due to atherosclerosis, medial degeneration and premature ageing of the aorta. Acute aortic syndrome consists of three pathologies. First, intramural haematomas occur when a bleed is contained within the aortic wall resulting from either focal disruption of the intima or fracturing of a fragile vasa vasorum. Second, a penetrating aortic ulcer manifests as an intense focus of atherosclerotic activity that erodes into the aortic wall leading to localised weakening of the media. Finally, an aortic dissection occurs when intimal tears cause the formation of a second false channel for blood to flow through separated by a dissection flap. Aortic dissections may occur *de novo* or as a secondary consequence of intramural haematomas or penetrating aortic ulcers. The three diseases are closely related.

Acute aortic syndrome is a dynamic condition with rapid and unpredictable clinical progression. Sudden weakening of the aortic wall threatens aortic rupture. Patients with acute aortic syndrome thus undergo intensive imaging surveillance with a view to detect disease propagation or morphological change.

The primary treatment modality in acute aortic syndrome is aggressive blood pressure control often with an intravenous beta-blocker infusion. The development of complications, such as impending rupture, visceral malperfusion or rapid growth are indications for surgical intervention. The emergence of endovascular therapy has revolutionised the management of acute aortic syndrome. Minimally invasive techniques such as thoracic endovascular aneurysm repair (TEVAR) involve accurate placement of aortic stents across intimal disruptions under fluoroscopic guidance. Patients with acute aortic syndrome, however, often present with complex aortic morphologies. Involvement of the ascending

aorta, proximity to visceral branches or underlying connective tissue disorders necessitates open surgical repair which, itself, carries significant comorbidity.

Acute aortic syndrome is unpredictable and determining risk of complications is challenging. Morphological aortic change is a late manifestation of disease progression. The development of novel imaging techniques enables clinicians to detect cellular pathologies that are otherwise hidden from conventional anatomical imaging. Our understanding of aortic wall biology in patients with thoracic aortopathy is improving. Novel circulating biomarkers may also one day aid detection of disease and improve risk prediction.

1.4 Anatomical vascular imaging

Anatomical imaging is diverse and flexible. The chief objectives are to detect morphological change and characterise atherosclerotic plaque. Imaging also allows a global assessment of calcification burden within the entire vascular territory. This information helps clinicians stratify the risk of future adverse events. Anatomical imaging can be used to detect both morphological change from medial degeneration and atherosclerosis.

1.4.1 Invasive Imaging

1.4.1.1 Catheter-based angiography

Catheter-based contrast angiography has historically been the most frequently used method to image the vascular system. Indeed, it is still used extensively to investigate certain vascular beds such as the peripheral or coronary arteries. This is largely because of the high spatial and temporal resolution that can be obtained. Catheter angiography is also a platform for intervention. However, catheter angiography alone merely provides a “lumenogram” of the circulation. It is unable to delineate intramural thrombus that is often present in expanding aortopathies.

Catheter based angiography has been superseded by non-invasive imaging modalities such as computed tomography and magnetic resonance imaging in the diagnostic process. It does, however, still play a major role in intervention for the accurate placement of

aortic stents during endovascular repairs.

1.4.1.2 Intravascular Ultrasound

Intravascular ultrasound (IVUS) offers extremely high-resolution characterisation owing to their proximity to diseased artery. IVUS packages a high-frequency ultrasound probe in a catheter that can directly visualise adjacent aortic wall from within the lumen. Its role in aortic imaging is still being evaluated. Investigators have reported the utility of IVUS to detect intimal disruptions in patients with intramural haematomas that were previously misdiagnosed using conventional CT imaging (Mileva et al. 2018). Similarly, a series of 15 patients characterised penetrating aortic ulcer morphology using IVUS. Interestingly, the authors found a further 4 aortic ulcers that were missed by conventional CT (Wei et al. 2006).

A potential use of IVUS is to provide peri-procedural aortic diameter measurements during endovascular intervention. A case series reports the experience of using IVUS to measure real-time aortic morphology in 57 patients with acute aortic syndrome undergoing endovascular therapy. IVUS accurately measured aortic diameter compared to conventional CT sizing within the thoracic aorta. IVUS, however, tended to overestimate aortic diameter around the aortic arch – a critical intervention zone in this cohort (Janosi et al. 2015).

IVUS has been used to characterise atherosclerotic plaque in smaller calibre vessels. It is well established in detecting and treating coronary (Jang et al. 2005; Brugaletta et al. 2011), carotid (Štěchovský et al. 2016) and lower limb [yin2017a] arteries.

1.4.1.3 Optical Coherence Tomography

Optical coherence tomography (OCT) provides exceptionally detailed images of the adjacent arterial wall using near infrared light delivered via a fibre optic wire. *Ex vivo* studies using OCT on tissue samples obtained during surgical repair of thoracic aortic aneurysms detected medial degeneration and foci of elastin disruption within the aortic wall. These findings correlated strongly with subsequent histological analysis (Real et al. 2013). OCT

has also been used to identify vessel wall abnormalities in mouse models of Marfan Syndrome (Lee et al. 2016). However, its utility as an *in vivo* imaging modality to investigate human aortas remains limited owing to narrow fields of views and requirement for proximity to the aortic wall.

In humans, OCT has been used in smaller calibre vessels. Here, OCT provides exceptionally high detail imaging of the adjacent vessel wall and is thus best suited for characterising atherosclerotic plaque (Jang et al. 2005). OCT is used clinically to detect vulnerable plaques and guide therapy in the coronary arteries (Bouma et al. 2003; Jang et al. 2002). OCT is now being used for these purposes in carotid artery stenosis (Dohad et al. 2017) and peripheral vascular disease (Schwindt et al. 2017). OCT remains a promising intravascular imaging modality that may one day find a use in larger calibre vessels such as the aorta.

1.4.2 Non-invasive Imaging

1.4.2.1 Ultrasound

The lack of ionising radiation makes ultrasound an ideal modality for situations that require repetitive imaging. Ultrasound is well suited to studying the aortic root and the abdominal aorta. Indeed, ultrasound is the imaging modality of choice in the United Kingdom abdominal aortic aneurysm screening programme. The remaining thoracic aorta, however, is shielded by bony structures necessitating cross-sectional imaging to investigate these structures. In patients with abdominal aortic aneurysms, contrast-enhanced ultrasound provides real-time characterisation of luminal flow. This has potential applications to visualise complications following endovascular repair such as endoleaks (Mirza et al. 2010).

Contrast agents containing a homogenous suspension of inert gas microbubbles (e.g. SF6) administered in the venous space can highlight specific features of arterial atherosclerotic plaque. In the carotid arteries, microbubbles identify neovascularisation in culprit lesions with a sensitivity and specificity greater than 80% (R. Huang et al. 2016).

Standardising the ultrasound assessment of vascular beds reduce the risk of inter-

observer variability. Vessel assessment is not always possible if the view is obscured by densely calcifying atherosclerotic disease. Similarly, bone or gas overlying the target vessel prevents adequate visualisation using ultrasound, limiting its use to easily arteries that are easily accessible.

1.4.2.2 Computed Tomography

The use of computed tomography angiography (CTA) is well established to assess the cardiovascular system. It is non-invasive and accessible. CTA has the added benefit of visualising the entire vessel from its origin to target structure, even in tortuous vessels. Among its many applications, CTA has the spatial resolution to detect morphological change and provide a global assessment of vascular disease (Figure 1.3A & D). Owing to the short acquisition times of new generation CT scanners, it is now possible to image mobile arterial structures in detail. Indeed, CTA is highly accurate in visualising arterial structures close to the heart such as the ascending aorta and coronary arteries. CTA is used throughout the vascular tree.

1.4.2.3 Magnetic Resonance Imaging

Angiography using magnetic resonance imaging (MRI) is best suited to imaging large stable vessels such as the carotid arteries. Multi-contrast magnetic resonance imaging (T1 weighted, T2 weighted, proton density) offers excellent soft tissue characterisation. This allows the constituents of aortic thrombus or atherosclerotic plaque to be investigated without the need for ionising radiation (Figure 1.3B). These properties make MRI useful in the longitudinal studies of chronic cardiovascular diseases. Administration of gadolinium (Gd)-based contrast media improves image acquisition and provides further structural information outlining differences between the blood pool and vessel wall (Fathi et al. 2018).

Ultrasmall paramagnetic particles of iron oxide (USPIOs) are 30-nm iron oxide nanoparticles stabilised with low-molecular-weight dextran. USPIOs accumulate in macrophages following phagocytosis and remain in the circulation for extended periods [kooi2003]. Areas rich in USPIO-positive macrophages have a low-signal intensity on T2 and T2* weighted MRI (Richards et al. 2011). In the carotid arteries, USPIO accumulation within

atherosclerotic lesions coincides with active plaque disease. These plaque exhibit intense macrophage infiltration (Trivedi et al. 2004.) USPIO also accumulate with high affinity in areas of macrophage infiltration within abdominal aortic aneurysms (Figure 1.3C) (McBride et al. 2015). Using smart MRI contrast agents to detect cellular activity within the vascular bed carries immense promise. These techniques may ultimately lead to the detection of active plaques at risk of imminent events and allow preventative therapy.

Magnetic resonance spectroscopy (MRS) combines the spatial imaging obtained from MRI with spectral analysis to detect the chemical composition and metabolic state of cardiovascular tissue. MRS is able to detect a range of atoms, including 1-Hydrogen (1H), 31-Phosphorus (31P), and 13-Carbon (13C) (Neubauer 2003). In vivo carotid studies using MRS have successfully quantified cholesteryl esters within atherosclerotic plaque (Zajicek et al. (1987); Saam et al. (2013)). Cholesteryl esters are the major class of lipids found in the lipid-rich necrotic core of vulnerable plaques. The chemical composition of structures is obtained using a chemical shift imaging sequence to acquire spectra over and around the atherosclerotic plaque. MRS spectroscopy amplitudes for specific metabolites, such as lipids, are then interpreted as a ratio to the amplitude of intrinsic water (Xin et al. (2015); Deelchand et al. (2010)). The final analysis allows detection and quantification of the lipid content of atherosclerotic plaque.

1.5 Biological imaging of the vascular system

Targeted biological tracers enable positron emission tomography (PET) to detect increased activity of specific disease processes, such as increased glycolytic activity or microcalcification. Biological radiotracer molecules typically consist of two components. One section has a ligand that targets sites of specific disease activity. The other component consists of a radioisotope. PET scanners can detect the intensity and distribution of radiotracer activity following molecular engagement with target disease processes. Molecular imaging in cardiovascular medicine has made substantial advances recently with an ever-expanding array of biological tracers targeting different processes. Ap-

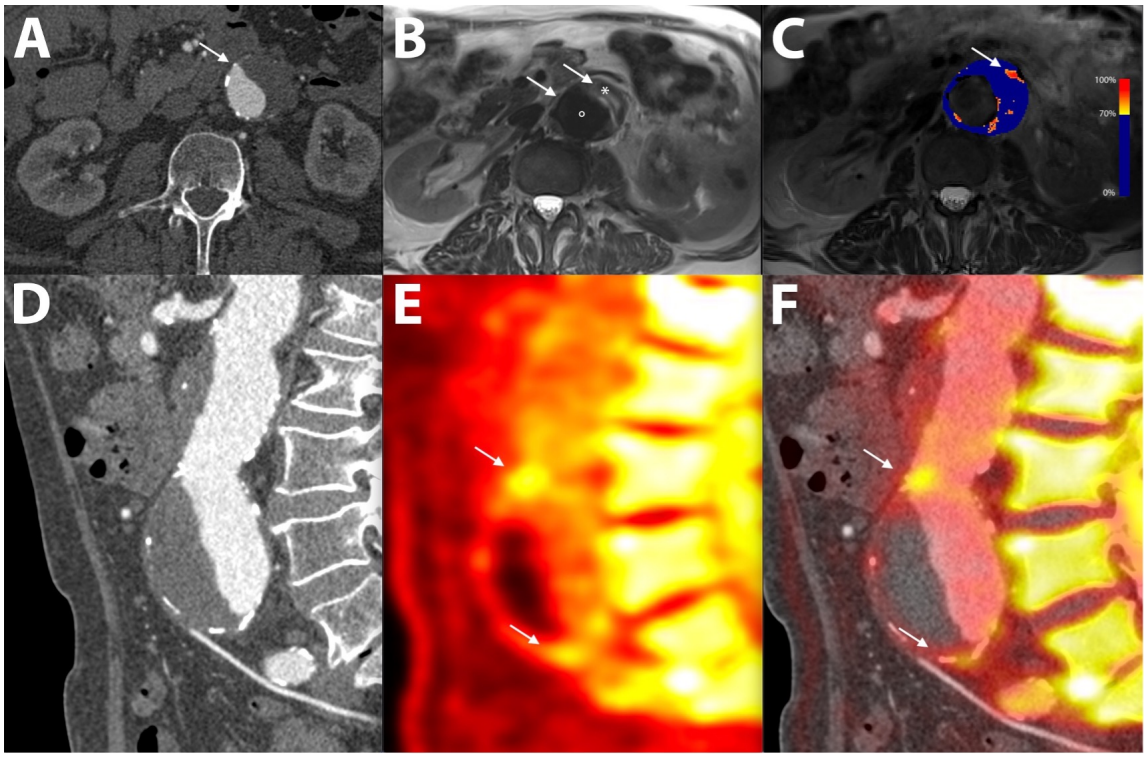

Figure 1.3: **Computed tomography, magnetic resonance imaging and positron emission tomography in a patient with a juxtarenal abdominal aortic aneurysm.** (**A**) Transverse view of the aneurysm as seen on computed tomography shows a dilated aorta with thrombus. (**B**) T2-weighted magnetic resonance imaging of the same aorta differentiates between the lumen (•), thrombus (∗) and adjacent structures. (**C**) A parametric map of the difference in T2* magnetic resonance imaging intensity before and after the administration of ultrasmall particles of iron oxide uptake shows high focal uptake in the anterior wall of the aneurysm (arrow). (**D**) The sagittal computed tomography view delineates the morphology of the aneurysm. (**E**) ^{18}F-Sodium fluoride PET shows uptake within the anterior aortic wall (arrows) detects areas of greatest vascular injury. (**F**) Superimposing positron emission tomography over the computed tomography confirms high ^{18}F-sodium Fluoride uptake at the aneurysm neck and near the bifurcation (arrows).

proaches to standardise quantification of radiotracer uptake has improved the reporting and reproducibility of results (Gholami et al. 2015).

1.5.1 Glucose and glycolysis

^{18}F-Fluorodeoxyglucose (^{18}F-FDG) is a glucose analogue. It is the most frequently used biological tracer in clinical practice. ^{18}F-FDG is taken up by metabolically active cells and its immediate metabolite is trapped within the cell following phosphorylation. This allows the quantification of cellular glycolytic activity. In vascular inflammation, uptake of ^{18}F-FDG is pronounced in smooth muscle cells, endothelial cells and macrophages (Folco et al. 2011). Because ^{18}F-FDG reflects global metabolic activity, its binding is non-specific and overlaps between diseased and healthy arterial tissues.

Up to 1-in-3 patients with acute aortic syndrome exhibit glycolytic activity within the aortic wall that is associated with detectable plasma c-reactive protein (CRP) and D-dimer (Kuehl et al. 2008). Interestingly, patients with acute aortic syndrome have increased ^{18}F-FDG binding compared to patients with chronic disease at the dissection flap and entry tear (Reeps et al. (2010)). This may represent the acute phase injury response of the vessel wall following acute aortic syndrome. A follow-up study by Gorla et al. (2015) reported 3-year outcomes in 60 patients with acute aortic syndrome. Again, the group found increased ^{18}F-FDG binding in over a third of patients with acute aortic syndrome, and again, radiotracer binding was associated with CRP and D-dimer concentrations.

Acute aortic syndrome is a rare condition and delivering research PET-imaging in this vulnerable patient cohort is challenging. Thus, PET/CT imaging studies in patients with acute aortic syndrome have recruited a heterogenous group of patients. Studies with well-characterised disease groups have recruited small samples. Within these limits, there is now encouraging data to suggest that ^{18}F-FDG PET/CT detects increased aortic glycolytic activity within the aortic wall of patients with acute aortic syndrome. Further studies are now required to better characterise ^{18}F-FDG PET/CT within defined patient cohorts and corrected for duration since initial presentation.

^{18}F-FDG PET/CT has been used more extensively to detect metabolic activity in vasculitic

diseases which exert a much more aggressive form of vascular inflammation affecting both the intima and media. Marked vessel wall hypertrophy causes arterial stenosis and can progress to complete occlusion. Morphological imaging is the basis of diagnosing vascular complications in aortitis and CT is highly sensitive in detecting diseased vessels in patients with large vessel vasculitis (Yamada et al. 1998). However, per-segment analysis of large vessels misses up to 40% of individual lesions (de Boysson et al. 2017). ^{18}F-FDG PET/CT improves the detection of aortitis beyond CT alone by detecting inflamed sections that look normal on CT. ^{18}F-FDG PET is also influenced by glucocorticoid and immunosuppressant therapy, which can be used to monitor the efficacy of treatment. However, this is a double-edged sword because late ^{18}F-FDG PET scans may miss vessel involvement if therapy has started (Versari et al. 2018).

The true sensitivity of ^{18}F-FDG PET in vasculitis is unknown. Longitudinal studies report that nearly half of vasculitis patients with biopsy proven disease do not exhibit significant ^{18}F-FDG uptake and this proportion reduces further with time (de Boysson et al. 2016). Although ^{18}F-FDG PET/CT may help detect inflammatory aortic disease, it is not robust enough to be used in isolation. Indeed, biopsy remains the gold standard for diagnosing large vessel vasculitis.

1.5.2 Microcalcification

Detecting microcalcification requires a different approach from established calcified plaque because CT does not have sufficient resolution to visualise the tiny calcium-containing crystals deposited within the arterial wall. ^{18}F-Sodium fluoride (also known as ^{18}F-fluoride or ^{18}F-NaF) is a promising radiotracer that binds to hydroxyapatite crystals deposited during microcalcification (Joshi et al. 2014). Due to surface area effects, it preferentially binds to areas of developing microcalcification, which is beyond the resolution of computed tomography (Vesey et al. 2017; Dweck et al. 2016).

In the vascular system, ^{18}F-sodium fluoride binds to microcalcification with great affinity (Marc R. Dweck, Chow, et al. 2012; Marc R. Dweck, Joshi, et al. 2012). This is true in nearly all metabolic processes that lead to vessel calcification, including atherosclerosis and medial degeneration (Marc R. Dweck, Chow, et al. 2012; Marc R. Dweck, Joshi, et al.

2012). Both are mediated by inflammation.

The Sodium Fluoride in Abdominal Aortic Aneurysm (SoFIA3) study investigated the role of ^{18}F-sodium fluoride in 72 patients with abdominal aortic aneurysms (Forsythe et al. 2018). It showed that aneurysmal aorta exhibit markedly increased ^{18}F-sodium fluoride uptake compared to non-diseased segments. Comparisons of ^{18}F-sodium fluoride binding between dilated and normal calibre aortae revealed increased tracer uptake in aneurysmal segments (Figure 1.3E-F).

Vessel wall calcification is universal in many aortopathies including aortic dissections and connective tissue disorders. The role of ^{18}F-sodium fluoride PET in these diseased states remains of great interest in vascular imaging.

1.5.3 Cellular Proliferation

^{18}F-Fluorothymidine becomes trapped within cells that are in the S-phase of their cell cycle (MacAskill et al. 2017). This phase is typically characterised by DNA replication prior to cell division. ^{18}F-FLT is retained within the cell following phosphorylation by thymidine-kinase-1 (TK-1) but is not incorporated within the DNA. This makes ^{18}F-FLT an ideal radiotracer to detect cellular proliferation – a property already exploited in oncology (Bertagna, Biasiotto, and Giubbini 2013).

In a pre-clinical apolipoprotein-E knockout (ApoE-/-) mouse-model of abdominal aortic aneurysm disease, ^{18}F-FLT PET/CT correlated with histological markers of cellular proliferation and aortic diameter at 14- and 28-day time points (SUV$_{max}$ control 0.007 ± 0.002 versus. 14-day 0.31±0.03 versus. 28-day 0.20±0.05, p<0.001). Within groups, Gandhi et al. (2019) found that the ^{18}F-FLT signal intensity peaks early in the disease cycle at 14-days (p<0.001) and co-localised to hypertrophied segments of the diseased aortic wall.

Gandhi et al. (2019) found that cellular proliferation is indeed elevated within the aorta of Angiotensin II-infused Apolipoprotein E-/- mice and that ^{18}F-FLT can non-invasively quantify this process. Moreover, the timing of ^{18}F-FLT uptake closely mirrored histological and proteomic analysis of aneurysmal tissue, with cellular proliferation appearing to be higher in the early stages of aneurysm development before later tailing off. This study therefore

provided novel insight into the cellular mechanisms observed in maturing aneurysmal tissue and demonstrated ^{18}F-FLT PET as a useful technique to detect these cellular changes.

1.5.4 Emerging radiotracers

There are several emerging radiotracers that visualise inflammatory activity by directly targeting cellular components of inflammation. Some of these are in the pre-clinical stage and have shown promise in directly detecting vascular inflammation (Table 1.1). These have been used predominantly to characterise atherosclerotic plaque.

Tracers that target macrophages directly, such as the somatostatin subtype 2 (SST2) receptor analogues, overcome the limitations caused by the poor specificity of ^{18}F-FDG. Here, the combination of a somatostatin ligand with a DOTA- (1,4,7,10-Tetraazacyclododecane-1,4,7,10-tetraacetic acid) or NOTA- (1,4,7-Tricarboxymethyl-1,4,7-Triazacyclononane) based “cage” has resulted in the development of various tracers. The cage houses a positron-emitting isotope, such as Gallium-68 (^{68}Ga) or Copper-64 (^{64}Cu). PET studies reveal that these agents exhibit preferential vascular uptake in patients with established cardiovascular risk factors and adverse Framingham risk scores (Malmberg et al. 2015). Histological comparison of carotid plaque with high ^{68}Ga-DOTA-TATE (1,4,7,10-Tetraazacyclododecane-N,N’,N“,N”’-Tetra-acetic acid]-D-Phe1, Tyr3-octreotate) uptake reveals selective binding of the radiotracer to CD68-positive macrophage-rich lesions. In a pilot study, ^{68}Ga-DOTA-TATE correctly identified metabolically active coronary and carotid lesions with good reproducibility and higher sensitivity than ^{18}F-FDG (Tarkin et al. 2017).

Targeting agent	Target	Imaging modality	Stage of development in aortic diseases
^{18}F-Fluorodeoxyglucose (^{18}F-FDG)	Glycolysis	PET	In clinical use
^{18}F-Sodium fluoride (^{18}F-NaF)	Microcalcification	PET	Clinical research
^{18}F-Fluorothymidine (^{18}F-FLT)	Cellular proliferation	PET	Pre-clinical research
Ultrasmall paramagnetic particles of iron oxide (USPIO)	Macrophages	MRI	Clinical research
^{18}F-DOTATATE	Macrophages	PET	Clinical research
Vascular cell adhesion molecule-1 (VCAM-1)	Macrophages	PET	Pre-clinical research
^{11}C-Choline	Macrophages	PET	Pre-clinical research
^{11}C-PK11195	Macrophages	PET	Pre-clinical research
^{18}F-Fluoromisonidazole (^{18}F-MISO)	Hypoxia	PET	None
^{18}F-Fluciclatide	Angiogenesis	PET	Clinical Research
^{18}F-Galacto-RGD	Angiogenesis	PET	Pre-clinical research
$\alpha_v\beta_3$ targeted paramagnetic particles	Angiogenesis	MRI	Pre-clinical research

Table 1.1: **Emerging radiotracers, their targets and stage of research development.**

Activated inflammatory cells within atherosclerotic plaque exhibit CXCR-4 receptors. Novel PET radiotracers, such as ^{68}Ga-Pentaxifor, can be used to target these receptors (Weiberg et al. 2018). In the coronary arteries, ^{68}Ga-Pentaxifor is high in culprit vessels following acute myocardial infarction (median SUVmax 1.96, IQR 1.55 – 2.31). These lesions also have high concentrations of CD68+ macrophages (Derlin et al. 2018).

^{18}F-Fluoromisonidazole (^{18}F-MISO) is a biological tracer that concentrates in hypoxic viable cells due to an accumulation of its metabolites in an oxygen-deprived environment. Animal models show ^{18}F-MISO correlates well with aortic atherosclerosis and areas of FDG uptake (Mateo et al. 2014). Exploratory human studies suggest that ^{18}F-MISO PET/CT corresponds to areas of vessel hypoxia, increased macrophage density and ^{18}F-FDG uptake in symptomatic carotid artery disease (Takasawa et al. 2007; Hong et al. 2011).

Angiogenic endothelial cells and hypoxic macrophages in atherosclerotic plaque express $\alpha_v\beta_3$ integrin cell surface glycoproteins. In animal models, $\alpha_v\beta_3$ targeted imaging with MRI sensitive paramagnetic particles identify areas of angiogenic proliferation (Winter et

al. 2003). ^{18}F-Fluciclatide is a novel $\alpha_v\beta_3$ -specific PET radiotracer that colocalises to areas of inflammation and angiogenesis (Jenkins et al. 2019). In a clinical cohort, ^{18}F-fluciclatide uptake was increased in patients with symptomatic coronary artery disease and was associated with coronary calcification score, total plaque volume and vessel wall thickness. A novel PET tracer, ^{18}F-Galacto-RGD, can also target $\alpha_v\beta_3$ integrin (Haubner et al. 2004) and in mice models of atherosclerosis, binds to sites of new atherosclerotic plaque. However, histological analysis in these mice models showed that uptake co-localised in macrophage-rich atherosclerotic plaque, as opposed to angiogenesis specifically (Laitinen et al. 2009). Culprit carotid plaques demonstrate increased ^{18}F-Galacto-RGD uptake on pre-operative PET/CT and post-operative autoradiography analysis. In a small sample of patients, ^{18}F-Galacto-RGD binding showed a tendency to bind to plaque rich in macrophages and those with increased vasa vasorum density (Beer et al. 2014).

1.6 Circulating biomarkers in Acute Aortic Syndrome

Circulating biomarkers offer a minimally invasive, yet powerful, way to detect disease. Acute aortic syndrome is a profound aortic injury associated with generalised inflammation, cytokine release, activation of thrombotic cascades, release of markers of aortic degeneration and the expression of circulating genetic material. It is possible to detect these disease processes in the blood of patients with acute aortic syndrome. Circulating biomarkers offer a global measure of metabolic activity within the body that is not necessarily distinct to a single target organ.

1.6.1 Clotting factors

Sudden disruption of the aortic wall leads to a widespread activation of prothrombotic and fibrinolytic pathways. D-dimer is a fibrin degradation product released in to the blood stream as a byproduct of fibrinolysis. D-dimer is used routinely for the diagnosis of prothrombotic conditions such as deep venous thrombosis, pulmonary embolus and disseminated intravascular coagulopathy. It was first described as a potential circulating biomarker in 2014 to diagnose acute aortic syndrome when all 16 patients in the study

were found to have increased concentrations of D-dimer comparable to pulmonary embolus (Eggebrecht et al. 2004). D-dimer has a reported sensitivity of 98% to detect acute aortic syndrome (Yang et al. 2020) and thus performs well as a rule-out test when levels are not raised. The magnitude of rise in D-dimer concentration appears proportional to the extent of false lumen thrombosis in contact with the circulation (Itagaki et al. 2018). A low D-dimer was found in patients with small localised tears in the aorta or when the false lumen was completely thrombosed at presentation (Itagaki et al. 2018).

Markers of fibrinolysis are associated with aortic expansion in patients with acute aortic syndrome (Sakalihasan et al. 2015a). Patients with aneurysmal progression were found to have increased D-dimer compared to those without aneurysmal progression in a prospective cohort study of patients with acute aortic syndrome. Other markers of fibrinolysis, such as plasmin-alpha2 antiplasmin (PAP) complexes were also raised in the aneurysm growth cohort. Interestingly, patients with aneurysmal expansion also had elevated markers of thrombosis such as thrombin-antithrombin (TAT) complexes and platelet-related P-selectin (Sakalihasan et al. 2015a). Concominant activation of the fibrinolytic and thrombotic pathways in patients with progressive disease is indicative of the dynamic nature of acute aortic syndrome. It is unclear if these coagulation pathways modulate disease progression. It is more likely that elevated coagulation factors are a by-product of rapidly evolving aortic morphology and consequent thrombosis from altered haemodynamic states.

1.6.2 Inflammatory markers

Acute aortic syndrome leads to a surge of inflammatory activity in multiple ways. First, medial degeneration itself may be driven by an inflammatory-mediated response leading to cystic medial necrosis, upregulation of matrix metalloproteinases, dysregulation of cellular architecture and upregulation of interleukins (Guo et al. 2020). Next, sudden tearing of the aorta may mount an inflammatory reparative response. Third, impaired perfusion to end-organs may cause ischaemia that can progress rapidly to a systemic inflammtory response. Finally, operative intervention leads to a second pro-inflammatory insult following the initial aortic event.

C-reactive protein (CRP) is a sensitive acute-phase response protein released in the circulation by the liver in response to macrophage and T-lymphocyte exposure to interleukin-6. CRP is thus highly sensitive to any pro-inflammatory reaction. Patients with acute aortic syndrome have elevated circulating CRP concentrations but these are modest (median CRP 13mg/L) and the prognostic ability of this circulating biomarker is limited by its poor specificity (Vrsalovic and Vrsalovic 2019; Hsieh et al. 2019).

The monocyte response following acute aortic syndrome appears to be independent of conventional inflammatory and genetic mediators. Lu et al. (2020) characterised the expression of CD14+ monocytes and blood mononuclear cells in patients with acute aortic syndrome. The monocyte response was independent of CRP and D-dimer. In a more detailed analysis, monocytes obtained from acute aortic syndrome patients had decreased expression of aortopathy-related genes such as TIMP1, TIMP2, transforming growth factor beta-1, SMAD3, and ACTA2 ($p<0.05$ for all, Lu et al. (2020)). The monocyte response, thus appears to be reactive to the aortic insult as opposed to being driven by underlying genetic mediators. Interestingly, patients that mount an aggressive biochemical inflammatory response, characterised by a high C-reactive protein or monocyte count, are more likely to experience aorta-related mortality in the hyperacute and acute phase of the disease (Erdolu and As 2020; Ma et al. 2020). A combination of monocyte-to-lymphocyte ratio, neutrophil-to-lymphocyte ratio and platelet count may have a small incremental role to predict 30-day mortality in patients with acute aortic syndrome (ROC 0.74, $p=0.021$) (Yiping Chen et al. 2020).

There has been intense interest in the role of interleukins on mediating aortopathy owing to their involvement in numerous inflammatory pathways. Over 50 have been described. Interleukin-6 is an acute phase reactant that facilitates B-cell differentiation. Patients with acute aortic syndrome have increased circulating interleukin-6 compared to healthy controls which peaks around day 2 and remains elevated for up to 30 days (S.-M. Yuan 2019). Similarly, interleukin-3 (Xu et al. 2018) and interleukin-11 (Liu et al. 2018) have increased expression in patients with acute aortic syndrome. These interleukins interact with lymphocytes, monocytes and plasma cells and are associated with matrix metalloproteinase expression. Interleukins thus have a strong theoretical basis for influencing aortic wall bi-

ology. Clinical studies, however, have failed to demonstrate a clear relationship between circulating interleukins and clinical outcomes in patients with acute aortic syndrome.

1.6.3 Elastin

Mature elastin forms in a circumferential orientation when insoluble tropoelastin is oxidised and cross-linked by desmosine on a fibrillin mesh (Karimi and Milewicz 2016). This mature elastin network is insoluble and provides the characteristic physiological properties necessary to maintain aortic morphology and function. Elastin has a long half-life and is rarely replenished once deposited in the aorta during embryological development (Duca et al. 2016). Thus, degradation of aortic elastin results in thinning of the medial layer and dysregulation of the otherwise tightly arranged components that conform structural stability.

1.6.3.1 Tropoelastin

Tropoelastin is a 60 to 72 kDa soluble monomer and a precursor to elastin formation. Tropoelastin is transported to the aortic media where it undergoes oxidation by the lysyl oxidase pathway and ultimately cross-linked into mature elastin during late foetal life. Thus, the healthy aorta contains an abundance of mature elastin but very little tropoelastin. Degeneration of the extracellular matrix leads to vascular smooth muscle cell phenotype change into a secretory state to produce tropoelastin. However, dysregulation of the extracellular matrix inhibits tropoelastin cross-linking due to down-regulation of the lysyl oxidase pathway. Accumulated tropoelastin within the cell wall drive inflammatory cell infiltration and over-expression of matrix metalloproteinases which drive further degeneration of the extracellular matrix. Tropoelastin has thus been hypothesised to be a promising marker for detecting elastin degeneration (Phinikaridou et al. 2018).

It is now possible to image tropoelastin directly. The elastin-specific MRI contrast agent (ESMA) uses a low molecular weight gadolinium chelate which binds to intra-arterial tropoelastin deposition (Phinikaridou et al. 2019). Mouse models of abdominal aortic aneurysms have used ESMA-MRI to demonstrate an accumulation of tropoelastin within the aortic wall on serial imaging following an infusion of angiotensin-II (Botnar et al. n.d.).

More recently, Gadolinium-ESMA enhanced MRI has characterised the accumulation of tropoelastin in relation to aortic diameter, again in animal models (Lavin et al. 2020).

Interestingly, human studies on aortic tissue obtained from 95 patients with acute aortic syndrome have pinpointed a single nucleotide polymorphism in the expression of tropoelastin messenger RNA which resulted in downregulation of both, elastin and tropoelastin (Qi et al. 2021). This highlights the inherent challenge in studying tropoelastin as a marker of elastin turnover in aortopathy. Patients that experience acute aortic syndrome may have reduced congenital cellular elastin content which is not replaced in the face of medial degeneration and hence do not produce tropoelastin as a reparative process. This may be a critical difference with animal models where aortic dilation is induced since these animals retain the genetic function to build new elastin reserves.

1.6.3.2 Desmosine

In contrast to tropoelastin, desmosine is a cross-linking molecule that is specific to mature elastin. Thus, its detection in the plasma is a more direct marker of mature elastin degradation rather than elastin turnover. Patients with aortopathy have reduced elastin content within the vessel wall associated with disease severity. Patients with abdominal aortic aneurysms were found to have increased plasma desmosine concentrations compared to healthy controls. Plasma desmosine concentration was associated with aortic size and predicted diseases progression (Mordi et al. 2019).

It is possible that patients with acute aortic syndrome, a condition characterised by reduced aortic elastin content, may also shed desmosine within the circulation. Desmosine thus may act as a marker of medial degeneration. Circulating desmosine in patients with acute aortic syndrome has never been investigated before. This novel biomarker of mature elastin degradation may play a role in detecting disease and improving risk stratification.

1.6.4 Micro Ribose Nucleic Acids

Micro-ribose nucleic acids (miRNA) are short non-coding fragments of RNA that modulate post-transcription gene function. miRNA are a relatively new discovery. The last two

decades has seen the identification of over two thousand miRNA and this number is growing. miRNA represent an interesting novel class of genetic modulators that may influence aortic wall composition and biology.

Individual miRNA likely interact with multiple genetic targets exerting their effect on numerous pathological processes. The composition of these miRNA are easily characterised and are typically around 22 base pairs long. It is thus possible to predict potential genetic-miRNA targets using computational algorithms (Yuhao Chen and Wang 2020). This information has been made available in open-source registries to facilitate novel research.

Thoracic aortopathy occurs in a range of clinical conditions, including Marfan syndrome, Loeys-Dietz syndrome, Vascular Ehlers-Danlos syndrome, osteogenesis imperfecta, bicuspid aortic valve disease and non-heritable thoracic aortic disease amongst more (Fletcher et al. 2020). Up to 22 individual genes have been implicated in the pathogenesis of these conditions, the most well characterised of which are the FBN1, SMAD and transforming growth factor-related genes. Identifying miRNA interactions with each of these genes is a complex task resulting in an overwhelming number of potential miRNA-genetic interactions.

Wang et al. (2015) tested a comprehensive panel of miRNA expression in patients with acute aortic syndrome. They identified 93 circulating miRNA that were either up- or down-regulated in this cohort. Similarly, Dong et al. (2017) compared circulating miRNA expression in 103 patients with aortic dissection to healthy controls and found two candidate miRNA that were associated with the presence of aortopathy. Both groups, however, focused on diagnosing acute aortic syndrome and did not correlate these findings with clinical state or aortic morphology. There was also poor overlap between the miRNA identified by each group as being potentially relevant in acute aortic syndrome patients. It is possible that expression of a select few miRNAs is associated with disease severity or longitudinal clinical outcomes.

Finding an overlap between miRNA that interact with known genetic defects and those demonstrated to have altered expression in acute aortic syndrome may enable researchers to short list candidate miRNA that play a central role in disease progression.

Known miRNA such as the hsa-let-7* and hsa-miR-30* families are known to interact with a broad range of genetic targets (Liao et al. 2011; Bridge et al. 2012). These include critical cellular functions related to the embryological development of the aortic media, angiogenesis, the transforming growth factor-beta pathway and lysyl oxidase function.

Interestingly, Qi et al. (2018) have identified a potential interaction of hsa-miR-144-3p with post transcription tropoelastin function in patients with aortic dissection. The group demonstrated that hsa-miR-144-3p binds to tropoelastin messenger RNA at the 3'-UTR site and thus inhibits protein translation of tropoelastin. This relationship was prominent in aortic tissue retrieved from patients with acute aortic syndrome which demonstrated that increased hsa-miR-144-3p in vascular smooth muscle cells was associated with inhibition of tropoelastin formation. Thus, miRNA may play an important regulatory role on the stability of the aorta media through their influence on gene function and protein translation within the medial layer.

1.7 Risk stratification

Involvement of the aortic root and ascending aorta is the most powerful predictor of adverse outcomes in acute aortic syndrome. Both, the DeBakey and Stanford Classification systems categorise patients based on anatomical location of the entry tear and are the clinical standard to plan therapy. The Stanford classification system divides patients with ascending aorta or proximal aortic arch involvement as Type A. Disease that affects the aorta distal to the origin of the left subclavian artery are categorised as Type B.

Patients with Stanford type A aortic dissection are at high risk of myocardial or cerebral ischaemia. They may also experience a retrograde extension to the aortic root manifesting as a cardiac tamponade. Consequently, patients with proximal aortic involvement in acute aortic syndrome are strongly considered for immediate surgical repair. In contrast, patients with uncomplicated Stanford type B disease may be treated conservatively with antihypertensive therapy alone. Rapid aortic expansion, impending aortic rupture and visceral ischaemia are markers of life-threatening complications. Clinical signs such as persistent hypertension and uncontrolled pain are further indicators of adverse outcomes.

These features of complicated type B aortic dissection are indication to offer surgical intervention.

Disease progression in uncomplicated Stanford type B disease is unpredicatable. Complications occur rapidly and at any stage of the disease process, sometimes many years following the initial aortic event. Patients thus undergo frequent surveillance cross-sectional imaging to study aortic morphology. This may be lifelong. Morphological features such as aortic size, false lumen morphology, involvement of the visceral arteries and false lumen thrombotic patterns are associated with poor clinical outcomes (G. Wang et al. 2021). Morphological change, however, is a late manifestation of aortic disease. Changes in aortic shape also adds complexity to surgical intervention.

The emergence of minimally invasive endovascular therapy provides a lower-risk alternative to open surgical repair for early intervention in patients with acute aortic syndrome (Chavan, Eldergash, and Thomas 2020; Xie et al. 2021). Thoracic endovascular aneurysm repair (TEVAR) involves placing a covered stent under fluoroscopic guidance across the site of intimal disruption (Liu et al. 2020; Pruitt et al. 2020). It is unclear whether prophylactically treating all patients with uncomplicated type B aortic dissection with endovascular therapy reduces long-term mortality. Modest-sized randomised controlled trials have not shown a clear benefit for this strategy (Brunkwall et al. 2014; Kamman et al. 2017; Nienaber et al. 2005). Longer term follow-up from these trials, however, now suggests that acute aortic syndrome patients may benefit from TEVAR over a 5-year period (Nienaber et al. 2013).

There is an imperative to identify the vulnerable aorta in patients with acute aortic syndrome. This may enable targeted therapy to patients at greatest risk to developing complications.

1.7.1 Morphological Features

1.7.1.1 Aortic Diameter

Aortic diameter is the clinical standard for risk stratification in expansive aortopathies. However, this unidimensional metric fails to capture the complex morphological changes

and biological activity affecting the aortic wall. In other aortopathies, such as aneurysms, aortic diameter is used as a threshold to trigger intervention. The role of aortic diameter in acute aortic syndrome is less clear. Aortic expansion is generally considered a marker of poor ouctomes.

G. Wang et al. (2021) characterised clinical and aortic morphological features associated with complicated acute aortic dissection at presentation from a large international registry over a 9 year period. This is the largest reported morphological dataset on patients with acute aortic syndrome consisting of 2820 patients. Interestingly, patients with complicated acute aortic syndrome were younger (55.8 versus 61.2 years), more likely to be male (79.7% versus 68.1%) and had a smaller total aortic diameter (4.0cm versus 4.9cm). Patients with uncomplicated disease were also more likely to have comorobidites such as coronary artery disease and chronic obstructive pulmonary disease. This is somewhat counter-intuitive. Aortic diameter at presentation was a poor discriminator of complications in patients presenting with complications.

The natural history of acute aortic syndrome consists of steady aortic expansion (S.-J. Lee et al. 2020), particularly in patients treated with best medical therapy alone (Brunkwall et al. 2014; van Bogerijen et al. 2014), those with connective tissue disorders (Donadille et al. 2020; Suzuki, Asai, and Kinoshita 2018) or the persistence of flow in the false lumen. A descending thoracic aorta threshold diameter of 4cm is reported as an adverse predictor of continued aortic expansion (Hysa et al. 2021; G. Wang et al. 2021; Oishi et al. 2020; van Bogerijen et al. 2014), although the positive predictive power of this metric is yet to be determined. Aortic expansion in the acute phase is rapid. Hence, the change in aortic diameter with respect to time may be a more relevant marker of aortic vulnerability. False lumen expansion within the first 14 days is associated with an increased likelihood of developing complications (Van Maele et al. 2021). Similarly, the extent of aortic involvement and the size of entry tear were associated with an increased likelihood of necessitating surgical intervention. This endpoint may be biased, however, because the variables being investigated are also triggers for surgical intervention. Interestingly, an entry tear on the inner surface of the aortic arch, persistence of the false lumen outflow, greater distal extension of the dissection flap and false lumen diameter were all associated with aortic

expansion (Van Maele et al. 2021).

1.7.1.2 False lumen morphology

The false lumen is prone to aneurysmal expansion. Song et al. (2007) found that a 22mm threshold of false lumen diameter is associated with false lumen expansion and adverse events (n=100, c-statistic 0.77 (95% CI 0.65-0.90)). This was later confirmed in a second study by Ueki et al. (2014). The true lumen-to-false lumen ratio has emerged as a potential metric for disease progression. Compression of the true lumen is associated with aortic events but not mortality (Evangelista et al. 2012; Tolenaar et al. 2013). Lavingia et al. (2015) performed a robust analysis of aortic morphology measurements and found that a true lumen to false lumen ratio of 0.8 or less was predictive of requiring aortic intervention whereas a ratio greater than 1.6 appeared to be protective. Finally, a circumferential morphology of the dissection flap was associated with a reduced aortic expansion (Kamman et al. 2017).

False lumen thrombosis affects haemodynamic flow within the aortic wall and may be associated with adverse clinical events. In a coagulation cascade simulation model, a high volume of fibrin was found to accumulate at the entry tear (Y. Wang et al. 2021) suggesting that there is a natural predisposition for thrombus formation at this site. Thrombosis of the false lumen may occur naturally or intentionally induced by endovascular therapy. The false lumen is prone to aneurysmal dilatation following aortic dissection. Excluding flow in the false lumen may therefore reduce aortic expansion and major adverse aortic events. Complete thromobosis of the false lumen is thus considered a favourable morphological marker of aortic remodelling. Thrombus in the false lumen is highly heterogenous and studies are thus inconsistent in their categorisation of thrombus groups (Spinelli et al. 2018). Parker et al. (2021) performed detailed haemodynamic simulations in patients with acute aortic syndrome stratified by well characterised false lumen thrombus states. Patients were categorised in to four groups: those with no thrombosis, proximal thrombosis, distal thrombosis and complete thrombosis. Interestingly, the presence of proximal thrombosis was associated with reduced pressure within the false lumen. This reduced false lumen perfusion pressure was also associated with reduced major adverse aortic

events. It is uncertain whether proximal thrombosis drives a reduction in fals elumen pressure or is simply a byproduct of reduced false lumen perfusion (Parker et al. 2021).

Miletic et al. (2021) present a case series of 51 patients intentionally undergoing false lumen embolisation using prosthetic plugs or coils to precipitate thrombosis of the false lumen following endovascular therapy. Increasing the thrombus burden of the false lumen was associated with a marginal decrease in total aortic diameter (64 mm to 61 mm), regression of the false lumen (37 mm to 26 mm) and corresponding expansion of the true lumen (25mm to 34mm). This is in line with secondary findings from the major clinical trials on endovascular therapy in acute aortic syndrome (Nienaber et al. 2010; Brunkwall et al. 2014). Thrombosis of the false lumen following endovascular therapy is associated with favourable aortic remodelling. However, aortic remodelling does not translate in to reduced all-cause mortality (Nienaber et al. 2005; Brunkwall et al. 2014; Qiu et al. 2020).

1.7.1.3 Visceral Artery Involvement

Patients with acute aortic syndrome affecting the proximal aorta or multiple aortic zones were more likely to experience ischaemic symptoms. These patients were also more likely to have visceral branch involvement necessitating mesenteric intervention (G. Wang et al. 2021). Patients with malperfusion were more likely to have increased serum creatinine at presentation and later go on to develop acute kidney injury. These patients were also likely to suffer spinal cord ischaemia - a devastating and disabling complication. However, despite the significant disparity in morphological features between patients with and without end-organ ischaemia, there was no difference in long-term survival between malperfusion and uncomplicated groups. In their case series of 44 patients, Lu et al. (2021) found that involvement of the superior mesenteric artery in the dissection process is associated with mesenteric malperfusion in nearly three quarters of affected patients. Patients with predominantly false lumen perfusion of the superior mesenteric artery (true lumen-to-false lumen ratio < 1) were more likely to encounter mesenteric ischaemia. Interestingly, this cohort was also more likely to present with lower limb ischaemic symptoms. Following TEVAR, thrombosis of the superior mesenteric artery true lumen was a signficant predictor of requiring mesenteric intervention.

1.7.1.4 Presence of Intramural Haematoma

The presence of an intramural haematoma may signify dyanmic and rapidly evolving disease. Jiang et al. (2021) investigated the presence of intramural haematomas in patients with symptomatic penetrating aortic ulcers undergoing endovascuar thearpy. In a cohort of 138 patients, the investigators found that intramural haematoma was associated with increased emergency admission rates, larger aortic diameter and increased incidence of peri-procedural entry tear formation. Stenting was associated with favourable clinical outcomes. However, the presence of intramural haematomas did not appear to influence survival. Similarly, Li et al. (2020) found that the presence of penetrating aortic ulcers and increased aortic diameter in patients with intramural haematomas was more likely to result in aorta-related mortality.

1.7.1.5 Isolated abdominal aortic dissections

This is a rare morphological state that behaves distinct from thoracic aortic dissection. Isolated abdominal aortic dissections are a relatively stable morphological state. Of 14 patients identified from a large multicentre database over a 10-year period, only two patients required intervention: one for aneurysmal disease and the other for aortic occlusion (Sen et al. 2021). Morbidity in this cohort was due to cardiac causes rather than aortopathy.

1.7.1.6 Haemodynamic changes

Haemodynamic changes are thought to play a critical role in the development and progression of acute aortic syndrome. Patients with acute aortic syndrome often present with profound hypertension. Again, it is uncertain if hypertension is the trigger of acute aortic syndrome or the response to profound aortic injury. Haemodynamic pressures across the initmal injury are influenced by, first, blood flow throughout the cardiac cycle, and second, the shape of the aorta and underlying thrombus.

Haemodynamic changes in the aorta can be measured in three ways. First, they can be estimated using computational models of blood flow in patient-specific aortic geometries

extracted from aortic imaging. Second, imaging modalities such as 4-dimensional MRI can estimated haemodynamic metrics during the cardiac cycle. Finally, pressures within the true or false lumens can be measured directly by placing a pressure-sensitive catheter within the aorta under fluoroscopic guidance. This final invasive strategy carries considerable risk.

Hsu et al. (2021) report the use of measuring contrast density during conventional computed tomography angiography as a means of estimating aortic flow in the false lumen. The authors studied surveillance imaging of patients that previously had endovascular therapy for type B aortic dissection and found that the presence of contrast half way down the false lumen was associated with increased aortic mortality and persistent aortic expansion. Indeed, false lumen perfusion is thought to be the major contributor towards false lumen expansion. Parker et al. (2021) demonstrated that false lumen perfusion pressure was independently associated with major adverse aortic events. Haemodynamic simulations in the dissected aorta is beyond the scope of clinical practice. Hsu et al. (2021) thus present a simple yet crude technique to estaimte false lumen perfusion.

Enhancement of the aortic wall with contrast during conventional CT angiography may be an imaging marker associated with aortic remodelling. Ito et al. (2020) report findings from 35 patients with uncomplicated Stanford type B aortic dissection. Patients with a 20 Hounsfield unit increase in the aortic wall between non-contrast and delayed phase imaging were considered to have aortic wall enhancement. The authors hypothesized that late-phase arterial wall enhancement was a product of improved arterial perfusion as a result of decreased pressure in the false lumen. In future studies, it would be interesting to compare late wall enhancement with haemodynamic metrics and histological features of the diseased aortic wall.

1.7.2 Molecular imaging

1.7.2.1 ^{18}F-Fluorodeoxyglucose PET/CT

Increased ^{18}F-FDG activity in patients with thoracic aortopathy was first described by Kuehl et al. (2008) who found that radiotracer uptake was associated with all-cause mor-

tality and disease progression. In a case-controlled study, Kato et al. (2010) found that radiotracer uptake in patients that died from acute aortic syndrome was greater than those that survived. The study groups, however, were small and insufficient to correct for confounders such as aortic diameter which was also increased in the mortality group. Reeps et al. (2010) described increased ^{18}F-FDG activity at the site of intimal disruption in acute patients (p=0.02) and concluded that PET imaging may aid in determining acuity of disease.

A longer prospective cohort study by Gorla et al. (2015) found that a combination of D-dimer and ^{18}F-FDG activity predicted a composite endpoint of aortic expansion or readmission to hospital with aortic complications. A more robust analysis found that ^{18}F-FDG, aortic diameter, partial thrombosis of the false lumen, male gender and hypertension were independent predictors of disease progression in a better characterised group of 23 patients with type B aortic dissection (Sakalihasan et al. 2015a). This study had a better characterised cohort of patients with aortic dissection. It was however unclear what phase of disease patients belonged to and whether this confounded the results.

1.7.2.2 ^{18}F-Sodium fluoride PET/CT

^{18}F-Sodium fluoride binds to vascular microcalcification with great affinity (Dweck et al. 2012). This is true in nearly all metabolic processes that lead to vessel calcification, including atherosclerosis and medial degeneration (Dweck et al. 2012). The Sodium Fluoride in Abdominal Aortic Aneurysm (SoFIA$_3$) study explored the role of ^{18}F-sodium fluoride in 72 patients with abdominal aortic aneurysms (Forsythe et al. 2018). It showed that aneurysmal aorta exhibit markedly increased ^{18}F-sodium fluoride uptake compared to non-diseased segments. Comparisons of ^{18}F-sodium fluoride binding between dilated and normal calibre aortae revealed increased tracer uptake in aneurysmal segments (Figure 1.3E-F). This binding pattern was independent of the aortic calcium score and aortic diameter. Histological comparisons of aortic tissue obtained following open aneurysm repair showed that ^{18}F-sodium fluoride binding correlates with microcalcification and aortic degradation in these subjects.

Vessel wall calcification is universal to many aortopathies including aortic dissections and

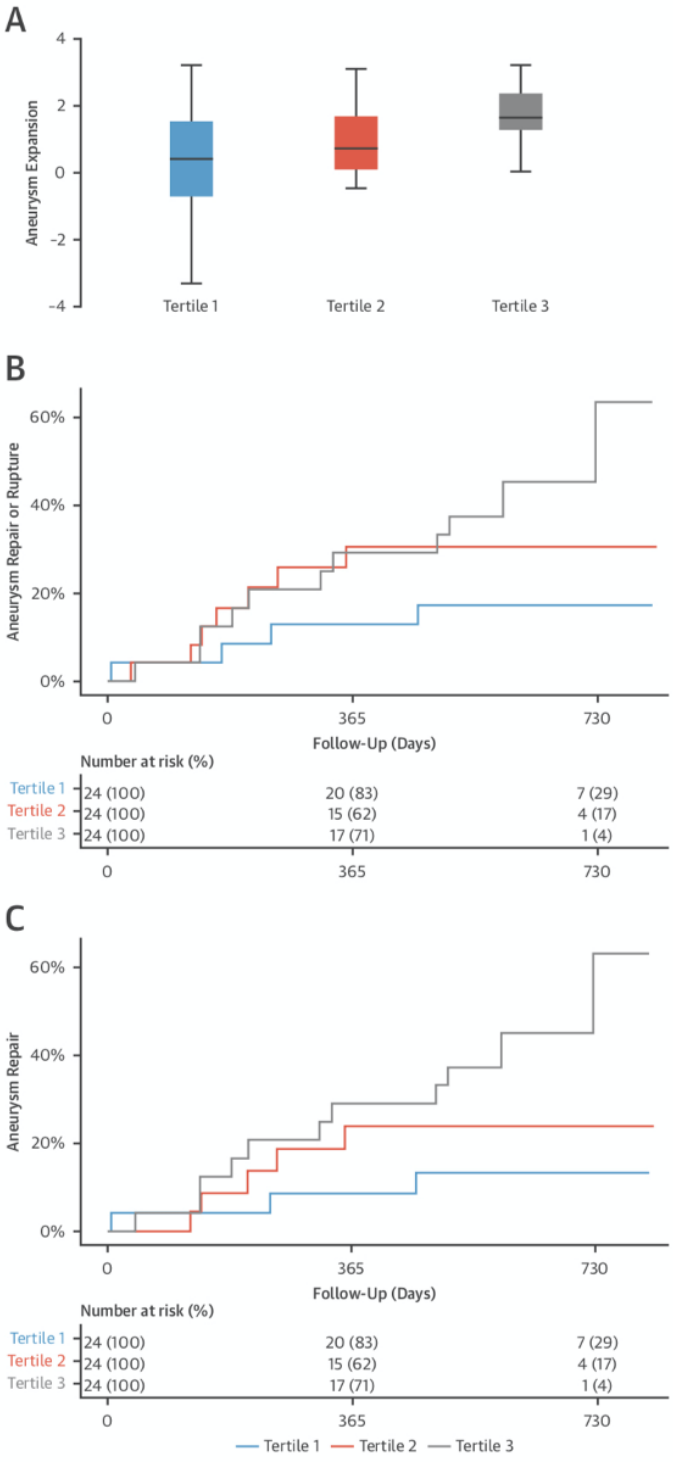

Figure 1.4: **Association of ^{18}F–sodium fluoride (^{18}F-sodium fluoride) uptake with disease progression and clinical outcome.** (**A**) Rate of aneurysm expansion (millimeters per year, $\log_2$ transformed) across the tertiles of ^{18}F-sodium fluoride uptake. The highest tertile expanded more rapidly than those in the lowest tertile (3.10 versus 1.24 mm/year respectively, p=0.008). Cumulative event rate (censored at date of death) across the tertiles of ^{18}F-sodium fluoride uptake for (**B**) abdominal aortic aneurysm repair or rupture (log-rank p=0.043) and (**C**) abdominal aortic aneurysm repair (log-rank p=0.014) (Forsythe et al. 2018).

connective tissue disorders. The role of ^{18}F-sodium fluoride PET in these diseased states remains of great interest in vascular imaging. Indeed, the pathological processes underlying aortic expansion in aortopathies share common pathways involving medial degeneration (Figure 1.5). Preliminary data suggests focal uptake of ^{18}F-sodium fluoride within the aortic wall following aortic dissections (Figure 1.6). Like abdominal aortic aneurysms, ^{18}F-sodium fluoride PET/CT may predict disease progression in these aortopathies as well.

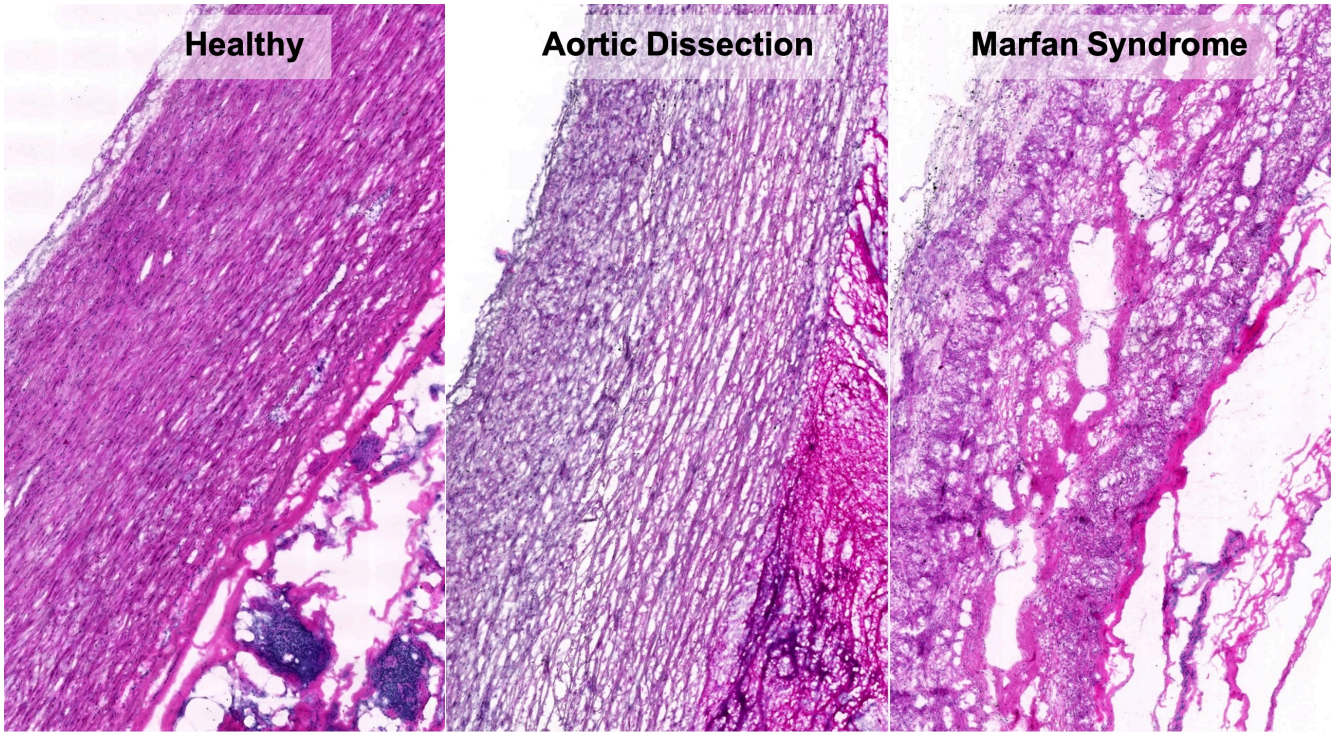

Figure 1.5: **Haematoxylin and eosin staining of aortic wall in acute aortic syndrome.** A healthy individual (**left**), a patient with aortic dissection (**middle**) and a patient with Marfan Syndrome (**right**). Compared to controls, patients with aortic dissection have reduced medial cellular density. Patients with Marfan Syndrome, who are at extremely high risk of acute aortic syndrome, have complete disruption of the medial architecture and marked reduction in cellular density.

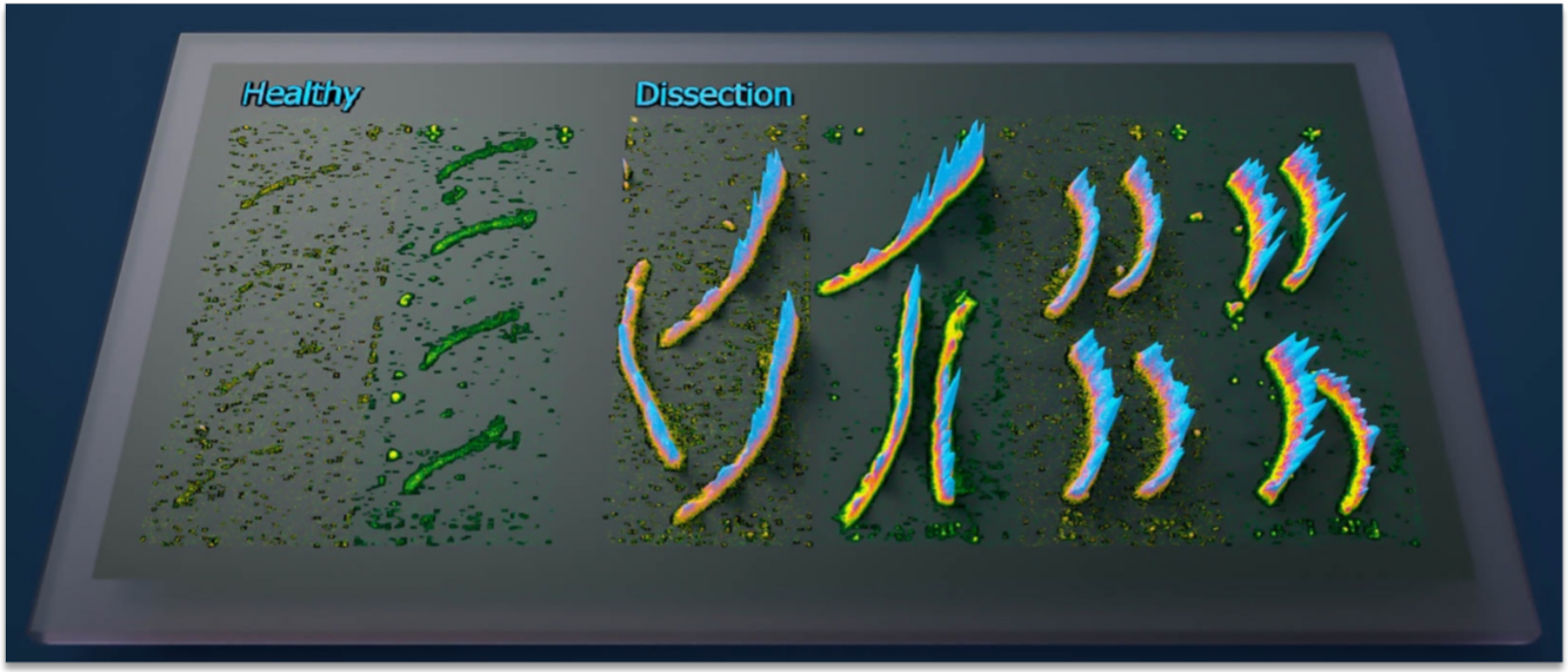

Figure 1.6: **Pre-clinical comparison of aortic ^{18}F-sodium fluoride binding in controls and patients with aortic dissection from cadaveric specimens.** A three-dimensional displacement map visualises the intensity of ^{18}F-sodium fluoride binding.

1.8 Aims of this thesis

The primary objective of this PhD thesis is to characterise the role of a novel multimodality imaging technique, ^{18}F-sodium fluoride PET/CT in patients with acute aortic syndrome and relate our findings to clinical features and disease severity (see **Chapter 3**). Next, we aim to investigate the relationship of ^{18}F-sodium fluoride PET/CT findings with aortic expansion and major adverse aortic events in patients with aortic dissection or intramural haematoma (see **Chapter 4**).

The secondary objectives of this thesis are to investigate two novel circulating biomarkers in patients with acute aortic syndrome. First, we will investigate the concentration of plasma desmosine in patients with acute aortic syndrome and relate these findings to clinical features and disease progression (see **Chapter 5**). Finally, we will investigate the miRNA expression in the serum of patients with acute aortic syndrome. Again, we relate these to disease severity and progression (see **Chapter 6**).

Chapter 2

Methods

This prospective single-centre cohort study investigated the role of ^{18}F-sodium fluoride positron emission tomography, plasma desmosine and circulating serum micro-ribonucleic acid (miRNA) expression in patients with acute aortic syndrome.

2.1 Study regulation

2.1.1 External peer-review of study proposals

The study proposal underwent external peer-review by the British Heart Foundation in a critical process to fund a Clinical Research Training Fellowship. This involved a detailed description of the study background, aims of the study, proposed methodology, sample size calculation, image analysis technique, circulating biomarker analysis and prospects for disseminating findings. The final study proposal was approved and funded by the British Heart Foundation (FS/18/31/33676).

2.1.2 Ethical approval

The East-of-Scotland Research Ethics Committee (REC 18/ES/0070) performed an independent critical review of the study proposal and its associated documentation (EoSRES 2021). The study was approved on the 9^{th} of July 2018.

2.1.3 Radiation protection

2.1.3.1 Ionising Radiation (Medical Exposure) Regulations (IR(ME)R)

Exposure to medical radiation is regulated by two legislations: The Ionising Radiation (Medical Exposure) Regulation 2017, and The Ionising Radiation (Medical Exposure)(Amendment) Regulation 2018. These legislations aim to minimise unintended, excessive and incorrect medical exposure, ensure that each exposure outweighs the risks, and that diagnostic doses are as low as reasonably possible for their intended use.

2.1.3.2 Administration of Radioactive Substances Advisory Committee (ARSAC)

The Administration of Radioactive Substance Advisory Committee (ARSAC) advises licensing authorities on applications for research involving radioactive materials. This study was subject to ARSAC approval owing to the administration of ^{18}F-sodium fluoride PET radiotracer. Exposure to radiation from CT Angiography was considered standard-of-care because this component of the research scan substituted normal surveillance imaging for study participants.

A detailed assessment of radiation exposure during the study period was performed by qualified radiophysicists with expertise in positron emission tomography and computed tomography. This was used to estimate the maximum risk of harm to patients through participation in the study and weighed against its potential benefits. The ARSAC committee approved the administration of radioactive substances under Regulation 11(1)(d) of IR(ME)R 2017 (GB) and IR(ME)(NI)R 2018 (Research ID 109, Procedure Codes ^{18}F-66-100, ^{18}F-66-21).

2.1.4 Declaration of Helsinki

This study conforms to the Declaration of Helsinki. The Declaration of Helsinki is a consensus set of ethical principles aimed at physicians involved with human research. It emphasises the core principles of acting in a patient's best interest and not exposing them to undue harm. The Declaration of Helsinki ensures that the benefit of research outweighs potential risks. It also protects patients, particularly vulnerable groups, by advising evalu-

ation of study proposals by an independent ethics committee. Patient confidentiality and autonomy are paramount. Research involving human subjects must be registered in a publicly accessible database.

2.1.5 Study registration

This study was registered on the clinicaltrials.gov database prior to recruitment of the first patient: ^{18}F Sodium Fluoride PET/CT in Acute Aortic Syndrome (FAASt), NCT03647566.

2.1.6 Sponsorship and compliance

This study was sponsored by the Academic and Clinical Central Office for Research and Development (ACCORD) which is a collaborative regulatory partnership between NHS Lothian and the University of Edinburgh (Academic and Clinical Central Office for Research and Development 2020). A detailed study proposal, study protocol, funding application (BHF RG/18/31/33676), service level agreement, ethical approval (DL/18/ES/0070), ARSAC approval (R109), NHS R&D approval and documentation for patients were approved by ACCORD to obtain sponsorship for this research.

This research was conducted in compliance with the principles of the International Conference on Harmonisation Tripartite Guideline for Good Clinical Practice (ICH GCP). All members of the research team were trained in and held a valid certificate for Good Clinical Practice. The conduct of this study also complied with the Medicines for Human Use (Clinical Trials) Regulations 2004, as amended.

All Investigators and study site staff involved with this study complied with the requirements of the Data Protection Act 1998 regarding the collection, storage, processing and disclosure of personal information and upheld the Act's core principles. Access to collated participant data was restricted to those clinicians treating the participants, representatives of the sponsor(s) and representatives of regulatory authorities. Computers used to collate the data had limited access measures via usernames and passwords. Published results do not contain any personal data that could allow identification of individual participants.

2.2 Study Objectives

2.2.1 Study 1: ^{18}F-Sodium fluoride PET in acute aortic syndrome

The *primary objective* of the study is to investigate maximum tissue-to-background ^{18}F-sodium fluoride binding in the most diseased segment (MDS TBR$_{max}$) of the aorta in patients with acute aortic syndrome compared to healthy controls. *Secondary objectives* of the study were to characterise ^{18}F-sodium fluoride MDS TBR$_{max}$ in relation to patient and disease characteristics. Patient characteristics consisted of participant age, sex and past medical history. Disease characteristics included aortic diameter and underlying pathology.

2.2.2 Study 2: Risk-stratification using ^{18}F-sodium fluoride PET

The *primary objective* of this study is to investigate aortic ^{18}F-sodium fluoride MDS TBR$_{max}$ in relation to change in aortic diameter with respect to time. The *secondary objective* is to investigate aortic radiotracer binding (MDS TBR$_{max}$) with respect to major adverse aortic events consisting of aortic repair, aortic rupture or aortic death over a 12 to 24-month follow-up period.

2.2.3 Study 3: Plasma desmosine in acute aortic syndrome

The *primary objective* of this study is to compare plasma desmosine in patients with acute aortic syndrome compared to healthy controls with no history of acute aortic syndrome. The *secondary objective* is to study plasma desmosine concentrations in relation to change in aortic diameter over time.

2.2.4 Study 4: Serum miRNA in acute aortic syndrome

The *primary objective* is to compare candidate serum miRNA expression in patients with acute aortic syndrome to healthy controls. The *secondary objective* of this study is to investigate disease progression in patients with acute aortic syndrome. This study also aims to determine a potential miRNA signature associated with major adverse aortic events in

patients with acute aortic syndrome. Again, major adverse aortic events are defined as aortic repair, aortic rupture or aortic death over a 12-to-24-month follow-up period.

2.3 Participant Selection

2.3.1 Patients with Acute Aortic Syndrome

Patients with acute aortic syndrome over the age of 25 years were eligible for inclusion. Acute aortic syndrome was defined in accordance with the European Society of Cardiology guidelines on aortic diseases: a combination of clinical symptoms consistent with aortic dissection or intramural hematoma which is confirmed by radiological investigation (Erbel et al. 2014).

Patients with Stanford classification type A and type B were eligible for inclusion, as well as patients who had received prior treatment but still had a residual section of aorta affected by acute aortic syndrome.

Consecutive patients hospitalized with acute aortic syndrome were screened for potential eligibility and were categorized as having an intramural hematoma or aortic dissection based on their admission diagnosis. Study participants needed to be clinically stable and retain capacity to consent for inclusion in the study. Individuals recruited to the study within 12 weeks of presentation were classified as having recent acute aortic syndrome. Patients with long-standing disease (>12 weeks) identified from aortic surveillance programmes were classified as having prior acute aortic syndrome.

Patients with traumatic dissections, chronic thoracic aneurysms and infective pseudoaneurysms were excluded. Other exclusion criteria consisted of chronic kidney disease (estimated glomerular filtration rate <30 mL/min/1.73 m^2), life-limiting malignancy, pregnancy, lack of capacity to consent, and allergy to CT contrast medium.

2.3.2 Control Subjects

2.3.2.1 ^{18}F-Sodium fluoride PET/CT studies

Control subjects had a normal calibre aorta identified from the abdominal aortic aneurysm screening programme and had no clinical evidence of acute aortic syndrome or aortic aneurysmal disease. Like the acute aortic syndrome groups, control subjects needed to have good renal function (estimated glomerular filtration rate > 30 mL/min/1.73m^2), no allergy to contrast medium and no life-limiting malignancy to be eligible for recruitment.

2.3.2.2 Plasma desmosine study

Healthy control subjects were recruited from the *United Kingdom Aneurysm Growth Study* (UKAGS, University of Leicester), *Desmosine in plasma and urine of Marfan Syndrome patients* study (DESMA, University of Dundee) and the National Health Centre, Singapore. The UKAGS is an ongoing prospective observational cohort study aiming to recruit 20,000 males with small abdominal aortic aneurysms. For the purposes of this study, healthy controls with an abdominal aortic aneurysm less than 30mm were selected at random in a 2:1 ratio (n = 106) with patients with acute aortic syndrome.

2.3.2.3 Serum micro-ribose nucleic acid (miRNA) study

Serum for healthy controls were obtained from the *Troponin to Risk Stratify Patients for Computed Tomography Coronary Angiography* (PRECISE-CTCA, NCT04549805) study (University of Edinburgh 2021). This prospective observational cohort study aims to recruit 250 patients with stable chest pain undergoing further evaluation of their coronary arteries using computed tomography coronary angiography. Healthy control subjects recruited from the PRECISE-CTCA study (n = 20) had biochemical and radiological confirmation of having no ischaemic heart disease or acute aortic syndrome.

2.4 Clinical assessment

A cardiovascular history was obtained, and clinical examination performed for all patients with acute aortic syndrome at recruitment. This included a review of the case notes and medications. Patients also had baseline blood tests. A full blood count, renal function tests, liver function tests, c-reactive protein and coagulation screen were performed as standard-of-care. A further 30 mL of blood was stored for research biomarker analysis.

2.5 Computed tomography angiography

Computed tomography angiography is the standard-of-care imaging modality to diagnose acute aortic syndrome and forms an essential part of the diagnostic criteria as outlined by the European Society of Cardiology guidelines on managing aortic diseases (Erbel et al. 2014). CT angiography is widely available and a has an excellent pooled-sensitivity of 100% and -specificity of 98% to detect acute aortic syndrome (Erbel et al. 2014; Shiga et al. 2006). The adoption of ECG-gated CT Angiography has increased the diagnostic accuracy of Stanford type A aortic dissection near the aortic root thus reducing the requirement for additional imaging modalities such as trans-thoracic echocardiography (Rogers et al. 2011).

A prospective ECG-gated contrast-enhanced CT aortogram was performed from the neck to the common femoral vessels (120 kV and 145 mAs, slice thickness 1 mm, field of view 300 mm). This was used for morphological analysis of the aorta.

2.5.1 Aortic diameter

Morphological analysis, including assessment of aortic diameter, was performed on centreline aortic reconstructions to reduce the risk of out-of-plane aortic diameter measurements. Centreline aortic measurements reduce inter-user variability and increase accuracy of aortic diameter measurements compared to transaxial imaging alone (Müller-Eschner et al. 2013). Aortic diameter measurement from contrast-enhanced computed tomography has excellent inter-user reproducibility in the ascending, descending and

abdominal aorta (inter-class correlation of 0.90, 0.92 and 0.93 respectively) (Houben et al. 2020).

We used the PACS Carestream image viewer for morphological analysis of the aorta. The PACS Carestream image viewer provides access to a comprehensive national database of radiographic investigations for patients in Scotland. This powerful DICOM image viewer is used as standard-of-care for clinical radiology. Add-ons to the base PACS Carestream software enable detailed aortic morphological analysis following centre-line reconstruction and multiplanar reconstructions.

Aortic diameter was measured in centreline reconstructions of the aorta obtained from computed tomography angiography scans as described by Müller-Eschner et al. (2013). Centrelines were constructed from the aortic root to the aortic bifurcation. Aortic diameter was measured in a cross-sectional plane to the centreline as is standard of care. An "outer-to-outer" aortic diameter was measured to incorporate the aortic wall. This strategy was adopted to include luminal thrombosis and intramural haematoma that may otherwise be missed using inner-to-inner aortic diameter measurements. The widest diameter of the aorta following multiplanar centreline reconstruction was considered the maximum aortic diameter.

2.5.2 Aortic growth

Serial aortic diameter measurements were made from all retrospective and prospective CT aortograms hosted on a comprehensive Picture Archiving and Communication System (PACS, Scottish Government 2012, 2011–17). This comprehensive imaging database allows clinicians to access all cross-sectional imaging for study participants. Again, the maximum aortic diameter was measured using centreline reconstruction of aortic segments affected by acute aortic syndrome as described above.

For each participant, aortic CT angiography from diagnosis to November 2020 were retrieved from the national PACS archive. Maximum aortic diameter was measured in each computed tomography.

Aortic expansion was measured during distinct growth periods. The first growth period

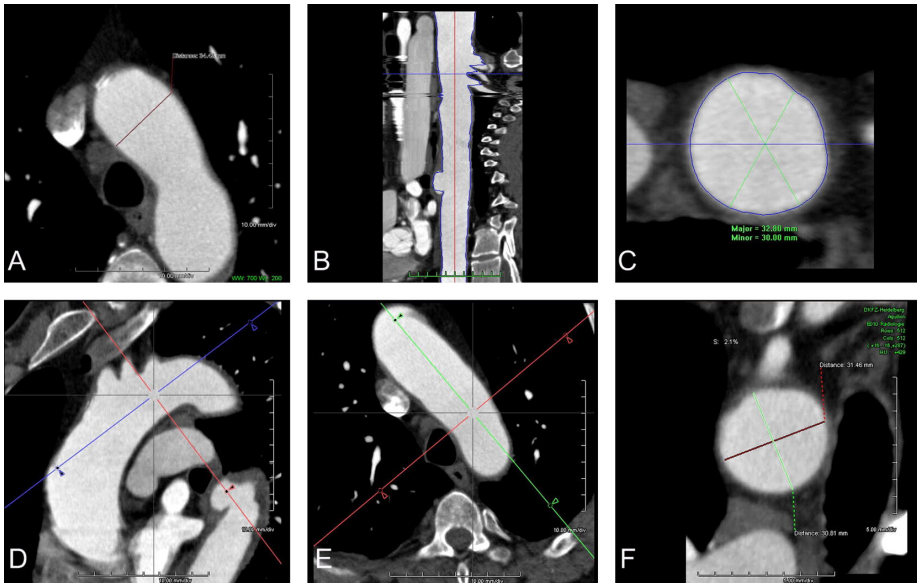

Figure 2.1: **Centreline reconstruction of the thoracic aorta.** Diameter assessment based on axial (**A**), double oblique multiplanar reformation (**D-F**) and centerline (**B-C**) techniques. Measuring on axial images, the course of the aorta can only be assessed visually (**A**), whereas MPR and centerline analysis allow for measurements in a plane perpendicular to the vessel course (**C, F**) (Müller-Eschner et al. 2013).

for each participant started at the point of diagnosis and was reset when intervention occurred or the date of most recent scan. If intervention occurred, a new growth period started.

Change in aortic diameter was measured as the total change in diameter corrected for the interval between scans within each growth period. This was subsequently annualised to obtain a change in aortic diameter per year during each growth period per participant.

2.6 Calcium scoring computed tomography

Computed tomography is excellent at detecting larger calcified plaques and thus measuring the volume of calcification within the thoracic aorta (Dudink et al. 2018). Aortic calcification can be quantified as both, a crude volume or as an Agatston score. The Agatston score is a graded scoring system that quantifies vascular calcification burden by combining calcium volume and Hounsfield units as a measure of calcification density (Agatston et al. 1990). Quantifying aortic calcium using dedicated computed tomography imaging

protocols is accurate with low inter-user variability (4% - 7%, Budoff et al. (2006)).

We performed an electrocardiogram (ECG)-gated prospective calcium scoring CT of the thoracic aorta (120 kV, 120 mAs, 3/3 mm; prospective ECG gating at 50% of the R-R interval) from the neck to the level of the L1 vertebra to include the entire thoracic aorta. Both calcium volume and aortic Agatston score (Dudink et al. 2018) were measured to determine macro-calcification burden in the thoracic aorta.

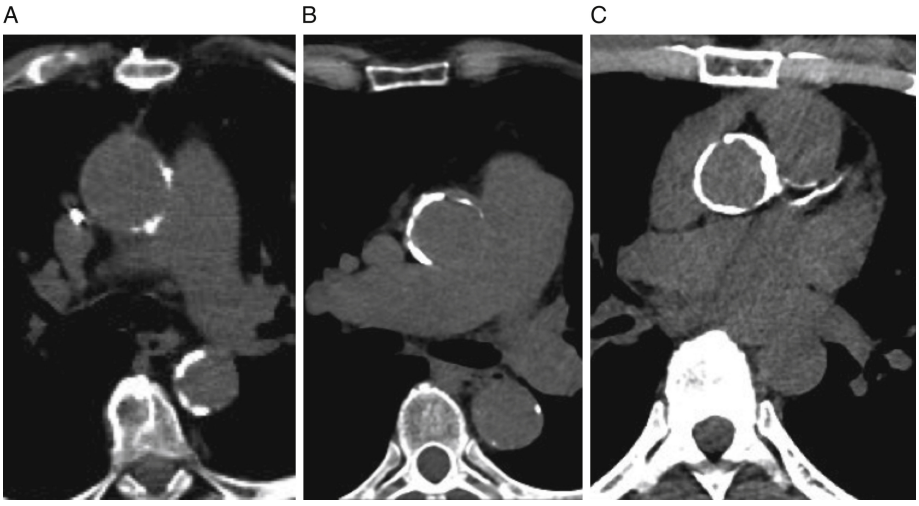

Figure 2.2: **Examples of thoracic aortic calcification.** A patient with mild (**A**), moderate (**B**) and circumferential (**C**) calcification of the thoracic aorta as detected by a calcium scoring CT scan (Desai et al. 2018).

2.7 ^{18}F-Sodium fluoride positron emission tomography and computed tomography

2.7.1 Image acquistion

In this study, participants were administered 125 MBq of ^{18}F-sodium fluoride intravenously one hour prior to their PET/CT scan. A low-dose attenuation correction CT (120 kV, 50 mAs, 5/3 mm) was followed by a PET scan in three 10-min bed positions to cover the whole aorta using a hybrid 128–detector array PET-CT scanner (Biograph mCT, Siemens Healthcare, Erlangen, Germany).

2.7.2 FusionQuant

^{18}F-Sodium fluoride uptake was measured using FusionQuant. This is an analytical tool to investigate positron emission tomography and was developed at Cedars-Sinai medical centre, California, United States of America. FusionQuant is designed specifically for the analysis of cardiovascular PET imaging. It enables co-registration of PET imaging with CT or MRI data. Built-in tools enables PET quantification along segments of a blood vessel. Recent advances now allow an estimate of PET signal along an entire vessel using centreline functionality (Tzolos et al. 2020; Fletcher et al. 2021). FusionQuant is fast and simple. It provides a streamlined pipeline for cardiovascular PET image analysis and has been validated to provide accurate measurements of PET uptake compared to commercially available PET image analysis software (Concordance Correlation Coefficient = 0.972 (95% CI 0.949–0.995) with OsiriX, Massera et al. (2020)).

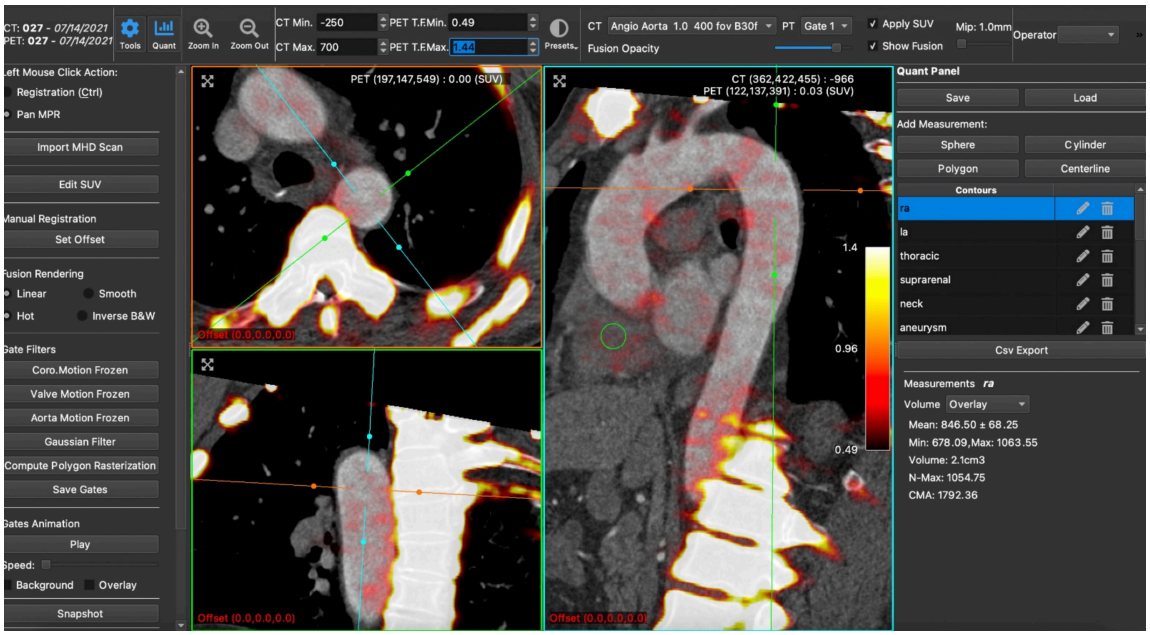

Figure 2.3: **^{18}F-Sodium fluoride positron emission tomography and computed tomography image analysis using FusionQuant.** The images have been loaded and coregistered. A region of interest is drawn by the user (green) to obtain standardised uptake values.

2.7.3 Image co-registration

FusionQuant automatically co-registers image stacks based on a coordinate system specified within the meta-data of the image sequence. Image co-registration is then confirmed by the user to align computed tomography angiography images with positron emission tomography scans within a three-dimensional space. Fixed anatomical structures with a high uptake of radiotracer were used to facilitate image co-registration. These include the kidneys which are a fixed retroperitoneal structure adjacent to the abdominal aorta, and the vertebra which remains fixed during respiration (Masuda et al. 2011).

2.7.4 Standardised Uptake Values (SUV)

^{18}F-Sodium fluoride binding was measured in standardised uptake values (SUV). This is a validated metric to measure PET signal intensity (Gonzalez-Galofre, Alcaide-Corral, and Tavares (2021); Kurdziel et al. (2012)). SUV are a measure of radiotracer signal intensity corrected for the duration between ^{18}F-sodium fluoride administration, the dose of radiotracer administered and the patient's body weight. SUVs are typically measured within a three-dimensional volume as guided by anatomical features obtained from image co-registration. Within this region of interest, a mean and maximum SUV can be calculated.

$$SUV(t) = \frac{c_{img}(t)}{ID/BW}$$

$SUV(t) =$ Standardised Uptake Value at time point t; $c_{img}(t) =$ radiotracer activity within the region of interest at timepoint t; $ID =$ the injected dose in Megabecquerels; $BW =$ the patient's body weight in kg.

2.7.5 Tissue-to-Background Ratio (TBR)

The tissue to background ratio is a technique used to adjust SUV values for background blood-pool activity and has been used extensively to quantify ^{18}F-sodium fluoride binding to diseased segments of the vascular system (Forsythe et al. 2018; Massera et al. 2020; Kwiecinski et al. 2020; Tzolos et al. 2020; Doris et al. 2020; Vesey et al. 2017; Fayad et al. 2011).

The maximum tissue to background (TBR_{max}) was obtained by first measuring maximum ^{18}F-sodium fluoride SUV in the aortic wall and then correcting this for background mean blood pool ^{18}F-sodium fluoride SUV in the right atrium.

$$TBR_{max} = \frac{SUV_{max}(target)}{SUV_{mean}(reference)}$$

TBR_{max} = maximum tissue-to-background ratio; $SUV_{max}(target)$ = Maximum standardised uptake value in the aorta; $SUV_{mean}(reference)$ = Mean standardised uptake value in the right atrium as a measure of background blood pool activity.

2.7.6 Most Diseased Segment (MDS)

The most diseased segment (MDS) is a systematic approach to determines peak radiotracer binding within the cardiovascular system whilst minimising signal artifact. It has excellent inter-user reproducibility to quantify ^{18}F-sodium fluoride uptake within the cardiovascular system, including highly mobile structures such as the aortic valve (inter-class correlation 0.80) (Pawade et al. 2016), and small arteries such as the coronary vessels (inter-class correlation 0.89) (Moss et al. 2019).

Aortic ^{18}F-sodium fluoride binding (TBR_{max}) was measured from the aortic root to the aortic bifurcation in 3mm intervals on the trans-axial plane in a similar manner to previous aortic studies (Fayad et al. 2011; Forsythe et al. 2018). Blood pool and vertebral radiotracer binding was used to threshold windowing of the PET images. This, combined with anatomical information obtained from CT angiograms was used to draw regions of interest over the aorta whilst excluding spill-over of radiotracer signal from bone and other adjacent viscera.

The most diseased segment was defined as peak TBR_{max} obtained from an average of three adjacent volumes (MDS TBR_{max}).

2.7.7 Aortic sections

The aorta was divided in to three sections to facilitate image analysis relative to the acute aortic syndrome pathology: the proximal aorta, the site of intimal disruption, and the distal

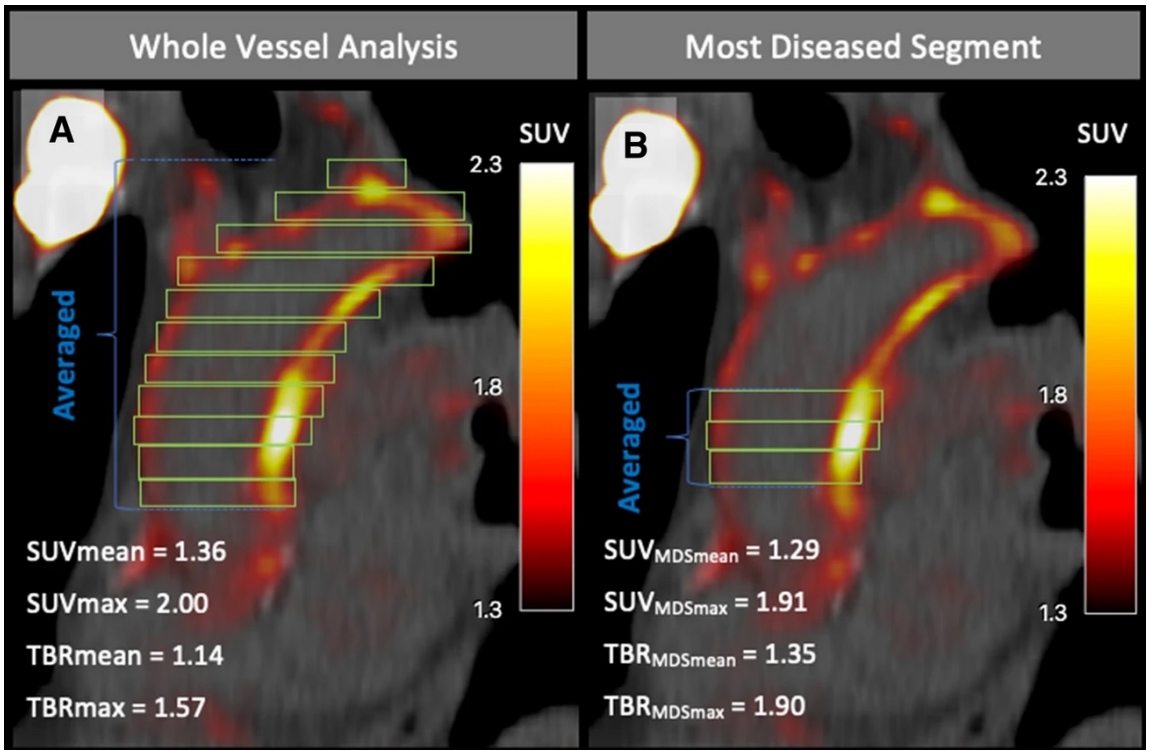

Figure 2.4: ^{18}**F-Sodium fluoride positron emission tomography and computed tomography in a patient with marked aortic wall uptake.** An illustrated representation of standard whole vessel (**A**) and most diseased segment (**B**) (Fletcher et al. 2021).

aorta. The site of intimal disruption was defined as a 10cm segment of aorta centred on the site of intimal tearing. These boundaries were then used to define the proximal and distal sections of aorta.

^{18}F-Sodium fluoride binding was measured in each section using the maximum tissue-to-background most diseased segment (MDS TBR$_{max}$) technique. Radiotracer binding at the site of intimal disruption and distal aorta was compared with radiotracer binding in the more proximal unaffected aorta.

2.7.8 Components of the aortic wall

The aortic wall affected by acute aortic syndrome was divided in to three components. First, the dissection flap was defined as the septum that divided the true- and false lumens. Next, the native outer aortic wall adjacent to the true lumen was determined. Finally, the outer aortic wall adjacent to the false lumen was identified. Again, ^{18}F-sodium fluoride uptake was measured in each component of the aortic wall using the most diseased segment (MDS TBR$_{max}$) technique.

2.8 Blood biomarker analysis

2.8.1 Sample processing

Blood obtained for research during the baseline and follow-up visits were stored as plasma, serum and whole blood. Plasma and serum were centrifuged at 800g for 10 minutes at 4° Celsius. Plasma and serum were then extracted and stored in 0.5 mL aliquots. All aliquots and whole blood were stored at -80° Celsius for future analysis (Biggs and Douglas 1953; Haeberle et al. 2006).

2.8.2 Plasma Desmosine

Plasma desmosine concentrations were analysed using a validated stable isotope dilution liquid chromatography–tandem mass spectrometry (LC-MS/MS) method. Briefly, the LC-MS/MS method quantifes plasma desmosine by first hydrolysing the sample using 11.8

N HCl (for 18h at 108° celsius) to separate desmosine bound to other circulating peptides. Next, the samples are mixed in a butanol/acetic acid and fixed to a compact cellulose layer. Finally, mass spectrometry is performed on the prepared samples to estimate plasma desmosine concentration (Albarbarawi et al. 2013). The reportable range for the assay is 0.1 to 160ng/mL with a co-efficient of variation of 5.7% (Albarbarawi et al. 2013; Miliotis et al. 2013; Mordi et al. 2019).

Plasma desmosine was measured by an independent team of researchers at the Department of Molecular and Clinical Medicine, University of Dundee. This group was blinded to the demographic and clinical details of study participants.

2.8.3 Serum micro-ribose nucleic acid

Serum miRNA measurements were performed at the British Heart Foundation Department for Cardiovascular Sciences, University of Edinburgh. This was performed on blood samples collected from study participants at baseline. Again, the researchers were blinded to the clinical and demographic details of study participants. Serum miRNA was measured using quantitative real-time polymerase chain reaction (qRT-PCR). This is the gold standard for micro RNA measurement in blood with an acceptable intra-platform reproducibility of 0.81 (standard deviation 0.07) that is comparable to other methods of quantifying micro RNA (Wang et al. 2011).

Aliquots of 50 µL serum were diluted with 150 µL of RNase-free water, followed by addition of 100 fmol of Caenorhabditis elegans miR-39 mimic (cel-miR-39 – Norgen Biotek, ON, Canada) as a spike-in control prior to RNA isolation. Total RNA was isolated by following the manufacturer's instructions in the miRNeasy Serum/Plasma Kit (Qiagen, Venlo, NL)(Kroh et al. 2010). Aliquots of 2.5 µL RNA were reverse transcribed using the miScript RT II Kit (Qiagen) and its supplied protocol for the generation of complementary DNA (cDNA) from miRNAs. Resulting cDNA was diluted 1:10 with nuclease-free water. qPCR was performed using the miScript SYBR Green PCR Kit (Qiagen) with reaction mixtures containing 1 µL of cDNA, 1 $\times$ QuantiTect SYBR Green PCR Master Mix, 1 $\times$ miScript Universal Primer, 1 $\times$ of miRNA-specific primer assay (Supplementary Table 1), and nuclease-free water up to 10 µL. qPCR was performed on the LightCycler 480 apparatus (Roche Diagnos-

tics, Burgess Hill, UK) utilising cycling parameters recommended for the miScript SYBR green system. The expression of each miRNA was normalised to the expression of the cel-miR-39 spike-in control.

2.9 Major adverse aortic events

Major adverse aortic events were defined as a composite of aortic rupture, aorta-related death or aortic intervention. A clinical adjudication committee was established to indepndently determine whether a major adverse aortic event had occurred. The committee consisted of members with expertise in vascular surgery, clinical radiology and independent physicians.

2.10 Statistical Analysis

2.10.1 Sample Size Calculation

A sample size calculation was performed by estimating most diseased segment SUV_{max} as the primary dependent variable from patients with acute and chronic aortic syndrome in a ratio of 3:1 for acute and chronic aortic syndrome, and control subjects. This allowed us to explore initial baseline differences but then assess long term follow up in the larger disease population as we have done previously (Forsythe et al. 2018). In the $SoFIA_3$ study, following log_2 transformation, the mean MDS SUV_{max} was 1.4±0.4 in patients with abdominal aortic aneurysms, and 1.0±0.4 in control subjects. Assuming similar mean MDS SUV_{max} uptake values in patients with aortic syndrome, we would need 42 patients and 14 controls subjects to detect a similar difference in uptake at 90% power and two-sided P<0.05.

2.10.2 Univariable Comparisons

Baseline demographics, blood tests and image analysis data were tabulated as either continuous, categorical, or ordinal variables. Continuous variables were assessed for normality and log-transformed if skewed to enable parametric statistical tests. A Student's t-test

was performed to compare normalised continuous variables across two categories. An analysis of variance (ANOVA) was used to compare continuous variables with a normal distribution across three or more categories. Non-parametric tests were used to compare skewed continuous variables. Chi-square analysis was used to compare categorical variables. A Fisher's exact test was used to compare categorical variables if the frequency count of the variable was below 5. A p-value less than 0.05 was considered statistically significant.

Univariable comparisons between disease and control groups was performed to identify potential confounding variables that may influence the end-point being investigated.

2.10.3 Linear Regression

Linear regression was used to fit continuous endpoints against potential confounders. The decision to include confounders was dictated by sample size, the result of univariate comparisons and clinical expertise. The effect-size of individual predictor variables was obtained as a beta-estimate with 95% confidence interval and a p-value.

2.10.3.1 ^{18}F-Sodium fluoride binding and aortic diameter

A linear regression model for ^{18}F-sodium fluoride MDS TBR$_{max}$ was fitted against aortic diameter, age, sex, participant smoking status, systolic blood pressure, duration since the index aortic event, Stanford classification and aortic pathology.

2.10.3.2 ^{18}F-Sodium fluoride and aortic expansion

Change in aortic diameter during each growth period (mm/yr) was fitted in a crude linear regression model against ^{18}F-sodium fluoride MDS TBR$_{max}$ in the wall adjacent to the false lumen. An adjusted model was developed to include time since acute aortic syndrome, endovascular intervention, or open surgery during the growth period as potential confounders of aortic expansion.

2.10.3.3 Plasma desmosine with respect to time since acute aortic syndrome

A cubic transformation was applied to the plasma desmosine concentration, which was fitted against time since acute aortic syndrome in study participants. A second regression model fitted plasma desmosine concentration (cubic-transformation) against time since acute aortic syndrome adjusted for age, gender, body mass index, diastolic blood pressure and smoking status.

2.10.3.4 Plasma desmosine and aortic expansion

Aortic growth was fitted in a crude linear regression model against plasma desmosine concentration. A second adjusted linear regression model for aortic growth also included aortic diameter, aortic Agatston score, time since acute aortic syndrome and aortic intervention in addition to plasma desmosine concentration.

2.10.4 Linear Discriminant Analysis (LDA)

Linear discriminant analysis (LDA) is a feature selection algorithm used to condense high-dimension data sets into fewer variables by scaling individual predictors against an optimum linear fit (Tharwat et al. 2017). In a two-dimensional LDA model, a single metric – the LDA score – can then be obtained for each participant as the sum of weighted variables included in the algorithm. This condensed LDA score can be investigated in isolation or used as an independent predictor in further statistical analyses (Rhys 2020).

2.10.4.1 LDA of serum miRNA expression in acute aortic syndrome

The expression of 16 individual miRNAs was fitted in a linear discriminant analysis model to stratify patients that experienced a major adverse aortic event during the study follow-up period. Weighting factors obtained from this analysis were used to produce a single miRNA LDA score per participant. miRNA LDA score was compared between patients that experienced a major adverse aortic event and those that remained event free using a Student's t-test.

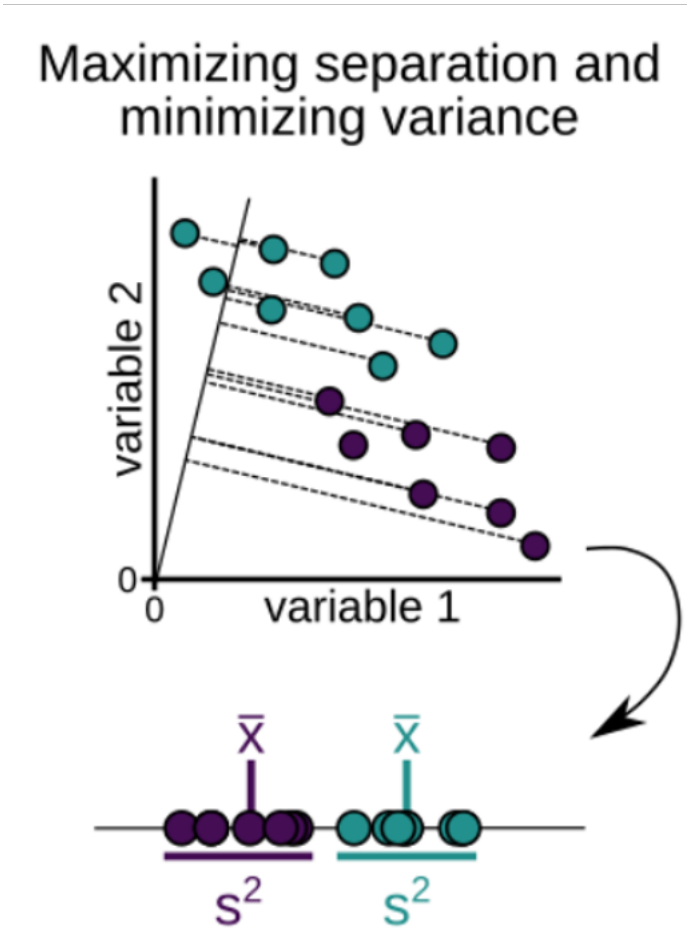

Figure 2.5: **Linear Discriminant Analysis.** An illustration of how linear discriminant analysis is used to determine the optimal linear fit between multiple continuous variables to stratify groups (Rhys 2020).

2.10.5 Survival analysis

Kaplan-Meier estimates were fitted to compare clinically significant events between groups and a log-rank test used to determine statistical significance. A proportional hazards Cox Regression model was used to fit survival against potentially significant confounders, again selected based on clinical significance or difference between groups on univariate comparison. A hazard ratio and 95% confidence interval were obtained by log-transforming the model estimate. A p-value of less than 0.05 was used to determine the statistical significance of predictors.

2.10.6 ^{18}F-Sodium fluoride as a predictor of Major Adverse Aortic Events

Median ^{18}F-sodium fluoride binding (MDS TBR$_{max}$) in the aortic wall adjacent to the true lumen was used to dichotomise patients as having high- or low- radiotracer binding groups. Kaplan-Meier estimates and log-rank tests were obtained to determine statistical significance between groups. A proportional hazards Cox regression model was fitted to investigate the influence of ^{18}F-sodium fluoride MDS TBR$_{max}$ in the aortic wall of the true lumen in a crude model. An adjusted model also incorporated participant age, sex, smoking status, aortic diameter, aortic pathology, time from index acute aortic syndrome and Stanford classification.

2.10.7 miRNA LDA score as a predictor of Major Adverse Aortic Events

The median miRNA score was used to dichotomise patients in to low- and high- miRNA LDA score groups. Kaplan-Meier estimates and log-rank testing was performed to compare major adverse aortic events between groups. Survival was then fitted to a proportional hazards Cox Regression model with miRNA LDA score in a crude analysis. A second proportional hazards Cox regression model was fitted to adjust for participant age, sex, aortic diameter and time since acute aortic syndrome in addition to miRNA LDA score.

2.10.8 Data management and analysis

Data was initially collated and cleaned in Microsoft Excel for Mac 2016. The data was stored in a password-encrypted document in a secure research environment. Statistical analysis was performed in R: A language and environment for statistical computing (R Foundation for Statistical Computing, Vienna, Austria, url: https://www.R-project.org/).

Chapter 3

^{18}F-Sodium fluoride PET in acute aortic syndrome

3.1 Abstract

3.1.1 Background

In patients with abdominal aortic aneurysm, we have previously demonstrated that ^{18}F-sodium fluoride positron emission tomography and computed tomography (^{18}F-NaF PET/CT) can identify aortic wall injury and predict aortic expansion and clinical outcome.

3.1.2 Objective

In a proof-of-concept study, we aimed to establish whether ^{18}F-NaF PET/CT could identify aortic disease in patients with acute aortic syndrome.

3.1.3 Methods

Patients with acute aortic syndrome (aortic dissection, intramural haematoma or penetrating aortic ulcer) and healthy control subjects underwent ^{18}F-NaF PET/CT and CT angiography of the aorta. ^{18}F-NaF uptake was measured at the most diseased segment of

the aorta and the maximum value corrected for background blood pool activity to obtain tissue-to-background ratios (TBR$_{max}$).

3.1.4 Results

Aortic ^{18}F-NaF uptake co-localized with histologically defined regions of microcalcification and elastin disruption. Compared to healthy volunteers, patients with acute aortic syndrome had increased ^{18}F-NaF uptake (TBR$_{max}$ 1.36 $\pm$ 0.39 (n=20) versus 2.08 $\pm$ 0.45 (n=56) respectively; p<0.001) with penetrating aortic ulcers having the highest uptake followed by aortic dissections and intramural haematomas (TBR$_{max}$ 2.38 $\pm$ 0.53 (n=9), 2.05 $\pm$ 0.42 (n=42) and 1.78 $\pm$ 0.29 (n=5) respectively). ^{18}F-NaF uptake was 32.5% [interquartile interval 24.8-41.0%] greater at the site of intimal disruption compared to proximal aorta.

3.1.5 Conclusion

^{18}F-Sodium fluoride uptake is increased in patients with acute aortic syndrome, occurs preferentially at sites of disease activity and is independent of aortic size. ^{18}F-Sodium fluoride holds promise as a non-invasive marker of disease activity and severity in patients with acute aortic syndrome.

3.2 Introduction

Acute aortic syndrome encompasses aortic dissections, intramural haematomas and penetrating aortic ulcers. These potentially catastrophic conditions result from degenerative processes that weaken the elastic connective tissue in the aortic wall. They are associated with abnormal reparative responses including the precipitation of calcium phosphate-rich crystals in the aortic media with microcalcification signifying a biologically active aortic state (Wanga et al. 2017) that may be a marker of vascular injury.

The vulnerable diseased aorta is at risk of haemorrhage within the wall manifesting as an intramural haematoma. Alternatively, a penetrating aortic ulcer can erode through the intimal and elastic lamella as a focus of intense inflammatory atherosclerotic activity. Such

processes expose the weakened medial layer to systemic arterial pressure. The resultant aortic dissection tears down the media adjacent to the outer adventitial layer. The damaged aorta is prone to aneurysmal dilatation and rupture leading to severe and often fatal bleeding (Evangelista et al. 2018).

It is difficult to predict aortic expansion or rupture following acute aortic syndrome. The current surveillance pathway relies on assessing aortic morphology and size with computed tomography (CT) or magnetic resonance angiography. Despite intensive blood pressure control and advances in endovascular surgery, the 3-year mortality from acute aortic syndrome remains unacceptably high at approximately 25% (X. Yuan et al. 2019).

Positron emission tomography (PET) can be used to assess the biological state of aortic tissue beyond anatomical imaging alone. We have previously shown that ^{18}F-sodium fluoride PET detects atherosclerotic microcalcification and offers a novel approach to quantify vascular injury (Irkle et al. 2015; Kwiecinski et al. 2020). In abdominal aortic aneurysms, ^{18}F-sodium fluoride uptake is increased in aneurysmal sections of the aorta (Forsythe et al. 2018).

In the present proof-of-concept study, we aimed to characterize ^{18}F-sodium fluoride PET/CT uptake in patients with acute aortic syndrome, and to establish its association with disease severity, concomitant risk factors and subcategories of disease.

3.3 Methods

This single-centre prospective cross-sectional case-control study assessed ^{18}F-sodium fluoride PET/CT in patients with acute aortic syndrome. This included patients with intramural haematoma, aortic dissection and penetrating aortic ulcers.

Detailed methodolgy is outlined in **Chapter 2**. Briefly, patients over the age of 25 years with acute aortic syndrome were eligible for recruitment. Those within 12 weeks of presentation were classified as having *recent* disease. Patients with long-standing disease identified from aortic surveillance programmes were classified as having *prior* acute aortic syndrome. Healthy control subjects were age-matched, had a normal calibre aorta

identified from the abdominal aortic aneurysm screening programme and had no clinical evidence of acute aortic syndrome or aortic aneurysmal disease (**Chapter 2.3**).

Aortic tissue obtained from open surgical intervention was stained with Verhoeff-van Gieson's stain for elastin and von Kossa's stain for calcium phosphate complexes. Autoradiography with ^{18}F-sodium fluoride and micro-PET/CT was performed on excised aortic specimens (**Chapter 2.4**).

A clinical assessment of all participants documented their past medical history, concomitant medication, clinical examination and clinical biochemistry and haematology (**Chapter 2.4**). Study participants underwent an ^{18}F-sodium fluoride PET/CT scan, an electrocardiogram (ECG)-gated prospective calcium scoring CT of the thoracic aorta, and a contrast-enhanced CT aortogram from the neck to the common femoral vessels (**Chapter 2.5**). Standardized uptake values (SUV) for peak ^{18}F-sodium fluoride uptake were measured in regions of interest. The maximum TBR in the most diseased segment (MDS TBR$_{max}$) was measured for the whole aorta, in relation to the intimal tear and within components of the aortic wall (**Chapter 2.7**).

Baseline characteristics of patients and healthy controls are presented as mean$\pm$standard deviation or median [interquartile interval] as appropriate. Normally distributed continuous variables were compared using a Students' t-test. Non-parametric tests were used to compare skewed variables. Chi-square or Fisher's exact tests were used to compare categorical variables. A linear regression model for MDS TBR$_{max}$ was fitted against age, gender, aortic diameter and Stanford classification as potential predictors. Secondary analysis of ^{18}F-sodium fluoride binding between aortic sub-pathologies was performed using a similar linear regression model (**Chapter 2.10**).

3.4 Results

3.4.1 Study Population

Of 135 patients with acute aortic syndrome, 89 were eligible to participate in the study. Fifty-six participants with acute aortic syndrome and 20 control subjects consented to

participate and were thus recruited. All patients were included in the final analysis.

The study population consisted of predominantly elderly men, half of whom reported a current or prior smoking habit (Table 3.1). Control subjects were also predominantly men and were matched for age, body-mass index, ischemic heart disease, diabetes mellitus and hypercholesterolemia. All participants tolerated the ^{18}F-sodium fluoride PET/CT scan well with no side-effects or adverse reactions.

3.4.2 Aortic Tissue Microcalcification

Tissue samples were obtained from two study participants who underwent emergency surgery (Figure 3.1). Specimens revealed a band of reduced elastin density and elastin breaks in the medial wall. Widespread microcalcification co-localized to areas adjacent to reduced elastin density. Autoradiography and micro-PET-CT demonstrated co-localization of ^{18}F-sodium fluoride uptake with areas of microcalcification and elastin disruption.

3.4.3 ^{18}F-Sodium Fluoride Positron Emission Tomography in Acute Aortic Syndrome

Aortic ^{18}F-sodium fluoride uptake was increased in patients with acute aortic syndrome (p<0.001, Figure 3.2 and 3.3) when assessed by either absolute standardized uptake values or tissue-to-background ratios at the most diseased segments of the aorta (Table 3.2).

The median interval from the initial clinical event to ^{18}F-sodium fluoride PET/CT was 30 weeks (range 3 days to 11 years) across both recent and prior acute aortic syndrome subgroups. A linear regression analysis corrected for age, gender, Stanford classification and acute disease categorization predicted ^{18}F-sodium fluoride MDS TBR$_{max}$ of 2.12 (95% confidence interval 1.92 – 2.32) in patients with acute aortic syndrome compared with 1.35 (95% confidence interval 1.15 – 1.54) in healthy control subjects: odds ratio 1.59 (95% confidence interval 1.14 – 2.22, p < 0.001) in a modelled 65-year old male. None of the other variables were independently associated with acute aortic syndrome.

Maximum aortic diameter was increased in patients with acute aortic syndrome compared to healthy control subjects (45.1 [40.2–49.5] versus 18.5 [16.0–19.0] mm, p<0.001). ^{18}F-

Table 3.1: **Patient Characteristics**

		Acute Aortic Syndrome (n=56)	Control Subjects (n=20)	p
Demographics	Age (years)	65 [51, 71]	65 [65, 65]	0.872
	Male (%)	41 (73%)	19 (95%)	0.083
	Body-mass Index (kg/m2)	28.8±5.16	29.3±6.4	0.752
	Systolic Blood Pressure (mmHg)	133±21	142±14	0.086
	Diastolic Blood Pressure (mmHg)	74±13	80±8	0.030*
	Heart Rate (beats per minute)	66±11	67±14	0.839
	Smoking Habit			0.002*
	Non-smoker	28 (50%)	15 (75%)	
	Ex-smoker	23 (41%)	0 (0%)	
	Current Smoker	5 (9%)	5 (25%)	
	Alcohol Consumption (any)	30 (54%)	12 (60%)	0.815
Aortic Characteristics	Aortic Diameter (mm)	44.9 [40.3, 49.4]	18.50 [16.0, 19.0]	<0.001*
	Pathology			
	Intramural Haematoma	5 (11%)	-	-
	Aortic Dissection	42 (73%)	-	-
	Penetrating Aortic Ulcer	9 (16%)	-	-
	Stanford Type B Classification	36 (64%)	-	-
	Recent Acute Aortic Syndrome	25 (45%)	-	-
	Prior Acute Aortic Syndrome	31 (55%)	-	-
Past Medical History	Hypertension	52 (93%)	6 (30%)	<0.001*
	Ischaemic Heart Disease	10 (18%)	1 (5%)	0.302
	Cerebrovascular Disease	8 (14%)	0 (0%)	-
	Diabetes Mellitus	2 (4%)	2 (10%)	0.602
	Hypercholesterolaemia	15 (27%)	7 (35%)	0.683
	Connective Tissue Disorder	5 (9%)	0 (0%)	-
Medications	Antiplatelet Therapy	27 (48%)	3 (15%)	0.019
	Anticoagulation Therapy	14 (26%)	1 (5%)	0.103
	Statin Therapy	33 (59%)	8 (40%)	0.231
	Beta-Blocker Therapy	49 (88%)	2 (10%)	<0.001*
	ACE-Inhibitor Therapy	27 (48%)	4 (20%)	0.053

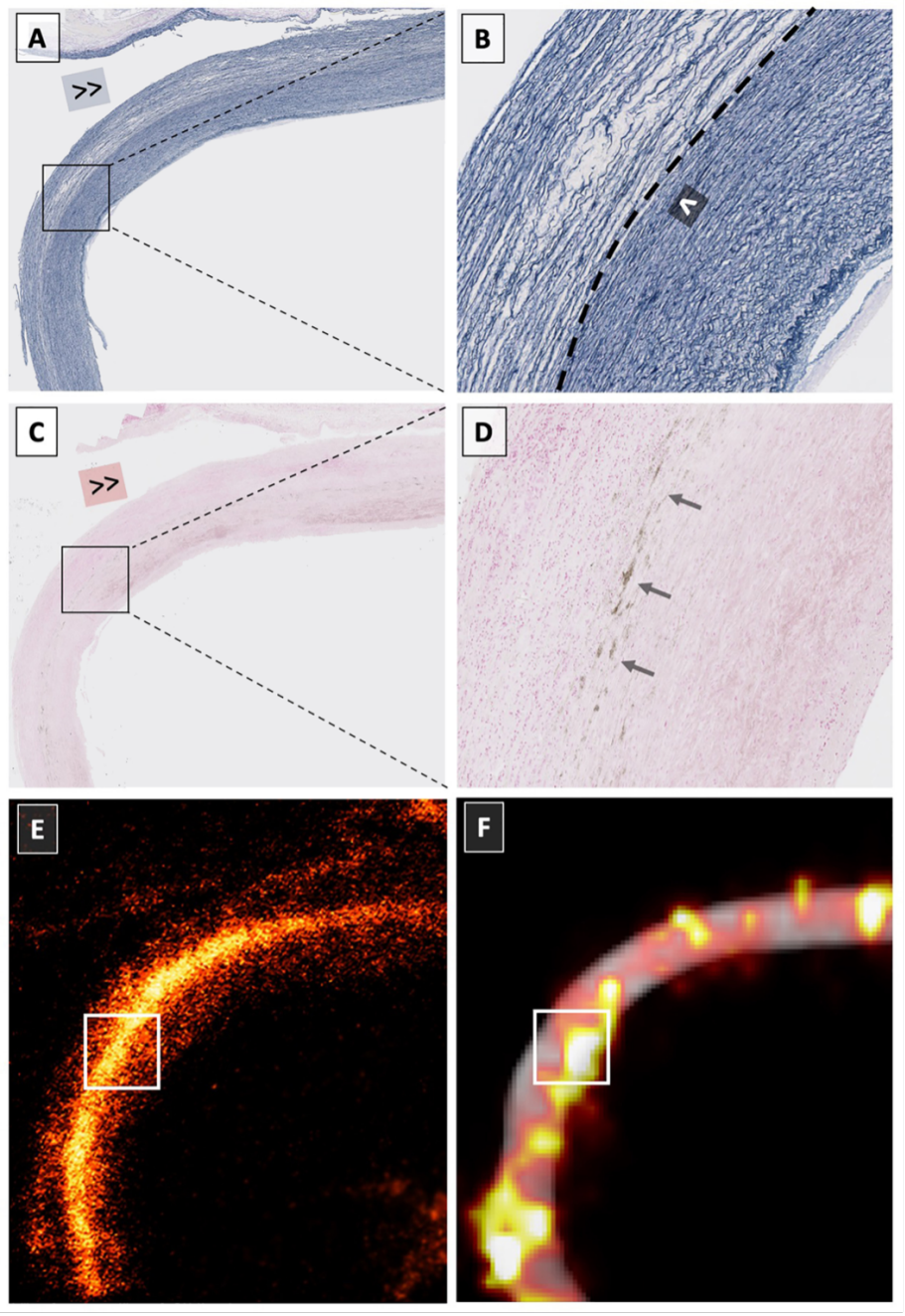

Figure 3.1: **Aortic medial degeneration and microcalcification in acute aortic syndrome.** Van Geisson's elastin stain shows a band of reduced elastin density (white arrow) along the outer circumference of the medial wall (**A**) and fractured elastin fibres (**B**) along the plane of aortic dissection (»). Von Kossa's stain for calcium and phosphate-rich hydroxyapatite crystals reveals a band of medial microcalcification adjacent to areas of reduced elastin density (grey arrows, **C** and **D**). High-resolution ^{18}F-sodium fluoride autoradiography confirms a band of aortic wall microcalcification throughout the specimen (**E**) that co-localizes with microcalcification and loss of elastin density (**C** and **D**). Focal concentrations of microcalcification (**E**) correlate with intense 18F-sodium fluoride binding on ex vivo micro-positron emission tomography and computed tomography of aortic specimens (**F**)

Sodium fluoride uptake was associated with maximum aortic diameter in a linear regression model adjusted for age, sex, time from initial presentation and Stanford Classification (Figure 3.4C, p=0.043).

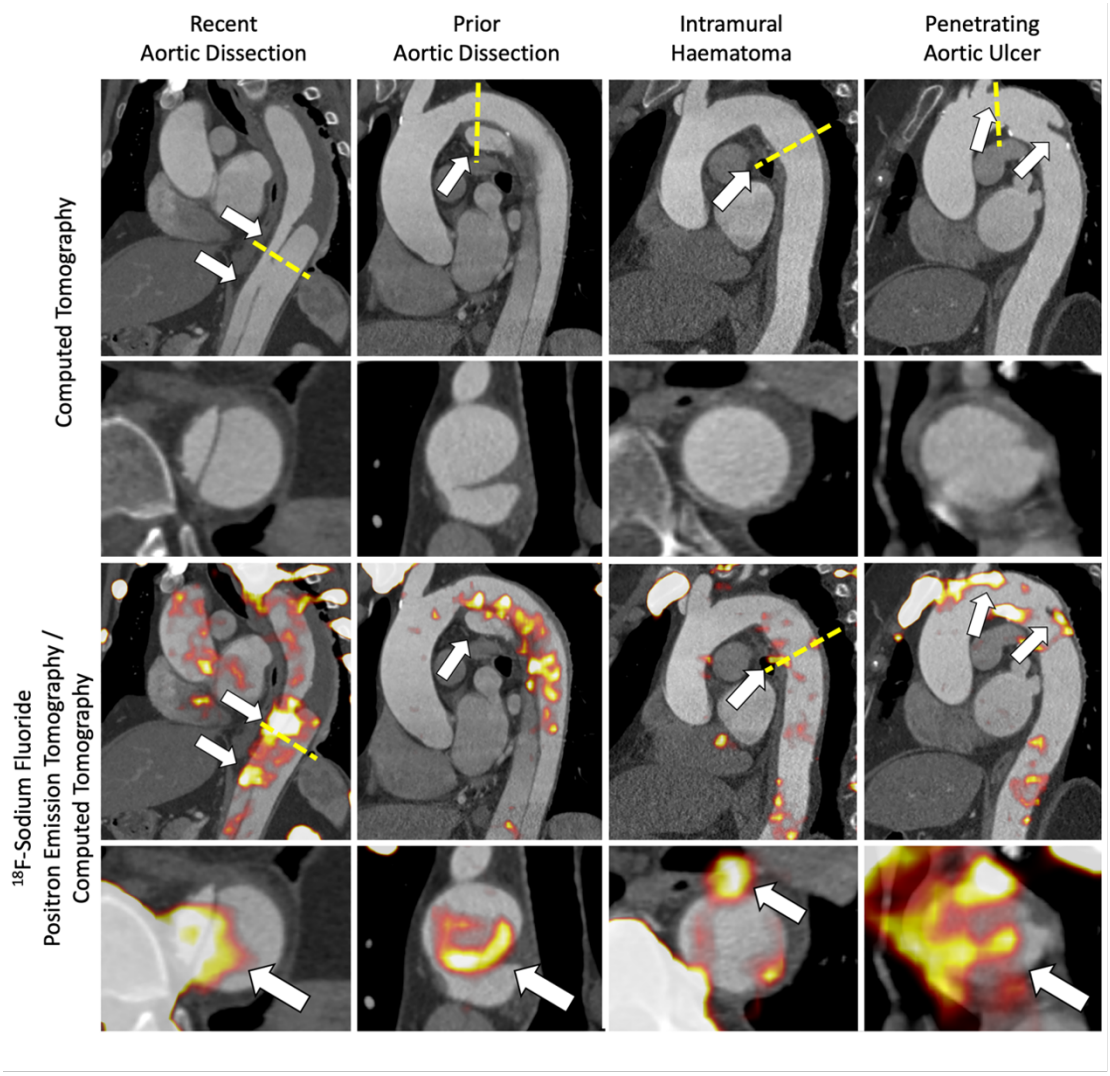

Figure 3.2: **Computed tomography angiography and combined ^{18}F-sodium fluoride positron emission tomography and computed tomography in patients with acute aortic syndrome.**

3.4.4 Subcategories of Acute Aortic Syndrome

Of the 56 recruited participants with acute aortic syndrome, 5 patients had an intramural haematoma, 42 patients had an aortic dissection and 9 patients had a penetrating aortic ul-

cer. Patients with aortic dissection were younger than those with intramural haematomas or penetrating aortic ulcers. The three groups were otherwise well matched for gender, body-mass index, aortic diameter and cardiovascular comorbidities. ^{18}F-Sodium fluoride PET/CT uptake was increased in all three subcategories of acute aortic syndrome compared to healthy controls (p<0.05, Table 3.2). Patients with recent acute aortic syndrome had similar ^{18}F-sodium fluoride uptake to those with long-standing disease (recent versus prior acute aortic syndrome (TBR±SD) 1.94±0.37 vs 2.04±0.51, p=0.497). Similarly, Stanford classification did not influence ^{18}F-sodium fluoride binding (TBR 1.98±0.49 for type A versus 2.00±0.44 for type B, p=0.851).

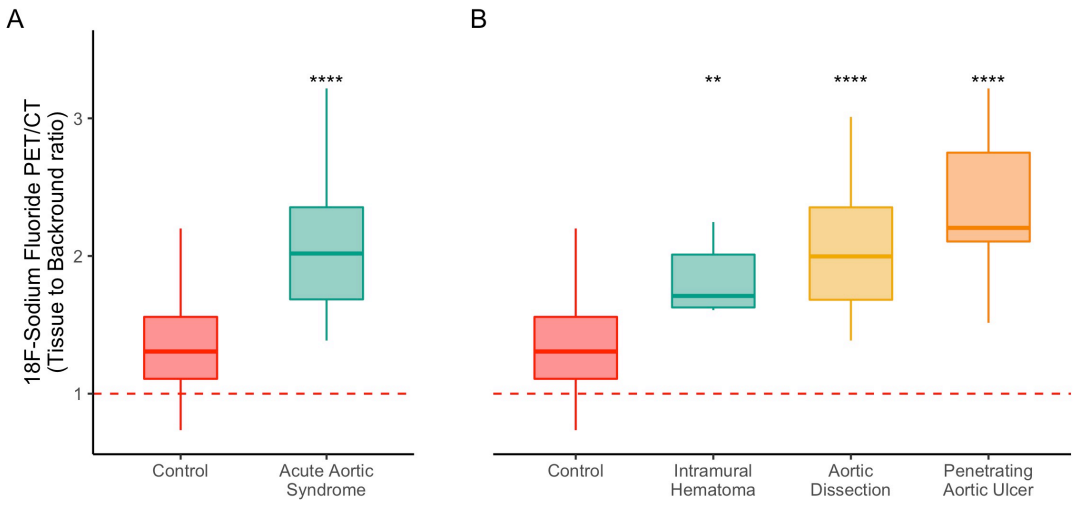

Figure 3.3: ^{18}**F-Sodium fluoride tissue-to-background ratio in subpopulations of patients with acute aortic syndrome.** (* = p < 0.05, *** = p < 0.001, **** = p < 0.0001).

3.4.5 Site of Intimal Disruption

In patients with Stanford type B acute aortic syndrome, ^{18}F-sodium fluoride uptake was seen at sites of intimal disruption compared to morphologically normal proximal aorta (median TBR$_{max}$: 1.61 [1.38-1.88] versus 1.18 [1.08-1.39] respectively; p<0.001; Figure 4). The percentage increase in ^{18}F-sodium fluoride uptake was greatest in penetrating aortic ulcers, followed by aortic dissection and thereafter intramural haematoma. Percentage increase in ^{18}F-sodium fluoride uptake at the site of intimal injury was similar in acute and

chronic disease (median percentage increase: 33.7 [24.7-37.4] % versus 31.3 [27.0-44.6] %; p=0.750).

3.4.6 Adverse clinical markers

Of the 18 patients with recent type B acute aortic syndrome, 10 patients presented with complicated disease. Of these, 6 patients encountered rapid expansion, 2 patients had resistant hypertension, 1 patient presented with impending aortic rupture and 1 patient presented with spinal cord ischaemia. ^{18}F-Sodium fluoride uptake was marginally increased in patients presenting with complicated disease however this did not reach statistical significance in this subgroup analysis (MDS TBRmax 2.02 $\pm$ 0.37 vs 2.29 $\pm$ 0.36; p=0.130). Similarly, there was no significant relationship between radiotracer uptake and visceral artery involvement (p=0.68), the distance of the entry tear from the left subclavian artery (R^2 = 0.01, p=0.98), the size of the entry tear (R^2 = 0.01, p=0.56) or the number of entry tears (1 entry tear vs >1 entry tear, n=19vs9, MDS TBR$_{max}$ 2.14 $\pm$ 0.30 vs 1.97 $\pm$ 0.42 respectively; p=0.246).

Table 3.2: **Binding of ^{18}F-sodium fluoride in acute aortic syndrome.** SUV, standardized up take value; TBR, tissue-to-background ratio; MDS, most diseased segment. Data presented as mean ± standard deviation or median [interquartile interval]. * p<0.05, compared to healthy controls.

	Whole Cohort		Subcategories of Acute Aortic Syndrome		
	Control (n=20)	Acute Aortic Syndrome (n=56)	Intramural Haematoma (n=6)	Aortic Dissection (n=41)	Penetrating Aortic Ulcer (n=9)
Aortic 18F-NaF binding (MDS SUVmax)	1.39 (0.73)	3.00 (0.98)*	2.59 (0.58)*	2.87 (0.68)*	3.87 (1.71)*
Aortic 18F-NaF binding (MDS TBRmax)	1.36 (0.39)	2.08 (0.45)*	1.78 (0.29)*	2.05 (0.42)*	2.38 (0.53)*
Proximal Aorta 18F-NaF TBR	-	1.18 [1.08, 1.39]	1.02 [1.01, 1.08]	1.17 [1.10, 1.28]	1.43 [1.21, 1.60]
At Intimal Disruption 18F-NaF TBR	-	1.61 [1.38, 1.88]	1.28 [1.23, 1.52]	1.43 [1.39, 1.68]	1.99 [1.74, 2.83]
Distal Aorta 18F-NaF TBR	-	1.31 [1.17, 1.44]	1.07 [0.99, 1.22]	1.31 [1.19, 1.34]	1.35 [1.24, 2.04]
Percentage increase in 18F-NaF at intimal disruption site vs healthy aorta	-	32.48% [24.78, 41.03]	19.73% [15.90, 46.90]	27.53% [25.14, 34.38]	44.64% [39.18, 62.86]

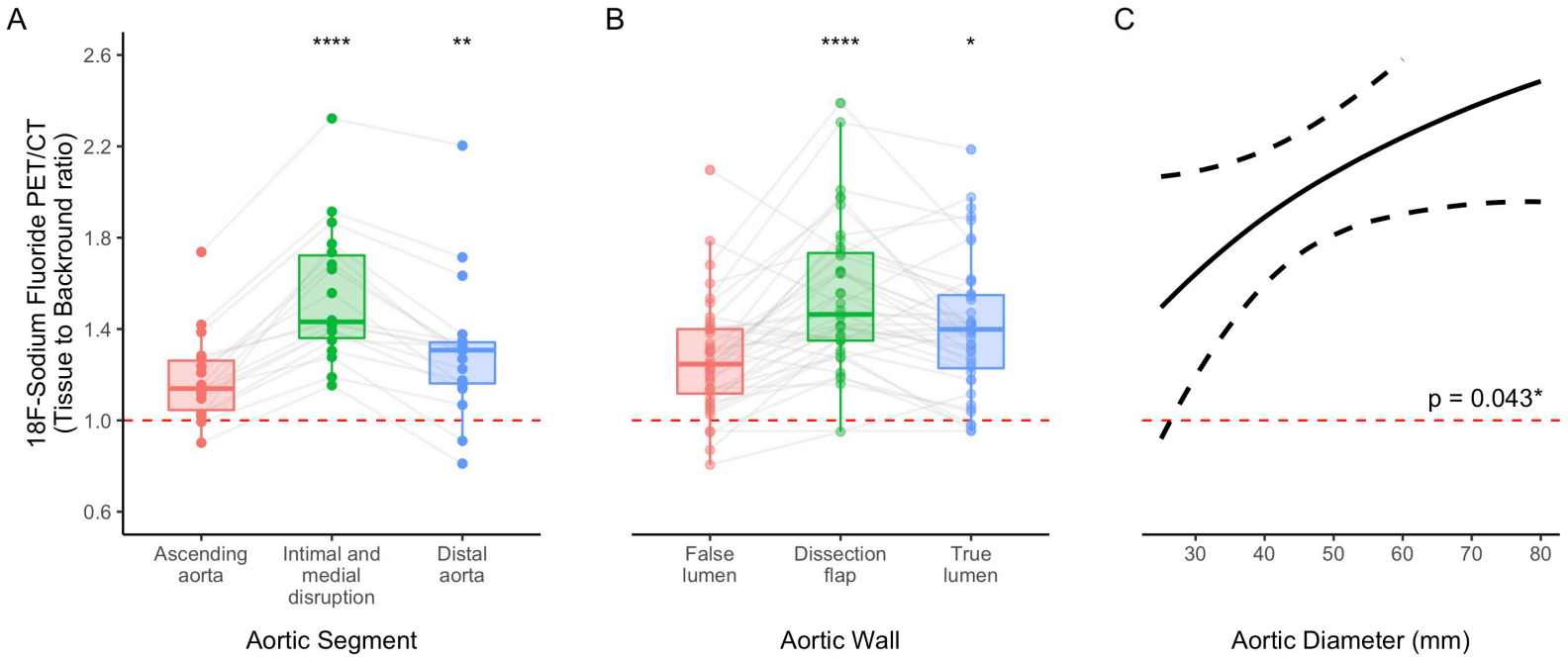

Figure 3.4: **Characteristics of ^{18}F-sodium fluoride binding in patients with acute aortic syndrome.** (**A**) ^{18}F-sodium fluoride binding at the site of intimal and medial disruption compared to proximal and distal aortic segments in patients with Stanford type B aortic dissection. (**B**) ^{18}F-sodium fluoride binding within different components of the aortic wall following aortic dissection. (**C**) Relationship between ^{18}F-sodium fluoride binding (log-transformed) and aortic diameter adjusted for age, sex, time from initial presentation to PET scan, and Stanford Classification. * = p < 0.05, *** = p < 0.001, **** = p < 0.0001

3.5 Discussion

This is the largest prospective positron emission tomography cohort study in patients with acute aortic syndrome and the first to characterize ^{18}F-sodium fluoride uptake. In this proof-of-principle study, we have demonstrated that there is increased aortic ^{18}F-sodium fluoride uptake which appears to vary by disease subtype. Moreover, ^{18}F-sodium fluoride uptake is particularly increased in diseased and pathological segments of the aorta, such as areas of intimal disruption and penetrating aortic ulcers. Radiotracer uptake is associated with aortic diameter and localizes to areas of medial disruption and microcalcification. We suggest that ^{18}F-sodium fluoride positron emission tomography holds potential promise as a marker of disease activity in acute aortic syndrome, which may predict future clinical outcome and guide patient management.

Acute aortic syndromes are a consequence of widespread degenerative changes within the aortic wall. Calcification is a common endpoint of aortic pathological processes that result from cellular destruction and the accumulation of intracellular material within the extracellular space (Aghagolzadeh et al. 2016). Two distinct pathological processes affect the aortic wall: atherosclerotic inflammatory changes within the intima and a chronic degenerative process weakening the aortic media. Both lead to vascular calcification (Fuery et al. 2017). Atherosclerosis is a focal intimal disease of macrophage-driven inflammation and cell death within a subendothelial lipid-rich necrotic core (Moore, Sheedy, and Fisher 2013; Syed et al. 2019). Conversely, medial degeneration is characterized by widespread dysregulation of the aortic extracellular matrix with collagen and elastin fibres losing their characteristic architecture (Mimler et al. 2019). Cellular density is decreased and cell death within the medial layer encourages phenotypical change of vascular smooth muscle cells favouring osteogenesis (Fuery et al. 2017). Atherosclerosis and medial degeneration are both characterized by the deposition of calcium phosphate crystals as precursors of calcified plaques (Fuery et al. 2017). We have confirmed that aortic tissue from patients with acute aortic syndrome had extensive medial degeneration and microcalcification: a pattern of medial disease that has been well described previously (Ahmadzadeh, Rausch, and Humphrey 2019). It is perhaps also important to highlight that we found microcalcification predominantly where elastin degeneration interfaces with adjacent healthier medial

wall. This probably underlies the ability of ^{18}F-sodium fluoride uptake to identify specific areas of disease activity that may be implicated in the initiation of the acute aortic syndrome.

We observed the greatest uptake of ^{18}F-sodium fluoride at the entry point and intimal tear of the aortic dissection. Patients with intramural haematomas and aortic dissections have apoptosis in the medial layer, potentially driven by an abnormally upregulated transforming growth factor-β pathway (Xu et al. 2001). This results in an aortic media devoid of cellular structures, pooling of glycoproteins, disorganization of the extracellular matrix and spillage of intracellular components within the extracellular space. These changes are observed throughout the vulnerable aorta and are most prominent at the site of intimal disruption (Sariola, Viljanen, and Luosto 1986). Foci of architecturally abnormal aortic media weakens the structural integrity of the aorta which is predisposed to tearing (Humphrey 2013). Tearing of the aorta is a profound vascular injury and may itself further accelerate calcification within the aortic wall (Yang et al. 2019). Our findings suggest that ^{18}F-sodium fluoride colocalizes to the site of intimal disruption in acute aortic syndrome although we cannot exclude that it may also detect the biological response to aortic injury.

Patients with penetrating aortic ulcers are typically comorbid and at high-risk of aortic complications if they become symptomatic (Geisbüsch et al. 2008). In these ulcers, aggressive atherosclerotic activity erodes through to the medial layer (Movsowitz et al. 1994). The effect is outpouching of a greatly weakened aortic wall that is prone to aortic dissection or rupture. This intense inflammatory response causes widespread cellular destruction and may explain why ^{18}F-sodium fluoride uptake was highest of all the subpopulations of acute aortic syndrome.

Our findings on the role of ^{18}F-sodium fluoride PET/CT in acute aortic syndrome mirror our earlier work on abdominal aortic aneurysms. The ^{18}F-Sodium Fluoride in Abdominal Aortic Aneurysm (SoFIA$_3$) study demonstrated that ^{18}F-sodium fluoride preferentially binds to diseased segments of abdominal aortic aneurysms (Forsythe et al. 2018). In both SoFIA$_3$ and the current study, individuals with aortopathy had greater ^{18}F-sodium fluoride uptake than healthy control subjects within the same vascular bed. Both studies have also found that ^{18}F-sodium fluoride uptake was independent of aortic size. In the SOFIA$_3$ study, we

had prolonged longitudinal follow up and we found that ^{18}F-sodium fluoride uptake was associated with aortic growth and was an independent predictor of aortic rupture or requiring surgical repair (Forsythe et al. 2018). This is the focus of the following chapter (**Chapter 4**).

Current strategies of long-term risk stratification of patients with aortic syndromes rely on anatomical characteristics rather than disease activity. Diameter is considered the strongest morphological predictor of aortic rupture. However, this unidimensional metric fails to capture the complex biological processes affecting the aortic wall. Aortic expansion is not linear and instead demonstrates a discontinuous staccato pattern of growth (Kurvers et al. 2004). Over half of patients with a subthreshold ascending aortic aneurysm (<5.5 cm) experience aortic rupture or dissection (Pape Linda A. et al. 2007). Conversely, many patients with larger aortas never rupture (Forsythe, Newby, and Robson 2016). We have demonstrated that PET/CT using ^{18}F-sodium fluoride allows us to detect aortic degeneration and informs us on the biological state of aortic tissue. Microcalcification occurs at a nanometre scale and is beyond the resolution of routine computed tomography or magnetic resonance imaging (Aghagolzadeh et al. 2016). This state of high biological activity is essentially silent. The non-invasive detection of microcalcification using ^{18}F-sodium fluoride PET/CT in patients with acute aortic syndrome therefore offers a major advantage to allow, for the first time, the identification and localization of destructive cellular processes affecting the aortic wall. The implications and ramifications of this will need to be further explored in future clinical studies.

We should acknowledge some limitations of our study. Intramural haematomas or penetrating aortic ulcers can evolve into aortic dissections and pathologies can co-exist. To standardize our analysis, we used the presenting diagnosis to determine aortic pathology. ^{18}F-Sodium fluoride PET/CT is associated with intense uptake of the radiotracer by bony structures such as the vertebrae and sternum. Overspill of tracer from these structures can therefore give a false impression of aortic uptake if this is not carefully excluded. Techniques to minimize or avoid overspill from bony ^{18}F-sodium fluoride uptake are in development (Akerele et al. 2019).

In conclusion, this single-centre study offers a proof-of-concept for ^{18}F-sodium fluoride

PET/CT in patients with acute aortic syndrome and demonstrates a potential application for the assessment of disease activity in these patients. Further investigation is warranted to determine whether this could predict acute aortic syndrome in those with aortopathies or be used to determine future clinical outcome in these potentially fatal conditions.

3.6 Clinical Perspectives

Aortic dissection, intramural haematomas and penetrating aortic ulcers are challenging conditions to treat owing to unpredictable disease progression and the significant consequences of intervention. Computed tomography angiography provides detailed anatomical information that is central to risk stratification in modern practice.

Positron emission tomography (PET) provides a unique insight into aortic wall biology. ^{18}F-Sodium fluoride PET is an emerging radiotracer that identifies microscopic calcification – an early biomarker of vascular injury. In a separate aortopathy, abdominal aortic aneurysms, ^{18}F-sodium fluoride PET/CT predicts aortic expansion and likelihood of requiring surgery or experiencing aortic rupture.

Our present study is the first description of ^{18}F-sodium fluoride PET/CT in patients with acute aortic syndrome. In this proof-of-concept study, we found that ^{18}F-sodium fluoride PET/CT binds to damaged segments of the aortic wall with greatest affinity at the site of intimal injury. This suggests that ^{18}F-sodium fluoride PET/CT can quantify and localize disease activity in patients with acute aortic syndrome, promising potential clinical applications in the risk stratification, clinical management and outcomes of these patients.

Multimodality imaging represents a holistic approach that integrates detailed morphological vessel assessment from computed tomography with the biological processes driving it. Future work will investigate the ability of ^{18}F-sodium fluoride PET/CT to improve risk prediction beyond conventional clinical and anatomical parameters in larger clinical cohorts.

Chapter 4

Risk-stratification using ^{18}F-sodium fluoride PET

4.1 Abstract

4.1.1 Background

Patients with aortic dissection or intramural haematoma experience rapid disease progression. We previously demonstrated increased uptake of ^{18}F-sodium fluoride in patients with acute aortic syndrome (**Chapter 3**).

4.1.2 Objective

In this longitudinal study, we aim to determine whether ^{18}F-sodium fluoride PET is associated with aortic disease progression and clinical outcomes in patients with aortid dissection or intramural haematomas.

4.1.3 Methods

Patients with aortic dissection or intramural haematomas and healthy controls underwent ^{18}F-sodium fluoride PET/CT and CT angiography of the aorta. ^{18}F-NaF uptake was measured at the most diseased segment of the aorta and the maximum value corrected for

background blood pool activity (maximum tissue-to-background ratio, TBR_{max}). Radiotracer binding was compared with change in aortic size, and major adverse aortic events (aortic rupture, aorta-related death or aortic repair) over 44.7($\pm$ 13) months.

4.1.4 Results

Overall, aortic growth occurred at a rate of +5.2 (95% CI 4.2 to 6.1) mm/yr but was influenced by the age of the acute aortic syndrome and intervention. ^{18}F-Sodium fluoride uptake in the false lumen was associated with aggressive aortic expansion (+7.1 (95% CI 1.7 - 13.1) mm/yr, p=0.011). ^{18}F-Sodium fluoride uptake in the outer aortic wall was independently associated with major adverse aortic events (hazard ratio 8.6 [95% CI, 1.1-68.1], p=0.041) adjusted for aortic diameter, time since acute aortic syndrome and clinical predictors.

4.1.5 Conclusion

In patients with acute aortic syndrome, ^{18}F-sodium fluoride uptake is associated with aortic growth and clinical events. ^{18}F-Sodium fluoride PET-CT holds promise as a non-invasive marker of disease severity and future risk in patients with acute aortic syndrome.

4.2 Introduction

Acute aortic syndrome comprises a range of potentially catastrophic conditions resulting from weakening in the elastic connective tissue of the aortic wall. Separation and fragmentation of aortic medial tissue can lead to contained hemorrhage resulting in an intramural hematoma exposing the aortic media to high systolic pressure that may permit ingress of blood resulting in an aortic dissection. This damaged aorta is prone to aneurysmal dilatation and rupture leading to severe and often fatal bleeding (Evangelista et al. 2018).

It is difficult to predict aortic expansion or rupture following acute aortic syndrome. The current surveillance pathway relies on assessing aortic morphology and size with computed tomography (CT) or magnetic resonance imaging (MRI). Despite intensive blood

pressure control and advances in endovascular surgery, the 3-year mortality from acute aortic syndrome remains unacceptably high at approximately 25% (X. Yuan et al. 2019).

The in-situ detection of pathobiological processes that drive morphological change holds great promise for risk prediction. Medial degeneration of the aortic wall is associated with abnormal reparative responses including the precipitation of calcium phosphate-rich crystals. The resultant microcalcification signifies a biologically active state (Wanga et al. 2017) that may be a marker of vascular injury. Positron emission tomography (PET) can be used to assess calcification activity and the biological state of aortic tissue beyond anatomical imaging alone. We have previously shown that ^{18}F-sodium fluoride PET detects atherosclerotic microcalcification and offers a novel approach to quantify vascular injury and disease activity (Irkle et al. 2015; Dweck, Rudd, and Newby 2014; Kwiecinski et al. 2020; Forsythe et al. 2018).

In this proof-of-concept study, we aimed to establish the association of ^{18}F-sodium fluoride PET/CT uptake in patients with acute aortic syndrome with disease disease progression and clinical outcomes.

4.3 Methods

The aim of this study was to evaluate the role of ^{18}F-sodium fluoride PET/CT as a means to predict aortic expansion and major adverse aortic events in patients with the fastest evolving pathologies, aortic dissection and intramural haematoma.

Detailed methodology has been summarised in **Chapter 2**. Briefly, this study reports longitudinal outcomes from the cohort recruited to our study characterising ^{18}F-sodium fluoride PET/CT in patients with acute aortic syndrome (**Chapter 3**). As earlier, ethical approval for the study as obtained by the East of Scotland Research Ethics Service (reference 18/ES/0070) and the study was registered in an open-source prospective database (NIH ClinicalTrials.gov, NCT 03647566). The study population consisted of patients over the age of 25 years with acute aortic syndrome and were categorised as having *recent* or *prior* disease as determined by a 12 week threshold from symptom onset to recruitement to the study. All patients underwent a clinical examination, ^{18}F-sdoium fluoride PET/CT

and CT angiography of the aorta at recruitement. The most diseased segment maximum tissue-to-background ratio method was used to quantify ^{18}F-sodium fluoride binding in the whole aorta and within each component of the aortic wall, namely the dissection flap, the wall adjacent to the true lumen and the wall adjacent to the false lumen.

Serial aortic diameter measurements were made from all prospective and retrospective CT angiograms hosted on a comprehensive Picture Archiving and Communication System (PACS). Again, the maximum aortic diameter was measured using centreline reconstruction of aortic segments affected by acute aortic syndrome. Change in aortic diameter was the primary endpoint of the longitudinal study. This was determined relative to aortic diameter at presentation or after intervention. A linear regression model was fitted to serial aortic diameter measurements against ^{18}F-sodium fluoride PET/CT uptake, time since initial presentation, endovascular therapy, open surgical repair.

Major adverse aortic events were defined as a composite of aortic repair, aortic rupture or aorta-related death. All endpoints were adjudicated by consensus of a clinical endpoint committee consisting of three independent vascular clinicians. Major adverse aortic events was the secondary endpoint of this study. Follow-up was censored at 10th November 2020 or at the time of event. A median threshold TBR$_{max}$ of 1.41 was used to dichotomise patients in to "high" and "low" ^{18}F-sodium fluoride groups. Kaplan-Meier analysis was performed to compare major adverse outcome events between ^{18}F-sodium fluoride groups. A proportional hazards Cox regression model was developed to study ^{18}F-sodium fluoride uptake with respect to major adverse aortic events, adjusted for participant age, sex, smoking status, maximum aortic diameter, aortic pathology, time from index acute aortic syndrome to PET scan and Stanford classification.

Baseline characteristics of patients and healthy controls are presented as mean ($\pm$ standard deviation) or median [interquartile interval] as appropriate. Normally distributed continuous variables were compared using a Students' t-test. Chi-square or Fisher's exact tests were used to compare categorical variables. Statistical analysis was performed in R, version 4.1.1 (R Foundation for Statistical Computing, Vienna, Austria). A two-tailed p-value less than 0.05 was considered statistically significant. The primary author had full access to all data in the study and takes responsibility for its integrity and analysis.

4.4 Results

4.4.1 Study Population

There are two components to this study. The first focuses on a subset of the study population reported in **Chapter 3** consisting only of patients with *aortic dissection* or *intramural haematoma*. Again, all patients with these pathologies were included in the analysis. For completeness, results for the entire study population are also included. The study population consisted of predominantly elderly men, half of whom reported a current or prior smoking habit (Table 4.1).

4.4.2 Aortic Growth

Maximum aortic diameter was obtained from 356 CT angiograms performed over a period of 93.4 (95% CI 68.4 to 118.4) months. Of these, 41 (11.5%) measurements were taken after patients had received endovascular therapy and 85 (23.9%) measurements were taken after open surgery. Mean aortic diameter at presentation for study participants was 46.1($\pm$ 11.6)mm. Aortic diameter gradually increased over time in patients with aortic dissection but regressed in patients with intramural haematomas. Patients with intramural haematomas experienced late aortic expansion beyond 2 years from the initial event (Figure 4.1).

Linear regression analysis for change in aortic diameter demonstrated that ^{18}F-sodium fluoride PET/CT uptake in the false lumen and time since presentation with acute aortic syndrome were associated with aortic growth (Table 4.2). Endovascular therapy resulted in regression of aortic diameter (Figure 4.2A). A similar trend was seen for patients who had received open surgical repair, but this did not reach statistical significance.

The unadjusted change in aortic diameter in the entire cohort was +5.2 (95% CI 4.2 to 6.1) mm/year. The mean adjusted change in aortic diameter was +7.1 (95% CI 5.8 to 8.4) mm/year in patients who received medical therapy alone, +5.9 (95% CI 3.6 to 8.2) mm/year following open surgery, +1.1 (95% CI -2.1 to 4.4) mm/year following endovascular therapy, and -0.1 (-3.9 to 3.8) mm/year following both open and endovascular repair (Figure 4.2B).

Table 4.1: Patient Characteristics

		Patients with Acute Aortic Syndrome (n=47)
Demographics	Age (years)	63 [53 to 70]
	Male (%)	35 (74.5)
	Body Mass Index (kg/m2)	28.8 ± 5.1
	Systolic Blood Pressure (mmHg)	128 ± 17
	Diastolic Blood Pressure (mmHg)	72 ± 11
	Heart Rate (beats per minute)	64 ± 10
	Smoking Habit (%)	
	Non-Smoker	24 (51%)
	Ex-Smoker	18 (38%)
	Smoker	5 (11%)
	Alcohol Consumption (any)	24 (51%)
Aortic Characteristics	Aortic Diameter (mm)	47.1 [41.4 to 49.5]
	Pathology (%)	
	Intramural Hematoma	5 (11%)
	Aortic Dissection	42 (89%)
	Stanford Type B Classification (%)	28 (60%)
	Recent Acute Aortic Syndrome (%)	22 (47%)
	Prior Acute Aortic Syndrome	25 (53%)
Past Medical History	Hypertension (%)	44 (94%)
	Ischemic heart disease (%)	6 (13%)
	Cerebrovascular disease (%)	6 (13%)
	Diabetes Mellitus (%)	2 (4%)
	Hypercholesterolemia (%)	12 (26%)
	Connective Tissue Disease (%)	5 (11%)
Medications	Beta Blocker (%)	43 (92%)
	ACE inhibitor (%)	24 (51%)
	Statin (%)	28 (60%)
	Antiplatelet Agent (%)	22 (47%)
	Anticoagulation (%)	14 (30%)

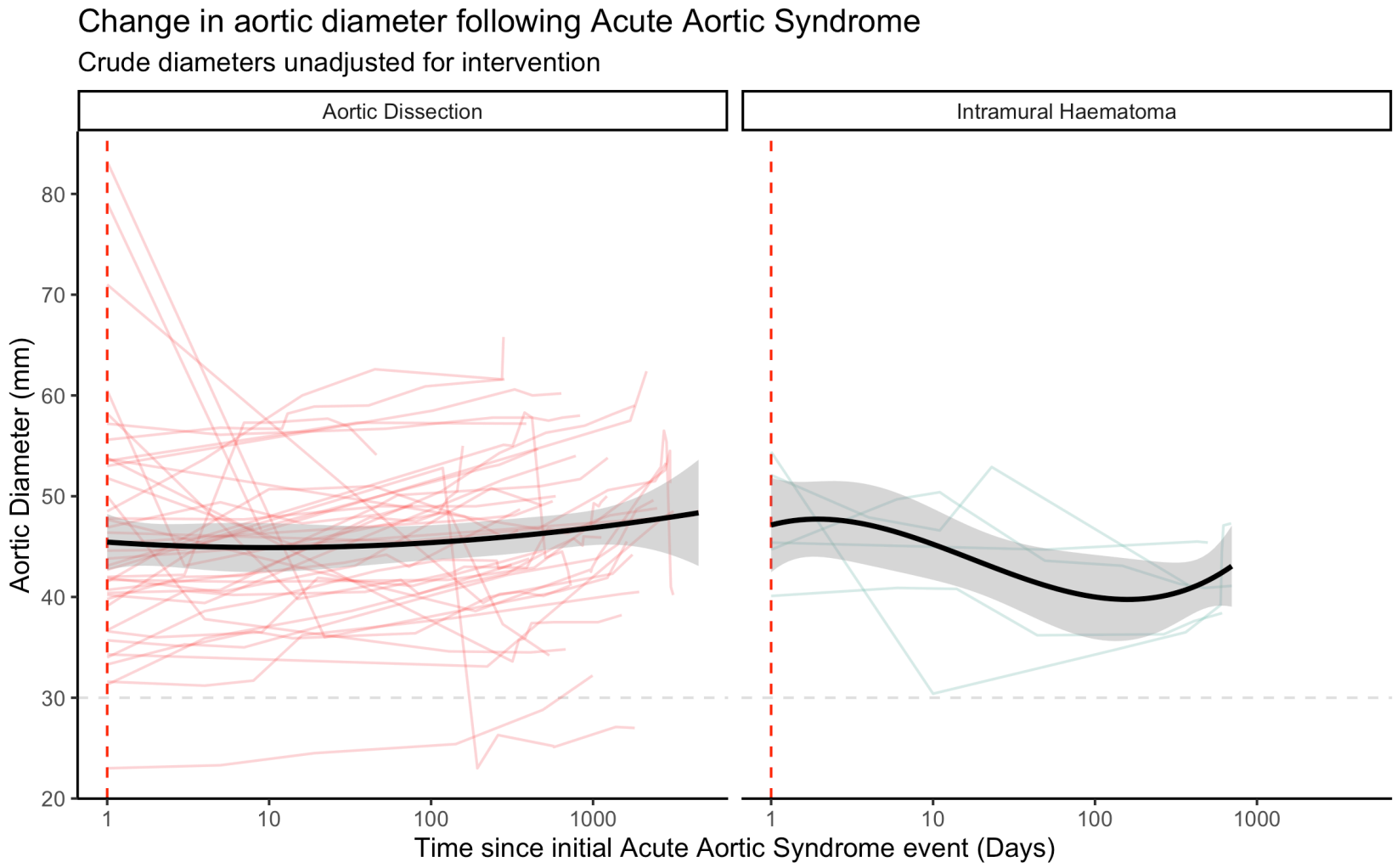

Figure 4.1: **Aortic diameter with respect to time in patients with acute aortic syndrome.** Crude values.

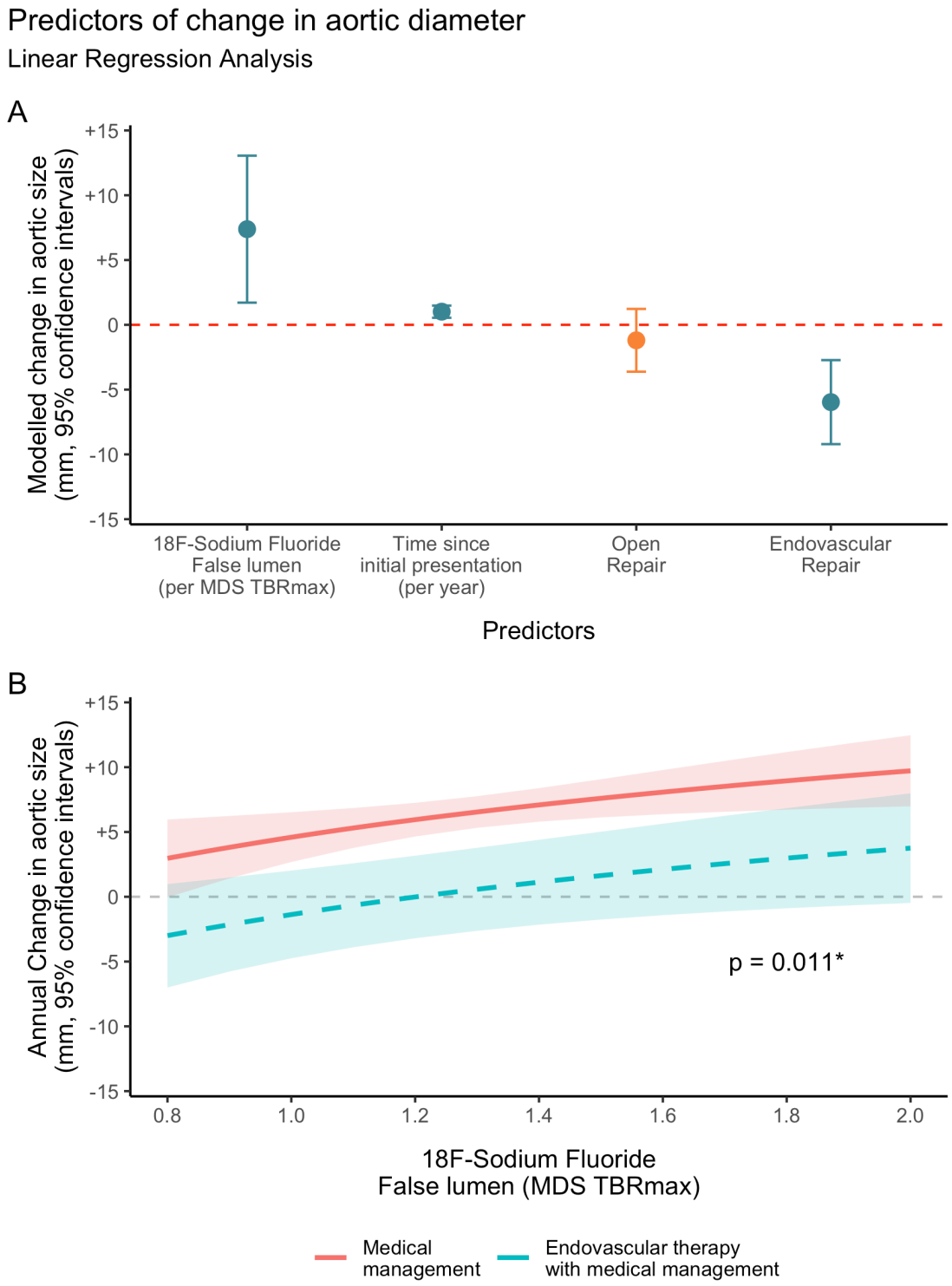

Figure 4.2: **Change in aortic size in relation to ^{18}F-sodium fluoride uptake in the false lumen.** (**A**) A linear regression model to investigate change in aortic size against ^{18}F-sodium fluoride uptake in the false lumen (log-transformed), duration since initial presentation with acute aortic syndrome (log-transformed), open surgical repair and endovascular repair. (**B**) The estimated aortic growth trajectory with increasing false lumen ^{18}F-sodium fluoride uptake in a model patient 1 year following acute aortic syndrome treated by either antihypertensives alone (**red**) or in conjunction with endovascular therapy (**blue**).

Table 4.2: **Change in maximum aortic diameter in relation to ^{18}F-Sodium Fluoride uptake within the aortic wall.** Linear regression analysis. Crude model includes ^{18}F-Sodium Fluoride uptake alone. Adjusted models also include time since presentation with acute aortic syndrome (log-transformed), endovascular repair and open repair.

	Crude Model			Adjusted Model		
Most Diseased Segment Tissue-to-Background ratio (log-transformed)	Beta estimate	95% Confidence Interval	p-value	Beta estimate	95% Confidence Interval	p-value
Whole aorta	0.5	(-4.1 to 5.1)	0.831	-0.8	(-5.1 to 3.6)	0.722
Outer aortic wall	3.0	(-2.1 to 8.0)	0.253	3.3	(-1.4 to 8.1)	0.169
Wall adjacent to true lumen	1.8	(-3.1 to 6.7)	0.461	2.4	(-2.2 to 7)	0.299
Wall adjacent to false lumen	9.1	(3.3 to 14.9)	0.002*	7.1	(1.7 to 13.1)	0.011*
Dissection flap	1.7	(-3.8 to 7.3)	0.541	0.1	(-5.3 to 5.4)	0.987

4.4.3 Adverse Aortic Events

The mean follow-up duration from ^{18}F-sodium fluoride PET/CT scan was 14.6 (95% CI 12.4 to 16.7) months. During this period, 12 (25.5%) patients encountered major adverse aortic events. Of these, two patients experienced aortic rupture and subsequent death. Open surgical repair was necessary in 8 patients and 2 patients required delayed endovascular stenting.

4.4.3.1 Patients with aortic dissection or intramural haematoma only

Patients with recent acute aortic syndrome had increased ^{18}F-sodium fluoride uptake in the outer wall of the aorta (Figure 4.3A, MDS TBR$_{max}$ 1.37 [1.19 to 1.55] vs 1.50 [1.40 to 1.85], p = 0.007). The median MDS TBR$_{max}$ of the outer wall was 1.41 and this was used to dichotomize patients into low and high ^{18}F-sodium fluoride uptake groups. Patients with recent acute aortic syndrome and high ^{18}F-sodium fluoride uptake in the outer aortic wall of the true lumen were at greater risk of encountering a major adverse aortic event than the remaining cohort (Figure 4.3B, log rank p < 0.001). A proportional hazards Cox regression model found that ^{18}F-sodium fluoride uptake in the aortic wall predicted major adverse aortic events in patients with aortic dissection or intramural hameatoma, but not when penetrating aortic ulcers were included in this cohort (Table 4.3).

4.4.3.2 Patients with aortic dissection, intramural haematoma or penetrating aortic ulcers

^{18}F-Sodium fluoride uptake was associated with major adverse aortic events in patients with recent acute aortic syndrome when the entire cohort of patients recruited to the original study were included. This consisted of patients with aortic dissection, intramural haematoma *or* penetrating aortic ulcers. Patients with recent acute aortic syndrome had an increased likelihood of experiencing major adverse aortic events when radiotracer uptake in the outer wall were stratified in halves or tertiles (Figure 4.4A-C). This relationship approached statistical significance when stratifying the entire cohort by median outer wall TBR$_{max}$ (Figure 4.4D).

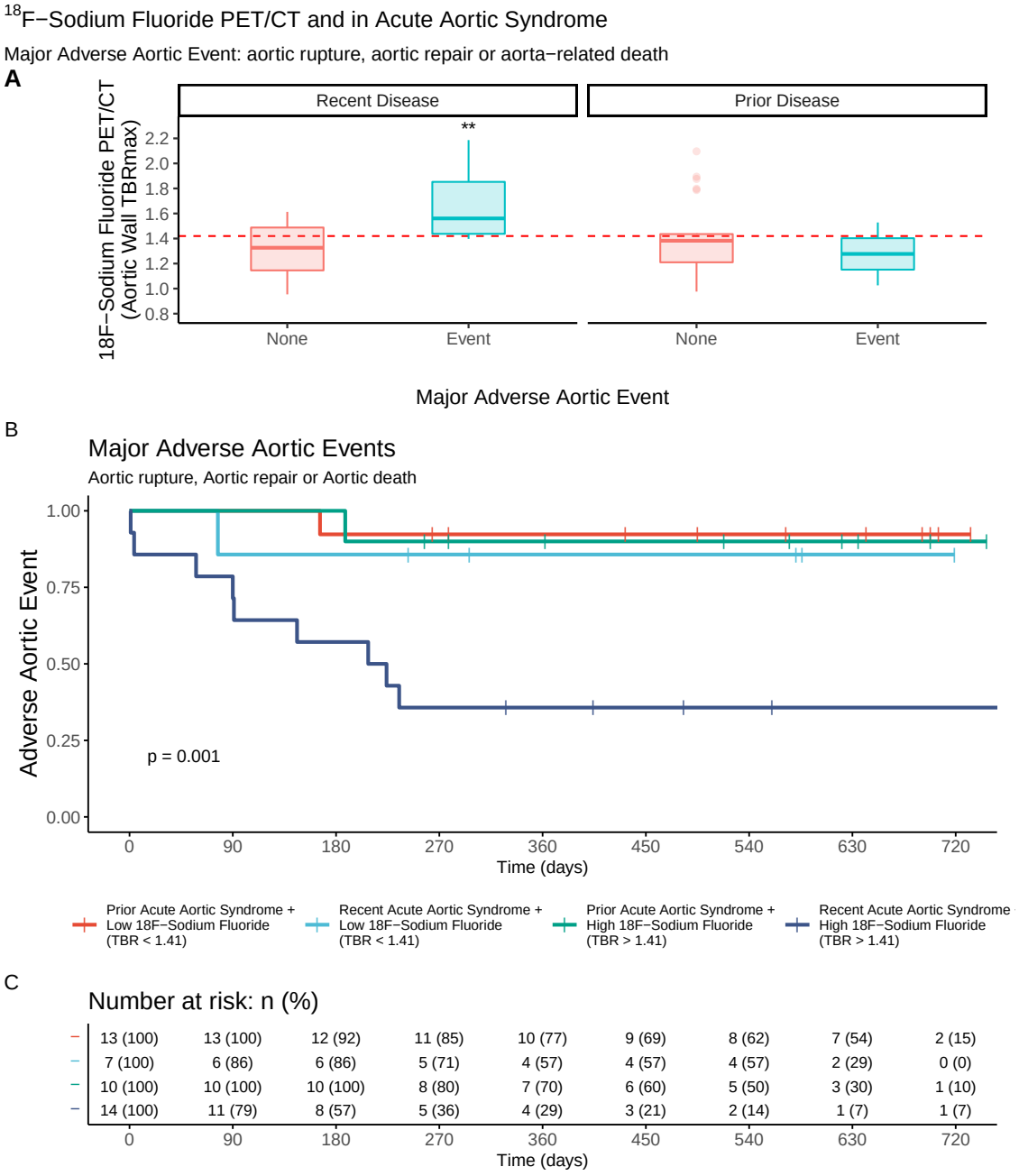

Figure 4.3: **Major adverse aortic events (aortic rupture, aortic repair or aorta-related death) following acute aortic syndrome.** (**A**) True lumen ^{18}F-sodium fluoride uptake in patients that experienced major adverse aortic events stratified by phase of disease. (**B**) Kaplan Meier estimates of major adverse aortic events following ^{18}F-sodium fluoride PET/CT scan stratified by phase of disease and aortic outer wall ^{18}F-sodium fluoride uptake category (using a threshold of TBR$_{max}$ 1.41). *** = p < 0.001

Table 4.3: **Major adverse aortic events in relation to ^{18}F-Sodium Fluoride uptake within the aortic wall.** Cox proportional hazard survival analysis. Crude model includes ^{18}F-Sodium Fluoride uptake alone. Adjusted models also include participant age, sex, smoking status, maximum aortic diameter, aortic pathology, time from index acute aortic syndrome to PET scan (log-transformed), and Stanford classification. MDS TBRmax = Most Diseased Segment Tissue-to-Background ratio, AD = Aortic dissection, IMH = Intramural haematoma, PAU = Penetrating aortic ulcer.

	MDS TBRmax		Crude Model			Adjusted Model		
	No Event (n=35)	Event (n=12)	Hazard Ratio	95% Confidence Interval	p-value	Hazard Ratio	95% Confidence Interval	p-value
AD and IMH only								
Whole aorta	1.98±0.4	2.11±0.3	1.6	(0.5 to 5.7)	0.437	2.4	(0.5 to 10.9)	0.265
Outer wall	1.38±0.3	1.59±0.3*	5.4	(1.0 to 29.2)	0.051	8.6	(1.1 to 68.1)	0.041*
Wall adjacent to true lumen	1.36±0.2	1.59±0.3*	7.2	(1.2 to 41)	0.027*	8.4	(1.1 to 63.6)	0.039*
Wall adjacent to false lumen	1.26±0.2	1.32±0.2	2.1	(0.2 to 19.3)	0.515	3.9	(0.2 to 73.6)	0.359
Dissection flap	1.51±0.3	1.67±0.3	3	(0.5 to 17.7)	0.224	3.6	(0.5 to 28)	0.228
AD, IMH and PAU								
Whole aorta	2.03±0.4	2.19±0.4	1.7	(0.6 - 4.8)	0.343	2	(0.7 - 6)	0.228
Outer wall	1.46±0.4	1.71±0.6	1.8	(0.8 - 4)	0.148	1.8	(0.7 - 4.3)	0.219

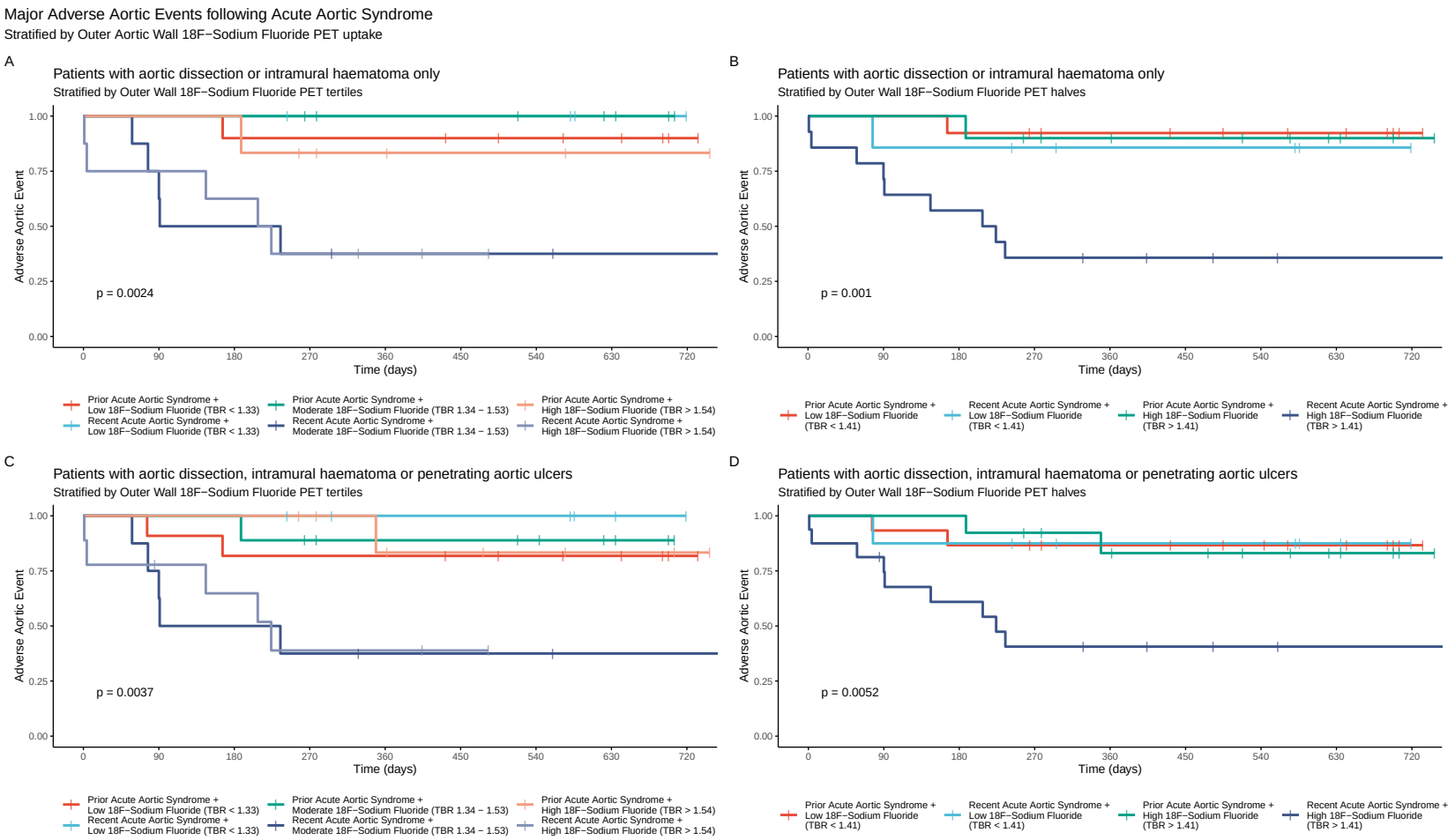

Figure 4.4: **Major adverse aortic events in patients with acute aortic syndrome.** Outcomes reported in patients with aortic dissection or intramural haematoma alone (**A, B**) and in the entire cohort (**C, D**). ^{18}F-Sodium fluoride binding in the outer aortic wall was stratified in tertiles (**A, C**) and halves (**B, D**).

4.4.4 Follow-up ^{18}F-sodium fluoride imaging

A preliminary comparison of baseline and follow-up 18F-sodium fluoride PET imaging found that radiotracer uptake was similar between scans (Figure 4.5). The mean interval between baseline and follow-up scans was 11.2 months. A total of 38 patients returned for follow-up imaging. Follow-up imaging was conducted during the COVID pandemic and the majority of patients lost to follow-up during this period were due to concerns related to visiting hospitals. Two patients passed away during the surveillance period and a further 4 had major open aortic surgery replacing their entire aorta.

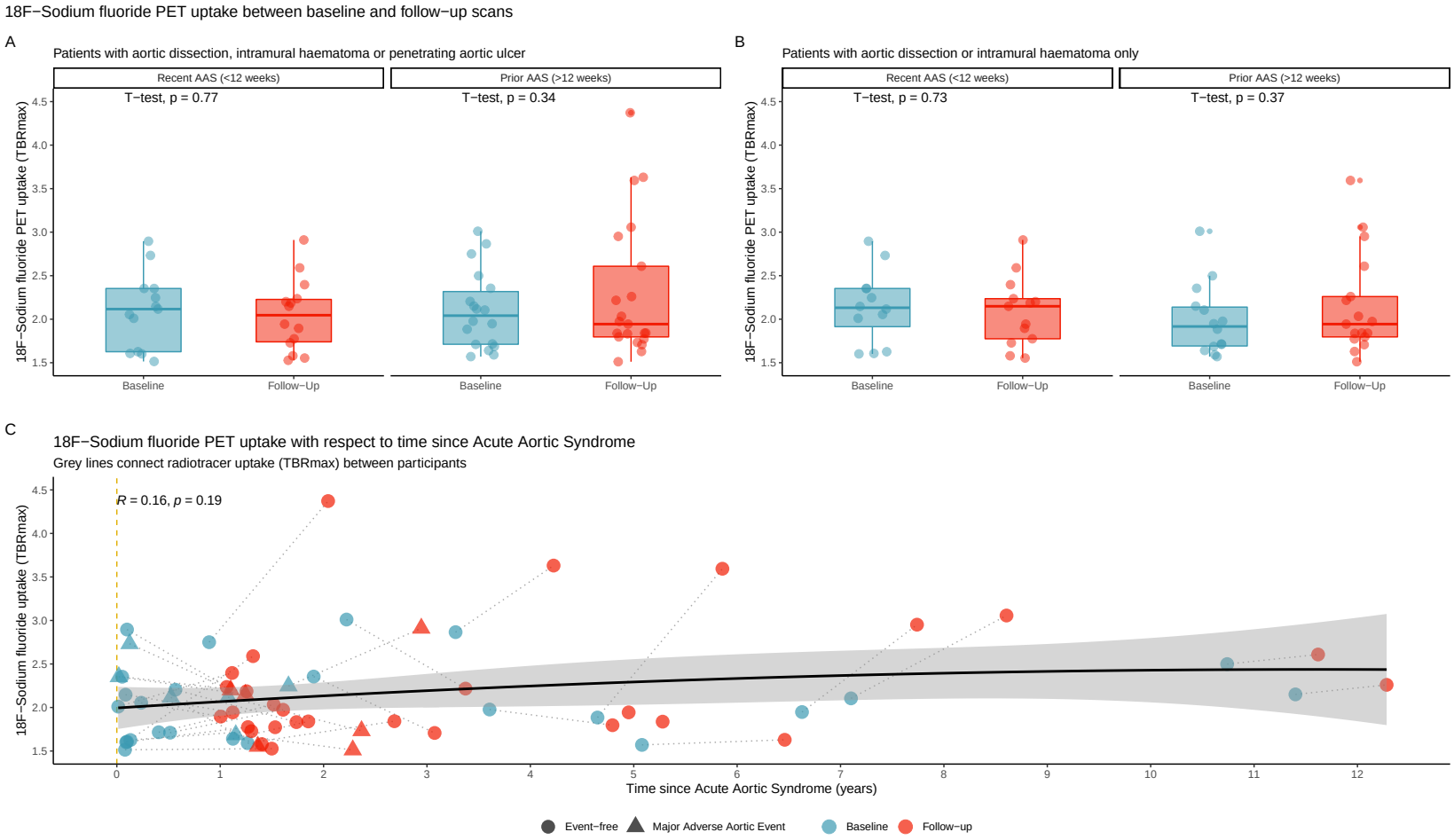

Figure 4.5: **A comparison of 18F-sodium fluoride binding between baseline and follow-up scans in patients with acute aortic syndrome.** Radiotracer binding was similar across groups in patients with aortic dissection or intramural haematoma alone (**A**) or the entire cohort which also included patients with penetrating aortic ulcers (**B**). There was no significant difference between radiotracer binding and the time since acute aortic syndrome when pooled analysis of baseline and follow-up ^{18}F-sodium fluoride uptake was performed (**C**).

4.5 Discussion

Having have previously described increased ^{18}F-sodium fluoride PET uptake in patients with acute aortic syndrome (**Chapter 3**), we now present findings related to disease progression in patients with aortic dissection or intramural haematoma. These are two rapidly evolving pathologies in patients with acute aortic syndrome and have a clear onset. Even with a modest sample size, aortic ^{18}F-sodium fluoride uptake is associated with disease progression and adverse clinical outcome, especially in those with a recent onset of disease. We suggest that ^{18}F-sodium fluoride PET holds promise as a marker of disease activity in acute aortic syndrome, which may predict future clinical outcome and guide patient management.

As described earlier, cellular death within the aortic wall leads to calcification. Cellular injury may be caused by atherosclerosis or by medial degeneration. Indeed, both pathological processes may lead to acute aortic syndrome. Cell death leads to the extracellular accumulation of calcium which triggers pathological differentiation of smooth muscle cells to adopt an osteoblastic phenotype, up-regulation of matrix metalloproteinases, reduction in cellular density and disruption of the medial architecture (**Chapter 1**). We initially found that patients with acute aortic syndrome had increased ^{18}F-sodium fluoride uptake and this may be a marker of cellular injury in the most vulnerable sections of the aorta. We now report that the burden of cellular injury in the aortic wall, as detected by ^{18}F-sodium fluoride PET, is associated with disease progression.

Aortic growth following acute aortic syndrome is complex. Sudden weakening of the aortic wall causes extreme aortic expansion in the acute and subacute phases. Beyond this period, we found that the rate of aortic growth slows but remains substantial. In addition, we found that endovascular or open repair further influences the rate of aortic growth in our cohort. Predicting change in aortic growth is thus challenging. We defined specific growth periods bordered by disease initiation and intervention to address this issue. Aortic expansion during these growth periods was more uniform. Our study found that ^{18}F-sodium fluoride uptake in the false lumen was independently associated with increasing aortic diameter. This remained true after adjusting for the duration since initial presen-

tation with acute aortic syndrome and intervention, suggesting that ^{18}F-sodium fluoride detects the most vulnerable aortas which are susceptible to aortic growth.

The outer wall of the false lumen contains a relatively small proportion of the aortic wall thickness. The majority of this aortic wall is contained away within the dissection flap. This perhaps explains why ^{18}F-sodium fluoride uptake within the outer wall of the false lumen appears to be lower than other components of the aortic wall. However, it is this weaker false lumen outer wall that is prone to expansion. We have found that ^{18}F-sodium fluoride PET can still identify diseased sections of the aortic wall adjacent to the false lumen despite the relatively low radiotracer signal intensity in this segment.

We observed a substantial rate of major adverse aortic events despite the modest sample size. Major adverse aortic events occurred predominantly in patients who had recently experienced acute aortic syndrome. Interestingly, 83% of major adverse aortic events occurred in patients with ^{18}F-sodium fluoride uptake above the median TBR$_{max}$ threshold of 1.41 in the aortic wall compared to only 2 patients below this level. Additionally, ^{18}F-sodium fluoride uptake was the only significant predictor of major adverse aortic events in a survival model that also included conventional clinical metrics such as aortic diameter, participant age and phase of disease. The ability of ^{18}F-sodium fluoride PET to provide independent risk stratification in patients with acute aortic syndrome is both remarkable and encouraging.

^{18}F-Sodium fluoride uptake in different components of the aortic wall is associated with specific aspects of disease progression. ^{18}F-Sodium fluoride activity in the false lumen was associated with aortic expansion. Indeed, this segment of aorta is prone to aneurysmal dilatation and ultimately rupture. In contrast, ^{18}F-sodium fluoride uptake in the whole aorta was associated with major adverse aortic events. This represents vascular injury to the full thickness of the aortic wall and likely better reflects global cardiovascular disease burden. Furthermore, we observed peak ^{18}F-sodium fluoride activity in other segments of the aorta that were unaffected by the acute aortic syndrome disease process. The whole aorta MDS TBR$_{max}$, however, was not associated with disease progression. This is perhaps not surprising as biological activity within the affected aortic segment likely drives disease progression. Interestingly, the age of acute aortic syndrome did not influence ra-

diotracer uptake. This may be related to a survival bias since those with the highest or the most progressive aortic MDS TBR$_{max}$ are less likely to survive in the longer term.

Our current findings mirror our earlier work on abdominal aortic aneurysms. The ^{18}F-Sodium Fluoride in Abdominal Aortic Aneurysm (SoFIA$_3$) study (Forsythe et al. 2018) demonstrated that ^{18}F-sodium fluoride colocalised with diseased segments of the aorta. Similarly, we have found that ^{18}F-sodium fluoride uptake is associated with aortic growth in both major aortopathies and has potential to improve risk stratification for major adverse aortic events beyond aortic size and other established risk factors.

Current strategies of long-term risk stratification of patients with aortic syndromes rely on anatomical characteristics rather than disease activity. Diameter is considered the strongest morphological predictor of aortic rupture. Aortic size at presentation is unable to stratify risk (G. Wang et al. 2021) in patients with acute aortic syndrome unless the aorta has already reached an aneurysmal size. Other morphological features such as partial thrombosis of the false lumen, size of the intimal disruption and morphology of the dissection flap are reported to stratify disease progression with mixed results (Ge et al. 2013; Watanabe et al. 2019; Schmitto et al. 2010; Wu et al. 2018). We have demonstrated that PET/CT using ^{18}F-sodium fluoride allows us to detect aortic degeneration and informs us on the biological state of aortic tissue.

We acknowledge limitations of our study. First, degenerative aortopathy disproportionately affects males and this demographic distribution is reflected in our patient cohort. Patient sex did not appear to influence ^{18}F-sodium fluoride uptake in our cohort but the inclusion of women was low. Second, techniques to minimize or to avoid overspill of ^{18}F-sodium fluoride from bony structures are in development (Akerele et al. 2019) and are not currently available for widespread. Third, there is no international consensus for intervention in thoracic aortopathy. In our study, surgical intervention was at the discretion of clinicians and although they were blinded to ^{18}F-sodium fluoride PET findings, variation in the surgical management of acute aortic syndrome may influence the relationship between ^{18}F-sodium fluoride uptake and major adverse aortic events. Finally, longitudinal data on disease progression and clinical outcomes in a larger, more homogenous cohort are now required to confirm whether ^{18}F-sodium fluoride PET/CT offers a predictive ad-

vantage over traditional clinical risk factors and anatomical imaging.

In conclusion, this single-centre study offers a proof-of-concept for ^{18}F-sodium fluoride PET/CT in patients with acute aortic syndrome and demonstrates a potential application for risk stratification in these patients by detecting disease activity. Our findings suggest that ^{18}F-sodium fluoride PET/CT is associated with aortic growth and may identify those at risk of major adverse aortic events. Further investigation is warranted to confirm whether ^{18}F-sodium fluoride PET/CT can predict future clinical outcomes so that we can intervene earlier to improve outcomes in this often fatal condition.

4.6 Clinical Perspectives

Predicting disease progression in patients with acute aortic syndrome is challenging. ^{18}F-Sodium fluoride PET/CT is associated with disease progression and may play a role in risk stratification. ^{18}F-Sodium fluoride PET/CT is a non-invasive multimodality imaging technique that detects vascular injury in patients with acute aortic syndrome. Radiotracer uptake in the false lumen is associated with aortic expansion. ^{18}F-Sodium fluoride PET activity in the damaged aorta is associated with major adverse aortic events when performed in the first 12 weeks. Future studies in larger homogenous cohorts are now required to establish the clinical utility of ^{18}F-sodium fluoride PET/CT in patients with acute aortic syndrome.

Chapter 5

Plasma desmosine in acute aortic syndrome

5.1 Abstract

5.1.1 Background

Acute aortic syndrome is a catastrophic condition resulting in rapid aortic expansion and potential vessel rupture. Its diagnosis requires computed tomography, often in critically unwell patients. Desmosine is a cross-linking structural molecule specific to mature elastin. It is released in the plasma of patients with aortopathy. We investigate plasma desmosine concentrations in patients with acute aortic syndrome.

5.1.2 Methods

Plasma desmosine concentration was compared between patients with acute aortic syndrome and propensity score-matched healthy controls. A cubic polynomial regression model was used to model plasma desmosine concentration with respect to time since acute aortic syndrome after adjusting for age, gender, body mass index, diastolic blood pressure and smoking history. Plasma desmosine was also investigated with respect to aortic diameter and vessel calcification. A linear regression model was used to investi-

gate aortic growth with respect to plasma desmosine after correcting for aortic diameter, Agatston score, time since acute aortic syndrome and surgical intervention.

5.1.3 Results

Fifty-three patients with acute aortic syndrome were matched with 106 healthy controls. Patients with acute aortic syndrome had a near two-fold increase in plasma desmosine compared to control subjects (0.58 $\pm$ 0.26 versus 0.27 $\pm$ 0.07 ng/mL, p<0.001). Plasma desmosine peaked in the acute phase and was detectable at presentation (0.82 $\pm$ 0.17 ng/mL, p<0.001), following which concentrations gradually declined over a 24-month period. Plasma desmosine was associated with aortic Agatston score (R=0.35, p=0.024) and inversely with aortic diameter (R=-0.33, p=0.016). Increased plasma desmosine was independently associated with aortic growth (β=+2mm/yr, p<0.001).

5.1.4 Conclusion

Plasma desmosine is a structural molecule that is raised in acute aortic syndrome and holds promise as a potential diagnostic biomarker. Plasma desmosine is also associated with imaging features of medial degeneration and may play a role in risk stratification by predicting aortic expansion.

5.2 Introduction

The acute aortic syndromes are catastrophic conditions. Aortic dissection, intramural haematoma and penetrating aortic ulcers are unpredictable in onset and clinical sequalae. Despite aggressive medical management, stringent surveillance and the emergence of minimally invasive surgical therapies, the mortality from acute aortic syndrome remains unacceptably high (Evangelista et al. 2018).

Elastin is an essential component of the aortic wall that contributes both structural integrity and recoil to the aorta. Elastin is formed when tropoelastin is first oxidised into an insoluble form and then cross-linked over an extracellular scaffold in a circumferential orientation (Karimi and Milewicz 2016). Desmosine, a structural amino acid, facilitates this

tropoelastin cross-linking and is uniquely found in mature elastin (Foster et al. 1974).

Patients with acute aortic syndrome have highly abnormal medial elastin (Agozzino et al. 2002). In acute aortic syndrome, the aorta experiences rapid structural instability resulting in cellular strain and degradation of the aortic media. Elastin fibres are fragmented and misaligned. Cellular density in the aortic media is reduced (Clarke et al. 2008). The resultant medial degeneration weakens the aorta and predisposes it to tearing, dilatation and ultimately rupture. Destruction of elastin fibres, as seen in acute aortic syndrome, may cause the release of desmosine into the blood stream.

The clinical presentation of acute aortic syndrome is varied. The characteristic symptoms of back, chest or abdominal pain overlap with other conditions. Visceral or limb ischaemia adds further complexity to the clinical presentation, and aortic rupture or cardiac tamponade may cause cardiovascular decompensation or rapid death. Prompt diagnosis requires a high index of suspicion and access to electrocardiography-gated contrast-enhanced computed tomography (Riambau et al. 2017). Resource availability and transferring unwell patients for investigations delays diagnosis. Indeed, there is a pressing need for the early and accurate identification of acute aortic syndrome when delivering emergency care.

Disease severity is currently determined by aortic morphology on cross-sectional anatomical imaging. No blood biomarker has translated into clinical practice owing to limitations in stratifying disease burden. In this context, plasma desmosine may be a promising novel biomarker for the detection or risk stratification of aortopathy. In this study, we aim to characterise plasma desmosine concentrations in patients with acute aortic syndrome.

The purpose of this study was to measure plasma desmosine concentration in patients with acute aortic syndrome in relation to disease charactersitics and compare this to healthy controls.

5.3 Methods

Plasma desmosine was measured in healthy controls and patients with acute aortic syndrome in a 2:1 ratio as described in **Chapter 2.3**. Plasma desmosine concentrations were analysed using a validated stable isotope dilution liquid chromatography–tandem mass spectrometry method. This validated assay has a range of 0.1 to 160 ng/mL (Albarbarawi et al. 2013) (**Chapter 2.8.2**).

Briefly, plasma desmosine concentrations were compared between disease and control groups, as well as between the acute aortic syndrome pathologies using a Student's t-test. A multivariable linear regression model corrected for demographic and clinical variables was used to compare adjusted plasma desmosine concentrations between control and acute aortic syndrome groups. Plasma desmosine concentration was also compared with phase of disease. A crude linear regression model of plasma desmosine concentration was fitted against a cubic polynomial transformation of time since acute aortic syndrome. An adjusted regression model also incorporated participant age, sex, body mass index, diastolic blood pressure and smoking status. Finally, plasma desmosine was compared with aortic diameter and Agatston's score. A multivariable linear regression model was used to investigate plasma desmosine concentration with respect to change in aortic diameter after accounting for aortic diameter, aortic Agatston score, time since acute aortic syndrome and participant age, sex and body mass index.

5.4 Results

5.4.1 Study Population

A total of 53 patients with acute aortic syndrome and 106 healthy controls were included (Table 5.1). The final 3 patients recruited to the original study did not have plasma desmosine measurements owing to limitations placed by the COVID-pandemic. The control group was younger, had more females and had lower body mass index. Patients with acute aortic syndrome had a lower heart rate and diastolic blood pressure, were more likely to smoke cigarettes and had a past medical history of hypertension.

Table 5.1: **Patient Characteristics**

		Healthy Control Subjects (n=106)	Acute Aortic Syndrome (n=53)
Demographics	Age (median [IQR])	53.00 [44.00, 60.00]	64.00 [53.00, 71.00]
	Sex (Male, %)	55 (51.9)	38 (71.7)
	Height (cm)	166.19 (9.55)	173.23 (9.55)
	Weight (kg)	68.17 (13.65)	86.75 (19.24)
	Body Mass Index (kg/m2)	24.52 (3.59)	28.76 (5.20)
	Heart rate (beats/min)	72.75 (10.90)	65.28 (10.42)
	Systolic blood pressure (mmHg)	131.22 (15.76)	132.87 (21.21)
	Diastolic blood pressure (mmHg)	78.06 (10.75)	73.87 (12.34)
	Smoking status (%)		
	Ex-smoker	15 (14.2)	22 (41.5)
	Non-smoker	89 (84.0)	26 (49.1)
	Smoker	2 (1.9)	5 (9.4)
	Alcohol (drinker, %)	-	29 (54.7)
Aortic Properties	Aortic diameter (mm,)	29.74 (4.09)	46.89 (8.55)
	Thoracic aorta Agatston Score (geometric mean)	-	146.9 (27.4)
	Pathology (%)		
	Aortic dissection	-	41 (77.4)
	Intramural haematoma	-	4 (7.5)
	Penetrating aortic ulcer	-	8 (15.1)
	Stanford Classification (Type B, %)		35 (66.0)
	Recent Acute Aortic Syndrome (%)	-	25 (47.2)
Past Medical History	Hypertension (%)	2 (1.9)	49 (92.5)
	Ischaemic Heart Disease (%)	-	9 (17.0)
	Cerebrovascular Disease (%)	-	7 (13.2)
	Diabetes Mellitus (%)	-	2 (3.8)
	Hypercholesterolaemia (%)	-	14 (26.4)
	Connective Tissue Disorder (%)	-	5 (9.4)

5.4.2 Plasma desmosine in Acute Aortic Syndromes

Patients with acute aortic syndrome had raised plasma desmosine concentrations compared to healthy control subjects (Figure 5.1). A similar trend was observed for sub-pathologies of acute aortic syndrome. A near two-fold increase was observed in patients with acute aortic syndrome compared to healthy controls following correction for potential confounders (acute aortic syndrome versus controls, plasma desmosine 0.27 versus 0.52 ng/mL, $p<0.001$, Table 2).

5.4.3 Time since Acute Aortic Syndrome

Plasma desmosine was increased in all phases of acute aortic syndrome (Figure 5.2). Peak desmosine was observed in the early stages of acute aortic syndrome. Plasma desmosine was detected at markedly elevated levels in samples obtained from patients presenting to the emergency department with acute aortic syndrome (Figure 5.3). These patients had symptom onset within 24 hours of acute aortic syndrome.

A polynomial regression model found that plasma desmosine decreased in a non-linear fashion with respect to time over many years after adjusting for participant age, sex, body mass index, diastolic blood pressure and smoking status (Table 5.4).

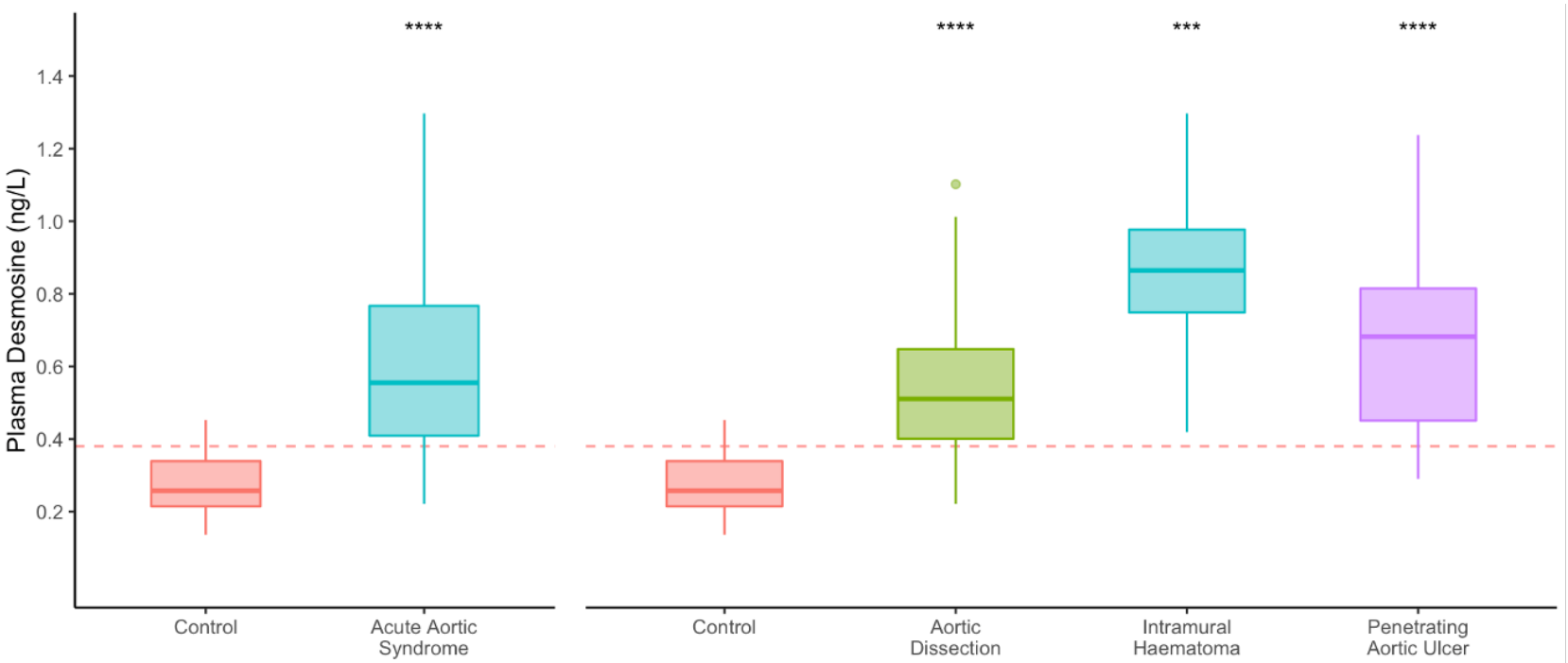

Figure 5.1: **Plasma desmosine concentration in patients with acute aortic syndrome and healthy control subjects.**

Table 5.2: **Plasma Desmosine in patients with Acute Aortic Syndrome.** Compared to healthy controls in a linear regression analysis. A crude model was fitted against pathology alone. A second, adjusted, model was adjusted for patient age, sex, body mass index, diastolic blood pressure and smoking status.

		Crude Model				Adjusted Model			
			95% CI				95% CI		
	Plasma Desmosine	beta estimate	lower	upper	p	beta estimate	lower	upper	p
Controls	0.27 ± 0.07	-	-	-	-	-	-	-	-
Acute Aortic Syndrome	0.58 ± 0.26	0.31	0.26	0.36	<0.001*	0.25	0.18	0.32	<0.001*
Aortic Dissection	0.54 ± 0.22	0.27	0.21	0.32	<0.001*	0.21	0.14	0.28	<0.001*
Intramural Haematoma	0.86 ± 0.36	0.59	0.44	0.74	<0.001*	0.52	0.36	0.69	<0.001*
Penetrating Aortic Ulcer	0.67 ± 0.31	0.39	0.29	0.5	<0.001*	0.35	0.23	0.47	<0.001*

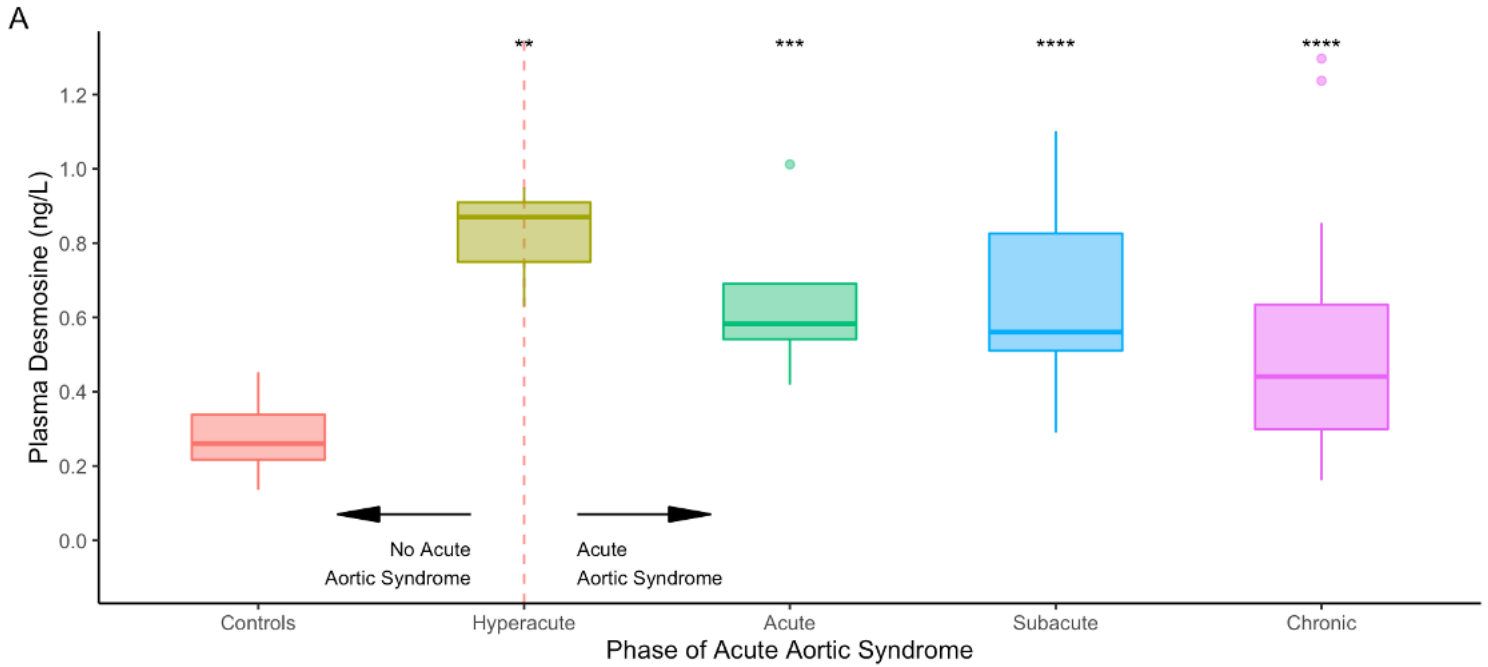

Figure 5.2: **Plasma desmosine by phase of Acute Aortic Syndrome.** Hyperacute = At presentation (first 24hrs), Acute = 24hrs – 14 days since presentation, Subacute = 15 – 90 days since presentation, Chronic = >90 days since presentation. ** $p < 0.01$, *** $p < 0.001$, **** $p < 0.0001$

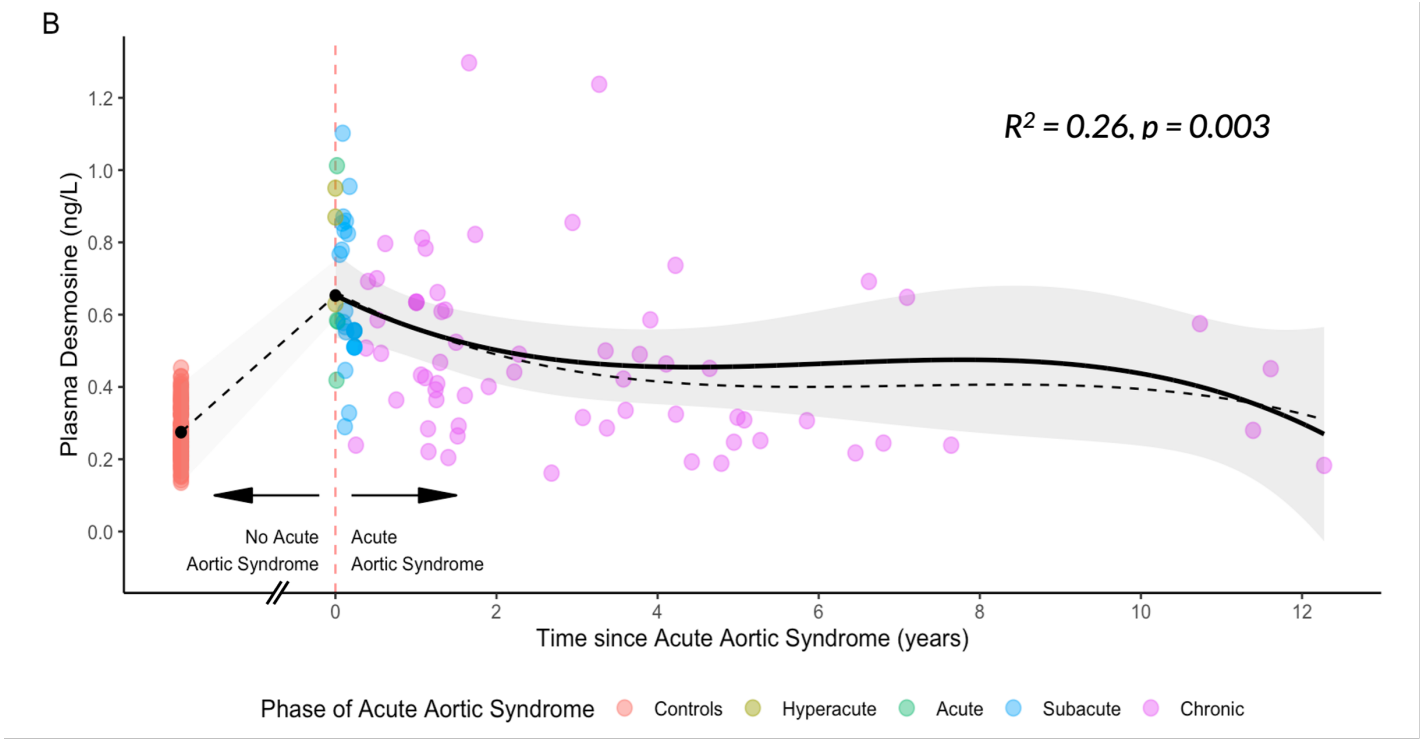

Figure 5.3: **A cubic polynomial fit of plasma desmosine concentrations following acute aortic syndrome with respect to time since acute aortic syndrome.** Dashed line = Crude plasma desmosine fit against time. Solid line = Adjusted pDes fit against time, age, sex, body mass index, diastolic blood pressure and smoking status. Ribbon = 95% confidence interval for adjusted pDes fit.

Table 5.3: **Change in plasma desmosine by phase of acute aortic syndrome compared to control subjects.** Linear regression analysis fitted against phase of disease and adjusted for patient age, sex, body mass index, diastolic blood pressure and smoking status.

	n	Plasma Desmosine	beta estimate	95% CI		p
				lower	upper	
Controls	106	0.27 ± 0.07	-	-	-	-
Presentation	3	0.82 ± 0.17	+0.54	+0.35	+0.73	< 0.001*
Acute	4	0.65 ± 0.25	+0.38	+0.21	+0.54	< 0.001*
Subacute	20	0.67 ± 0.21	+0.39	+0.31	+0.47	< 0.001*
Chronic	65	0.47 ± 0.23	+0.20	+0.15	+0.25	< 0.001*

Table 5.4: **Change in plasma desmosine with respect to time since acute aortic syndrome.** The duration since acute aortic syndrome was associated with a reduction in plasma desmosine concertation. In contrast, advancing age and body mass index were associated with increased plasma desmosine concentration

		95% CI		
	beta estimate	lower	upper	p
Time since Acute Aortic Syndrome (years, cubic polynomial)	-0.717	-1.187	-0.247	0.003*
Sex (male)	-0.103	-0.218	0.013	0.081
Age (years)	0.004	0.001	0.008	0.027*
Body Mass Index (kg/m2)	0.010	0.001	0.020	0.033*
Diastolic Blood Pressure (mmHg)	-0.001	-0.005	0.004	0.807
Smoker	0.008	-0.163	0.178	0.93

5.4.4 Aortic Diameter

In patients with acute aortic syndrome, mean aortic diameter was 46.9 $\pm$ 8.55mm and the thoracic aorta had a mean Agatston score of 146.9 $\pm$ 27.4 (geometric mean). The time interval between presentation and latest scan was 3.1 $\pm$ 2.8 years, during which 6 patients had endovascular intervention and 21 participants had open repair.

An inverse relationship was observed between increasing plasma desmosine and aortic diameter (Figure 5.4A). Plasma desmosine correlated positively with thoracic aorta Agatston score (Figure 5.4B) and change in aortic diameter over time (Figure 5.4C).

Change in aortic diameter fitted using a linear regression model found that plasma desmosine was a strong predictor of aortic growth. This was true independent of baseline aortic diameter, thoracic aorta Agatston score, time since acute aortic syndrome and aortic intervention (Figure 5.5).

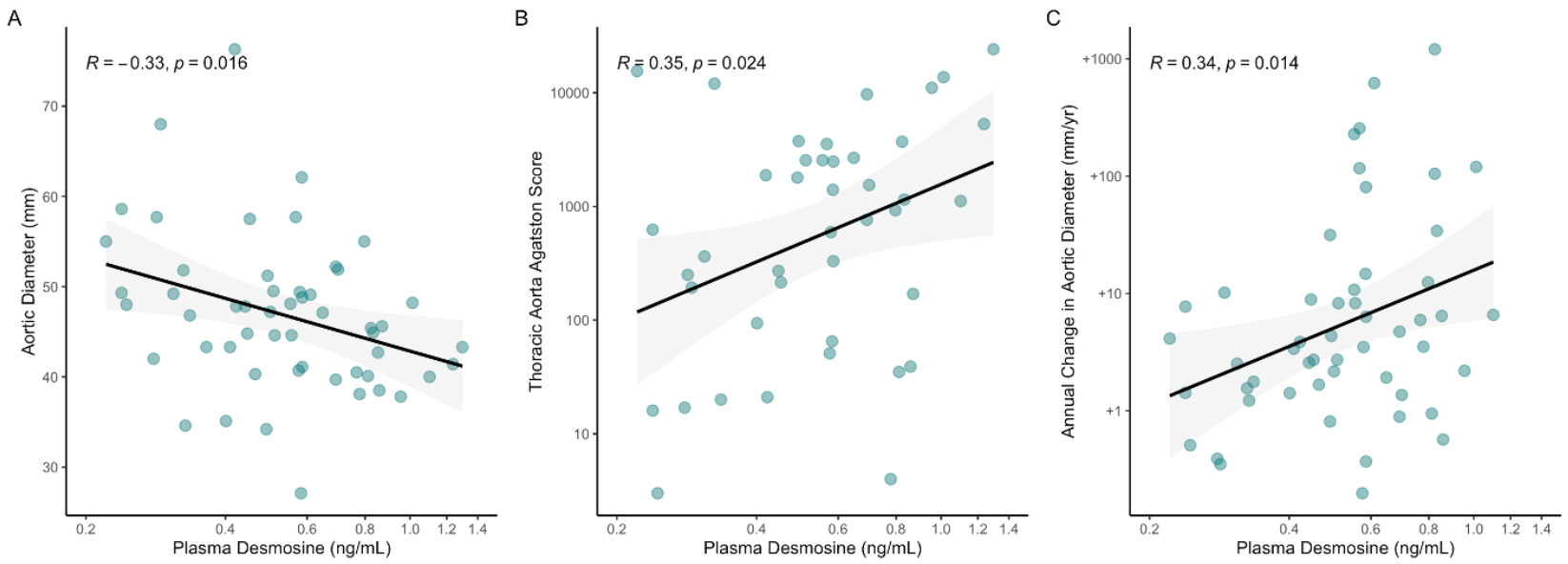

Figure 5.4: **Plasma desmosine and aortic characteristics.** Increased plasma desmosine concentration was associated with a decrease in aortic diameter (**A**). Both, thoracic aorta Agatston Score (**B**) and aortic expansion (**C**) were associated with plasma desmosine concetration.

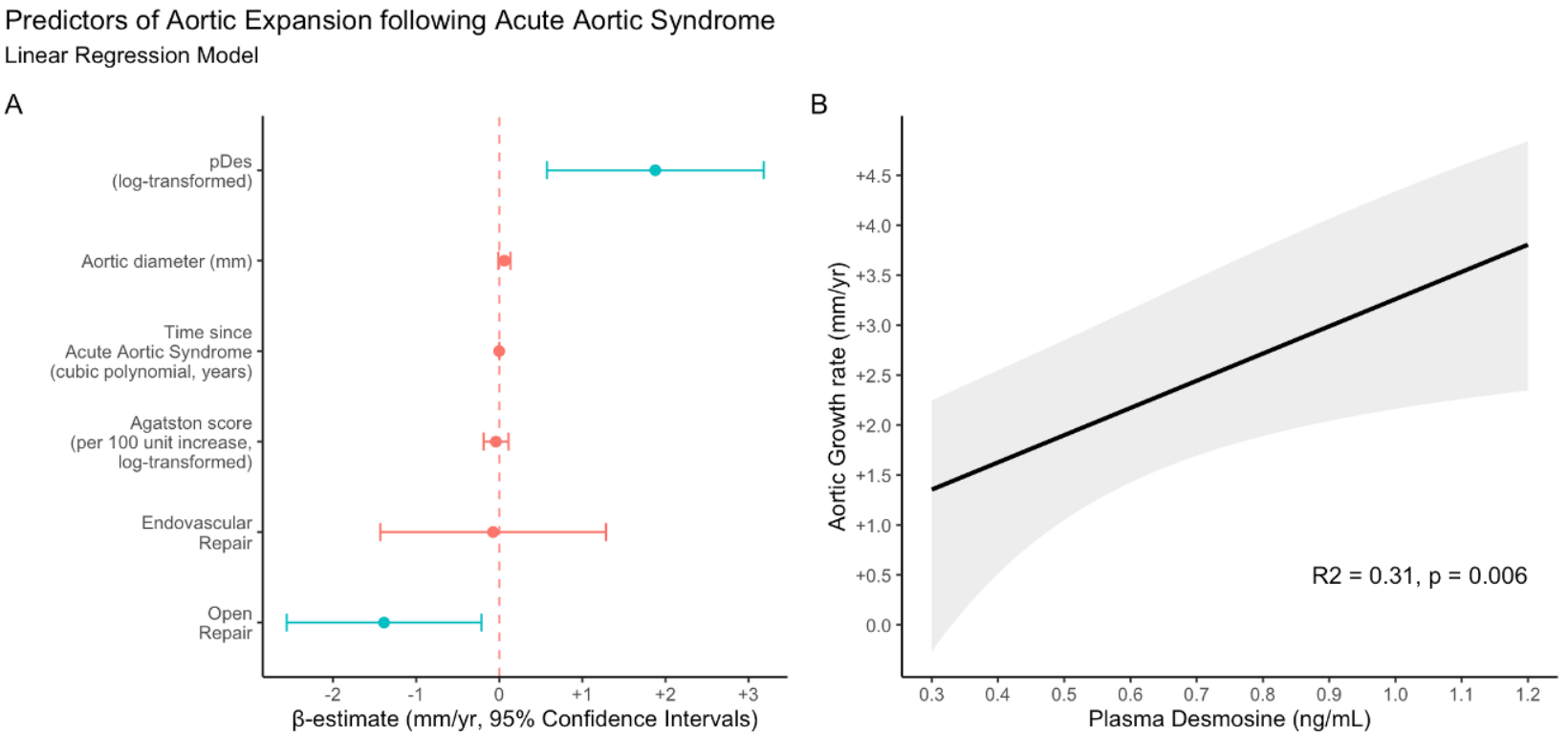

Figure 5.5: **Predictors of aortic expansion following acute aortic syndrome.** (**A**) Linear regression analysis of predictors of aortic expansion following acute aortic syndrome. (**B**) Estimated annual change in aortic diameter with increasing plasma Desmosine concentration following acute aortic syndrome. pDes = plasma desmosine.

5.4.5 Major Adverse Aortic Events

Plasma desmosine was not associated with major adverse aortic events (**Figure 5.6**) on Kaplan-Meier analysis. Similarly, a proportion hazards Cox regression model found that patient sex (HR 0.27 [95% CI 0.08 - 0.95], p=0.042) was the only significant predictor of major adverse aortic events independent of participant plasma desmosine concentration (HR 0.92 [95% CI 0.16-5.37], p=0.93), aortic diameter, time since acute aortic syndrome and smoking status.

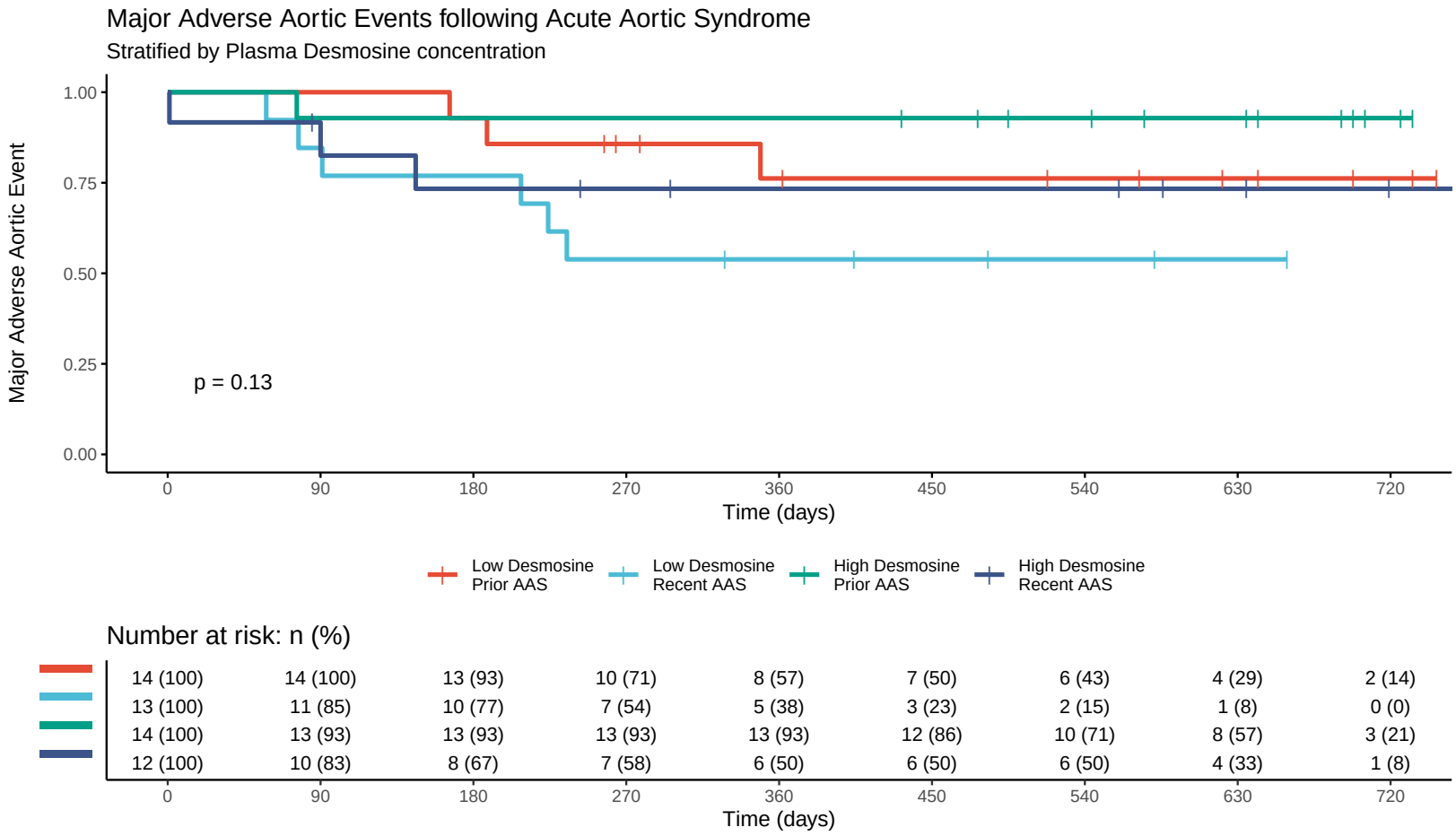

Figure 5.6: **Major adverse aortic events following acute aortic syndrome.** Stratified by median plasma desmosine concentration.

5.5 Discussion

This is the first study to characterise plasma desmosine in patients with acute aortic syndrome. We found that patients with acute aortic syndrome have increased plasma desmosine concentration compared to healthy control subjects. Interestingly, plasma desmosine was detectable in the hyperacute phase of the disease when patients presented to the emergency department. Plasma desmosine remains elevated in patients with acute aortic syndrome for many years compared to healthy controls, although the overall trend is towards a reduction in desmosine concentrations over time. Interestingly, plasma desmosine was also associated with aortic expansion suggesting a possible role in risk stratification.

Desmosine is a lysine-rich cross-linking structural molecule specific to mature elastin. Elastin is formed when vascular smooth muscle cells produce soluble tropoelastin that is ultimately oxidised and arranged circumferentially within the aortic wall in a process mediated by lysyl-oxidase (Karimi and Milewicz 2016). Desmosine cross-linked tropoelastin fibres are a critical component of mature elastin, which has an extremely long biological half life (Shapiro et al. 1991). Once produced in foetal life and early infancy, vascular elastin is rarely replenished (Duca et al. 2016). The aortic media is rich in mature elastin which is a critical structural component that maintains recoil.

Acute aortic syndrome is characterised by degeneration of the aortic media. Genetic abnormalities such as defects in the fibrillin-1 gene predispose to atypical fibre assembly resulting in dysregulated elastin formation (Mariko et al. 2011; Ju et al. 2014). Elastin degeneration occurs naturally within the ageing aorta. External insults such as hypertension and smoking accelerate elastin fibre fragmentation. Environmental insults also drive a phenotypical change in vascular smooth muscle cells which are reduced in density and now favour structural support over the production of extracellular precursors (Clément Marc et al. 2019). This shifts the balance of medial turnover towards destruction of the extracellular matrix thus placing additional strain on already damaged elastin fibres. The resultant destruction of mature elastin causes the release of desmosine into the systemic circulation at sufficient quantities to be detected within plasma.

We found increased plasma desmosine concentration in patients with acute aortic syndrome compared to healthy control subjects. This was the case in all three pathologies of acute aortic syndrome and reflects the burden of mature elastin damage. Intramural haematoma and aortic dissection cause profound damage to the aorta leading to the sudden disruption to elastic fibres in the medial wall. Penetrating aortic ulcers are caused by intense inflammatory atherosclerotic activity that weakens the media (Macura et al. 2003). Again, medial elastin is heavily damaged. Deterioration of the extracellular elastin matrix in all three pathologies comprising of acute aortic syndrome results in degradation of mature elastin and its eventual release into the blood stream.

Interestingly, elevated plasma desmosine was markedly elevated levels within 24 hours of patients experiencing symptoms and presenting to the emergency department. Acute aortic dissections and intramural haematomas are associated with the sudden destruction of the aortic wall which may cause a surge of desmosine release into the blood stream. Desmosine is a structural molecule within the aortic wall that is released in high concentrations when its target organ is damaged. Plasma desmosine may thus be a novel serum biomarker to diagnose acute aortic syndrome. The multiple fold increase in plasma desmosine within a few hours of patients experiencing symptoms presents the possibility of using this structural protein to identify aortic damage from acute aortic syndrome in the emergency department.

Plasma desmosine remained elevated in patients with acute aortic syndrome at various phases of the disease. The highest levels were detected in the sub-acute and acute phase, following which plasma desmosine remained elevated for many months following presentation. The half-life of desmosine once it is released into the circulation remains uncertain. However, a high concentration of desmosine in the urine of patients suggests that plasma desmosine is eventually excreted by the kidneys once released into the plasma (Lindberg et al. 2012). Hence, it is unclear whether elevated plasma desmosine in the subacute and chronic phases of acute aortic syndrome is the result of ongoing elastin degeneration or simply a remnant of the desmosine surge released following the initial aortic insult.

Curiously, plasma desmosine appeared to be negatively correlated with maximum aortic diameter. Aortic expansion occurs as a consequence of an architecturally abnormal aor-

tic wall being dilated by altered haemodynamic pressures. Dilated aortas typically have reduced elastin density and diminished vascular smooth muscle cells which are replaced by rigid collagen fibres and inflammatory infiltrates (Hellenthal et al. 2009). Indeed, histological analysis of tissue obtained from our own study revealed a similar trend towards a reduction in elastin fibre density in patients with acute aortic syndrome (**Chapter 3.4.2**). Thus, it is possible that patients with larger aortas in our study had decreased plasma desmosine levels because of reduced total elastin content within dilated vessels.

Vascular calcification occurs in response to medial degeneration. Cellular necrosis and the consequent spillage of calcium into the extracellular spaces causes phosphate-rich microscopic calcification crystals to precipitate within the aortic media. Cellular destruction causes a further pathological change in vascular smooth muscle cells which adopt an osteoblastic-like synthetic phenotype. This stimulates further vascular calcification. Eventually, microcalcification coalesces into larger plaques of sufficient size to be detected by computed tomography. Vascular calcification is the common pathological endpoint of medial degeneration and signifies advanced diseased. In our study, vascular calcification was associated with plasma desmosine in patients with acute aortic syndrome. It is possible that elastin degeneration and vascular calcification share a common link leading to disease progression. Elastinolysis is a product of medial degeneration and the pathological processes that lead to elastin fragmentation also ultimately result in vascular calcification.

The common findings of reduced plasma desmosine in dilated aortic walls and increased in vascular calcification provides insight into the biological properties of the aortic wall that eventually leads to aortic expansion. In our study, patients with increased plasma desmosine were more likely to experience aortic growth independent of other potential confounders such as aortic diameter, phase of disease, vascular calcification and surgical intervention. Thus, our findings suggest that in the latter stages of acute aortic syndrome, plasma desmosine concentration is a biomarker of disease activity and holds promise as a potential marker for risk stratification.

We should acknowledge limitations of our study. Elastin, and hence desmosine, is not specific to vascular tissue. Indeed, smokers and patients with chronic obstructive pulmonary

disease have also been observed to have increased plasma desmosine concentrations. Although initially considered to be a result of elastin breakdown within the alveoli, novel findings suggest that raised desmosine in smokers may instead reflect vascular damage within the alveolar-capillary complex of the lung (Huang et al. 2016). Indeed, the largest plasma desmosine study to date in patients with chronic obstructive pulmonary disease found that plasma desmosine was associated with major adverse cardiovascular events but not decline in respiratory function (Rabinovich et al. 2016). In our results, a history of smoking did not independently predict plasma desmosine decline over time following acute aortic syndrome but plasma desmosine was associated with vascular disease progression. A larger prospective study with longer follow-up will be required to determine whether plasma desmosine also predicts major adverse events such as aortic rupture, the need for surgical intervention or aorta-related death.

The detection of plasma desmosine requires further development. The current method to identify plasma desmosine uses mass-spectrometry technology that is highly accurate but also time-consuming. There is a pressing logistical requirement for the timely quantification of plasma desmosine concentrations if it is to be considered a biomarker for acute disease. Newly developed enzyme-linked immunosorbent assays for human plasma desmosine are still unreliable with an error tolerance of ±0.04ng/mL (MyBioSource 2021) which approaches nearly 30% variation for our control cohort. Developing a rapid and accurate measurement technique is essential for plasma desmosine to be considered a biomarker for acute aortic syndrome.

5.6 Conclusion

This first-in-man descriptive study suggests that plasma desmosine is a promising biomarker for elastin degeneration in acute aortic syndrome. Desmosine is a cross-linking structural molecule specific to mature elastin and is raised in patients with acute aortic syndrome compared to healthy controls. Desmosine peaks in the acute phase of disease and is detectable when patients with acute aortic syndrome present to the emergency department, thus acting as a potential diagnostic biomarker. Plasma desmo-

sine was also associated with imaging markers of medial degeneration such as aortic calcification and aortic growth. Hence plasma desmosine may also play an important role in risk stratification for aortic disease progression. The next step is to assess the sensitivity and specificity of plasma desmosine to diagnose acute aortic syndrome and longer follow-up in a larger cohort is required to determine its ability to predict major adverse aortic events.

Chapter 6

Serum micro-RNA in acute aortic syndrome

6.1 Abstract

6.1.1 Background

Acute aortic syndrome may cause catastrophic aortic rupture or death. MicroRNAs (miRNA) are non-coding fragments that modulate post-transcription protein function. The significance of miRNAs in acute aortic syndrome is uncertain.

6.1.2 Objective

To investigate the relationship of serum miRNAs with markers of acute aortic syndrome disease activity and major adverse aortic events.

6.1.3 Methods

miRNAs that interact with at least 5 genes known to cause thoracic aortopathy and validated in a miRNA screening study were measured in the serum of patients with aortic dissection, intramural haematoma or penetrating aortic ulcer. Serial CT angiography and ^{18}F-sodium fluoride PET/CT was used to measure aortic diameter, aortic Agatston score

and cellular injury. A linear discriminant analysis (LDA) weighted individual miRNA expression to obtain a unifying miRNA LDA score per participant. This was investigated in a proportional hazards Cox regression model for major adverse aortic events (aortic repair, aortic rupture or aortic death).

6.1.4 Results

A total of 53 patients with acute aortic syndrome and 20 control subjects underwent serum miRNA testing. Serum hsa-miR-29c-5p and -30b-5c were associated with aortic diameter whereas hsa-miR-130a-5p, -30a-5p, -30c-5p and -30d-5p were related with aortic expansion. Serum hsa-miR-130a-5p and 29a-5p were associated with progression in aortic Agatston score. Serum hsa-miR-149-5p, -29c-5p and the entire hsa-miR-30* family was associated with progression of ^{18}F-sodium fluoride binding in the true lumen. MicroRNA LDA score predicted major adverse aortic events independent of aortic diameter (hazard ratio 3.32(1.71-6.46), p<0.001).

6.1.5 Conclusion

Circulating miRNAs are associated with interrelated pathological pathways in acute aortic syndrome. Identification of a miRNA signature in patients with acute aortic syndrome may improve risk stratification.

6.2 Introduction

Acute aortic syndrome is characterised by cellular degeneration and weakening of the aortic media. A contained haemorrhage within the aortic wall manifests as an intramural haematoma whereas aggressive atherosclerotic activity may invade through the intima to form a penetrating aortic ulcer. High-pressure arterial blood flow may then strip the medial layer open to form an aortic dissection. These dramatic pathological changes predispose the aorta to dilatation and rupture, a catastrophic and often fatal event.

A complex interaction of genetic and environmental risk factors drives acute aortic syndrome. Our improved understanding of genetic pathways and their varying phenotype

have identified potential pathways that predispose to developing aortopathy. In practice, however, many patients with acute aortic syndrome are never demonstrated to have a defined genetic abnormality (Fletcher et al. 2020). Micro-ribonucleic acids (miRNA) are short non-coding segments of post-transcription RNA that modulate gene expression (Zeng 2006). Over two thousand miRNA have been characterised. This number is increasing. Over- and under-expression of specific circulating miRNAs has been observed in patients with acute aortic syndrome (Wang et al. 2015). However, the clinical significance of this variation is uncertain.

In this study, we first identified validated miRNAs that are predicted to interact with known genetic defects leading to thoracic aortopathy. We then identified expression of these miRNAs in the serum of patients with acute aortic syndrome. Finally, we aimed to investigate candidate miRNA expression in relation to clinical characteristics and disease progression.

The aim of this study was to identify candidate miRNA that may be associated with acute aortic syndrome, and investigate their expression in relation to disease characteristics and major adverse aortic events. This is a sub-study of the ^{18}F-sodium fluoride positron emission tomography in Acute Aortic Syndrome (FAASt, NCT03647566) study. Detailed methodology are described in **Chapter 2.3**.

6.3 Methods

6.3.1 Identifying and measuring candidate miRNA

Briefly, candidate miRNAs were shortlisted if they interacted with at-least 5 known genes that cause thoracic aortopathy with a certainty >98% and had been previously shown to be up- or down-regulated in acute aortic syndrome. Serum miRNA expression was investigated in patients with acute aortic syndrome and compared to healthy controls with radiological and biochemical evidence of no cardiac or aortic disease **Chapter 2.8.3**. qRT-PCR was performed on the LightCycler 480 apparatus (Roche Diagnostics, Burgess Hill, UK) utilising cycling parameters recommended for the miScript SYBR green system. The expression of each miRNA was normalised to the expression of the cel-miR-39 spike-in

control.

6.3.2 Disease characteristics

Maximum aortic diameter was determined from CT angiography performed at the same time as serum collection. Serial retro- and prospective CT angiography was used to determine aortic growth as described in **Chapter 2.5**. Similarly, aortic Agatston score was calculated from calcium scoring CT images obtained at the same time point as serum collection. Patients underwent 18F-sodium fluoride PET/CT at this time point and again one year later, the latter of which was used to determine progression of 18F-sodium fluoride uptake. The expression of each miRNA was compared with aortic diameter using linear regression in a crude model, and one adjusted for participant age and time since acute aortic syndrome. Longitudinal analysis compared miRNA with change in aortic size, progression of Agatston score and progression of ^{18}F-sodium fluoride radiotracer binding. Again, comparisons were made using linear regression in a crude model, and one adjusted for participant age, time since acute aortic syndrome and aortic diameter.

6.3.3 Major adverse aortic events

Major adverse aortic events were described as aortic rupture, aortic repair or aorta-related death. Clinical endpoints were determined by consensus of an adjudication committee consisting of three vascular clinicians. The final follow-up date for all study participants was 10th November 2020. Individual miRNA expression were compared between study participants that experienced a major adverse aortic event and those that remained event-free. A linear discriminant analysis (LDA) with respect to major adverse aortic events was used to weight and combine all miRNA into a single condensed metric (the miRNA LDA score). The miRNA LDA score was compared between patients that experienced major adverse aortic events and those that did. The median miRNA LDA score was used to stratify patients in to “high” and “low” miRNA LDA score categories which were compared using Kaplan-Meier analysis. A cox regression model for major adverse aortic event was fitted against participant age, sex, aortic diameter, time since acute aortic syndrome and miRNA LDA score.

6.4 Results

6.4.1 Candidate miRNAs

A total of 16 miRNAs met the criteria for inclusion in the study (Figure 6.1). These included hsa-let-7a-3p, hsa-let-7b-3p, hsa-let-7f-1-3p, hsa-miR-130a-3p, hsa-miR-130a-5p, hsa-miR-145-5p, hsa-miR-149-3p, hsa-miR-29a-3p, hsa-miR-29c-3p, hsa-miR-30a-5p, hsa-miR-30b-5p, hsa-miR-30c-5p, hsa-miR-30d-5p and hsa-miR-30e-5p.

6.4.2 Study Population

Fifty three out of 56 patients from the original imaging study (94.6%) were included in this sub-analysis. As was true in **Chapter 5**, the final three participants recruited did not have blood samples collected owing to the COVID pandemic. Study participants had increased aortic diameter compared to healthy control subjects but were otherwise well matched for age, sex, body-mass index and smoking history. Patients were more likely to be on antihypertensive therapy and consequently had a lower blood pressure than controls.

6.4.3 miRNA expression in patients with acute aortic syndrome

miRNAs expression in patients with acute aortic syndrome was varied compared to controls subjects with morphologically normal aortas. Certain miRNAs, such as hsa-miR-30a, -30c, -30d, -30e, -126-5p and -29a were detected in all healthy controls and in 91% of patients (48/53). Other miRNAs, such as hsa-miR-130a-5p, 130a-3p, -149, -30b and -29c were detected in less than a quarter of healthy controls but expressed in up to three quarter of patients with acute aortic syndrome (Figure 6.2).

When miRNAs were detected, expression of 11 miRNAs was reduced, 5 miRNAs had a similar expression, and hsa-miR-126-3p was the only one with increased expression in the serum of patients with acute aortic syndrome compared to controls (Table 6.2).

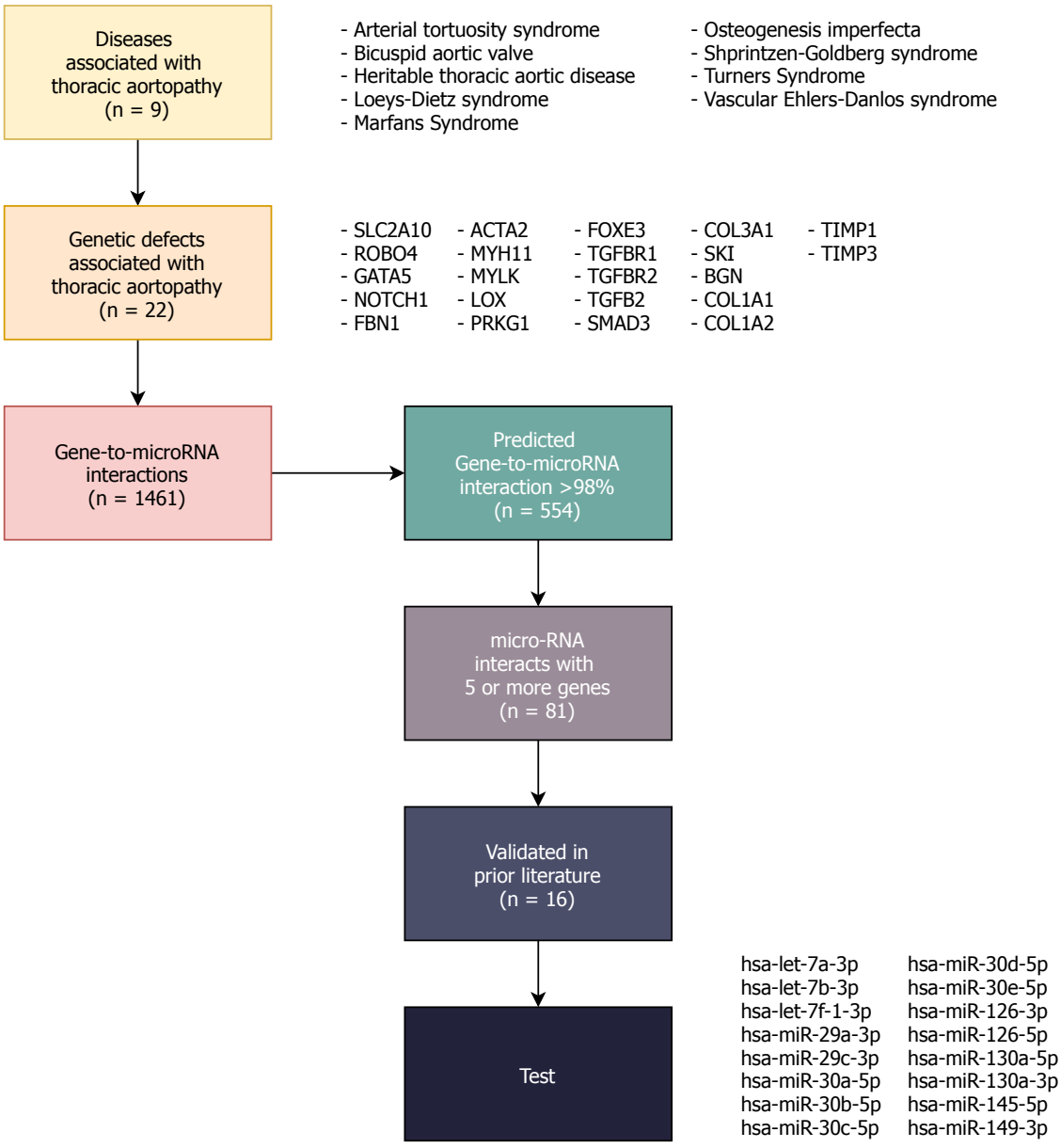

Figure 6.1: **Identification of candidate micro-RNA (miRNA) in patients with acute aortic syndrome.**

Table 6.1: **Patient Characteristics**

Characteristic	Acute Aortic Syndrome, N = 53	Control Subjects, N = 20	p-value
Demographics			
Age (years)	64 (53, 71)	56 (54, 63)	0.290
Sex (male, n (%))	39 (74%)	10 (50%)	0.056
Body Mass Index (kg/m2)	28.1 (25.6, 31.6)	26.4 (25.5, 27.7)	0.106
Heart rate, beats per minute	63 (59, 71)	68 (61, 82)	0.117
Systolic blood pressure (mmHg)	128 (119, 142)	155 (138, 174)	<0.001*
Current or Ex-Smoker (n, (%))	27 (51%)	10 (50%)	0.943
Aortic Characteristics			
Aortic Diameter (mm)	47 (41, 50)	32 (30 - 35)	<0.001*
Pathology (n, (%))			-
Intramural Haematoma	4 (7.5%)	-	-
Aortic Dissection	41 (77%)	-	-
Penetrating Aortic Ulcer	8 (15%)	-	-
Stanford Classification (Type B, %)	34 (64%)	-	-
Recent Acute Aortic Syndrome	24 (45%)	-	-
Medical History			
Hypertension (n, (%))	49 (92%)	3 (15%)	<0.001*
Ischaemic Heart Disease (n, (%))	9 (17%)	9 (45%)	0.030*
Cerebrovascular Disease (n, (%))	8 (15%)	0 (0%)	0.097
Diabetes Mellitus (n, (%))	2 (3.8%)	1 (5.0%)	>0.999
Hypercholesterolaemia (n, (%))	13 (25%)	5 (25%)	>0.999
Connective Tissue Disorder (n, (%))	5 (9.4%)	0 (0%)	>0.999
Medications			
Beta-Blocker (n, (%))	47 (89%)	6 (30%)	<0.001
Statin (n, (%))	32 (60%)	3 (15%)	<0.001
Antiplatelet agent (n, (%))	26 (49%)	3 (15%)	0.008*
Anticoagulation (n, (%))	14 (26%)	2 (10%)	0.205

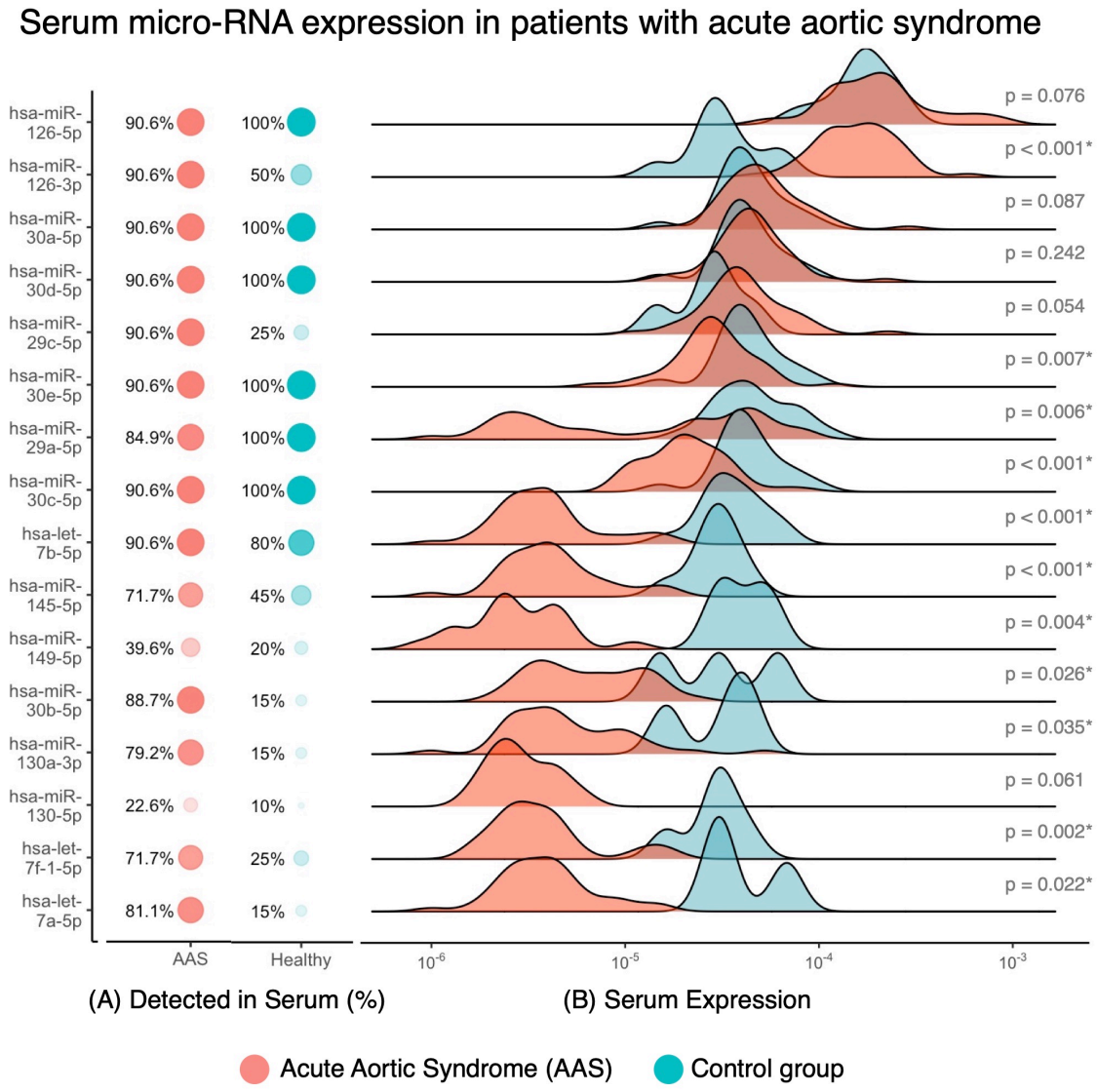

Figure 6.2: **Serum micro-RNA (miRNA) expression in patients with a history of Acute Aortic Syndrome.** (**A**) Serum miRNA detection rate in acute aortic syndrome patients and healthy controls. (**B**) Distribution of miRNA concertation in patients with acute aortic syndrome compared to healthy controls. * $p < 0.05$.

Table 6.2: **miRNA expression in patients with acute aortic syndrome.** * p<0.05

miRNA	Detectable (%)		Expression (log10[IQR])		
	Acute Aortic Syndrome (n=53)	Control Subjects (n=20)	Acute Aortic Syndrome (n=53)	Control Subjects (n=20)	p
hsa-let-7a-5p	81.1	15	-5.40 [-5.54, -5.21]	-4.50 [-4.52, -4.33]	0.022*
hsa-let-7b-5p	90.6	80	-5.40 [-5.56, -5.22]	-4.47 [-4.53, -4.35]	<0.001*
hsa-let-7f-1-5p	71.7	25	-5.44 [-5.58, -5.33]	-4.53 [-4.53, -4.49]	0.002*
hsa-miR-130a-3p	79.2	15	-5.34 [-5.53, -5.00]	-4.45 [-4.62, -4.40]	0.035*
hsa-miR-130a-5p	22.6	10	-5.53 [-5.63, -5.36]	-4.43 [-4.46, -4.40]	0.061
hsa-miR-145-5p	71.7	45	-5.36 [-5.53, -5.12]	-4.53 [-4.59, -4.45]	<0.001*
hsa-miR-126-3p	90.6	50	-3.76 [-3.94, -3.63]	-4.52 [-4.57, -4.41]	<0.001*
hsa-miR-126-5p	90.6	100	-3.68 [-3.85, -3.45]	-3.77 [-3.84, -3.68]	0.076
hsa-miR-149-5p	39.6	20	-5.58 [-5.66, -5.37]	-4.40 [-4.49, -4.30]	0.004*
hsa-miR-29a-5p	84.9	100	-4.64 [-5.47, -4.31]	-4.36 [-4.48, -4.18]	0.006*
hsa-miR-29c-5p	90.6	25	-4.39 [-4.47, -4.22]	-4.54 [-4.58, -4.50]	0.054
hsa-miR-30a-5p	90.6	100	-4.30 [-4.42, -4.11]	-4.37 [-4.44, -4.29]	0.087
hsa-miR-30b-5p	88.7	15	-5.15 [-5.41, -4.88]	-4.52 [-4.67, -4.36]	0.026*
hsa-miR-30c-5p	90.6	100	-4.66 [-4.76, -4.50]	-4.39 [-4.45, -4.30]	<0.001*
hsa-miR-30d-5p	90.6	100	-4.33 [-4.43, -4.18]	-4.39 [-4.45, -4.30]	0.242
hsa-miR-30e-5p	90.6	100	-4.54 [-4.61, -4.36]	-4.39 [-4.45, -4.30]	0.007*

miRNA expression was similar between Stanford Classification and underlying Pathology. hsa-miR-30c-5p was the only miRNA that was increased in patients in the acute phase of disease compared to those with long-standing disease.

6.4.4 Aortic characteristics

In a linear regression model adjusted for demographic and clinical risk factors, hsa-miR-29c-5p and hsa-miR-30b-5p were associated with aortic diameter. Increasing serum expression of both miRNAs was inversely associated with reduced aortic diameter.

No microRNA was associated with aortic calcification in either crude or adjusted model. However, hsa-miR-145-5p was inversely associated with ^{18}F-sodium fluoride binding in the aortic wall adjacent to the false lumen. Again, an inverse relationship existed between hsa-miR-145-5p and false lumen ^{18}F-sodium fluoride binding intensity.

6.4.5 Disease progression

Increased expression of hsa-miR-130a-5p, -30a-5p, -30c-5p and -30d-5p were associated with aortic expansion in a linear regression model adjusted for participant age, time since acute aortic syndrome and baseline aortic diameter (Table 6.3).

Increased hsa-miR-130a-5p was associated with slower progression in Agatston score whereas hsa-miR-29a-5p exhibited a positive correlation with percent increase in Agatston score. On serial ^{18}F-sodium fluoride PET/CT imaging, hsa-miR-130a-3p was associated with progression of radiotracer binding within the aortic flap. In the true lumen, hsa-miR-149-5p, -29c-5p, -30a-5p, -30b-5p, -30c-5p, -30d-5p and -30e-5p were all associated with progression of ^{18}F-sodium fluoride signal binding.

Table 6.3: **Serum miRNA and disease characteristics in patients with acute aortic syndrome.** Linear regression analysis in a Crude model and once adjusted for participant age, time since acute aortic syndrome and baseline aortic diameter.

			Crude Model			Adjusted Model		
			Beta	95% CI	p	Beta	95% CI	p
Disease severity	Aortic diameter (mm)	hsa-miR-29c-5p	-0.07	-0.15 to 0	0.051	-0.08	-0.15 to -0.01	0.037*
		hsa-miR-30b-5p	-0.06	-0.11 to 0	0.034*	-0.06	-0.12 to -0.01	0.023*
	18F-Sodium Fluoride in the false lumen (MDS TBRmax)	hsa-miR-145-5p	-0.04	-0.08 to -0.01	0.019*	-0.04	-0.08 to -0.01	0.024*
Disease Progression	Aortic expansion (mm/yr)	hsa-miR-130a-5p	0.1	-0.18 to 0.38	0.478	0.24	0.02 to 0.46	0.034*
		hsa-miR-30a-5p	0.77	-0.15 to 1.69	0.099	0.76	0.02 to 1.5	0.043*
		hsa-miR-30c-5p	0.9	-0.02 to 1.83	0.054	0.78	0.04 to 1.53	0.039*
		hsa-miR-30d-5p	0.91	-0.03 to 1.86	0.058	0.83	0.07 to 1.6	0.033*
	Agatston Score (% change/yr)	hsa-miR-130a-5p	-316.85	-617.3 to -16.36	0.039*	-322.6	-635.3 to -9.84	0.044*
		hsa-miR-29a-5p	771.67	281.74 to 1261.6	0.003*	996.74	438.88 to 1554.6	0.001*
	18F-Sodium Fluoride in the true lumen (% MDS TBRmax/yr)	hsa-miR-149-5p	4.12	0.92 to 7.32	0.014*	4.54	0.57 to 8.51	0.027*
		hsa-miR-29c-5p	-11.41	-25.32 to 2.51	0.104	-16.13	-31.31 to -0.95	0.038*
		hsa-miR-30a-5p	-14.58	-28.57 to -0.58	0.042*	-17.03	-31.73 to -2.33	0.025*
		hsa-miR-30b-5p	-14.14	-26.95 to -1.32	0.032*	-16.32	-29.95 to -2.69	0.021*
		hsa-miR-30c-5p	-15.62	-30.57 to -0.67	0.041*	-18.05	-34.11 to -1.99	0.029*
		hsa-miR-30d-5p	-16.84	-32.14 to -1.54	0.032*	-19.21	-35.23 to -3.19	0.021*
		hsa-miR-30e-5p	-14.16	-28.93 to 0.62	0.06	-16.53	-32.22 to -0.85	0.040*

6.4.6 Adverse Aortic Events

miRNA expression was similar between patients that experienced major adverse aortic events and those that remained event-free. No individual miRNA was associated with major adverse aortic events on crude- and adjusted Cox regression analysis.

Linear discriminate analysis (LDA) weighted individual miRNA expression to condense these into a single continuous miRNA LDA score for each study participant (Figure 6.3). The miRNA LDA score stratified patients that experienced major adverse aortic events from those that remained event-free (miRNA LDA score 1.19 $\pm$ 1.13 vs. -0.35 $\pm$ 0.96 respectively, p<0.001). Kaplan-Meier analysis confirmed that patients with a high miRNA LDA score had an increased likelihood of experiencing a major adverse aortic event compared to patients with a low miRNA LDA score (Log-rank p = 0.007, Figure 6.4).

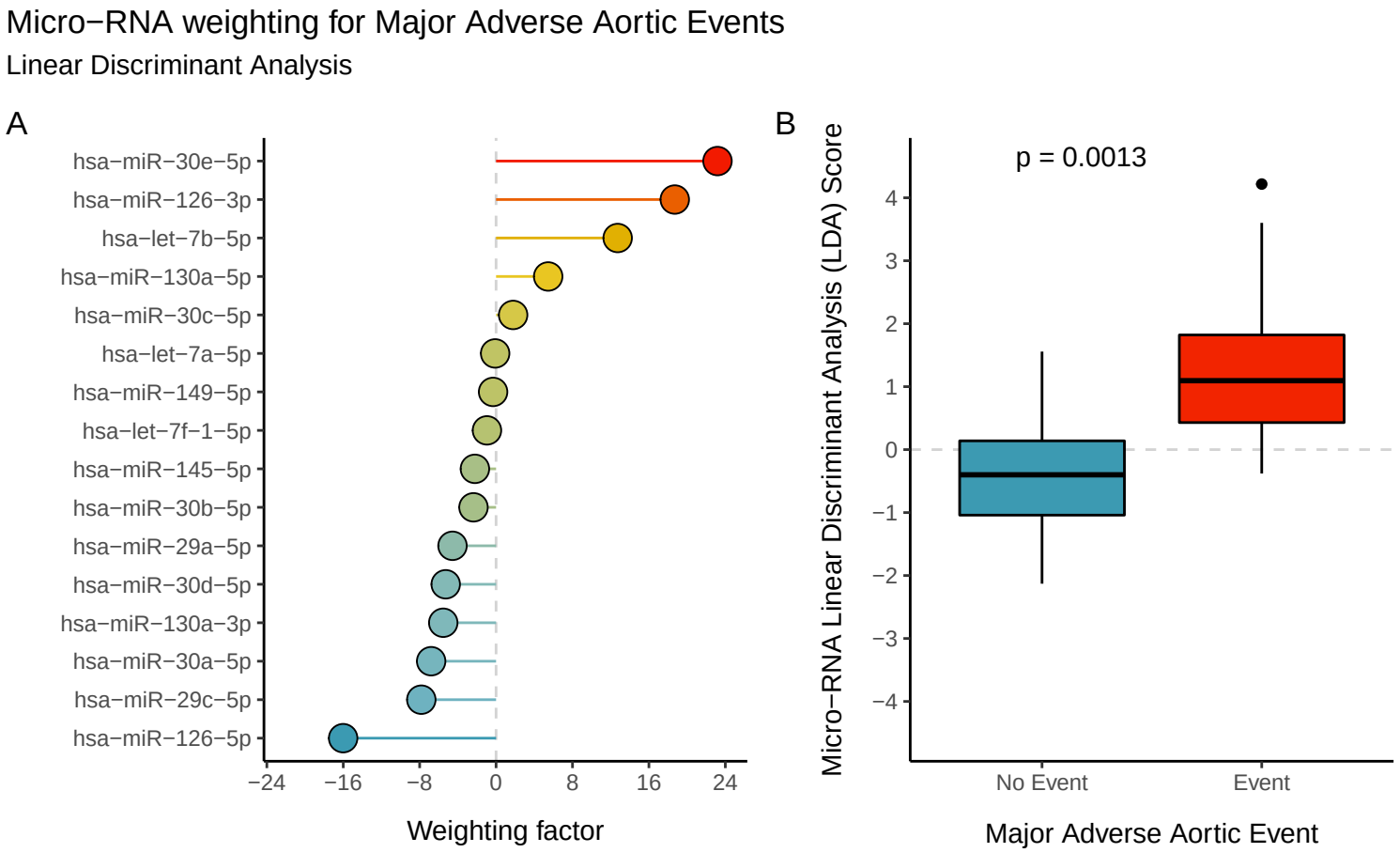

Figure 6.3: **Weighting factor for serum micro-RNA (miRNA) concentrations to optimise stratification for major adverse aortic events in patients with acute aortic syndrome.** Linear Discriminant Analysis. (**A**) Weighting factor for individual miRNAs. (**B**) miRNA linear discriminant analysis (LDA) score in patients that experienced aortic rupture, aortic repair or aortic death.

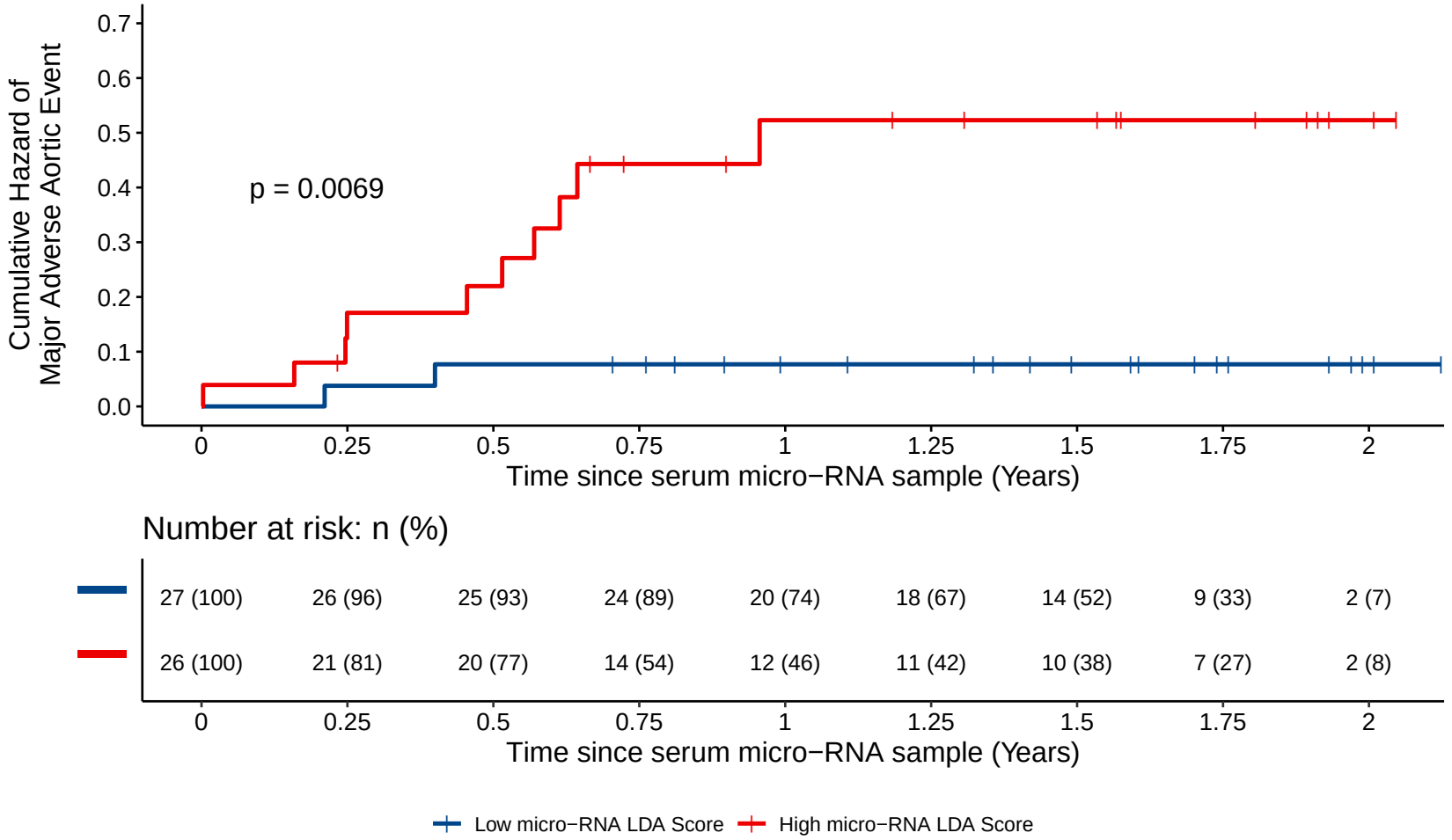

Figure 6.4: **Cumulative hazard of major adverse aortic events in patients with acute aortic syndrome.** Kaplan-Meier estimates stratified by micro-RNA (miRNA) linear discriminant analysis score.

In a proportional hazards Cox-regression analysis, miRNA LDA score and patient sex were the only significant predictors of major adverse aortic events in patients with acute aortic syndrome independent of participant age, aortic diameter, systolic blood pressure and duration since acute aortic syndrome (Cox-regression analysis table).

Table 6.4: **Major adverse aortic events following acute aortic syndrome.** Proportional hazards Cox regression model for aortic rupture, aortic repair or aortic death.

	Crude Model				Adjusted Model			
		95% CI				95% CI		
	Hazard Ratio	Lower	Upper	p	Hazard Ratio	Lower	Upper	p
miRNA LDA Score	2.97	1.86	4.73	<0.001*	3.32	1.71	6.46	<0.001*
Age (per year)	-	-	-	-	1.05	0.98	1.12	0.166
Sex (Male)	-	-	-	-	0.25	0.07	0.90	0.034*
Aortic Diameter (per 5mm)	-	-	-	-	1.08	0.76	1.54	0.659
Systolic Blood Pressure (per 10mmHg)	-	-	-	-	1.18	0.77	1.82	0.451
Time since acute aortic syndrome (per year)	-	-	-	-	0.79	0.52	1.19	0.262

6.5 Discussion

This is the first study to correlate serum miRNA expression in patients with acute aortic syndrome to aortic morphology and longitudinal clinical outcomes. Acute aortic syndrome is a heterogenous group of aortic conditions characterised by medial degeneration leading to intimal and medial disruption. Cellular degeneration of the aortic media is associated with a reduced cellular density, fracturing of the extracellular matrix, pooling of proteoglycans and progressive calcification of the aortic wall (Yamada et al. 2015; Sariola, Viljanen, and Luosto 1986). miRNA function in patients with acute aortic syndrome appears both, complex and interrelated. We found that several miRNAs are associated with aortic size, aortic calcification, progression of aortic disease and ultimately clinical events. In this study, we identified potentially relevant miRNAs from predicted interactions with known genetic defects that cause thoracic aortopathy. We have found that certain candidate miRNAs are correlated with clinical and imaging markers of disease severity. Finally, we used a feature discriminant algorithm to identify optimal weighting for each miRNA to predict major adverse aortic events.

miRNAs are short non-coding segments of RNA that act as signalling modulators for protein transcription and post-transcription protein function. Over 2000 miRNA interactions have been described in humans. This number is growing. The precise mechanism of action of many miRNA is still being understood. Gene-to-miRNA interactions can be predicted using computational algorithms, the analysis of which are stored in large-scale open-source databases (Yuhao Chen and Wang 2020; Wang 2008). We adopted a systematic approach to identify miRNAs with a high probability of interacting with multiple genes that cause thoracic aortopathy. This led to the identification of 16 candidate miRNAs that may play a role in modulating aortic biology in patients with acute aortic syndrome.

A comparison of serum miRNAs expression in patients with acute aortic syndrome and healthy controls revealed two important findings. First, the presence of circulating miRNAs in patients with acute aortic syndrome is varied compared to healthy subjects. Second, acute aortic syndrome was associated with a reduction in circulating miRNA expression for most candidates. Only hsa-miR-126-3p was upregulated in acute aortic syndrome

patients compared to healthy controls. We observed no difference in miRNAs expression between Stanford Classification groups and underlying pathology suggesting miRNAs expression is related to progressive medial degeneration that drives acute aortic syndrome rather than the clinical presentation of disease itself.

The hsa-miR-30 family is emerging as a significant potential modulator of aortic disease in patients with acute aortic syndrome (Liao et al. 2011). In our cohort, members of the hsa-miR-30 family were readily detected in patients but at a lower or similar expression to healthy controls. Reduced serum expression of members of the hsa-miR-30 family were associated with increased aortic diameter and approached statistical significance to predict aortic expansion after correcting for confounders. These miRNAs were also associated with progression of ^{18}F-sodium fluoride binding in the true lumen which is suggestive of continuous microscopic cellular injury (**Chapter 3** and **4**).

The transforming growth factor beta (TGF-β) pathway is a major regulator of medial integrity within the aortic wall (Humphrey 2013; Benke et al. 2013). The hsa-miR-30 family interacts strongly with transforming growth factor receptor-$\beta 1$ (TGFBR2) and -$\beta 2$ (TGFBR1) genes. These genes typically regulate cellular proliferation through protein transcription in smooth muscle cells and cardiomyocytes. The TGFBR1 and TGFBR2 genes are further modulated by the SMAD3 gene – another target of the hsa-miR-30 family. Defects in the TGF-β pathway are thought to play a primary role in connective tissue disorders such as Marfan and Loeys-Dietz syndrome that lead to acute aortic syndrome through premature ageing and reduced cellular density of the aortic media. The hsa-miR-30 family also interacts with the myosin heavy 11 (MYH11) and myosin light chain kinase (MYLK) genes. Combined, these genes are responsible for the production and functioning of the major contractile apparatus of smooth muscle cells (Karimi and Milewicz 2016). Within the extracellular space, the hsa-miR-30 family interacts with the lysyl oxidase (LOX) gene. In smooth muscle cells, the LOX gene is responsible for catalysing oxidation of lysine to form cross-links within the extracellular matrix. These elucidate a second possible mechanism by which the hsa-miR-30 family interacts with vascular connective tissue – through the functioning of the major contractile units and extracellular matrix of the aortic media. Finally, the hsa-miR-30 family plays a role in angiogenesis. Increased expression of these

miRNAs are associated with angiogenic proliferation (Bridge et al. 2012) through modulation of the DLL4 protein. DLL4 mediates cell-to-cell interactions within the aortic endothelium that drives Notch-dependent vessel growth (Pitulescu et al. 2017). Conversely, blocking the hsa-miR-30 family in animal models leads to aortic dilation [bridge2012]. We observed a similar finding of reduced expression of members of the hsa-miR-30 family being associated with increased aortic diameter in human subjects.

Another miRNA associated with progression of ^{18}F-sodium fluoride PET/CT signal in the true lumen was hsa-miR-149-5c. Like the hsa-miR-30 family, hsa-miR-149-5c also interacts with the lysyl oxidase and transforming growth factor-$\beta 2$ (TGFB2) genes suggesting an interrelated role in disease progression. ^{18}F-sodium fluoride PET/CT signal in the true lumen itself is a predictor of major adverse aortic events in patients with acute aortic syndrome. The identification of miRNAs associated with imaging markers of cellular injury in the aortic wall may elucidate potential mechanisms of action through which the diseased aorta is damaged.

The interaction between miRNAs and the clinical manifestation of disease is complex. No individual miRNA was associated with all clinical markers of disease activity and neither predicted major adverse aortic events. Linear discriminant analysis is a feature extraction algorithm (Le et al. 2020; Rhys 2020) that optimises the weighting of individual miRNA expression associated with major adverse aortic events and condenses this information into a single metric. The use of such an algorithm has two advantages when working with multiple biomarkers. First, it provides a measure of which miRNAs appear to influence the clinical endpoint relative to other biomarkers in the study. We found that hsa-miR-126-3p, hsa-let-7b, members of the hsa-miR-30 family (-e, -b and -c) were scaled positively, whereas hsa-miR-126-5p, hsa-miR-29c-5p and other members of the hsa-miR-30 family (-a and -d) were scaled negatively. Second, condensing the expression of several microRNAs into a single metric reduces complexity within the dataset and simplifies subsequent regression modelling. Linear discriminate analysis thus provides us with a miRNA signature in the serum of patients with acute aortic syndrome that may be associated with adverse clinical outcomes.

In our cohort, the miRNA LDA score was able to stratify patients that experienced acute aor-

tic syndrome from those that remained event free. This was true independent of conventional clinical risk factors such as aortic diameter and blood pressure. This miRNA signature provides a template to identify potentially significant serum biomarkers for risk stratification in patients with acute aortic syndrome. The miRNAs that underwent the greatest positive scaling were hsa-miR-30e-5p and hsa-miR-126-3p. We found that patients with acute aortic syndrome had significantly increased circulating hsa-miR-126-3p than healthy controls. This miRNA is a potent modulator of angiogenesis and plays a critical role in maintaining vascular integrity. High expression of hsa-miR-126-3p inhibit the vascular endothelial growth factor (VEGF) pathway (Fish et al. 2008) resulting in loss of vascular integrity. Inhibition of the VEGF pathway in the developing foetus results in haemorrhage (Siekmann, Covassin, and Lawson 2008), whereas in adults, reduced VEGF pathway activity mimics the effects of cigarette smoking through inhibition of hypoxia-inducible factor-1α resulting in highly abnormal irregular angiogenesis (Michaud et al. 2003).

We should acknowledge limitations of our study. First, we adopted a balanced approach to identify a comprehensive range of miRNAs whilst maintain feasibility of the study. Indeed, to the authors knowledge, no precedence exists for clinically validating miRNAs that interact with multiple genetic defects to cause a common clinical endpoint. We chose candidate miRNAs based on algorithmic predictions with genetic abnormalities associated with acute aortic syndrome. It is likely that accelerated discovery of novel miRNAs will yield additional relevant biomarkers. Second, we identified circulating miRNAs rather than the tissue expression of miRNA. Comparing these would further investigation. The specificity of circulating miRNA to vascular tissue is uncertain. However, testing miRNA expression in aortic tissue necessitates major surgical intervention or death – a strategy that is unsuitable for early risk stratification. Third, we tested circulating miRNA expression in the serum of patients. It is possible that activated platelets in the coagulation cascade influence miRNA expression and thus a direct comparison of miRNA expression between serum and plasma is not possible (Wang et al. 2012; Foye et al. 2017). Finally, no individual miRNA was associated with all markers of disease activity or adverse clinical event. We have thus used a feature extraction statistical algorithm to weight the significance of individual miRNAs and condense these into a single metric. This condensed

miRNA LDA score now needs to be validated in an external cohort.

6.6 Conclusion

miRNAs are associated with aortic morphology and biological processes within the aortic related to disease progression. The interaction between miRNAs and disease progression is complex. The hsa-miR-30 family is expressed abundantly in patients with acute aortic syndrome and is associated with aortic diameter, aortic expansion, and progression of aortic microcalcification in the true lumen. No individual miRNA predicted adverse aortic event. It is possible to combine candidate miRNAs using a feature extraction algorithm to obtain a miRNA signature to stratify patients at risk of experiencing major adverse aortic events. Future work now needs to elucidate the function of candidate miRNAs and validate these findings in a larger external cohort.

6.7 Clinical Perspectives

Acute aortic syndrome has an unpredictable clinical course. It is a dynamic condition with the capacity to cause major morbidity and death. Hence, there is a pressing need to improve risk stratification in this vulnerable cohort. Genetic abnormalities associated with acute aortic syndrome have varying phenotypical penetration and thus may remain silent.

miRNAs may bridge the genetic expression of proteins and post-transcription protein function. Identifying relevant circulating miRNAs and understanding their relationship with clinically significant adverse events holds great promise. Patient serum is easily accessible and timely miRNA detection is feasible.

In this study, we have identified numerous individual miRNAs that are associated with different markers of disease progression, thus suggesting miRNAs play physiological roles in wide array of pathological processes. We have also estimated a miRNA signature that is associated with major adverse aortic events.

A larger study that validates these findings in an external cohort is now required to determine the prognostic value of miRNAs in patients with acute aortic syndrome.

Chapter 7

Conclusions

7.1 Main findings

This thesis aimed to investigate the role of ^{18}F-sodium fluoride positron emission tomography and computed tomography, plasma desmosine concentration and circulating miRNA expression in patients with acute aortic syndrome.

7.1.1 ^{18}F sodium fluoride PET/CT in acute aortic syndrome

We performed tissue analysis from the aortas of patients with acute aortic syndrome and found that areas of medial degeneration co-localised with microscopic calcification that could be detected using ^{18}F-sodium fluoride. We then characterised, for the first time, ^{18}F-sodium fluoride PET/CT uptake in patients with acute aortic syndrome and found that this signal is increased particularly around areas of cellular injury such as the site of intimal disruption and the dissection flap. This was the largest PET study in patients with acute aortic syndrome and the first to use ^{18}F-Sodium fluoride. Interestingly, we found that ^{18}F-sodium fluoride PET/CT uptake in the outer wall adjacent to the false lumen was associated with aortic expansion and this relationship remained true independent of confounders such as the time since acute aortic syndrome and surgical intervention. Next, ^{18}F-sodium fluoride PET uptake in the outer aortic wall emerged as a predictor of major adverse aortic events in patients with recent disease. Again, this was independent of con-

ventional clinical risk factors such as aortic diameter, age and comorbidities.

Our findings on the use of ^{18}F-sodium fluoride PET/CT in patients with acute aortic syndrome highlight the powerful insights to be gained through the non-invasive biological imaging of the aorta. The pathophysiological processes detected by ^{18}F-sodium fluoride would otherwise be silent because they are beyond the resolution of conventional anatomical imaging. Morphological aortic change is a late-feature of disease and is unable to adequately stratify risk in the early stages of acute aortic syndrome. The application of multimodality molecular imaging holds immense promise to advance our knowledge of the disease processes that drive morphological change and improve risk stratification in a vulnerable patient cohort.

7.1.2 Plasma desmosine in acute aortic syndrome

Acute aortic syndrome is a degenerative aortopathy that is challenging to diagnose, unpredictable and catastrophic. We investigated the concentration of plasma desmosine in patients with acute aortic syndrome which is released in to the circulation when mature elastin breaks down. We characterised, for the first time, plasma desmosine concentration in patients with acute aortic syndrome and found that levels were markedly increased compared to healthy controls. Interestingly, plasma desmosine was detectable within 24 hours of symptom onset in patients presenting to the emergency department with acute aortic syndrome - a clinical state associated with rapid aortic destruction. The early spike of plasma desmosine makes it an attractive potential biomarker for the diagnosis of acute aortic syndrome. Indeed, prompt diagnosis of acute aortic syndrome is a major unmet clinical need.

Plasma desmosine concentration was also associated with disease states of the aorta. Aortic expansion occurs as a result of loss of elastin structure. It is perhaps not surprising that patients with large aortas had reduced circulating plasma desmosine. Plasma desmosine concentration, however, *was* associated with aortic Agatston score. Aortic calcification is a maker of cellular degeneration and its relationship with plasma desmosine supports the hypothesis that medial destruction within the aortic wall is associated with the release of desmosine in to the circulation. Finally, we found that increased circu-

lating desmosine was associated with aortic expansion independent of confounders such as aortic diameter, the time since acute aortic syndrome, and prior intervention.

7.1.3 miRNA in acute aortic syndrome

Finally, we investigated circulating miRNA expression in patients with acute aortic syndrome in relation to disease characteristics and progression. miRNA are non-coding fragments that modulate post-transcription protein function. We identified 16 candidate miRNA and found that these were deferentially expressed between study participants and healthy controls. We found that individual miRNAs were associated with multiple aspects of disease severity and progression, including aortic size, calcification and expansion. We used machine-learning statistical techniques to gain a better understanding of miRNA expression and its relation to major adverse aortic event. Our miRNA signature outperformed traditional clinical paramters such as aortic diameter to identify patients that encountered major adverse aortic events. This is the largest miRNA study in patients with acute aortic syndrome and the first to characterise miRNA expression with longitudinal disease outcomes. This novel finding opens multiple possible avenues to explore the pathobiology that may drive medial degeneration. Interestingly, many of the miRNA we investigated were under-expressed suggesting a deficiency in post-transcription modulation of genetic targets. The identification of a key miRNA-axis that drives disease progression may one day even translate to a potential therapeutic target by replenishing deficient miRNA.

7.1.4 Detecting vascular injury

Detecting vascular injury is challenging. Processes such as cellular destruction, microscopic calcification and elastin fragmentation are beyond the scope of conventional anatomical imaging and are thus silent. Morphological aortic change is a late manifestation of disease which may be predated by altered biological properties of the aortic wall. Consequently, two aortas with relatively similar morphological features may have different biological properties with varying clinical consequences. The ability to study biological activity in the aorta thus holds immense promise for the early detection of

vascular injury.

We performed ^{18}F-sodium fluoride PET/CT in patients with acute aortic syndrome as a means to detect microscopic calcification within the aortic wall. This had never been done in patients with acute aortic syndrome before. We first demonstrated that ^{18}F-sodium fluoride is able to detect microcalcification associated with cellular injury in tissue specimens. In our clinical cohort, we found that ^{18}F-sodium fluoride PET/CT uptake was increased in patients with both, *recent* and *prior* acute aortic syndrome, and that this activity concentrated around areas of cellular destruction: the site of intimal injury, the base of penetrating aortic ulcers and the dissection flap itself. As we had hypothesised, our clinical study found that patients with acute aortic syndrome had aortic microcalcfication that was now detectable using ^{18}F-sodium fluoride PET/CT.

Our histological specimens also demonstrated dramatic rupturing of elastin fibres in the aortic wall. Indeed, disruption of the extracellular matrix and loss of cellular architecture in acute aortic syndrome is well described (Wanga et al. 2017). We thus hypothesised that circulating biomarkers of mature elastin degeneration, such as desmosine, may be indicative of medial degeneration. We found that plasma desmosine was elevated in all phases of acute aortic syndrome. Plasma desmosine was thus found to be elevated in acute aortic syndrome and was detectable within 24 hours of symptom onset as an acute marker of profound vascular injury. This has exciting implications for plasma desmosine as a diagnostic blood test for acute aortic syndrome. Future work will now determine the predictive ability of plasma desmosine to detect and differentiate acute aortic syndrome from competing pathologies such as myocardial infarction and pulmonary embolus.

Both, ^{18}F-sodium fluoride uptake and plasma desmosine concentration are associated with cellular injury in patients with acute aortic syndrome. ^{18}F-Sodium fluoride is a promising multimodality imaging technique that provides a topicological map of cellular injury in the disease aorta. It is thus highly specific for aortic tissue. In contrast, plasma desmosine provides a measure of global elastin degeneration with the potential to detect sudden aortic disruption through a surge in circulating desmosine.

7.1.5 The vulnerable aorta

Predicting risk in acute aortic syndrome is challenging. Failing to detect potential complications is associated with catastrophic and often fatal complications. Thus, identifying the vulnerable aorta is a major unmet clinical need in acute aortic syndrome. Having had detected aortic injury in these patients, the next objective of this work was to understand how ^{18}F-sodium fluoride PET, plasma desmosine and circulating miRNA may improve risk stratification.

The current strategy for predicting risk is to enroll patients to an imaging surveillance program to monitor morphological change. Simply observing progressive aortic expansion carries risks. Rapid disease progression may occur between interval scans and there is a risk of sub-threshold aortic rupture. In addition, the use of aortic diameter as a unidimensional metric fails to capture the complex biological features associated with acute aortic syndrome. Finally, there is no obvious adverse morphological feature that predicts major adverse aortic events.

We propose that studying the biological properties of the aorta can improve our ability to predict aortic expansion or major adverse aortic events. Indeed, we found that ^{18}F-sodium fluoride activity in the outer wall of the false lumen, which is most vulnerable to dilatation, is associated with aortic expansion. This was independent of traditional risk factors such as aortic diameter and prior intervention. Similarly, we found that patients that experienced the most rapid aortic expansion also had the greatest concentration of circulating desmosine. Finally, we identified multiple miRNA interactions that were associated with aortic diameter and aortic expansion. We have found that the most vulnerable aortas prone to expansion exhibit biological characteristics that are closely related to the burden of cellular injury and medial degeneration. Identifying vascular injury can thus potentially identify the vulnerable aorta at risk of expansion.

Aortic expansion may lead to major adverse aortic events such as aortic rupture, aortic death or the need for aortic intervention. Again, waiting for morphological change is a high-risk strategy owing to the unpredicatable nature of acute aortic syndrome. We found that ^{18}F-sodium fluoride uptake in the outer aortic wall independently predicted major adverse

aortic events by quantifying microcalcification as a global measure of vascular health. We also found a distinct miRNA signature in patients with acute aortic syndrome. This signature emerged as a potential tool that identifies patients with a three-fold increased risk of encountering a major adverse aortic event. Again, this was the first time that ^{18}F-sodium fluoride PET or miRNAs had been investigated in patients with acute aortic syndrome to predict clinical outcomes. We found that moving beyond morphological features to incorporate multimodality imaging and molecular genetics can inform us of the biological activity in the aortic wall to identify the vulnerable aortas following acute aortic syndrome.

7.1.6 Limitations

We must recognise limitations of our work. This was the first time ^{18}F-sodium fluoride PET, plasma desmosine or miRNA were being investigated in patients with acute aortic syndrome. Hence the study population consisted of a relatively heterogeneous group of patients consisting of both, Stanford type A and type B disease across a spectrum of timepoints within the disease. This strategy allows us to describe radiotracer binding in a variety of clinical and aortic morphological states. However, the variability in our cohort also makes it challenging to draw conclusions with regards to clinical subgroups. Acute aortic syndrome typically has an extremely varied presentation that likely drives unpredictable clinical outcomes. Even subpopulations within the same Stanford classification group may present with very different morphological changes, some of whom experience rapid aortic growth. This adds a further degree of heterogeneity within our cohort. Despite this shortcoming, however, we were able to detect a relationship between radiotracer binding and aortic expansion in a relatively modest sample size suggesting a positive underlying relationship must exist and is in need for further characterisation.

It is difficult to determine whether the radiotracer binding we observed was due to the dissection process itself or because of medial degeneration leading to aneurysmal transformation. It would be interesting to compare radiotracer binding between acute aortic syndrome patients and those with de-novo thoracic aortic aneurysms to better understand the pathological processes that drive ^{18}F-sodium fluoride binding. In this first analysis on patients with acute aortic syndrome, we considered it prudent to compare ^{18}F-sodium flu-

oride binding with healthy controls with no background of aortopathy.

Our exclusion criteria for this study included patients that were unable to consent and those with significant renal injury. These are devastating potential consequences of acute aortic syndrome itself. Indeed, patients that were excluded from the study may represent the most vulnerable cohort – those that experienced renal ischaemia or a cerebrovascular accident as consequence of the disease process. Thus our study investigates patients that remained relatively well following their initial presentation with acute aortic syndrome.

We adopted a robust systematic approach to optimise exclusion of radiotracer signal from adjacent structures such as bone and neighbouring viscera. However, there is still a degree of user-dependent subjectivity when establishing regions of interest within an aorta that may have undergone significant morphological distortion. ^{18}F-Sodium fluoride MDS TBR$_{max}$ was calculated at point of image acquisition thus reducing bias towards longitudinal outcomes. Novel techniques to computationally reduce bony interference of ^{18}F-sodium fluoride signal are under development and may be instrumental to differentiate cardiovascular signal uptake from adjacent osseous structures (Akerele et al. 2020, 2019). The MDS TBR$_{max}$ method of quantifying ^{18}F-sodium fluoride method is validated and the gold standard for measuring radiotracer binding within the aorta. However, it detects peak radiotracer binding within a small segment of aorta. This approach is beneficial in situations where foci of disease activity manifest as radiological hotspots. Newer techniques, such as the aortic microcalcification activity (AMA) score, are now being validated that offer a global measure of ^{18}F-sodium fluoride binding within the entire vessel (Fletcher et al. 2021). The AMA score is akin to conventional calcium scoring performed on conventional CT scans by providing a metric that reflects the total burden of microcalcification in the entire vessel, corrected for vessel volume and background blood pool activity. The AMA method has been validated in the quantification of ^{18}F-sodium fluoride in the ascending aorta and is currently being evaluated in infrarenal aortic aneurysms. Further work will be required to confirm its utility in patients with acute aortic syndrome.

We used conventional statistical techniques to compare normally distributed variables between groups. All three statistical techniques used in this thesis, namely linear regression, proportional hazards Cox regression, and linear discriminant analysis models assume a

normal distribution of continuous predictor variables with little covariance. Each of these models attempts to fit a linear relationship which can be adjusted by transforming the distribution of predictors. However, it is possible that the relationships observed were not related in a linear fashion and thus suppressed or exaggerated by our modelling technique. More complex statistical models, such as decision trees, have the strength of fitting non-linear relationships. However, these models work better with larger sample sizes thus reducing the likelihood of overfitting data to "noise". A future study with a larger data set would benefit from such statistical techniques to find non-linear relationships associated with aortic expansion or major adverse aortic events.

Finally, there is a large variation in clinical practice and no international consensus on the optimum management of patients with acute aortic syndrome. Thus, the threshold for intervention following acute aortic syndrome varies between clinicians owing to differences in perceived risk determined by clinical and radiological disease progression. Variation in the management of acute aortic syndrome influences our clinical end points for aortic repair. External validation in a future larger study would be required to increase generalisability of our findings.

7.2 Future Direction

We have identified ^{18}F-sodium fluoride PET/CT as a promising imaging biomarker in patients with acute aortic syndrome. We have also investigated plasma desmosine and serum miRNA expression in patients with acute aortic syndrome. Each of these biomarkers offers potential to detect disease and improve risk stratification. However, we have also highlighted several limitations of this early exploratory work.

7.2.1 ^{18}F-sodium fluoride PET imaging in patients with acute aortic syndrome

Future research should now focus on investigating ^{18}F-sodium fluoride binding in a larger and sub-selected cohort of patients with acute aortic syndrome followed up for a longer period. There are several interesting questions raised by our work. Namely, how does ^{18}F-sodium fluoride binding influence disease progression within specific subtypes of acute

aortic syndrome? Does the pattern of radiotracer binding change with respect to time on serial imaging? What are the implications of endovascular or surgical intervention on ^{18}F-sodium fluoride risk stratification? And can ^{18}F-sodium fluoride ultimately aid clinicians to target the vulnerable aorta with early intervention? There is now a need to better characterise ^{18}F-sodium fluoride binding in focussed subgroups of patients with acute aortic syndrome, thus increasing generalisability of this research and understanding its role in clinical practice.

There remains considerable uncertainty on the optimum approach to treat patients with uncomplicated Stanford type B aortic dissections. Patients have traditionally been treated with antihypertensive therapy alone. The emergence of endovascular therapy has revolutionised the treatment of thoracic aortopathy. Although endovascular therapy improves aortic remodelling, such a strategy in an unselected cohort of patients has failed to demonstrate a clear benefit. ^{18}F-sodium fluoride PET/CT may bridge this critical knowledge gap by identifying the vulnerable aorta prone to expansion or rupture thus aiding targeted endovascular therapy. In the first instance, a future study would aim to better characterise ^{18}F-sodium fluoride in a homogenous group of patients with uncomplicated Stanford type B aortic dissection managed with medical intervention alone. We have already demonstrated that patients with Stanford type B acute aortic syndrome exhibit increased radiotracer binding. A future study would build on this knowledge by investigating ^{18}F-sodium fluoride binding with respect to known high-risk aortic features, adverse clinical metrics and ultimately disease progression requiring intervention or experiencing a major adverse aortic event. Based on the findings from our study, a sample size of nearly 125 patients would be required to detect a difference of 20% between patient groups stratified by ^{18}F-sodium fluoride PET/CT as observed in this study, powered at 90% to an alpha threshold of 0.05. Such a study is feasible but requires a multicentre effort to deliver the largest PET/CT study in patients with acute aortic syndrome. Such a study could identify the unique combination of clinical and multimodality imaging features likely associated with disease progression. Detailed characterisation of ^{18}F-sodium fluoride binding in patients with uncomplicated type B aortic dissection would then provide a criterion to stratify patients in to high- and low-risk of adverse clinical events and thus being targeted with inter-

vention in the form of a randomised controlled study.

Similarly, in patients with Stanford type A aortic dissection, the natural history of disease progression within the remaining distal aorta is unpredictable. Patients with type A aortic dissection are often investigated intensively during the perioperative period to repair the ascending aorta. However, surveillance in the chronic phase of disease is less intensive and patients are consequently lost to follow-up. ^{18}F-Sodium fluoride PET/CT in this group of patients may, again, help identify the vulnerable aorta with the aim of targeting surveillance and subsequent intervention.

A further major clinical need is the identification of the vulnerable aorta in patients with connective tissue disorders or congenital bicuspid aortic valves. These patients are 100 times more likely to experience an acute aortic syndrome compared to the general population. Intervention is currently driven by aortic diameter. However, in at-risk individuals, up to 70% of aortic dissections occur below this size threshold. Aortic diameter is the clinical standard to direct intervention however it is a single unidimensional metric that oversimplifies a complex disease process.

7.2.2 ^{18}F-sodium fluoride PET in other aortopathies

Current work at the British Heart Foundation Centre for Cardiovascular Science, University of Edinburgh is using ^{18}F-sodium fluoride detect vascular injury in the aorta of patients with congenital aortopathies and bicuspid aortic valves. We have already demonstrated that ^{18}F-sodium fluoride binds to areas of medial degeneration characterised by a reduction in elastin content and the precipitation of microscopic calcium-rich hydroxyapatite crystals. We have also characterised the ^{18}F-sodium fluoride binding pattern in patients that do experience acute aortic syndrome. The research team is now investigating tissue samples from high-risk patients with congenital aortopathy in a three-part study. First, we intend to investigate myocyte and myofibroblast function within the media of patients with congenital aortopathy. We have already demonstrated expertise in ^{18}F-sodium fluoride pre-clinical and human studies. Cellular expression of myocyte function will be performed in collaboration of a specialist histology team at the University of British Columbia. Histological and autoradiography findings will be correlated with the

biomechanical properties of freshly acquired specimens in a collaboration with a team of biomechanical engineers at the University of Liverpool. Second, we will perform ^{18}F-sodium fluoride PET/MRI in 60 patients with thoracic aortopathy (30 patients with Marfan's syndrome and 30 with Turner's Syndrome) and compare this to radiotracer binding in age- and sex-matched healthy controls to characterise ^{18}F-sodium fluoride binding in disease groups. Finally, we like the present thesis, we intend to gain early exploratory data on the clinical implications of ^{18}F-sodium fluoride PET/MRI in patients with thoracic aortopathies and disease progression. There is clear potential to gain a better understanding of the pathophysiological processes that drive aortopathy using ^{18}F-sodium fluoride PET/MRI to ultimately improve the care received by extremely high-risk patients.

A second related imaging project at the British Heart Foundation Centre for Cardiovascular Science is investigating the role of ^{18}F-sodium fluoride PET/CT in patients with abdominal aortic aneurysms treated by endovascular aneurysm repair (EVAR). The emergence of EVAR has provided a minimally invasive alternative to abdominal aortic aneurysm repair. The procedure involves placing a stent within the abdominal aortic aneurysm under fluoroscopic guidance with the aim of excluding the aneurysm sac from perfusion and thus reducing the risk of aortic rupture. Despite advances in second and third generation stents, there remains a risk of blood continuing to perfuse the aneurysm sac and presenting a risk of aortic rupture. A leak may develop around the stent, arise from back-bleeding from a visceral branch, or result from stent migration or fracture. Indeed, the aortic wall is a biologically active medium that is both, diseased but also integral to securing the stent in place. The utility of EVAR has thus been undermined by concerns of stent durability. Investigating biological activity within the native aortic wall using ^{18}F-sodium fluoride PET/CT holds promise to identify patients that may encountered continued degenerative and morphological change despite stent placement and thus proceed to developing EVAR-related complications.

The proposed study consists of two parts. First, a cross-sectional study will characterise ^{18}F-sodium fluoride PET/CT in 20 patients with and 20 patients without EVAR-related complications including endoleaks. Second, a prospective longitudinal study will perform ^{18}F-sodium fluoride PET/CT in 80 patients prior to EVAR therapy to identify adverse morpholog-

ical and PET features associated with post-procedural complications such as endoleaks. This study will ultimately aim to identify vulnerable sections of aorta in patients undergoing EVAR therapy for abdominal aortic aneurysm and lay the foundation for a future study to select patients who will benefit most from EVAR. This is a major unmet clinical need.

7.2.3 Plasma desmosine as a marker of elastin degeneration

Desmosine is a marker of mature elastin degradation. It is a highly stable molecule that can be readily detected in the plasma of patients with acute aortic syndrome. We have demonstrated two potential roles for plasma desmosine in patients with acute aortic syndrome. First, plasma desmosine was detectable within 24 hours of symptoms onset and thus may play a role in the early diagnosis of acute aortic syndrome in the emergency department. Second, plasma desmosine concentration was associated with aortic calcification and expansion and may be an important marker for risk stratification in patients with acute aortic syndrome.

Our early explanatory analysis of plasma desmosine detected raised circulating concentrations in patients with acute aortic syndrome. However, more work is required to characterise plasma desmosine, particularly in relation to alternative causes of chest pain if it is to be used as a diagnostic biomarker. This is essential to determine the specificity and sensitivity of plasma desmosine to detect acute aortic syndrome in the emergency setting. Work is now underway to characterise plasma desmosine concentrations in patients presenting with alternative diagnoses for chest pain. These include 20 patients with myocardial infarction, 20 with pulmonary embolus and 20 with non-specific chest pain, in addition to 20 patients with acute aortic syndrome. This early exploratory cross-sectional analysis will provide insight on the concentration of plasma desmosine in the most common presentations of chest pain and lay the foundation for a prospective cohort study that will investigate the predictive power of plasma desmosine for diagnosing acute aortic syndrome in a larger study. Again, this will require a larger multicentre effort.

Similarly, there is a need to gain a better understanding of circulating biomarker expression in patients with acute aortic syndrome which will likely require a multicentre collaborative effort. Like the future research in ^{18}F-sodium fluoride PET studies, there is a need now

to characterise plasma desmosine concentrations in targeted subpopulations of patients with acute aortic syndrome. This includes patients at specific stages of the disease, and those belonging to a single Stanford classification group. This step is essential to determine the role of plasma desmosine as a viable risk stratification tool in patients with acute aortic syndrome. We noted a 2-fold increase in plasma desmosine concentrations in patients with acute aortic syndrome compared to healthy controls. A larger cohort study is now required to prospectively measure plasma desmosine concentrations in a homogenous subgroup of patients with acute aortic syndrome and followed-up to determine their risk of aortic expansion.

7.2.4 miRNA expression in patients with aortopathy

We found a potential miRNA signature in patients with acute aortic syndrome that may be associated with major adverse aortic events. Again, miRNA expression now needs to be validated in a larger sample size of a more homogenous subpopulation of patients with acute aortic syndrome, with crucially, a standardised approach to intervention. We know very little about the molecular influence of miRNA in patients with acute aortic syndrome. This novel class of circulating modulators likely interact with multiple genes in different tissue beds thus exerting a significant influence on the expression of key pathological pathways. This exciting new class of biological modulators represents both, a daunting but also promising potential to enhance our understanding of disease processes. miRNAs are also being investigated as potential therapeutic targets.

Circulating miRNA may originate from any part of the body. There is now a need to obtain fresh-frozen aortic tissue from patients undergoing surgical repair for acute aortic syndrome and measuring miRNA expression in these specimens. A future study would investigate relationships between the histological structure of diseased aortic tissue, miRNA expression, markers of cellular function such as vascular smooth muscle immunohistochemistry or osteopontin expression, and clinical or demographic characteristics such as patient smoking history.

Preparing and fixing fresh-frozen aortic specimens from patients with acute aortic syndrome presents a significant logistical challenge as most open repairs are now performed

in emergency situations involving the ascending aorta. Our previous work on the histological characterisation of tissue, however, has demonstrated that it is possible to obtain aortic histology from a modest cohort of 75 patients through collaborative networks. A future study on the miRNA expression in acute aortic syndrome would aim to investigate the aortic expression of candidate miRNAs directly in tissue and within the peripheral circulation.

We found that many candidate miRNAs were under expressed in patients with acute aortic syndrome compared to healthy controls. The absence of these miRNAs was associated with morphological changes in the aorta such as increased likelihood to undergo aortic expansion or calcification. Thus, we may have started identifying molecular pathways that lead to medial degeneration and disease progression through a deficiency of miRNA signalling. There is now a need to characterise the biological pathways within the aorta of the most promising miRNA candidates such as those belonging to the hsa-miR-30* family. Initial animal models suggest that blocking the hsa-miR-30* family leads to aortic expansion in mice and we found a similar relationship in patients with acute aortic syndrome. Further, targeted animal models may now be developed to determine the influence of manipulating candidate miRNAs on the biology and phenotype of aortas. This would improve our understanding of the mechanisms that lead to aortic expansion and possibly to acute aortic syndrome. miRNA have been investigated as potential therapeutic agents by replacing them using novel drug-delivery techniques. Indeed, identifying critical miRNA pathways in degenerative aortopathies may one day lead to novel drug discoveries. This would represent a significant advance for the medical management of aortopathy and represents a major unmet clinical need.

7.2.5 Novel analytical techniques

Scotland hosts a unique dataset of comprehensive patient-level data for hospital admissions, surgical intervention, drug prescriptions, diabetes mellitus, cancer and death over a 30-year period. Access to this data is governed by clinical need and secured through the Public Benefit and Privacy Panel for Health and Social Care. We now have anonymised linked data for all patients that have presented to a Scottish hospital with a diagnosis of

acute aortic syndrome since inception of the database. This is now the largest and most comprehensive national dataset of aortic diseases and provides a sample set sufficient to go beyond traditional audit reporting.

The emergence of novel supervised prediction algorithms that use retrospective observational data to find recurring patterns to aid classification. Examples of such algorithms include random forest regression, k-nearest neighbour and extreme gradient boosting. These models can detect non-linear relationships between predictor variables and perform best with larger datasets. In contrast to popular belief, these models are also entirely explainable, and it is possible to obtain the predictive significance of individual variables across their entire distribution. Indeed, we used a similar machine learning algorithm, the linear discriminant analysis, in our investigation of miRNA expression in patients with acute aortic syndrome. We now plan to investigate this substantial dataset of patients admitted to Scottish hospitals with a diagnosis of aortopathy in relation to surgical outcomes. We will use novel statistical techniques to find patterns in patient presentation to identify and characterise the relationship between clinical risk factors and outcomes. This investigation will form the basis of future prospective observational studies that ultimately hold the potential to inform randomised clinical trials.

Novel analytical techniques leverage advanced computational algorithms and off-site commercially available computing platforms to classify or predict user-defined outcomes. Indeed, the emergence of unsupervised learning algorithms can now identify abstract clustering patterns within data that may go unrecognised on manual inspection. There is growing interest in automated image interpretation algorithms that detect disease, improve risk stratification and eventually aid clinical decision making. Such algorithms are suited to identifying subtle relationships in subjective data sets such as images. Radiological investigations such as CT and MRI image stacks contain a large amount of unstructured data that requires interpretation and thus subjectivity to extract useful information. In contrast, an automated algorithm accepts the entire raw image stack and identifies relationships within the data by treating it as a large three-dimensional matrix. These techniques require significant computational power and technical expertise to optimise. However, the final product carries potential to identify imaging features that

play a role in predicting a clinical endpoint. For instance, patients with acute aortic syndrome have highly varied aortic morphology which is often condensed to a single metric such as aortic diameter or tortuosity. Much of the morphological data from the aorta of these patients is lost. An automated learning algorithm, such as a deep-neural network, could potentially identify a combination of morphological features that predict disease progression beyond conventional clinical metrics. A model algorithm would first automatically extract geometries of structures within and around the aorta and then investigating imaging properties, such as Hounsfield unit intensity within thrombus or peri-aortic fat, with the aim of predicting adverse features associated with disease progression. Indeed, such algorithms have already been tested in other structures such as the brain and retinal scans. We have also made initial progress to automatically segment aortic morphology from CT angiography using deep neural networks. The British Heart Foundation Department for Cardiovascular Science has excellent in-house expertise and a wide collaborative network to facilitate a project of this ambition. The University of Edinburgh also has access to in-house supercomputer facilities that can be used to tune and train resource-intensive algorithms.

7.3 Conclusion

Acute aortic syndrome is a devastating and unpredicatable condition. Diagnosis is challenging and conventional risk stratification relies on detecting morphological change which is a late feature. Studying aortic wall biology in patients with acute aortic syndrome may help detect cellular injury and predict disease progression or clinical outcomes.

In this exploratory proof-of-concept analysis, we found ^{18}F-Sodium fluoride PET/CT to be a promising imaging modality that detects cellular injury such as the site of intimal disruption and the dissection flap. ^{18}F-Sodium fluoride PET/CT was independently associated with aortic expansion and major adverse aortic events thus suggesting a potential role in risk stratification. We also investigated two novel circulating biomarkers of medial degeneration. First, we found that plasma desmosine, a by-product of mature elastin degradation, was increased in patients with acute aortic syndrome and detectable within 24 hours

of symptoms onset. This has exciting implications for the use of plasma desmosine as a diagnostic biomarker in acute aortic syndrome. Plasma desmosine concentration was also associated with aortic expansion. Second, we identified candidate miRNA and characterised their expression in the serum of patients with acute aortic syndrome with respect to aortic morphology. We found that these miRNA were associated with aortic diameter, aortic growth and aortic calcification. We then identified a miRNA signature that was indepndently associated with major adverse aortic events.

^{18}F-Sodium fluoride PET CT, plasma desmosine and miRNA carry exciting potential to detect the vulnerable aorta and aid risk stratification in patients with acute aortic syndrome. The next step is to now validate our findings in a larger, well characterised sub-population of patients with acute aortic syndrome.

Publications, prizes and achievements

Journal Publications and Book Chapters

Syed, Maaz B. J., Alexander J. Fletcher, and Marc R. Dweck. 2019. 'Imaging Cellular Activity and Proliferation in the Aortic Wall.' *Journal of Nuclear Cardiology : Official Publication of the American Society of Nuclear Cardiology*, December. https://doi.org/10.1007/s12350-019-01987-3

Syed, Maaz B. J., Alexander J. Fletcher, Marc R. Dweck, Rachael Forsythe, and David E. Newby. 2019. 'Imaging Aortic Wall Inflammation.' *Trends in Cardiovascular Medicine* 29 (8): 440–48. https://doi.org/10.1016/j.tcm.2018.12.003

Syed, Maaz Bj, Alexander J. Fletcher, Rachael O. Forsythe, Jakub Kaczynski, David E. Newby, Marc R. Dweck, and Edwin Jr van Beek. 2019. 'Emerging Techniques in Atherosclerosis Imaging.' *The British Journal of Radiology* 92 (1103): 20180309. https://doi.org/10.1259/bjr.20180309

Syed, Maaz B. J., Mhairi Doris, Marc Dweck, Rachael Forsythe, and David E. Newby. 2019. 'Chapter 9 - Imaging Vascular Calcification: Where Are We Headed'. In Coronary Calcium, edited by Aloke Virmani Finn, 203–46. *Academic Press*. https://doi.org/10.1016/B978-0-12-816389-4.00009-8

Syed, Maaz B. J., Jakub Kaczynski, and David E. Newby. 2020. '18F-Sodium Fluoride Positron Emission Tomography/Computed Tomography Imaging of the Peripheral Vasculature'. In Sodium Fluoride PET/CT in Clinical Use, edited by Kalevi Kairemo and Homer A. Macapinlac, 85–94. Clinicians' Guides to Radionuclide Hybrid Imaging. *Cham: Springer*

International Publishing. https://doi.org/10.1007/978-3-030-23577-2_11

Akerele, Mercy I., Nicolas A. Karakatsanis, Daniel Deidda, Jacobo Cal-Gonzalez, Rachael O. Forsythe, Marc R. Dweck, **Maaz Syed**, et al. 2020. 'Comparison of Correction Techniques for the Spill in Effect in Emission Tomography.' *IEEE Transactions on Radiation and Plasma Medical Sciences* 4 (4): 422–32. https://doi.org/10.1109/TRPMS.2020.2980443

Akerele, Mercy I., Nicolas A. Karakatsanis, Rachael O. Forsythe, Marc R. Dweck, **Maaz Syed**, Robert G. Aykroyd, Steven Sourbron, David E. Newby, and Charalampos Tsoumpas. 2019. 'Iterative Reconstruction Incorporating Background Correction Improves Quantification of [(18)F]-NaF PET/CT Images of Patients with Abdominal Aortic Aneurysm.' *Journal of Nuclear Cardiology : Official Publication of the American Society of Nuclear Cardiology*, November. https://doi.org/10.1007/s12350-019-01940-4

Akerele, Mercy I., Nouf A. Mushari, Rachael O. Forsythe, **Maaz Syed**, Nicolas A. Karakatsanis, David E. Newby, Marc R. Dweck, and Charalampos Tsoumpas. 2020. 'Assessment of Different Quantification Metrics of [(18)F]-NaF PET/CT Images of Patients with Abdominal Aortic Aneurysm.' *Journal of Nuclear Cardiology : Official Publication of the American Society of Nuclear Cardiology*, June. https://doi.org/10.1007/s12350-020-02220-2

Deidda, Daniel, Mercy I. Akerele, Robert G. Aykroyd, Marc R. Dweck, Kelley Ferreira, Rachael O. Forsythe, Warda Heetun, David E. Newby, **Maaz Syed**, and Charalampos Tsoumpas. 2021. 'Improved Identification of Abdominal Aortic Aneurysm Using the Kernelized Expectation Maximization Algorithm.' *Philosophical Transactions. Series A, Mathematical, Physical, and Engineering Sciences* 379 (2200): 20200201. https://doi.org/10.1098/rsta.2020.0201

Doris, Mhairi K., Mohammed N. Meah, Alastair J. Moss, Jack P. M. Andrews, Rong Bing, Rebecca Gillen, Nick Weir … **Maaz B. J. Syed**, et al. 2020. 'Coronary (18)F-Fluoride Uptake and Progression of Coronary Artery Calcification.' *Circulation.* Cardiovascular Imaging 13 (12): e011438. https://doi.org/10.1161/CIRCIMAGING.120.011438

Doyle, Barry J., Nikhilesh Bappoo, **Maaz B. J. Syed**, Rachael O. Forsythe, Janet T. Powell, Noel Conlisk, Peter R. Hoskins, et al. 2020. 'Biomechanical Assessment Predicts Aneurysm Related Events in Patients with Abdominal Aortic Aneurysm.' *European Journal*

of Vascular and Endovascular Surgery : The Official Journal of the European Society for Vascular Surgery 60 (3): 365–73. https://doi.org/10.1016/j.ejvs.2020.02.023

Fletcher, Alexander J., Maria Lembo, Jacek Kwiecinski, **Maaz B. J. Syed**, Jennifer Nash, Evangelos Tzolos, Rong Bing, et al. 2021. 'Quantifying Microcalcification Activity in the Thoracic Aorta.' *Journal of Nuclear Cardiology : Official Publication of the American Society of Nuclear Cardiology*, January. https://doi.org/10.1007/s12350-020-02458-w

Fletcher, Alexander J., **Maaz B. J. Syed**, Timothy J. Aitman, David E. Newby, and Niki L. Walker. 2020. 'Inherited Thoracic Aortic Disease: New Insights and Translational Targets.' *Circulation* 141 (19): 1570–87. https://doi.org/10.1161/CIRCULATIONAHA.119.043756

Parker, Louis P., Benedikt Reutersberg, **Maaz B. J. Syed**, Bijit Munshi, Samantha Richards, Lachlan J. Kelsey, Natzi Sakalihasan, Hans-Henning Eckstein, Paul E. Norman, and Barry J. Doyle. 2021. 'Proximal False Lumen Thrombosis Is Associated with Low False Lumen Pressure and Fewer Complications in Type B Aortic Dissection.' *Journal of Vascular Surgery*, November. https://doi.org/10.1016/j.jvs.2021.10.035

Pawade, Tania A., Mhairi K. Doris, Rong Bing, Audrey C. White, Laura Forsyth, Emily Evans, Catriona Graham … **Maaz B. J. Syed**, et al. 2021. 'Effect of Denosumab or Alendronic Acid on the Progression of Aortic Stenosihttps: A Double-Blind Randomized Controlled Trial.' *Circulation* 143 (25): 2418–27. https://doi.org/10.1161/CIRCULATIONAHA.121.053708

Sandeman, Dennis, **Maaz B. J. Syed**, Dorien M. Kimenai, Kuan Ken Lee, Atul Anand, Shruti S. Joshi, Lorraine Dinnel, et al. 2021. 'Implementation of an Early Rule-out Pathway for Myocardial Infarction Using a High-Sensitivity Cardiac Troponin T Assay.' *Open Heart* 8 (2> https://doi.org/10.1136/openhrt-2021-001769

Letters and Abstracts

Forsythe, Rachael O., **Maaz Syed**, and David E. Newby. 2018. 'Response to Letter Regarding Article, "Aortic Wall Inflammation Predicts Abdominal Aortic Aneurysm Expansion, Rupture, and Need for Surgical Repair".' *Circulation* 137 (12): 1295–96. https://doi.org/10.1161/CIRCULATIONAHA.117.032344

Doris, Mhairi, Alastair Moss, Jack Andrews, **Maaz Syed**, Rong Bing, Michelle Williams, Edwin J. R. van Beek, et al. 2019. '4 18F-Sodium Fluoride Positron Emission Tomography Predicts Progression of Coronary Calcification'. *Heart* 105 (Suppl 6): A5–6. https://doi.org/10.1136/heartjnl-2019-BCS.4

Fletcher, Alexander, Evangelos Tzolos, Shruti Joshi, Jacek Kwiecinski, Rong Bing, **Maaz Syed**, Mhairi Doris, et al. 2021. '157 18F-Sodium Fluoride Positron Emission Tomography, Aortic Disease Activity and Ischaemic Stroke Risk'. *Heart* 107 (Suppl 1): A122–A122. https://doi.org/10.1136/heartjnl-2021-BCS.154

Syed, Maaz B. J., Alexander J. Fletcher, Rachael O. Forsythe, Marc R. Dweck, Andrew L. Tambyraja, Edwin van Beek, and David E. Newby. 2019. 'Preliminary Findings from 18F-Sodium Fluoride Positron Emission Tomography/Computed Tomography in Acute Aortic Syndrome'. *European Journal of Vascular and Endovascular Surgery* 58 (6): e588–90. https://doi.org/10.1016/j.ejvs.2019.09.063

Syed, Maaz, Alexander Fletcher, Samuel Debono, Rachael Forsythe, Michelle Williams, Marc Dweck, Adriana Tavares, et al. 2021. '161 18F-Sodium Fluoride Positron Emission Tomography in Acute Aortic Syndrome'. *Heart* 107 (Suppl 1): A125–26. https://doi.org/10.1136/heartjnl-2021-BCS.158

Syed, Maaz, Zaid Iskander, Alexander Fletcher, Samuel Debono, Marc Dweck, Jeffrey T. J. Huang, Calvin Chin, David Newby, and Anna Maria Choy. 2021. 'BS7 Plasma Desmosine as a Biomarker in Acute Aortic Syndrome'. *Heart* 107 (Suppl 1): A159–A159. https://doi.org/10.1136/heartjnl-2021-BCS.205

Press Coverage

Hudson, Jocelyn. 2021. **'Collaborative effort key to investigating potential biomarker of acute aortic syndrome'.** *Vascular News (blog)*. 10 December 2021. https://vascularnews.com/collaborative-effort-key-to-investigating-potential-biomarker-of-acute-aortic-syndrome/

Hudson, Jocelyn. 2020. **'Sodium Fluoride Positron Emission Tomography Shows**

Promise as Multimodality Imaging Technique in Acute Aortic Syndrome'. *Vascular News (blog)*. 30 October 2020. https://vascularnews.com/sodium-fluoride-positron-emission-tomography-shows-promise-as-multimodality-imaging-technique-in-acute-aortic-syndrome/

On-Air Interview: Good Morning Scotland. 08:10AM, 07 June 2021. **'Plasma desmosine as a biomarker for acute aortic syndrome'.** *BBC Radio Scotland*.

Wilson, Caroline. 2021. **'Simple Blood Test Could Protect Thousands at Risk of Deadly Heart Condition'.** *Herald Scotland*, 7 June 2021. https://www.heraldscotland.com/news/19350283.acute-aortic-syndrome-scottish-study-hope-patients/

Prizes

Sol Cohen Prize 2021 for best research paper (oral abstract). Vascular Society Annual Scientific Meeting (December 2021). Title: Plasma Desmosine as a Biomarker in Acute Aortic Syndrome.

Sol Cohen Prize 2020 for best research paper (oral abstract). Vascular Society Annual Scientific Meeting (November 2020). Title: 18F-Sodium Fluoride PET/CT in Acute Aortic Syndrome.

Oral Abstract Runner-up Prize 2020. European Society of Vascular Surgery Annual Meeting (2020). Title: 18F-Sodium Fluoride PET/CT in Acute Aortic Syndrome.

Best Oral Abstract 2019. Scottish Heart and Arterial Disease Prevention (SHARP) ASM (Crieff, 2019). Title: Preliminary findings of 18F-Sodium Fluoride PET/CT in Acute Aortic Syndrome.

Oral Abstract Runner-up Prize 2019. The Society of Cardiovascular CT (SCCT) Winter Meeting (Dublin, 2019). Title: Early Experience of 18F-Sodium Fluoride PET/CT in Acute Aortic Syndrome

Bibliography

Agatston, Arthur S., Warren R. Janowitz, Frank J. Hildner, Noel R. Zusmer, Manuel Viamonte, and Robert Detrano. 1990. "Quantification of Coronary Artery Calcium Using Ultrafast Computed Tomography." *Journal of the American College of Cardiology* 15 (4): 827–32. https://doi.org/10.1016/0735-1097(90)90282-T.

Aghagolzadeh, Parisa, Matthias Bachtler, Rakesh Bijarnia, Christopher Jackson, Edward R. Smith, Alex Odermatt, Ramin Radpour, and Andreas Pasch. 2016. "Calcification of Vascular Smooth Muscle Cells Is Induced by Secondary Calciprotein Particles and Enhanced by Tumor Necrosis Factor-α." *Atherosclerosis* 251 (August): 404–14. https://doi.org/10.1016/j.atherosclerosis.2016.05.044.

Agozzino, L., F. Ferraraccio, S. Esposito, A. Trocciola, A. Parente, A. Della Corte, M. De Feo, and M. Cotrufo. 2002. "Medial Degeneration Does Not Involve Uniformly the Whole Ascending Aorta: Morphological, Biochemical and Clinical Correlations." *European Journal of Cardio-Thoracic Surgery* 21 (4): 675–82. https://doi.org/10.1016/S1010-7940(02)00022-2.

Ahmadzadeh, H., M. K. Rausch, and J. D. Humphrey. 2019. "Modeling Lamellar Disruption Within the Aortic Wall Using a Particle-Based Approach." *Scientific Reports* 9 (1): 15320. https://doi.org/10.1038/s41598-019-51558-2.

Akerele, Mercy I., Nicolas A. Karakatsanis, Daniel Deidda, Jacobo Cal-Gonzalez, Rachael O. Forsythe, Marc R. Dweck, Maaz Syed, et al. 2020. "Comparison of Correction Techniques for the Spill in Effect in Emission Tomography." *IEEE Transactions on Radiation and Plasma Medical Sciences* 4 (4): 422–32. https://doi.org/10.1109/TRPMS.2020.2980443.

Akerele, Mercy I., Nicolas A. Karakatsanis, Rachael O. Forsythe, Marc R. Dweck, Maaz Syed, Robert G. Aykroyd, Steven Sourbron, David E. Newby, and Charalampos Tsoumpas. 2019. "Iterative Reconstruction Incorporating Background Correction Improves Quantification of [18F]-NaF PET/CT Images of Patients with Abdominal Aortic Aneurysm." *Journal of Nuclear Cardiology*, November. https://doi.org/10.1007/s12350-019-01940-4.

Albarbarawi, Osama, Alun Barton, Douglas Miller, Charles McSharry, Rekha Chaudhuri, Neil C Thomson, Colin NA Palmer, Graham Devereux, and Jeffrey T-J Huang. 2013. "Characterization and Validation of an Isotope-Dilution LC–MS/MS Method for Quantification of Total Desmosine and Isodesmosine in Plasma and Serum." *Bioanalysis* 5 (16): 1991–2001. https://doi.org/10.4155/bio.13.164.

Beer, Ambros J., Jaroslav Pelisek, Peter Heider, Antti Saraste, Christian Reeps, Stephan Metz, Stefan Seidl, et al. 2014. "PET/CT Imaging of Integrin AVβ3 Expression in Human Carotid Atherosclerosis." *JACC: Cardiovascular Imaging* 7 (2): 178–87. https://doi.org/10.1016/j.jcmg.2013.12.003.

Benke, Kálmán, Bence Ágg, Bálint Szilveszter, Ferenc Tarr, Zsolt B. Nagy, Miklós Pólos, László Daróczi, Béla Merkely, and Zoltán Szabolcs. 2013. "The Role of Transforming Growth Factor-Beta in Marfan Syndrome." *Cardiology Journal* 20 (3): 227–34. https://doi.org/10.5603/CJ.2013.0066.

Bersi, M. R., R. Khosravi, A. J. Wujciak, D. G. Harrison, and J. D. Humphrey. 2017. "Differential Cell-Matrix Mechanoadaptations and Inflammation Drive Regional Propensities to Aortic Fibrosis, Aneurysm or Dissection in Hypertension." *Journal of the Royal Society Interface* 14 (136): 20170327.

Bertagna, Francesco, Giorgio Biasiotto, and Raffaele Giubbini. 2013. "The Role of F-18-Fluorothymidine PET in Oncology." *Clinical and Translational Imaging* 1 (2): 77–97. https://doi.org/10.1007/s40336-013-0014-2.

Biggs, Rosemary, and A. S. Douglas. 1953. "The Thromboplastin Generation Test." *Journal of Clinical Pathology* 6 (1): 23–29. https://www.ncbi.nlm.nih.gov/pmc/articles/PMC1023525/.

Botnar, René M., Andrea J. Wiethoff, Ullrich Ebersberger, Sara Lacerda, Ulrike Blume, Alice Warley, Christian H. P. Jansen, et al. n.d. "In Vivo Assessment of Aortic Aneurysm Wall Integrity Using Elastin-Specific Molecular Magnetic Resonance Imaging." *Circulation: Cardiovascular Imaging*. Accessed September 18, 2018. https://www.ahajournals.org/doi/abs/10.1161/circimaging.113.001131.

Bouma, B. E., G. J. Tearney, H. Yabushita, M. Shishkov, C. R. Kauffman, D. DeJoseph Gauthier, B. D. MacNeill, et al. 2003. "Evaluation of Intracoronary Stenting by Intravascular Optical Coherence Tomography." *Heart* 89 (3): 317–20. https://doi.org/10.1136/heart.89.3.317.

Bridge, Gemma, Rui Monteiro, Stephen Henderson, Victoria Emuss, Dimitris Lagos, Dimitra Georgopoulou, Roger Patient, and Chris Boshoff. 2012. "The microRNA-30 Family Targets DLL4 to Modulate Endothelial Cell Behavior During Angiogenesis." *Blood* 120 (25): 5063–72. https://doi.org/10.1182/blood-2012-04-423004.

Brugaletta, Salvatore, Hector M. Garcia-Garcia, Patrick W. Serruys, Sanneke de Boer, Jurgen Ligthart, Josep Gomez-Lara, Karen Witberg, et al. 2011. "NIRS and IVUS for Characterization of Atherosclerosis in Patients Undergoing Coronary Angiography." *JACC: Cardiovascular Imaging* 4 (6): 647–55. https://doi.org/10.1016/j.jcmg.2011.03.013.

Brunkwall, J., P. Kasprzak, E. Verhoeven, R. Heijmen, P. Taylor, P. Alric, L. Canaud, et al. 2014. "Endovascular Repair of Acute Uncomplicated Aortic Type B Dissection Promotes Aortic Remodelling: 1 Year Results of the ADSORB Trial." *European Journal of Vascular and Endovascular Surgery* 48 (3): 285–91. https://doi.org/10.1016/j.ejvs.2014.05.012.

Budoff, Matthew J., Junichiro Takasu, Ronit Katz, Songshou Mao, David M. Shavelle, Kevin D. O'Brien, Roger S. Blumenthal, J. Jeffrey Carr, and Richard Kronmal. 2006. "Reproducibility of CT Measurements of Aortic Valve Calcification, Mitral Annulus Calcification, and Aortic Wall Calcification in the Multi-Ethnic Study of Atherosclerosis." *Academic Radiology* 13 (2): 166–72. https://doi.org/10.1016/j.acra.2005.09.090.

Chavan, Ajay, Osama Eldergash, and Rohit Philip Thomas. 2020. "Role of Endoluminal Techniques in the Management of Acute Type B Aortic Dissection and Intramural Haematoma." *Cardiovascular and Interventional Radiology* 43 (12): 1798–1807.

https://doi.org/10.1007/s00270-020-02652-w.

Chen, Yiping, Yanjuan Lin, Haoruo Zhang, Yanchun Peng, Sailan Li, and Xizhen Huang. 2020. "Relationship of Platelet Counts and Inflammatory Markers to 30-Day Mortality Risk in Patients with Acute Type a Aortic Dissection." *BioMed Research International* 2020: 1057496. https://doi.org/https://dx.doi.org/10.1155/2020/1057496.

Chen, Yuhao, and Xiaowei Wang. 2020. "miRDB: An Online Database for Prediction of Functional microRNA Targets." *Nucleic Acids Research* 48 (D1): D127–D131. https://doi.org/10.1093/nar/gkz757.

Clarke, Murray C. H., Trevor D. Littlewood, Nichola Figg, Janet J. Maguire, Anthony P. Davenport, Martin Goddard, and Martin R. Bennett. 2008. "Chronic Apoptosis of Vascular Smooth Muscle Cells Accelerates Atherosclerosis and Promotes Calcification and Medial Degeneration." *Circulation Research* 102 (12): 1529–38. https://doi.org/10.1161/CIRCRESAHA.108.175976.

Clément Marc, Chappell Joel, Raffort Juliette, Lareyre Fabien, Vandestienne Marie, Taylor Annabel L., Finigan Alison, et al. 2019. "Vascular Smooth Muscle Cell Plasticity and Autophagy in Dissecting Aortic Aneurysms." *Arteriosclerosis, Thrombosis, and Vascular Biology* 39 (6): 1149–59. https://doi.org/10.1161/ATVBAHA.118.311727.

Davignon, Jean, and Peter Ganz. 2004. "Role of Endothelial Dysfunction in Atherosclerosis." *Circulation* 109 (23 suppl 1): III–27.

de Boysson, Hubert, Anael Dumont, Eric Liozon, Marc Lambert, Jonathan Boutemy, Gwenola Maigne, Nicolas Martin Silva, et al. 2017. "Giant-Cell Arteritis: Concordance Study Between Aortic CT Angiography and FDG-PET/CT in Detection of Large-Vessel Involvement." *European Journal of Nuclear Medicine and Molecular Imaging* 44 (13): 2274–9. https://doi.org/10.1007/s00259-017-3774-5.

de Boysson, Hubert, Eric Liozon, Marc Lambert, Jean-Jacques Parienti, Nicolas Artigues, Loik Geffray, Jonathan Boutemy, et al. 2016. "18F-Fluorodeoxyglucose Positron Emission Tomography and the Risk of Subsequent Aortic Complications in Giant-Cell Arteritis: A Multicenter Cohort of 130 Patients." *Medicine* 95 (26): e3851. https://doi.org/10.1097/

MD.0000000000003851.

Deelchand, Dinesh Kumar, Pierre-François Van de Moortele, Gregor Adriany, Isabelle Iltis, Peter Andersen, John P. Strupp, J. Thomas Vaughan, Kâmil Uğurbil, and Pierre-Gilles Henry. 2010. "In Vivo 1H NMR Spectroscopy of the Human Brain at 9.4 T: Initial Results." *Journal of Magnetic Resonance* 206 (1): 74–80.

Derlin, Thorsten, Daniel G. Sedding, Jochen Dutzmann, Arash Haghikia, Tobias König, L. Christian Napp, Christian Schütze, et al. 2018. "Imaging of Chemokine Receptor CXCR4 Expression in Culprit and Nonculprit Coronary Atherosclerotic Plaque Using Motion-Corrected [68Ga]Pentixafor PET/CT." *European Journal of Nuclear Medicine and Molecular Imaging* 45 (11): 1934–44. https://doi.org/10.1007/s00259-018-4076-2.

Devereux, Richard B., Giovanni de Simone, Donna K. Arnett, Lyle G. Best, Eric Boerwinkle, Barbara V. Howard, Dalane Kitzman, et al. 2012. "Normal Limits in Relation to Age, Body Size and Gender of Two-Dimensional Echocardiographic Aortic Root Dimensions in Persons $\geq$15 Years of Age." *The American Journal of Cardiology* 110 (8): 1189–94. https://doi.org/10.1016/j.amjcard.2012.05.063.

Dietz, HC, and RE Pyeritz. 1995. "Mutations in the Human Gene for Fibrillin-1 (FBN1) in the Marfan Syndrome and Related Disorders." *Human Molecular Genetics* 4 (suppl_1): 1799–1809. https://doi.org/10.1093/hmg/4.suppl_1.1799.

Dohad, Suhail, Alexander Zhu, Sandeep Krishnan, Frances Wang, Serena Wang, Justin Cox, and Timothy D. Henry. 2017. "Optical Coherence Tomography Guided Carotid Artery Stent Procedure: Technique and Potential Applications." *Catheterization and Cardiovascular Interventions* 91 (3): 521–30. https://doi.org/10.1002/ccd.27344.

Donadille, Bruno, Sophie Tuffet, Clement Cholet, Mariana Nedelcu, Nathalie Bourcigaux, Laurence Iserin, Laurence Monnier-Cholley, Alexandra Rousseau, and Sophie Christin-Maitre. 2020. "Prevalence and Progression of Aortic Dilatation in Adult Patients with Turner Syndrome: A Cohort Study." *European Journal of Endocrinology* 183 (4): 463–70. https://doi.org/10.1530/EJE-20-0284.

Dong, Jian, Junmin Bao, Rui Feng, Zhiqing Zhao, Qingsheng Lu, Guokun Wang, Haiyan Li,

et al. 2017. “Circulating microRNAs: A Novel Potential Biomarker for Diagnosing Acute Aortic Dissection.” *Scientific Reports* 7 (1): 12784. https://doi.org/10.1038/s41598-017-13104-w.

Doris, Mhairi K., Mohammed N. Meah, Alastair J. Moss, Jack P. M. Andrews, Rong Bing, Rebecca Gillen, Nick Weir, et al. 2020. “Coronary 18F-Fluoride Uptake and Progression of Coronary Artery Calcification.” *Circulation. Cardiovascular Imaging* 13 (12): e011438. https://doi.org/10.1161/CIRCIMAGING.120.011438.

Duca, Laurent, Sébastien Blaise, Béatrice Romier, Muriel Laffargue, Stéphanie Gayral, Hassan El Btaouri, Charlotte Kawecki, et al. 2016. “Matrix Ageing and Vascular Impacts: Focus on Elastin Fragmentation.” *Cardiovascular Research* 110 (3): 298–308. https://doi.org/10.1093/cvr/cvw061.

Dudink, Elton A. M. P., Frederique E. C. M. Peeters, Sibel Altintas, Luuk I. B. Heckman, Rutger J. Haest, Hans Kragten, Bas L. J. H. Kietselaer, et al. 2018. “Agatston Score of the Descending Aorta Is Independently Associated with Coronary Events in a Low-Risk Population.” *Open Heart* 5 (2): e000893. https://doi.org/10.1136/openhrt-2018-000893.

Dweck, Marc R., Elena Aikawa, David E. Newby, Jason M. Tarkin, James H. F. Rudd, Jagat Narula, and Zahi A. Fayad. 2016. “Noninvasive Molecular Imaging of Disease Activity in Atherosclerosis.” *Circulation Research* 119 (2): 330–40. https://doi.org/10.1161/CIRCRESAHA.116.307971.

Dweck, Marc R., Marcus W. L. Chow, Nikhil V. Joshi, Michelle C. Williams, Charlotte Jones, Alison M. Fletcher, Hamish Richardson, et al. 2012. “Coronary Arterial 18F-Sodium Fluoride Uptake: A Novel Marker of Plaque Biology.” *Journal of the American College of Cardiology* 59 (17): 1539–48. https://doi.org/10.1016/j.jacc.2011.12.037.

Dweck, Marc R, Marcus W L Chow, Nikhil V Joshi, Michelle C Williams, Charlotte Jones, Alison M Fletcher, Hamish Richardson, et al. 2012. “Coronary Arterial 18F-Sodium Fluoride Uptake: A Novel Marker of Plaque Biology.” *Journal of the American College of Cardiology* 59 (17): 1539–48. https://doi.org/10.1016/j.jacc.2011.12.037.

Dweck, Marc R., Francis R. Joshi, David E. Newby, and James HF Rudd. 2012. “Noninvasive

Imaging in Cardiovascular Therapy: The Promise of Coronary Arterial 18F-Sodium Fluoride Uptake as a Marker of Plaque Biology." *Expert Review of Cardiovascular Therapy* 10 (9): 1075–7. https://doi.org/10.1586/erc.12.104.

Dweck, Mark R., James HF Rudd, and David E. Newby. 2014. "Positron Emission Tomography Evaluation of Aortic Stenosis." In *Multimodality Imaging for Transcatheter Aortic Valve Replacement*, 189–96. Springer.

Eggebrecht, Holger, Christoph K. Naber, Christian Bruch, Knut Kröger, Clemens von Birgelen, Axel Schmermund, Marc Wichert, Thomas Bartel, Klaus Mann, and Raimund Erbel. 2004. "Value of Plasma Fibrin D-Dimers for Detection of Acute Aortic Dissection." *Journal of the American College of Cardiology* 44 (4): 804–9. https://doi.org/10.1016/j.jacc.2004.04.053.

Emberson, Jonathan, Kennedy R Lees, Patrick Lyden, Lisa Blackwell, Gregory Albers, Erich Bluhmki, Thomas Brott, et al. 2014. "Effect of Treatment Delay, Age, and Stroke Severity on the Effects of Intravenous Thrombolysis with Alteplase for Acute Ischaemic Stroke: A Meta-Analysis of Individual Patient Data from Randomised Trials." *The Lancet* 384 (9958): 1929–35. https://doi.org/10.1016/S0140-6736(14)60584-5.

Erbel, Raimund, Victor Aboyans, Catherine Boileau, Eduardo Bossone, Roberto Di Bartolomeo, Holger Eggebrecht, Arturo Evangelista, Volkmar Falk, and Herbert Frank. 2014. "2014 ESC Guidelines on the Diagnosis and Treatment of Aortic Diseases: Document Covering Acute and Chronic Aortic Diseases of the Thoracic and Abdominal Aorta of the Adult the Task Force for the Diagnosis and Treatment of Aortic Diseases of the European Society of Cardiology (ESC)." *European Heart Journal* 35 (41): 2873–2926.

Erdolu, Burak, and Ahmet Kagan As. 2020. "C-Reactive Protein and Neutrophil to Lymphocyte Ratio Values in Predicting Inhospital Death in Patients with Stanford Type a Acute Aortic Dissection." *The Heart Surgery Forum* 23 (4): E488–E492. https://doi.org/https://dx.doi.org/10.1532/hsf.3055.

Evangelista, Arturo, Eric M. Isselbacher, Eduardo Bossone, Thomas G. Gleason, Marco Di Eusanio, Udo Sechtem, Marek P. Ehrlich, Santi Trimarchi, Alan C. Braverman, and Truls Myrmel. 2018. "Insights from the International Registry of Acute Aortic Dissection: A 20-

Year Experience of Collaborative Clinical Research." *Circulation* 137 (17): 1846–60.

Evangelista, Artur, Armando Salas, Aida Ribera, Ignacio Ferreira-Gonzalez, Hug Cuellar, Victor Pineda, Teresa Gonzalez-Alujas, Bart Bijnens, Gaieta Permanyer-Miralda, and David Garcia-Dorado. 2012. "Long-Term Outcome of Aortic Dissection with Patent False Lumen: Predictive Role of Entry Tear Size and Location." *Circulation* 125 (25): 3133–41. https://doi.org/10.1161/CIRCULATIONAHA.111.090266.

Fathi, Amir, Jonathan R Weir-McCall, Allan D Struthers, Brian J Lipworth, and Graeme Houston. 2018. "Effects of Contrast Administration on Cardiac MRI Volumetric, Flow and Pulse Wave Velocity Quantification Using Manual and Software-Based Analysis." *The British Journal of Radiology*, January, 20170717. https://doi.org/10.1259/bjr.20170717.

Fayad, Zahi A., Venkatesh Mani, Mark Woodward, David Kallend, Markus Abt, Tracy Burgess, Valentin Fuster, Christie M. Ballantyne, Evan A. Stein, and Jean-Claude Tardif. 2011. "Safety and Efficacy of Dalcetrapib on Atherosclerotic Disease Using Novel Non-Invasive Multimodality Imaging (Dal-PLAQUE): A Randomised Clinical Trial." *The Lancet* 378 (9802): 1547–59.

Fish, Jason E., Massimo M. Santoro, Sarah U. Morton, Sangho Yu, Ru-Fang Yeh, Joshua D. Wythe, Kathryn N. Ivey, Benoit G. Bruneau, Didier Y. R. Stainier, and Deepak Srivastava. 2008. "miR-126 Regulates Angiogenic Signaling and Vascular Integrity." *Developmental Cell* 15 (2): 272–84. https://doi.org/10.1016/j.devcel.2008.07.008.

Fletcher, Alexander J., Maria Lembo, Jacek Kwiecinski, Maaz B. J. Syed, Jennifer Nash, Evangelos Tzolos, Rong Bing, et al. 2021. "Quantifying Microcalcification Activity in the Thoracic Aorta." *Journal of Nuclear Cardiology: Official Publication of the American Society of Nuclear Cardiology*, January. https://doi.org/10.1007/s12350-020-02458-w.

Fletcher, Alexander J., Maaz B. J. Syed, Timothy J. Aitman, David E. Newby, and Niki L. Walker. 2020. "Inherited Thoracic Aortic Disease: New Insights and Translational Targets." *Circulation* 141 (19): 1570–87. https://doi.org/10.1161/CIRCULATIONAHA.119.043756.

Folco, Eduardo J., Yuri Sheikine, Viviane Z. Rocha, Thomas Christen, Eugenia Shvartz, Galina K. Sukhova, Marcelo F. Di Carli, and Peter Libby. 2011. "Hypoxia but Not

Inflammation Augments Glucose Uptake in Human Macrophages: Implications for Imaging Atherosclerosis with 18Fluorine-Labeled 2-Deoxy-D-Glucose Positron Emission Tomography." *Journal of the American College of Cardiology* 58 (6): 603–14. https://doi.org/10.1016/j.jacc.2011.03.044.

Forsythe, Rachael O., Marc R. Dweck, Olivia M. B. McBride, Alex T. Vesey, Scott I. Semple, Anoop S. V. Shah, Philip D. Adamson, et al. 2018. "18FSodium Fluoride Uptake in Abdominal Aortic Aneurysms: The SoFIA3 Study." *Journal of the American College of Cardiology* 71 (5): 513–23. https://doi.org/10.1016/j.jacc.2017.11.053.

Forsythe, Rachael O., David E. Newby, and Jennifer MJ Robson. 2016. "Monitoring the Biological Activity of Abdominal Aortic Aneurysms Beyond Ultrasound." *Heart* 102 (11): 817–24.

Foster, Judith Ann, Lisa Rubin, Herbert M. Kagan, Carl Franzblau, Eveline Bruenger, and Lawrence B. Sandberg. 1974. "Isolation and Characterization of CrossLinked Peptides from Elastin." *Journal of Biological Chemistry* 249 (19): 6191–6. http://www.jbc.org/content/249/19/6191.

Foye, Catherine, Irene K. Yan, Waseem David, Neha Shukla, Yacob Habboush, Lori Chase, Kristen Ryland, Vivek Kesari, and Tushar Patel. 2017. "Comparison of miRNA Quantitation by Nanostring in Serum and Plasma Samples." *PLOS ONE* 12 (12): e0189165. https://doi.org/10.1371/journal.pone.0189165.

Fuery, Michael A., Lusha Liang, Frederick S. Kaplan, and Emile R. Mohler. 2017. "Vascular Ossification: Pathology, Mechanisms, and Clinical Implications." *Bone* [In Press] (July). https://doi.org/10.1016/j.bone.2017.07.006.

Gandhi, Richa, Christopher Cawthorne, Lucinda J. L. Craggs, John D. Wright, Juozas Domarkas, Ping He, Joanna Koch-Paszkowski, et al. 2019. "Cell Proliferation Detected Using [18F]FLT PET/CT as an Early Marker of Abdominal Aortic Aneurysm." *Journal of Nuclear Cardiology*, November. https://doi.org/10.1007/s12350-019-01946-y.

Ge, Xing-Yi, Jia-Lu Li, Xing-Lou Yang, Aleksei A. Chmura, Guangjian Zhu, Jonathan H. Epstein, Jonna K. Mazet, et al. 2013. "Isolation and Characterization of a Bat SARS-Like

Coronavirus That Uses the ACE2 Receptor." *Nature* 503 (7477): 535–38. https://doi.org/10.1038/nature12711.

Geisbüsch, Philipp, Drosos Kotelis, Tim F. Weber, Alexander Hyhlik-Dürr, Hans-Ulrich Kauczor, and Dittmar Böckler. 2008. "Early and Midterm Results After Endovascular Stent Graft Repair of Penetrating Aortic Ulcers." *Journal of Vascular Surgery* 48 (6): 1361–8. https://doi.org/10.1016/j.jvs.2008.07.058.

Gholami, Saeid, Ali Salavati, Sina Houshmand, Thomas J. Werner, and Abass Alavi. 2015. "Assessment of Atherosclerosis in Large Vessel Walls: A Comprehensive Review of FDG-PET/CT Image Acquisition Protocols and Methods for Uptake Quantification." *Journal of Nuclear Cardiology* 22 (3): 468–79. https://doi.org/10.1007/s12350-015-0069-8.

Gonzalez-Galofre, Zaniah N., Carlos J. Alcaide-Corral, and Adriana A. S. Tavares. 2021. "Effects of Administration Route on Uptake Kinetics of 18F-Sodium Fluoride Positron Emission Tomography in Mice." *Scientific Reports* 11 (1): 5512. https://doi.org/10.1038/s41598-021-85073-0.

Gorla, Riccardo, Raimund Erbel, Hilmar Kuehl, Philipp Kahlert, Konstantinos Tsagakis, Heinz Jakob, Amir-Abbas Mahabadi, et al. 2015. "Prognostic Value of 18F-Fluorodeoxyglucose PET-CT Imaging in Acute Aortic Syndromes: Comparison with Serological Biomarkers of Inflammation." *The International Journal of Cardiovascular Imaging* 31 (8): 1677–85. https://doi.org/10.1007/s10554-015-0725-8.

Guo, Ling-Ling, Meng-Tao Wu, Li-Wei Zhang, Yong-Xin Chu, Peng Tian, Zai-Ping Jing, Jia-Si Li, Yu-Dong Sun, Kak K Yeung, and Lei Zhang. 2020. "Blocking Interleukin-1 Beta Reduces the Evolution of Thoracic Aortic Dissection in a Rodent Model." *European Journal of Vascular and Endovascular Surgery : The Official Journal of the European Society for Vascular Surgery* 60 (6): 916–24. https://doi.org/https://dx.doi.org/10.1016/j.ejvs.2020.08.032.

Haeberle, Stefan, Thilo Brenner, Roland Zengerle, and Jens Ducrée. 2006. "Centrifugal Extraction of Plasma from Whole Blood on a Rotating Disk." *Lab on a Chip* 6 (6): 776–81. https://doi.org/10.1039/B604145K.

Haubner, Roland, Bertrand Kuhnast, Christian Mang, Wolfgang A. Weber, Horst Kessler,

Hans-Jürgen Wester, and Markus Schwaiger. 2004. "[18F]Galacto-RGD: Synthesis, Radiolabeling, Metabolic Stability, and Radiation Dose Estimates." *Bioconjugate Chemistry* 15 (1): 61–69. https://doi.org/10.1021/bc034170n.

Hellenthal, Femke A. M. V. I., Irma L. A. Geenen, Joep A. W. Teijink, Sylvia Heeneman, and Geert Willem H. Schurink. 2009. "Histological Features of Human Abdominal Aortic Aneurysm Are Not Related to Clinical Characteristics." *Cardiovascular Pathology* 18 (5): 286–93. https://doi.org/10.1016/j.carpath.2008.06.014.

Hirsch, Danielle, Reuven Azoury, Sara Sarig, and Howard S. Kruth. 1993. "Colocalization of Cholesterol and Hydroxyapatite in Human Atherosclerotic Lesions." *Calcified Tissue International* 52 (2): 94–98. https://doi.org/10.1007/BF00308315.

Holm, Tammy M., Jennifer P. Habashi, Jefferson J. Doyle, Djahida Bedja, YiChun Chen, Christel van Erp, Mark E. Lindsay, et al. 2011. "Noncanonical TGFβ Signaling Contributes to Aortic Aneurysm Progression in Marfan Syndrome Mice." *Science (New York, N.Y.)* 332 (6027): 358–61. https://doi.org/10.1126/science.1192149.

Hong, Young T, John S Beech, Rob Smith, Jean-Claude Baron, and Tim D Fryer. 2011. "Parametric Mapping of [18F]Fluoromisonidazole Positron Emission Tomography Using Basis Functions." *Journal of Cerebral Blood Flow and Metabolism : Official Journal of the International Society of Cerebral Blood Flow and Metabolism* 31 (2): 648–57. https://doi.org/10.1038/jcbfm.2010.141.

Houben, Ignas B., Theodorus M. J. van Bakel, Nicholas S. Burris, Frans L. Moll, Joost A. van Herwaarden, and Himanshu J. Patel. 2020. "Critical Appraisal of Multidimensional CT Measurements Following Acute Open Repair of Type A Aortic Dissection." *Journal of Cardiac Surgery* 35 (3): 634–44. https://doi.org/10.1111/jocs.14446.

Hsieh, Wan Chin, Brandon Michael Henry, Chong Chao Hsieh, Pavel Maruna, Mohamed Omara, and Jaroslav Lindner. 2019. "Prognostic Role of Admission c-Reactive Protein Level as a Predictor of in-Hospital Mortality in Type-a Acute Aortic Dissection: A Meta-Analysis." *Vascular and Endovascular Surgery* 53 (7): 547–57. https://doi.org/https://dx.doi.org/10.1177/1538574419858161.

Hsu, Hung-Lung, Yun-Ning Chiu, Tai-Wei Chen, Chun-Yang Huang, Chun-Che Shih, and Chiao-Po Hsu. 2021. "Flow Density of Computed Tomography Aortography for Predicting Early Unfavorable Aortic Remodeling After TEVAR in Type IIIb Aortic Dissection." *International Journal of Cardiology* 332 (gqw, 8200291): 41–47. https://doi.org/10.1016/j.ijcard.2021.04.010.

Huang, Jeffrey T. J., Charlotte E. Bolton, Bruce E. Miller, Ruth Tal-Singer, Roberto A. Rabinovich, Colin N. A. Palmer, Neil C. Thomson, and William MacNee. 2016. "Age-Dependent Elastin Degradation Is Enhanced in Chronic Obstructive Pulmonary Disease." *European Respiratory Journal*, September. https://doi.org/10.1183/13993003.01125-2016.

Huang, Runqing, Sahar S. Abdelmoneim, Caroline A. Ball, Lara F. Nhola, Ann M. Farrell, Steven Feinstein, and Sharon L. Mulvagh. 2016. "Detection of Carotid Atherosclerotic Plaque Neovascularization Using Contrast Enhanced Ultrasound: A Systematic Review and Meta-Analysis of Diagnostic Accuracy Studies." *Journal of the American Society of Echocardiography* 29 (6): 491–502. https://doi.org/10.1016/j.echo.2016.02.012.

Humphrey, J. D. 2013. "Possible Mechanical Roles of Glycosaminoglycans in Thoracic Aortic Dissection and Associations with Dysregulated Transforming Growth Factor-β." *Journal of Vascular Research* 50 (1): 1–10. https://doi.org/10.1159/000342436.

Hysa, Lisa, Sara Khor, Benjamin W Starnes, Warren B Chow, Matthew P Sweet, Jimmy Nguyen, and Sherene Shalhub. 2021. "Cause-Specific Mortality of Type B Aortic Dissection and Assessment of Competing Risks of Mortality." *Journal of Vascular Surgery* 73 (1): 48–60.e1. https://doi.org/10.1016/j.jvs.2020.04.499.

Irkle, Agnese, Alex T. Vesey, David Y. Lewis, Jeremy N. Skepper, Joseph L. E. Bird, Marc R. Dweck, Francis R. Joshi, et al. 2015. "Identifying Active Vascular Microcalcification by 18F-Sodium Fluoride Positron Emission Tomography." *Nature Communications* 6. https://doi.org/10.1038/ncomms8495.

Itagaki, Ryo, Naoyuki Kimura, Makiko Mieno, Daijiro Hori, Satoshi Itoh, Kei Akiyoshi, Koichi Yuri, Keisuke Tanno, Koji Kawahito, and Atsushi Yamaguchi. 2018. "Characteristics and Treatment Outcomes of Acute Type A Aortic Dissection with Elevated D-Dimer Concentration." *Journal of the American Heart Association* 7 (14). https://doi.org/10.1161/JAHA.1

18.009144.

Ito, Eisaku, Takao Ohki, Naoki Toya, Soichiro Fukushima, Yuri Murakami, Hikaru Nakagawa, Ryosuke Nishie, and Takeyuki Misawa. 2020. "Aortic Wall Enhancement Detected by Contrast Computed Tomography Scan Predicts Aortic Remodeling After Conservative Therapy for Acute Uncomplicated Type B Dissection." *Annals of Vascular Surgery* 68 (avs, 8703941): 361–68. https://doi.org/10.1016/j.avsg.2020.04.036.

Jang, Ik-Kyung, Brett E. Bouma, Dong-Heon Kang, Seung-Jung Park, Seong-Wook Park, Ki-Bae Seung, Kyu-Bo Choi, et al. 2002. "Visualization of Coronary Atherosclerotic Plaques in Patients Using Optical Coherence Tomography: Comparison with Intravascular Ultrasound." *Journal of the American College of Cardiology* 39 (4): 604–9. https://doi.org/10.1016/S0735-1097(01)01799-5.

Jang, Ik-Kyung, Guillermo J. Tearney, Briain MacNeill, Masamichi Takano, Fabian Moselewski, Nicusor Iftima, Milen Shishkov, et al. 2005. "In Vivo Characterization of Coronary Atherosclerotic Plaque by Use of Optical Coherence Tomography." *Circulation* 111 (12): 1551–5. https://doi.org/10.1161/01.CIR.0000159354.43778.69.

Janosi, Rolf Alexander, Riccardo Gorla, Kim Rogmann, Philipp Kahlert, Konstantinos Tsagakis, Daniel-Sebastian Dohle, Daniel Wendt, et al. 2015. "Validation of Intravascular Ultrasound for Measurement of Aortic Diameters: Comparison with Multi-Detector Computed Tomography." *Minimally Invasive Therapy & Allied Technologies : MITAT : Official Journal of the Society for Minimally Invasive Therapy* 24 (5): 289–95. https://doi.org/10.3109/13645706.2015.1051053.

Jenkins, William S., Alex T. Vesey, Anna Vickers, Anoushka Neale, Catriona Moles, Martin Connell, Nikhil Vilas Joshi, et al. 2019. "In Vivo Alpha-V Beta-3 Integrin Expression in Human Aortic Atherosclerosis." *Heart* 105 (24): 1868–75. https://doi.org/10.1136/heartjnl-2019-315103.

Jiang, Xiaolang, Tianyue Pan, Lingwei Zou, Bin Chen, Junhao Jiang, Yun Shi, Tao Ma, et al. 2021. "Outcomes of Endovascular Stent Graft Repair for Penetrating Aortic Ulcers with or Without Intramural Hematoma." *Journal of Vascular Surgery* 73 (5): 1541–8. https://doi.org/10.1016/j.jvs.2020.10.022.

Joshi, Nikhil V, Alex T Vesey, Michelle C Williams, Anoop S V Shah, Patrick A Calvert, Felicity H M Craighead, Su Ern Yeoh, et al. 2014. "18F-Fluoride Positron Emission Tomography for Identification of Ruptured and High-Risk Coronary Atherosclerotic Plaques: A Prospective Clinical Trial." *Lancet (London, England)* 383 (9918): 705–13. https://doi.org/10.1016/S0140-6736(13)61754-7.

Ju, X., T. Ijaz, H. Sun, W. LeJeune, G. Vargas, T. Shilagard, A. Recinos, D. M. Milewicz, A. R. Brasier, and R. G. Tilton. 2014. "IL-6 Regulates Extracellular Matrix Remodeling Associated with Aortic Dilation in a Fibrillin-1 Hypomorphic mgR/mgR Mouse Model of Severe Marfan Syndrome." *Journal of the American Heart Association* 3 (1): e000476–e000476. https://doi.org/10.1161/JAHA.113.000476.

Kamman, Arnoud V, Jan Brunkwall, Eric L Verhoeven, Robin H Heijmen, Santi Trimarchi, and ADSORB trialists. 2017. "Predictors of Aortic Growth in Uncomplicated Type B Aortic Dissection from the Acute Dissection Stent Grafting or Best Medical Treatment (ADSORB) Database." Edited by Alric P Kasprzak P Heijmen R. *Journal of Vascular Surgery*, Comment in: J Vasc Surg. 2020 May;71(5):1817; PMID: 32334736 [https://www.ncbi.nlm.nih.gov/pubmed/32334736], 65 (4): 964–971.e3. https://doi.org/10.1016/j.jvs.2016.09.033.

Karimi, Ashkan, and Dianna M. Milewicz. 2016. "Structure of the Elastin-Contractile Units in the Thoracic Aorta and How Genes That Cause Thoracic Aortic Aneurysms and Dissections Disrupt This Structure." *Canadian Journal of Cardiology* 32 (1): 26–34. https://doi.org/10.1016/j.cjca.2015.11.004.

Kato, Kimihiko, Akiko Nishio, Noriyuki Kato, Hisashi Usami, Tetsuo Fujimaki, and Toyoaki Murohara. 2010. "Uptake of 18F-FDG in Acute Aortic Dissection: A Determinant of Unfavorable Outcome." *Journal of Nuclear Medicine : Official Publication, Society of Nuclear Medicine* 51 (5): 674–81. https://doi.org/10.2967/jnumed.109.065227.

Kuehl, H, H Eggebrecht, T Boes, G Antoch, S Rosenbaum, S Ladd, A Bockisch, J Barkhausen, and R Erbel. 2008. "Detection of Inflammation in Patients with Acute Aortic Syndrome: Comparison of FDG-PET/CT Imaging and Serological Markers of Inflammation." *Heart (British Cardiac Society)* 94 (11): 1472–7.

Kurdziel, Karen A., Joanna H. Shih, Andrea B. Apolo, Liza Lindenberg, Esther Mena, Yolanda Y. McKinney, Stephen S. Adler, et al. 2012. "The Kinetics and Reproducibility of 18F-Sodium Fluoride for Oncology Using Current PET Camera Technology." *Journal of Nuclear Medicine* 53 (8): 1175–84. https://doi.org/10.2967/jnumed.111.100883.

Kurvers, Harrie, Frank J. Veith, Evan C. Lipsitz, Takao Ohki, Nicholas J. Gargiulo, Neal S. Cayne, William D. Suggs, et al. 2004. "Discontinuous, Staccato Growth of Abdominal Aortic Aneurysms." *Journal of the American College of Surgeons* 199 (5): 709–15. https://doi.org/10.1016/j.jamcollsurg.2004.07.031.

Kwiecinski, Jacek, Evangelos Tzolos, Philip D. Adamson, Sebastien Cadet, Alastair J. Moss, Nikhil Joshi, Michelle C. Williams, et al. 2020. "Coronary 18F-Sodium Fluoride Uptake Predicts Outcomes in Patients with Coronary Artery Disease." *Journal of the American College of Cardiology* 75 (24): 3061–74. https://doi.org/10.1016/j.jacc.2020.04.046.

Laitinen, Iina, Antti Saraste, Eliane Weidl, Thorsten Poethko, Axel W. Weber, Stephan G. Nekolla, Pia Leppänen, Seppo Ylä-Herttuala, Gabriele Hölzlwimmer, and Axel Walch. 2009. "Evaluation of αVβ3 Integrin-Targeted Positron Emission Tomography Tracer 18F-Galacto-RGD for Imaging of Vascular Inflammation in Atherosclerotic MiceCLINICAL PERSPECTIVE." *Circulation: Cardiovascular Imaging* 2 (4): 331–38.

Lavin, Begoña, Sara Lacerda, Marcelo E Andia, Silvia Lorrio, Robert Bakewell, Alberto Smith, Imran Rashid, René M Botnar, and Alkystis Phinikaridou. 2020. "Tropoelastin: An in Vivo Imaging Marker of Dysfunctional Matrix Turnover During Abdominal Aortic Dilation." *Cardiovascular Research* 116 (5): 995–1005. https://doi.org/10.1093/cvr/cvz178.

Lavingia, Kedar S, Sebastian Larion, Sadaf S Ahanchi, Chad P Ammar, Mohit Bhasin, Aleem K Mirza, David J Dexter, and Jean M Panneton. 2015. "Volumetric Analysis of the Initial Index Computed Tomography Scan Can Predict the Natural History of Acute Uncomplicated Type B Dissections." *Journal of Vascular Surgery*, Erratum in: J Vasc Surg. 2016 Apr;63(4):1133 Note: Larion, Sebastion [corrected to Larion, Sebastian]Comment in: J Vasc Surg. 2015 Oct;62(4):899; PMID: 26210492 [https://www.ncbi.nlm.nih.gov/pubmed/26210492], 62 (4): 893–9. https://doi.org/10.1016/j.jvs.2015.04.449.

Le, Khuyen T., Caroline Chaux, Frédéric J. P. Richard, and Eric Guedj. 2020. "An Adapted Linear Discriminant Analysis with Variable Selection for the Classification in High-Dimension, and an Application to Medical Data." *Computational Statistics & Data Analysis* 152 (December): 107031. https://doi.org/10.1016/j.csda.2020.107031.

Lee, Jae Hoon, Junmo Kim, Sun-Jae Lee, Young-Ah Kim, Young-In Maeng, and Kwan-Kyu Park. 2020. "Apoptosis and Fibrosis of Vascular Smooth Muscle Cells in Aortic Dissection: An Immunohistochemical Study." *International Journal of Clinical and Experimental Pathology* 13 (8): 1962–9. https://www.ncbi.nlm.nih.gov/pmc/articles/PMC7476953/.

Lee, Ling, Jason Z. Cui, Michelle Cua, Mitra Esfandiarei, Xiaoye Sheng, Winsey Audrey Chui, Michael Haoying Xu, et al. 2016. "Aortic and Cardiac Structure and Function Using High-Resolution Echocardiography and Optical Coherence Tomography in a Mouse Model of Marfan Syndrome." *PLOS ONE* 11 (11): e0164778. https://doi.org/10.1371/journal.pone.0164778.

Lee, Seung-Jun, Woong Chol Kang, Young-Guk Ko, Yeongmin Woo, Chul-Min Ahn, Jong Youn Won, Do-Yun Lee, et al. 2020. "Aortic Remodeling and Clinical Outcomes in Type B Aortic Dissection According to the Timing of Thoracic Endovascular Aortic Repair." *Annals of Vascular Surgery* 67 (avs, 8703941): 322–31. https://doi.org/10.1016/j.avsg.2020.03.022.

Li, Zilun, Chenshu Liu, Ridong Wu, Jian Zhang, Hong Pan, Jinghong Tan, Zhuang Guo, et al. 2020. "Prognostic Value of Clinical and Morphologic Findings in Patients with Type B Aortic Intramural Hematoma." *Journal of Cardiothoracic Surgery* 15 (1): 49. https://doi.org/10.1186/s13019-020-1067-8.

Liao, Mingfang, Sili Zou, Jianfeng Weng, Lewei Hou, Lin Yang, Zhiqing Zhao, Junmin Bao, and Zaiping Jing. 2011. "A microRNA Profile Comparison Between Thoracic Aortic Dissection and Normal Thoracic Aorta Indicates the Potential Role of microRNAs in Contributing to Thoracic Aortic Dissection Pathogenesis." *Journal of Vascular Surgery* 53 (5): 1341–1349.e3. https://doi.org/10.1016/j.jvs.2010.11.113.

Lindberg, C. A., G. Engström, M. Gerhardsson de Verdier, U. Nihlén, M. Anderson, K. Forsman-Semb, and M. Svartengren. 2012. "Total Desmosines in Plasma and

Urine Correlate with Lung Function." *European Respiratory Journal* 39 (4): 839–45. https://doi.org/10.1183/09031936.00064611.

Liu, Chang, Congcong Zhang, Lixin Jia, Boya Chen, Luxin Liu, Jie Sun, Wenmei Zhang, et al. 2018. "Interleukin-3 Stimulates Matrix Metalloproteinase 12 Production from Macrophages Promoting Thoracic Aortic Aneurysm/Dissection." *Clinical Science (London, England : 1979)* 132 (6): 655–68. https://doi.org/https://dx.doi.org/10.1042/CS20171529.

Liu, Donghai, Hong Luo, Shuang Lin, Lixuan Zhao, and Chenhui Qiao. 2020. "Comparison of the Efficacy and Safety of Thoracic Endovascular Aortic Repair with Open Surgical Repair and Optimal Medical Therapy for Acute Type B Aortic Dissection: A Systematic Review and Meta-Analysis." *International Journal of Surgery (London, England)*, Comment in: Int J Surg. 2020 Dec;84:93; PMID: 33127588 [https://www.ncbi.nlm.nih.gov/pubmed/33127588]Comment in: Int J Surg. 2021 Mar;87:105901; PMID: 33626416 [https://www.ncbi.nlm.nih.gov/pubmed/33626416], 83 (101228232): 53–61. https://doi.org/10.1016/j.ijsu.2020.08.051.

Lu, Li, Yuanhao Tong, Wenwen Wang, Yayi Hou, Huan Dou, and Zhao Liu. 2020. "Characterization and Significance of Monocytes in Acute Stanford Type B Aortic Dissection." *Journal of Immunology Research* 2020: 9670360. https://doi.org/https://dx.doi.org/10.1155/2020/9670360.

Lu, Weifeng, Weiguo Fu, Lixing Wang, Daqiao Guo, Xin Xu, Bin Chen, and Junhao Jiang. 2021. "Morphologic Characteristics and Endovascular Management of Acute Type B Dissection Patients with Superior Mesenteric Artery Involvement." *Journal of Vascular Surgery* 74 (2): 528–536.e2. https://doi.org/10.1016/j.jvs.2020.12.099.

Ma, Mingjia, Juan Shi, Xin Feng, Jing Wang, Ligang Liu, and Xiang Wei. 2020. "The Elevated Admission White Blood Cell Count Relates to Adverse Surgical Outcome of Acute Stanford Type a Aortic Dissection." *Journal of Cardiothoracic Surgery* 15 (1): 48. https://doi.org/https://dx.doi.org/10.1186/s13019-020-1078-5.

MacAskill, Mark G., Adriana S. Tavares, Junxi Wu, Christophe Lucatelli, Joanne C. Mountford, Andrew H. Baker, David E. Newby, and Patrick W. F. Hadoke. 2017. "PET Cell Tracking

Using 18F-FLT Is Not Limited by Local Reuptake of Free Radiotracer." *Scientific Reports* 7. https://doi.org/10.1038/srep44233.

Macura, Katarzyna J., Frank M. Corl, Elliot K. Fishman, and David A. Bluemke. 2003. "Pathogenesis in Acute Aortic Syndromes: Aortic Dissection, Intramural Hematoma, and Penetrating Atherosclerotic Aortic Ulcer." *American Journal of Roentgenology* 181 (2): 309–16. https://doi.org/10.2214/ajr.181.2.1810309.

Malmberg, Catarina, Rasmus S Ripa, Camilla B Johnbeck, Ulrich Knigge, Seppo W Langer, Jann Mortensen, Peter Oturai, Annika Loft, Anne Mette Hag, and Andreas Kjaer. 2015. "64Cu-DOTATATE for Noninvasive Assessment of Atherosclerosis in Large Arteries and Its Correlation with Risk Factors: Head-to-Head Comparison with 68Ga-DOTATOC in 60 Patients." *Journal of Nuclear Medicine : Official Publication, Society of Nuclear Medicine* 56 (12): 1895–1900. https://doi.org/10.2967/jnumed.115.161216.

Mariko, Boubacar, Mylène Pezet, Brigitte Escoubet, Stéphanie Bouillot, Jean-Pierre Andrieu, Barry Starcher, Daniela Quaglino, et al. 2011. "Fibrillin-1 Genetic Deficiency Leads to Pathological Ageing of Arteries in Mice." *The Journal of Pathology* 224 (1): 33–44. https://doi.org/10.1002/path.2840.

Massera, Daniele, Mhairi K. Doris, Sebastien Cadet, Jacek Kwiecinski, Tania A. Pawade, Frederique E. C. M. Peeters, Damini Dey, David E. Newby, Marc R. Dweck, and Piotr J. Slomka. 2020. "Analytical Quantification of Aortic Valve 18F-Sodium Fluoride PET Uptake." *Journal of Nuclear Cardiology* 27 (3): 962–72. https://doi.org/10.1007/s12350-018-01542-6.

Masuda, Miha, Hajime Kurosawa, Junichi Ohishi, Daisuke Kobayashi, and Masahiro Kohzuki. 2011. "Spinal Behavior During Tidal and Deep Breathing in Healthy Male Subjects." *European Respiratory Journal* 38 (Suppl 55). https://erj.ersjournals.com/content/38/Suppl_55/p2114.

Mateo, Jesus, David Izquierdo-Garcia, Juan J. Badimon, Zahi A. Fayad, and Valentin Fuster. 2014. "Noninvasive Assessment of Hypoxia in Rabbit Advanced Atherosclerosis Using 18F-Fluoromisonidazole Positron Emission Tomographic ImagingCLINICAL PERSPECTIVE." *Circulation: Cardiovascular Imaging* 7 (2): 312–20. https:

//doi.org/10.1161/CIRCIMAGING.113.001084.

McBride, Olivia M. B., Colin Berry, Paul Burns, Roderick T. A. Chalmers, Barry Doyle, Rachael Forsythe, O. James Garden, et al. 2015. "MRI Using Ultrasmall Superparamagnetic Particles of Iron Oxide in Patients Under Surveillance for Abdominal Aortic Aneurysms to Predict Rupture or Surgical Repair: MRI for Abdominal Aortic Aneurysms to Predict Rupture or Surgerythe MA3RS Study." *Open Heart* 2 (1): e000190. https://doi.org/10.1136/openhrt-2014-000190.

Michaud, Sophie-Élise, Catherine Ménard, Louis-Georges Guy, Giuseppa Gennaro, and Alain Rivard. 2003. "Inhibition of Hypoxia-Induced Angiogenesis by Cigarette Smoke Exposure: Impairment of the HIF-Lalpha/VEGF Pathway." *The FASEB Journal* 17 (9): 1150–2. https://doi.org/10.1096/fj.02-0172fje.

Michel, Jean-Baptiste, Guillaume Jondeau, and Dianna M Milewicz. 2018. "From Genetics to Response to Injury: Vascular Smooth Muscle Cells in Aneurysms and Dissections of the Ascending Aorta." *Cardiovascular Research* 114 (4): 578–89. https://doi.org/10.1093/cvr/cvy006.

Miletic, Kyle G, Bogdan A Kindzelski, Kevin E Hodges, Jocelyn Beach, Michael Z Tong, Faisal Bakaeen, Douglas R Johnston, Milind Desai, Sean Lyden, and Eric E Roselli. 2021. "Impact of Endovascular False Lumen Embolization on Thoracic Aortic Remodeling in Chronic Dissection." *The Annals of Thoracic Surgery*, Comment in: Ann Thorac Surg. 2021 Feb;111(2):501-502; PMID: 32791061 [https://www.ncbi.nlm.nih.gov/pubmed/32791061], 111 (2): 495–501. https://doi.org/10.1016/j.athoracsur.2020.04.093.

Mileva, Niya, Dobrin Vassilev, Robert Gil, and Gianluca Rigatelli. 2018. "Misdiagnosed Aortic Intramural Hematoma and the Role of Intravascular Ultrasound Imaging in Detection of Acute Aortic Syndrome: A Case Report." *Cardiovascular Innovations and Applications* 2 (4): 447–49. https://doi.org/10.15212/CVIA.2017.0028.

Miliotis, Tasso, Claes Lindberg, Kristina Forsman Semb, Marleen van Geest, and Sven Kjellström. 2013. "Quantitative High-Performance Liquid Chromatography–Tandem Mass Spectrometry Method for the Analysis of Free Desmosines in Plasma and Urine." *Journal of Chromatography A* 1308 (September): 73–78. https://doi.org/10.1016/j.chroma.2

013.06.063.

Mimler, Teresa, Clemens Nebert, Eva Eichmair, Birgitta Winter, Thomas Aschacher, Marie-Elisabeth Stelzmueller, Martin Andreas, Marek Ehrlich, Guenther Laufer, and Barbara Messner. 2019. "Extracellular Matrix in Ascending Aortic Aneurysms and Dissections What We Learn from Decellularization and Scanning Electron Microscopy." *PLoS ONE* 14 (3). https://doi.org/10.1371/journal.pone.0213794.

Mirza, T. A., A. Karthikesalingam, D. Jackson, S. R. Walsh, P. J. Holt, P. D. Hayes, and J. R. Boyle. 2010. "Duplex Ultrasound and Contrast-Enhanced Ultrasound Versus Computed Tomography for the Detection of Endoleak After EVAR: Systematic Review and Bivariate Meta-Analysis." *European Journal of Vascular and Endovascular Surgery* 39 (4): 418–28. https://doi.org/10.1016/j.ejvs.2010.01.001.

Moore, Kathryn J., Frederick J. Sheedy, and Edward A. Fisher. 2013. "Macrophages in Atherosclerosis: A Dynamic Balance." *Nature Reviews Immunology* 13 (10): 709–21. https://doi.org/10.1038/nri3520.

Mordi, Ify R., Rachael O Forsythe, Corry Gellatly, Zaid Iskandar, Olivia M. B. McBride, Athanasios Saratzis, Roderick Chalmers, et al. 2019. "Plasma Desmosine and Abdominal Aortic Aneurysm Disease." *Journal of the American Heart Association* 8 (20): e013743. https://doi.org/10.1161/JAHA.119.013743.

Moss, Alastair J., Mhairi K. Doris, Jack P. M. Andrews, Rong Bing, Marwa Daghem, Edwin J. R. van Beek, Laura Forsyth, et al. 2019. "Molecular Coronary Plaque Imaging Using 18F-Fluoride." *Circulation: Cardiovascular Imaging* 12 (8): e008574. https://doi.org/10.1161/CIRCIMAGING.118.008574.

Movsowitz, Herman D., Craig Lampert, Larry E. Jacobs, and Morris N. Kotler. 1994. "Penetrating Atherosclerotic Aortic Ulcers." *American Heart Journal* 128 (6): 1210–7. https://doi.org/10.1016/0002-8703(94)90753-6.

Mullick, Adam E., Katrin Soldau, William B. Kiosses, Thomas A. Bell, Peter S. Tobias, and Linda K. Curtiss. 2008. "Increased Endothelial Expression of Toll-Like Receptor 2 at Sites of Disturbed Blood Flow Exacerbates Early Atherogenic Events." *Journal of Experimental*

Medicine 205 (2): 373–83. https://doi.org/10.1084/jem.20071096.

Müller-Eschner, M., F. Rengier, S. Partovi, T. F. Weber, A. Kopp-Schneider, P. Geisbüsch, H. -U. Kauczor, and H. von Tengg-Kobligk. 2013. "Accuracy and Variability of Semiautomatic Centerline Analysis Versus Manual Aortic Measurement Techniques for TEVAR." *European Journal of Vascular and Endovascular Surgery* 45 (3): 241–47. https://doi.org/10.1016/j.ejvs.2012.12.003.

Neubauer, Stefan. 2003. "Cardiac Magnetic Resonance Spectroscopy." *Current Cardiology Reports* 5 (1): 75–82. https://doi.org/10.1007/s11886-003-0041-0.

New, Sophie EP, Claudia Goettsch, Masanori Aikawa, Julio F. Marchini, Manabu Shibasaki, Katsumi Yabusaki, Peter Libby, Catherine M. Shanahan, Kevin Croce, and Elena Aikawa. 2013. "Macrophage-Derived Matrix Vesicles: An Alternative Novel Mechanism for Microcalcification in Atherosclerotic Plaques." *Circulation Research* 113 (1): 72–77.

Newby, Andrew C. 2016. "Metalloproteinase Production from Macrophages a Perfect Storm Leading to Atherosclerotic Plaque Rupture and Myocardial Infarction." *Experimental Physiology* 101 (11): 1327–37. https://doi.org/10.1113/EP085567.

Nienaber, Christoph A., Stephan Kische, Ibrahim Akin, Hervé Rousseau, Holger Eggebrecht, Rossella Fattori, Tim C. Rehders, et al. 2010. "Strategies for Subacute/Chronic Type B Aortic Dissection: The Investigation of Stent Grafts in Patients with Type B Aortic Dissection (INSTEAD) Trial 1-Year Outcome." *The Journal of Thoracic and Cardiovascular Surgery*, Proceedings of the Aortic Symposium 2010, 140 (6, Supplement): S101–S108. https://doi.org/10.1016/j.jtcvs.2010.07.026.

Nienaber, Christoph A, Stephan Kische, Herve Rousseau, Holger Eggebrecht, Tim C Rehders, Guenther Kundt, Aenne Glass, et al. 2013. "Endovascular Repair of Type B Aortic Dissection: Long-Term Results of the Randomized Investigation of Stent Grafts in Aortic Dissection Trial." Edited by Pierangeli A Meinertz T Fattori R. *Circulation. Cardiovascular Interventions*, Comment in: Circ Cardiovasc Interv. 2013 Aug;6(4):326-8; PMID: 23963578 [https://www.ncbi.nlm.nih.gov/pubmed/23963578], 6 (4): 407–16. https://doi.org/10.1161/CIRCINTERVENTIONS.113.000463.

Nienaber, Christoph A, Simona Zannetti, Barbara Barbieri, Stephan Kische, Wolfgang Schareck, Tim C Rehders, and INSTEAD study collaborators. 2005. "INvestigation of STEnt Grafts in Patients with Type B Aortic Dissection: Design of the INSTEAD Trial–a Prospective, Multicenter, European Randomized Trial." *American Heart Journal* 149 (4): 592–9.

Oishi, Yasuhisa, Yoshiyuki Yamashita, Satoshi Kimura, Hiromichi Sonoda, Sho Matsuyama, Tomoki Ushijima, Satoshi Fujita, Hideki Tatewaki, Yoshihisa Tanoue, and Akira Shiose. 2020. "Preoperative Distal Aortic Diameter Is a Significant Predictor of Late Aorta-Related Events After Endovascular Repair for Chronic Type B Aortic Dissection." *General Thoracic and Cardiovascular Surgery* 68 (10): 1086–93. https://doi.org/10.1007/s11748-020-01318-1.

Pape Linda A., Tsai Thomas T., Isselbacher Eric M., Oh Jae K., O'Gara Patrick T., Evangelista Arturo, Fattori Rossella, et al. 2007. "Aortic Diameter $\geq$5.5 Cm Is Not a Good Predictor of Type A Aortic Dissection." *Circulation* 116 (10): 1120–7. https://doi.org/10.1161/CIRCULATIONAHA.107.702720.

Parker, Louis P., Benedikt Reutersberg, Maaz B. J. Syed, Bijit Munshi, Samantha Richards, Lachlan J. Kelsey, Natzi Sakalihasan, Hans-Henning Eckstein, Paul E. Norman, and Barry J. Doyle. 2021. "Proximal False Lumen Thrombosis Is Associated with Low False Lumen Pressure and Fewer Complications in Type B Aortic Dissection." *Journal of Vascular Surgery*, November. https://doi.org/10.1016/j.jvs.2021.10.035.

Paruchuri, Vijayapraveena, Kahled F. Salhab, Gregory Kuzmik, George Gubernikoff, Hai Fang, John A. Rizzo, Bulat A. Ziganshin, and John A. Elefteriades. 2015. "Aortic Size Distribution in the General Population: Explaining the Size Paradox in Aortic Dissection." *Cardiology* 131 (4): 265–72. https://doi.org/10.1159/000381281.

Pawade, Tania, Tim Cartlidge, William S. A. Jenkins, Philip Adamson, Phillip Robson, Christophe Lucatelli, Edwin Jacques Rudolph van Beek, et al. 2016. "Optimization and Reproducibility of Aortic Valve 18F-Fluoride Positron Emission Tomography in Patients with Aortic Stenosis." *Circulation: Cardiovascular Imaging* 9 (10). https://doi.org/10.1161/CIRCIMAGING.116.005131.

Phinikaridou, A., B. Lavin, S. Lacerda, M. Andia, I. Rashid, and R. Botnar. 2019. "Tropoelastin: A New Imaging Biomarker of Dysfunctional Extracellular Matrix Remodelling in Atherosclerosis and Aortic Aneurysm." *Atherosclerosis* 287 (August): e49–e50. https://doi.org/10.1016/j.atherosclerosis.2019.06.142.

Phinikaridou, Alkystis, Sara Lacerda, Begoña Lavin, Marcelo E. Andia, Alberto Smith, Prakash Saha, and René M. Botnar. 2018. "Tropoelastin." *Circulation: Cardiovascular Imaging* 11 (8): e007303. https://doi.org/10.1161/CIRCIMAGING.117.007303.

Pirillo, Angela, Fabrizia Bonacina, Giuseppe Danilo Norata, and Alberico Luigi Catapano. 2018. "The Interplay of Lipids, Lipoproteins, and Immunity in Atherosclerosis." *Current Atherosclerosis Reports* 20 (3): 12. https://doi.org/10.1007/s11883-018-0715-0.

Pitulescu, Mara E., Inga Schmidt, Benedetto Daniele Giaimo, Tobiah Antoine, Frank Berkenfeld, Francesca Ferrante, Hongryeol Park, et al. 2017. "Dll4 and Notch Signalling Couples Sprouting Angiogenesis and Artery Formation." *Nature Cell Biology* 19 (8): 915–27. https://doi.org/10.1038/ncb3555.

Proudfoot, Diane, Jeremy N. Skepper, Laszlo Hegyi, Martin R. Bennett, Catherine M. Shanahan, and Peter L. Weissberg. 2000. "Apoptosis Regulates Human Vascular Calcification in Vitro: Evidence for Initiation of Vascular Calcification by Apoptotic Bodies." *Circulation Research* 87 (11): 1055–62. https://doi.org/10.1161/01.RES.87.11.1055.

Pruitt, Eric Y, Salvatore T Scali, Dean J Arnaoutakis, Martin R Back, George J Arnaoutakis, Tomas D Martin, Thomas M Beaver, Thomas S Huber, and Gilbert R Upchurch. 2020. "Complicated Acute Type B Aortic Dissection: Update on Management and Results." *The Journal of Cardiovascular Surgery* 61 (6): 697–707. https://doi.org/10.23736/S0021-9509.20.11555-6.

Qi, Youfei, Chang Shu, Sahua Liu, Hao Chen, and Wenbo Zhang. 2021. "Association Between Single Nucleotide Polymorphisms of Tropoelastin Gene and Aortic Dissection." *Zhong Nan Da Xue Xue Bao Yi Xue Ban = Journal of Central South University. Medical Sciences* 46 (5): 458–66. https://doi.org/10.11817/j.issn.1672-7347.2021.200624.

Qi, You-Fei, Chang Shu, Zhan-Xiang Xiao, Ming-Yao Luo, Kun Fang, Yuan-Yuan Guo, Wen-Bo

Zhang, and Jie Yue. 2018. “Post-Transcriptional Control of Tropoelastin in Aortic Smooth Muscle Cells Affects Aortic Dissection Onset.” *Molecules and Cells* 41 (3): 198–206. https://doi.org/10.14348/molcells.2018.2193.

Qiu, Peng, Binshan Zha, Xu Zhang, Kaichuang Ye, Jinbao Qin, Xinrui Yang, Zhiyou Peng, Junchao Liu, and Xinwu Lu. 2020. “A Meta-Analysis of Combined Proximal Stent Grafting with or Without Adjunctive Distal Bare Stent for the Management of Aortic Dissection.” *Journal of Vascular Surgery*, Comment in: J Vasc Surg. 2020 Sep;72(3):1121; PMID: 32829767 [https://www.ncbi.nlm.nih.gov/pubmed/32829767], 72 (3): 1109–1120.e6. https://doi.org/10.1016/j.jvs.2020.02.052.

Rabinovich, Roberto A., Bruce E. Miller, Karolina Wrobel, Kareshma Ranjit, Michelle C. Williams, Ellen Drost, Lisa D. Edwards, et al. 2016. “Circulating Desmosine Levels Do Not Predict Emphysema Progression but Are Associated with Cardiovascular Risk and Mortality in COPD.” *European Respiratory Journal* 47 (5): 1365–73. https://doi.org/10.1183/13993003.01824-2015.

Real, Eusebio, Alma Eguizabal, Alejandro Pontón, Marta Calvo Diez, Jose Fernando Val-Bernal, Marta Mayorga, José M. Revuelta, José M. López-Higuera, and Olga M. Conde. 2013. “Optical Coherence Tomography Assessment of Vessel Wall Degradation in Thoracic Aortic Aneurysms.” *Journal of Biomedical Optics* 18 (12): 126003. https://doi.org/10.1117/1.JBO.18.12.126003.

Reeps, Christian, Jaroslav Pelisek, Ralph A Bundschuh, Manuela Gurdan, Alexander Zimmermann, Stefan Ockert, Martin Dobritz, Hans-Henning Eckstein, and Markus Essler. 2010. “Imaging of Acute and Chronic Aortic Dissection by 18F-FDG PET/CT.” *Journal of Nuclear Medicine : Official Publication, Society of Nuclear Medicine* 51 (5): 686–91. https://doi.org/10.2967/jnumed.109.072298.

Reynolds, Joanne L., Alexis J. Joannides, Jeremy N. Skepper, Rosamund McNair, Leon J. Schurgers, Diane Proudfoot, Willi Jahnen-Dechent, Peter L. Weissberg, and Catherine M. Shanahan. 2004. “Human Vascular Smooth Muscle Cells Undergo Vesicle-Mediated Calcification in Response to Changes in Extracellular Calcium and Phosphate Concentrations: A Potential Mechanism for Accelerated Vascular Calcification in ESRD.” *Journal of*

the American Society of Nephrology 15 (11): 2857–67. https://doi.org/10.1097/01.ASN.0000141960.01035.28.

Rhys, Hefin. 2020. *Machine Learning with R, the Tidyverse, and Mlr*. Shelter Island, NY: Manning publications.

Riambau, V., D. Böckler, J. Brunkwall, P. Cao, R. Chiesa, G. Coppi, M. Czerny, et al. 2017. "Editor's Choice Management of Descending Thoracic Aorta Diseases: Clinical Practice Guidelines of the European Society for Vascular Surgery (ESVS)." *European Journal of Vascular and Endovascular Surgery* 53 (1): 4–52. https://doi.org/10.1016/j.ejvs.2016.06.005.

Richards, Jennifer M J, Scott I Semple, Thomas J MacGillivray, Calum Gray, Jeremy P Langrish, Michelle Williams, Marc Dweck, et al. 2011. "Abdominal Aortic Aneurysm Growth Predicted by Uptake of Ultrasmall Superparamagnetic Particles of Iron Oxide: A Pilot Study." *Circulation. Cardiovascular Imaging* 4 (3): 274–81. https://doi.org/10.1161/CIRCIMAGING.110.959866.

Rogers, Ian S., Dahlia Banerji, Emily L. Siegel, Quynh A. Truong, Brian B. Ghoshhajra, Thomas Irlbeck, Suhny Abbara, et al. 2011. "Usefulness of Comprehensive Cardiothoracic Computed Tomography in the Evaluation of Acute Undifferentiated Chest Discomfort in the Emergency Department (CAPTURE)." *The American Journal of Cardiology* 107 (5): 643–50. https://doi.org/10.1016/j.amjcard.2010.10.039.

Saam, Tobias, Holger Hetterich, Verena Hoffmann, Chun Yuan, Martin Dichgans, Holger Poppert, Thomas Koeppel, Ulrich Hoffmann, Maximilian F. Reiser, and Fabian Bamberg. 2013. "Meta-Analysis and Systematic Review of the Predictive Value of Carotid Plaque Hemorrhage on Cerebrovascular Events by Magnetic Resonance Imaging." *Journal of the American College of Cardiology* 62 (12): 1081–91.

Sakalihasan, Natzi, Christoph A Nienaber, Roland Hustinx, Pierre Lovinfosse, Mounia El Hachemi, Jean-Paul Cheramy-Bien, Laurence Seidel, et al. 2015a. "(Tissue PET) Vascular Metabolic Imaging and Peripheral Plasma Biomarkers in the Evolution of Chronic Aortic Dissections." *European Heart Journal Cardiovascular Imaging* 16 (6): 626–33. https://doi.org/10.1093/ehjci/jeu283.

Sakalihasan, Natzi, Christoph A Nienaber, Roland Hustinx, Pierre Lovinfosse, Mounia El Hachemi, Jean-Paul Cheramy-Bien, Laurence Seidel, et al. n.d.b. "(Tissue Pet) Vascular Metabolic Imaging and Peripheral Plasma Biomarkers in the Evolution of Chronic Aortic Dissections." *European Heart Journal Cardiovascular Imaging* 16 (6): 626–33. https://doi.org/https://dx.doi.org/10.1093/ehjci/jeu283.

Sariola, H., T. Viljanen, and R. Luosto. 1986. "Histological Pattern and Changes in Extracellular Matrix in Aortic Dissections." *Journal of Clinical Pathology* 39 (10): 1074–81. https://doi.org/10.1136/jcp.39.10.1074.

Schmitto, Jan D, Aron F Popov, Kasim O Coskun, Martin Friedrich, Samuel Sossalla, Vassilios Didilis, Friedrich A Schoendube, and Masoud Mirzaie. 2010. "Morphological Investigations of Type A Aortic Dissection." *Annals of Thoracic and Cardiovascular Surgery : Official Journal of the Association of Thoracic and Cardiovascular Surgeons of Asia* 16 (5): 331–4.

Schwindt, Arne G., J. Gray Bennett, William H. Crowder, Suhail Dohad, Sean F. Janzer, Jon C. George, Barry Tedder, et al. 2017. "Lower Extremity Revascularization Using Optical Coherence TomographyGuided Directional Atherectomy: Final Results of the EValuatIon of the PantheriS OptIcal COherence Tomography ImagiNg Atherectomy System for Use in the Peripheral Vasculature (VISION) Study." *Journal of Endovascular Therapy* 24 (3): 355–66. https://doi.org/10.1177/1526602817701720.

Sen, Indrani, Mario D'Oria, Salome Weiss, Thomas C Bower, Gustavo S Oderich, Manju Kalra, Jill Colglazier, and Randall R DeMartino. 2021. "Incidence and Natural History of Isolated Abdominal Aortic Dissection: A Population-Based Assessment from 1995 to 2015." *Journal of Vascular Surgery* 73 (4): 1198–1204.e1. https://doi.org/10.1016/j.jvs.2020.07.090.

Shapiro, S. D., S. K. Endicott, M. A. Province, J. A. Pierce, and E. J. Campbell. 1991. "Marked Longevity of Human Lung Parenchymal Elastic Fibers Deduced from Prevalence of D-Aspartate and Nuclear Weapons-Related Radiocarbon." *The Journal of Clinical Investigation* 87 (5): 1828–34. https://doi.org/10.1172/JCI115204.

Shen, Ying H., and Scott A. LeMaire. 2017. "Molecular Pathogenesis of Genetic and Sporadic Aortic Aneurysms and Dissections." *Current Problems in Surgery* 54 (3): 95–155.

https://doi.org/10.1067/j.cpsurg.2017.01.001.

Shiga, Toshiya, Zen'ichiro Wajima, Christian C. Apfel, Tetsuo Inoue, and Yoko Ohe. 2006. "Diagnostic Accuracy of Transesophageal Echocardiography, Helical Computed Tomography, and Magnetic Resonance Imaging for Suspected Thoracic Aortic Dissection: Systematic Review and Meta-Analysis." *Archives of Internal Medicine* 166 (13): 1350–6. https://doi.org/10.1001/archinte.166.13.1350.

Siekmann, Arndt F., Laurence Covassin, and Nathan D. Lawson. 2008. "Modulation of VEGF Signalling Output by the Notch Pathway." *BioEssays* 30 (4): 303–13. https://doi.org/10.1002/bies.20736.

Sluimer, Judith C., Jean-Marie Gasc, Job L. van Wanroij, Natasja Kisters, Mathijs Groeneweg, Maarten D. Sollewijn Gelpke, Jack P. Cleutjens, et al. 2008. "Hypoxia, Hypoxia-Inducible Transcription Factor, and Macrophages in Human Atherosclerotic Plaques Are Correlated with Intraplaque Angiogenesis." *Journal of the American College of Cardiology* 51 (13): 1258–65. https://doi.org/10.1016/j.jacc.2007.12.025.

Sonesson, Björn, Toste Länne, Flemming Hansen, and Thomas Sandgren. 1994. "Infrarenal Aortic Diameter in the Healthy Person." *European Journal of Vascular Surgery* 8 (1): 89–95. https://doi.org/10.1016/S0950-821X(05)80127-6.

Song, Jong-Min, Sung-Doo Kim, Jeong-Hoon Kim, Mi-Jeong Kim, Duk-Hyun Kang, Joon Beom Seo, Tae-Hwan Lim, Jae Won Lee, Meong-Gun Song, and Jae-Kwan Song. 2007. "Long-Term Predictors of Descending Aorta Aneurysmal Change in Patients with Aortic Dissection." *Journal of the American College of Cardiology*, Comment in: J Am Coll Cardiol. 2007 Aug 21;50(8):805-7; PMID: 17707187 [https://www.ncbi.nlm.nih.gov/pubmed/17707187], 50 (8): 799–804.

Spinelli, Domenico, Filippo Benedetto, Rocco Donato, Gabriele Piffaretti, Massimiliano M Marrocco-Trischitta, Himanshu J Patel, Kim A Eagle, and Santi Trimarchi. 2018. "Current Evidence in Predictors of Aortic Growth and Events in Acute Type B Aortic Dissection." *Journal of Vascular Surgery* 68 (6): 1925–1935.e8. https://doi.org/10.1016/j.jvs.2018.05.232.

Stary, Herbert C., A. Bleakley Chandler, Robert E. Dinsmore, Valentin Fuster, Seymour Glagov, William Insull, Michael E. Rosenfeld, Colin J. Schwartz, William D. Wagner, and Robert W. Wissler. 1995. "A Definition of Advanced Types of Atherosclerotic Lesions and a Histological Classification of Atherosclerosis: A Report from the Committee on Vascular Lesions of the Council on Arteriosclerosis, American Heart Association." *Circulation* 92 (5): 1355–74. https://doi.org/10.1161/01.CIR.92.5.1355.

Suzuki, Tomoaki, Tohru Asai, and Takeshi Kinoshita. 2018. "Predictors for Late Reoperation After Surgical Repair of Acute Type A Aortic Dissection." *The Annals of Thoracic Surgery* 106 (1): 63–69. https://doi.org/10.1016/j.athoracsur.2018.01.071.

Syed, Maaz Bj, Alexander J. Fletcher, Rachael O. Forsythe, Jakub Kaczynski, David E. Newby, Marc R. Dweck, and Edwin Jr van Beek. 2019. "Emerging Techniques in Atherosclerosis Imaging." *The British Journal of Radiology* 92 (1103): 20180309. https://doi.org/10.1259/bjr.20180309.

Štěchovský, Cyril, Petr Hájek, Martin Horváth, Miloslav Špaček, and Josef Veselka. 2016. "Near-Infrared Spectroscopy Combined with Intravascular Ultrasound in Carotid Arteries." *The International Journal of Cardiovascular Imaging* 32 (1): 181–88. https://doi.org/10.1007/s10554-015-0687-x.

Tabas, Ira, and Karin E. Bornfeldt. 2016. "Macrophage Phenotype and Function in Different Stages of Atherosclerosis." *Circulation Research* 118 (4): 653–67. https://doi.org/10.1161/CIRCRESAHA.115.306256.

Takasawa, Masashi, John S Beech, Tim D Fryer, Young T Hong, Jessica L Hughes, Keiji Igase, P Simon Jones, et al. 2007. "Imaging of Brain Hypoxia in Permanent and Temporary Middle Cerebral Artery Occlusion in the Rat Using 18F-Fluoromisonidazole and Positron Emission Tomography: A Pilot Study." *Journal of Cerebral Blood Flow and Metabolism : Official Journal of the International Society of Cerebral Blood Flow and Metabolism* 27 (4): 679–89. https://doi.org/10.1038/sj.jcbfm.9600405.

Tarkin, Jason M., Francis R. Joshi, Nicholas R. Evans, Mohammed M. Chowdhury, Nichola L. Figg, Aarti V. Shah, Lakshi T. Starks, et al. 2017. "Detection of Atherosclerotic Inflammation by 68Ga-DOTATATE PET Compared to [18F]FDG PET Imaging." *Journal of the Ameri-*

can College of Cardiology 69 (14): 1774–91. https://doi.org/10.1016/j.jacc.2017.01.060.

Teague, Heather L., Mark A. Ahlman, Abass Alavi, Denisa D. Wagner, Andrew H. Lichtman, Matthias Nahrendorf, Filip K. Swirski, et al. 2017. "Unraveling Vascular Inflammation: From Immunology to Imaging." *Journal of the American College of Cardiology* 70 (11): 1403–12. https://doi.org/10.1016/j.jacc.2017.07.750.

Tharwat, Alaa, Tarek Gaber, Abdelhameed Ibrahim, and Aboul Ella Hassanien. 2017. "Linear Discriminant Analysis: A Detailed Tutorial." *AI Communications* 30 (2): 169–90. https://doi.org/10.3233/AIC-170729.

Tolenaar, Jip L, Jasper W van Keulen, Santi Trimarchi, Frederik H W Jonker, Joost A van Herwaarden, Hence J M Verhagen, Frans L Moll, and Bart E Muhs. 2013. "Number of Entry Tears Is Associated with Aortic Growth in Type B Dissections." *The Annals of Thoracic Surgery* 96 (1): 39–42. https://doi.org/10.1016/j.athoracsur.2013.03.087.

Trivedi, Rikin A., Jean-Marie U-King-Im, Martin J. Graves, Justin J. Cross, Jo Horsley, Martin J. Goddard, Jeremy N. Skepper, et al. 2004. "In Vivo Detection of Macrophages in Human Carotid Atheroma: Temporal Dependence of Ultrasmall Superparamagnetic Particles of Iron Oxide-Enhanced MRI." *Stroke* 35 (7): 1631–5. https://doi.org/10.1161/01.STR.0000131268.50418.b7.

Tzolos, Evangelos, Jacek Kwiecinski, Martin Lyngby Lassen, Sebastien Cadet, Philip D. Adamson, Alastair J. Moss, Nikhil Joshi, et al. 2020. "Observer Repeatability and Interscan Reproducibility of 18F-Sodium Fluoride Coronary Microcalcification Activity." *Journal of Nuclear Cardiology: Official Publication of the American Society of Nuclear Cardiology*, June. https://doi.org/10.1007/s12350-020-02221-1.

Ueki, Chikara, Genichi Sakaguchi, Takeshi Shimamoto, and Tatsuhiko Komiya. 2014. "Prognostic Factors in Patients with Uncomplicated Acute Type B Aortic Dissection." *The Annals of Thoracic Surgery* 97 (3): 767–73. https://doi.org/10.1016/j.athoracsur.2013.10.038.

van Bogerijen, Guido H. W., Jip L. Tolenaar, Vincenzo Rampoldi, Frans L. Moll, Joost A. van Herwaarden, Frederik H. W. Jonker, Kim A. Eagle, and Santi Trimarchi. 2014. "Predictors

of Aortic Growth in Uncomplicated Type B Aortic Dissection." *Journal of Vascular Surgery* 59 (4): 1134–43. https://doi.org/10.1016/j.jvs.2014.01.042.

Van Maele, Margaux, Hozan Mufty, Geert Maleux, Sabrina Houthoofd, Kim Daenens, and Inge Fourneau. 2021. "Predictive Factors of Operative Need in Medically Managed Type B Aortic Dissections." *Annals of Vascular Surgery* 71 (avs, 8703941): 437–43. https://doi.org/10.1016/j.avsg.2020.07.060.

Versari, Annibale, Nicolo Pipitone, Massimiliano Casali, Francois Jamar, and Giulia Pazzola. 2018. "Use of Imaging Techniques in Large Vessel Vasculitis and Related Conditions." *The Quarterly Journal of Nuclear Medicine and Molecular Imaging : Official Publication of the Italian Association of Nuclear Medicine (AIMN) [and] the International Association of Radiopharmacology (IAR), [and] Section of the Society Of...* 62 (1): 34–39. https://doi.org/10.23736/S1824-4785.17.03044-8.

Vesey, Alex T., William SA Jenkins, Agnese Irkle, Alastair Moss, Greg Sng, Rachael O. Forsythe, Tim Clark, Gemma Roberts, Alison Fletcher, and Christophe Lucatelli. 2017. "18 F-Fluoride and 18 F-Fluorodeoxyglucose Positron Emission Tomography After Transient Ischemic Attack or Minor Ischemic Stroke." *Circulation: Cardiovascular Imaging* 10 (3): e004976.

Virmani, Renu, Allen P. Burke, Frank D. Kolodgie, and Andrew Farb. 2003. "Pathology of the Thin-Cap Fibroatheroma: A Type of Vulnerable Plaque." *Journal of Interventional Cardiology* 16 (3): 267–72.

Vrsalovic, Mislav, and Presecki Ana Vrsalovic. 2019. "Admission c-Reactive Protein and Outcomes in Acute Aortic Dissection: A Systematic Review." *Croatian Medical Journal* 60 (4): 309–15.

Wang, Bin, Paul Howel, Skjalg Bruheim, Jingfang Ju, Laurie B. Owen, Oystein Fodstad, and Yaguang Xi. 2011. "Systematic Evaluation of Three microRNA Profiling Platforms: Microarray, Beads Array, and Quantitative Real-Time PCR Array." *PLOS ONE* 6 (2): e17167. https://doi.org/10.1371/journal.pone.0017167.

Wang, Grace, Benjamin M Jackson, Scott M Damrauer, Venkat Kalapatapu, Julia Glaser,

Michael A Golden, and Darren Schneider. 2021. “Unique Characteristics of the Type B Aortic Dissection Patients with Malperfusion in the Vascular Quality Initiative.” *Journal of Vascular Surgery* 74 (1): 53–62. https://doi.org/10.1016/j.jvs.2020.11.047.

Wang, Kai, Yue Yuan, Ji-Hoon Cho, Sara McClarty, David Baxter, and David J. Galas. 2012. “Comparing the MicroRNA Spectrum Between Serum and Plasma.” *PLOS ONE* 7 (7): e41561. https://doi.org/10.1371/journal.pone.0041561.

Wang, Xiao-Jian, Bi Huang, Yan-Min Yang, Liang Zhang, Wen-Jun Su, Li Tian, Tian-Yi Lu, Shu Zhang, Xiao-Han Fan, and Ru-Tai Hui. 2015. “Differential Expression of microRNAs in Aortic Tissue and Plasma in Patients with Acute Aortic Dissection.” *Journal of Geriatric Cardiology : JGC* 12 (6): 655–61. https://doi.org/10.11909/j.issn.1671-5411.2015.06.013.

Wang, Xiaowei. 2008. “miRDB: A microRNA Target Prediction and Functional Annotation Database with a Wiki Interface.” *RNA* 14 (6): 1012–7. https://doi.org/10.1261/rna.965408.

Wang, Yan, Kun Luo, Yonghui Qiao, and Jianren Fan. 2021. “An Integrated Fluid-Chemical Model Toward Modeling the Thrombus Formation in an Idealized Model of Aortic Dissection.” *Computers in Biology and Medicine* 136 (doc, 1250250): 104709. https://doi.org/10.1016/j.compbiomed.2021.104709.

Wanga, Shaynah, Stijntje Hibender, Yanto Ridwan, Cindy van Roomen, Mariska Vos, Ingeborg van der Made, Nicole van Vliet, et al. 2017. “Aortic Microcalcification Is Associated with Elastin Fragmentation in Marfan Syndrome: Microcalcification and Elastin Fragmentation in Marfan Syndrome.” *The Journal of Pathology* 243 (3): 294–306. https://doi.org/10.1002/path.4949.

Watanabe, Toshitaka, Toshiro Ito, Hiroshi Sato, Takuma Mikami, Ryosuke Numaguchi, Naomi Yasuda, Junji Nakazawa, Yosuke Kuroda, Ryo Harada, and Nobuyoshi Kawaharada. 2019. “Morphological Predictor of Remodelling of the Descending Thoracic Aortic False Lumen That Remains Patent After Repair of Acute Type A Dissection.” *Interactive Cardiovascular and Thoracic Surgery* 28 (4): 629–34. https://doi.org/10.1093/icvts/ivy284.

Wei, Hu, Francois Schiele, Nicolas Meneveau, Marie-France Seronde, Pierre Legalery, Fiona Caulfield, Jean-François Bonneville, Sidney Chocron, and Jean-Pierre Bassand. 2006. "The Value of Intravascular Ultrasound Imaging in Diagnosis of Aortic Penetrating Atherosclerotic Ulcer." *EuroIntervention* 1 (4): 432–37.

Weiberg, Desiree, James T. Thackeray, Guenter Daum, Jan M. Sohns, Saskia Kropf, Hans-Juergen Wester, Tobias L. Ross, Frank M. Bengel, and Thorsten Derlin. 2018. "Clinical Molecular Imaging of Chemokine Receptor CXCR4 Expression in Atherosclerotic Plaque Using 68Ga-Pentixafor PET: Correlation with Cardiovascular Risk Factors and Calcified Plaque Burden." *Journal of Nuclear Medicine* 59 (2): 266–72. https://doi.org/10.2967/jnumed.117.196485.

Winter, Patrick M., Anne M. Morawski, Shelton D. Caruthers, Ralph W. Fuhrhop, Huiying Zhang, Todd A. Williams, John S. Allen, et al. 2003. "Molecular Imaging of Angiogenesis in Early-Stage Atherosclerosis with $\alpha_V\beta_3$-IntegrinTargeted Nanoparticles." *Circulation* 108 (18): 2270–4. https://doi.org/10.1161/01.CIR.0000093185.16083.95.

Wu, Jin-Lin, Liang Zhang, Jun-Tao Qiu, and Cun-Tao Yu. 2018. "Morphological Features of the Thoracic Aorta and Supra-Aortic Branches in Patients with Acute Type A Aortic Dissection in China." *Interactive Cardiovascular and Thoracic Surgery* 27 (4): 555–60. https://doi.org/10.1093/icvts/ivy110.

Xie, Enmin, Fan Yang, Yuan Liu, Ling Xue, Ruixin Fan, Nianjin Xie, Lyufan Chen, Jitao Liu, and Jianfang Luo. 2021. "Timing and Outcome of Endovascular Repair for Uncomplicated Type B Aortic Dissection." *European Journal of Vascular and Endovascular Surgery : The Official Journal of the European Society for Vascular Surgery*, Comment in: Eur J Vasc Endovasc Surg. 2021 May;61(5):798; PMID: 33431293 [https://www.ncbi.nlm.nih.gov/pubmed/33431293], 61 (5): 788–97. https://doi.org/10.1016/j.ejvs.2021.02.026.

Xin, Lijing, Bernard Lanz, Hongxia Lei, and Rolf Gruetter. 2015. "Assessment of Metabolic Fluxes in the Mouse Brain in Vivo Using 1H-[13C] NMR Spectroscopy at 14.1 Tesla." *Journal of Cerebral Blood Flow and Metabolism: Official Journal of the International Society of Cerebral Blood Flow and Metabolism* 35 (5): 759–65. https://doi.org/10.1038/jcbfm.20

14.251.

Xiong, Wanfen, Yong Zhao, Amy Prall, Timothy C. Greiner, and B. Timothy Baxter. 2004. "Key Roles of CD4+ T Cells and IFN-γ in the Development of Abdominal Aortic Aneurysms in a Murine Model." *Journal of Immunology* 172 (4): 2607–12. https://nebraska.pure.elsevier.com/en/publications/key-roles-of-cd4supsup-t-cells-and-ifn-%CE%B3-in-the-development-of-ab.

Xu, Chengpei, Sheila Lee, Tej M. Singh, Eiketsu Sho, Xiangqi Li, Mien Sho, Hirotake Masuda, and Christopher K. Zarins. 2001. "Molecular Mechanisms of Aortic Wall Remodeling in Response to Hypertension." *Journal of Vascular Surgery* 33 (3): 570–78. https://doi.org/10.1067/mva.2001.112231.

Xu, Yao, Jing Ye, Menglong Wang, Yuan Wang, Qingwei Ji, Ying Huang, Tao Zeng, et al. 2018. "Increased Interleukin-11 Levels in Thoracic Aorta and Plasma from Patients with Acute Thoracic Aortic Dissection." *Clinica Chimica Acta; International Journal of Clinical Chemistry* 481: 193–99. https://doi.org/https://dx.doi.org/10.1016/j.cca.2018.03.014.

Yamada, Hiroshi, Noriyuki Sakata, Hideichi Wada, Tadashi Tashiro, and Eiki Tayama. 2015. "Age-Related Distensibility and Histology of the Ascending Aorta in Elderly Patients with Acute Aortic Dissection." *Journal of Biomechanics* 48 (12): 3267–73. https://doi.org/10.1016/j.jbiomech.2015.06.025.

Yamada, I, T Nakagawa, Y Himeno, F Numano, and H Shibuya. 1998. "Takayasu Arteritis: Evaluation of the Thoracic Aorta with CT Angiography." *Radiology* 209 (1): 103–9. https://doi.org/10.1148/radiology.209.1.9769819.

Yang, Chih-Jen, Shih-Hung Tsai, Jen-Chun Wang, Wei-Chou Chang, Chih-Yuan Lin, Zun-Cheng Tang, and Hsian-He Hsu. 2019. "Association Between Acute Aortic Dissection and the Distribution of Aortic Calcification." *PLoS ONE* 14 (7). https://doi.org/10.1371/journal.pone.0219461.

Yang, Guifang, Wen Peng, Yang Zhou, Huaping He, Xiaogao Pan, Yuzhong Cai, and Xiangping Chai. 2020. "Characteristics and Prognosis of Acute Type a Aortic Dissection with Negative d-Dimer Result." *The American Journal of Emergency Medicine* 38 (9): 1820–4.

https://doi.org/https://dx.doi.org/10.1016/j.ajem.2020.05.055.

Yuan, Shi-Min. 2019. "Profiles and Predictive Values of Interleukin-6 in Aortic Dissection: A Review." *Brazilian Journal of Cardiovascular Surgery* 34 (5): 596–604. https://doi.org/https://dx.doi.org/10.21470/1678-9741-2018-0287.

Yuan, Xun, Andreas Mitsis, Yida Tang, and Christoph A. Nienaber. 2019. "The IRAD and Beyond: What Have We Unravelled so Far?" *General Thoracic and Cardiovascular Surgery* 67 (1): 146–53. https://doi.org/10.1007/s11748-017-0817-6.

Zajicek, Jaroslav, Justin D. Pearlman, Michael B. Merickel, Carlos R. Ayers, James R. Brookeman, and Michael F. Brown. 1987. "High-Resolution Proton NMR Spectra of Human Arterial Plaque." *Biochemical and Biophysical Research Communications* 149 (2): 437–42.

Zeng, Y. 2006. "Principles of Micro-RNA Production and Maturation." *Oncogene* 25 (46): 6156–62. https://doi.org/10.1038/sj.onc.1209908.